TARGETED DELIVERY OF HYDROGEN SULFIDE: SYNTHESIS AND APPLICATION OF SMALL MOLECULE HYDROGEN SULFIDE DONORS

by

ANNIE K. GILBERT

A DISSERTATION

Presented to the Department of Chemistry and Biochemistry
and the Division of Graduate Studies of the University of Oregon
in partial fulfillment of the requirements
for the degree of
Doctor of Philosophy

June 2022

DISSERTATION APPROVAL PAGE

Student: Annie K. Gilbert

Title: Targeted Delivery of Hydrogen Sulfide: Synthesis and Application of Small Molecule Hydrogen Sulfide Donors

This dissertation has been accepted and approved in partial fulfillment of the requirements for the Doctor of Philosophy degree in the Department of Chemistry and Biochemistry by:

Dr. Ramesh Jasti	Chairperson
Dr. Michael D. Pluth	Advisor
Dr. Amanda Cook	Core Member
Dr. Marian Hettiaratchi	Core Member
Dr. Diana Libuda	Institutional Representative

and

Krista Chronister	Vice Provost for Graduate Studies

Original approval signatures are on file with the University of Oregon Division of Graduate Studies.

Degree awarded June 2022

DISSERTATION ABSTRACT

Annie K. Gilbert

Doctor of Philosophy

Department of Chemistry and Biochemistry

June 2022

Title: Targeted Delivery of Hydrogen Sulfide: Synthesis and Application of Small Molecule Hydrogen Sulfide Donors

Hydrogen sulfide (H_2S) is an important gaseous signaling molecule that is endogenously produced. Over the past couple of decades, several biological functions of H_2S have been recognized, including the ability of H_2S to promote angiogenesis, osteogenesis, anti-inflammation, and antioxidant effects. Although these physiological effects make H_2S an ideal therapeutic for regenerative medicine, the gaseous state and high reactivity of H_2S make the small molecule challenging to administer to biological systems. To address these challenges, small molecule H_2S donors have been developed that react with biological analytes or environments to produce H_2S in a slow, sustained manner. Despite the expansive library of H_2S donors, several of these H_2S sources still lack spatial control over H_2S delivery which leads to inefficiency and significantly different biological outcomes due to off-target H_2S effects.

The research in this dissertation follows two main aims 1) to improve the localization of H_2S delivery by developing targeted H_2S donors and 2) to develop and apply H_2S donors to bone healing applications. Chapter I is a review of activatable COS-based H_2S donors that build a foundation for developing targeted H_2S donor platforms. Chapter II uses a passive localization approach in developing an acid-labile COS-based H_2S donor that produces H_2S within a specific pH window. Chapter III describes the development of

a library of organelle-targeted COS-based H_2S donors to study subcellular H_2S effects. Chapter IV is a review of the roles of reactive sulfur species in bone and serves as a transition into work towards targeting H_2S delivery in bone healing applications. Chapter V provides an H_2S-releasing biomaterial using the previously developed *N*-acetylcysteine tetrasulfide ($NACS_4$) H_2S donor. Furthermore, this chapter investigates the effects of $NACS_4$ on the osteogenic differentiation of human mesenchymal stem cells to predict the therapeutic activity of $NACS_4$-loaded biomaterials in healing bone defects. Lastly, Chapter VI reports the development of an alkaline phosphatase activated COS-based H_2S donor to target H_2S delivery within the bone healing process. This dissertation includes previously published and unpublished co-authored materials.

CURRICULUM VITAE

NAME OF AUTHOR: Annie K. Gilbert

GRADUATE AND UNDERGRADUATE SCHOOLS ATTENDED:

University of Oregon, Eugene

DEGREES AWARDED:

Doctor of Philosophy, Chemistry, 2022, University of Oregon
Bachelor of Science, Chemistry, 2017, University of Oregon

AREAS OF SPECIAL INTEREST:

Reactive Sulfur Species in Biology
Small Molecule Organic Synthesis
Chemical tool development

PROFESSIONAL EXPERIENCE:

NSF Graduate Research Fellow, Department of Chemistry and Biochemistry, University of Oregon, Eugene, OR, 2019-2022

Graduate Teaching Fellow, Department of Chemistry and Biochemistry, University of Oregon, Eugene, OR, 2017-2019

GRANTS, AWARDS, AND HONORS:

NSF Graduate Research Fellowship 2019-2022

SFRBM Young Investigator Award 2020

LeRoy H. Klemm Award 2017

UOWGS Sara J. Staggs Undergraduate Transition Award 2017

Presidential Undergraduate Research Scholar 2016-2017

Summit Scholar 2013-2017

PUBLICATIONS:

Gilbert, A.K.; Pluth, M.D. Subcellular Delivery of Hydrogen Sulfide via Small Molecule Donors. *Manuscript in preparation*.

Gilbert, A.K.; Newton, T.D.; Hettiaratchi, M.H.; Pluth, M.D. Reactive Sulfur and Selenium Species in the Regulation of Bone Homeostasis. *Submitted to Free Radic. Biol. Med.*

Fosnacht, K.G.; Hammers, M.D.; Earp, M.S.; **Gilbert, A.K.**; Pluth, M.D. A Cell Trappable Methyl Rhodol-Based Fluorescent Probe for Hydrogen Sulfide Detection. *Submitted to Asian J. Chem.*

Gilbert, A.K.; Pluth, M.D. "COS-based H_2S Donors" *Hydrogen Sulfide: Chemical Biology Basics, Detection Methods, Therapeutic Applications, and Case Studies,* Pluth, M.D.; Wiley, *in press*.

Gilbert, A.K.; Zhao, Y.; Otteson, C.E.; Pluth, M.D. Development of Acid-Mediated H_2S/COS Donors That Respond to a Specific pH Window. *J. Org. Chem.* **2019**, *84*, 14469-14475.

Bolton, S.G; Cerda, M.M; **Gilbert, A.K.**; Pluth, M.D. Effects of sulfane sulfur content in benzyl polysulfides on thiol-triggered H_2S release and cell proliferation. *Free Radic. Biol. Med.* **2019**, *131*, 393-398.

Eytel, L.M.; **Gilbert, A.K.**; Görner, P.; Zakharov, L.N.; Johnson, D.W.; Haley, M.M. Do CH-Anion and Anion-π Interactions Alter the Mechanism of 2:1 Host-Guest Complexation in Arylethynyl Monourea Anion Receptors? *Chem. Eur. J.* **2017**, *23*, 4051-4054.

ACKNOWLEDGMENTS

First, I would like to thank my family. To my parents Kandis and Richard Hulteng, and Randal and Tina Gilbert. Thank you for your support in my education and upbringing. To my siblings, Tyler, Kara, Meryl, and Elaine.

Next, I would like to thank my advisor, Professor Mike Pluth – thank you for letting me figure out what I was passionate about and supporting me along the way. Thank you to Professor Marian Hettiaratchi for welcoming me into her lab as an honorary member. To the rest of my committee, Professors Ramesh Jasti, Amanda Cook, and Diana Libuda. I would like to thank my mentors along the way, including my undergraduate mentor, Professor Lisa Eytel. Thank you to my undergraduate advisors, Professors Darren Johnson, and Michael Haley. To my graduate student mentors, Drs. Matthew Cerda, Brittany White, and Christy McDevitt.

Thank you to my lab, which has changed so much over the years but has always made me feel welcome and comfortable to ask for help and be myself. Special thanks to Carrie Levinn for taking up drinking coffee to get me through advancement. To my undergraduate student, Mia Ramos – I have loved getting to work with you. To the current lab: Dr. Toby Sherbow, Turner Newton, Arman Garcia, Kaylin Fosnacht, Olivia Apicella, Haley Smith, and Andy Davis. And to the Hettiaratchi lab for making me feel welcome in their lab space, providing helpful feedback on presentations and projects, and including me in all their lab festivities. Thank you to the chemistry department and student communities – CBGReAT, WGS, CMiS, and ADSE. To the various sports teams, Alkynes of Trouble, Basis Sets, Bump Traps, Perovspikes, and Buckyballers. To all my UO friends and the UO

Chemistry department. To my cat, Olive, for being my study buddy during many late nights. Finally, to my best friend and companion, John. Thank you for everything.

Lastly, I'd like to thank the University of Oregon, and the funding for the research in this dissertation: National Science Foundation (NSF/GRFP DGE-1842486), and the National Institute of Health (R01GM113030).

To my family – thank you for everything

TABLE OF CONTENTS

Chapter Page

Chapter Page

LIST OF FIGURES

CHAPTER I

HYDROGEN SULFIDE DELIVERY VIA COS-BASED H_2S DONORS

This chapter includes material from Gilbert A.K.; Pluth, M.D. COS-based H_2S Donors. *Hydrogen Sulfide: Chemical Biology Basics, Detection Methods, Therapeutic Applications, and Case Studies,* Pluth, M.D.; Wiley, *in press*. This review was written by Annie K. Gilbert, with editorial assistance from Professor Michael D. Pluth.

1.1 Introduction

Hydrogen sulfide (H_2S) has recently been established as an endogenously produced gaseous signaling molecule. H_2S is produced from cysteine and homocysteine by three main enzymes including cystathionine β-synthase, cystathionine γ-lyase, and 3-mercaptopyruvate sulfur transferase. Upon production, H_2S contributes to a wide range of physiological effects, including vasodilation, angiogenesis, anti-inflammation, and the reduction of oxidative stress.[1-2] Unusual H_2S metabolism is also associated with certain diseases, including diabetes and Alzheimer disease.[3-4] Although there is potential for the use of H_2S as a therapeutic small molecule, H_2S is a gas and highly reactive, which make controlled delivery of H_2S to areas of therapeutic need challenging, yet essential.

Small molecule hydrogen sulfide (H_2S) donors have been developed to provide controlled-releasing sources of H_2S that contrast the large bolus release of inorganic sulfide salts. With slower sustained release, these H_2S donors can better mimic endogenous H_2S production. Moreover, the slower release profiles can allow for diffusion into areas of therapeutic need (i.e., oxidative environments, areas of inflammation, etc.). Despite this progress, scaffolds that produce H_2S

directly often have limited tunability and generally lack widely used control compounds to delineate effects of H_2S from resulting byproducts. As a strategy to overcome these limitations, our group as well as other researchers have developed modular and tunable H_2S donors that function by the intermediate release of precursors that are quickly converted to H_2S. Inspired by the enzymatic conversion of carbonyl sulfide (COS) to H_2S, our lab reasoned that COS could serve as a vehicle for H_2S delivery.[5] No longer tied to releasing H_2S directly, COS-based H_2S donors provide access to established prodrug platforms and chemistry that has been known for years but not recognized as a potential platform for H_2S delivery. This general approach has provided COS/H_2S donors that can be activated by biological stimuli, deliver fluorophores and prodrugs alongside COS/H_2S, and can incorporate targeting groups to further localize H_2S delivery.[6-7] In this chapter, we highlight the basic properties of COS and summarize current COS-based H_2S delivery strategies.

1.2 Properties of COS

COS was initially misidentified as a mixture of CO_2 and H_2S, both of which are hydrolysis byproducts of COS and thus common impurities found in COS gas.[8] On its own, COS is a colorless and odorless gas that was discovered by Than in 1867 when mixing carbon monoxide with excess sulfur in a glowing porcelain tube.[9] This initial method to prepare COS contained significant carbon monoxide (CO) impurities. A more reliable synthesis of COS relies on the acid-mediated hydrolysis of thiocyanate salts and subsequent purification through a series of washing steps.[10]

COS is the most abundant sulfur-containing gas in the atmosphere (~0.5 ppb) and is emitted by a variety of abiotic, biotic, and anthropogenic sources including volcanoes, oceans, microorganisms, and coal.[10] Beyond its identity as a major atmospheric gas in the global sulfur

cycle, prior work suggests that COS could be an important biological molecule and a potential gasotransmitter.[5] For example, exposure of α-amino acids to COS under prebiotic conditions generates peptides, implicating the possible role of COS in origin of life peptide ligation (Figure 1.1).[11-12] COS has also been detected in various biological tissues and in the exhaled breath of humans, further supporting its significance in biology, although enzymatic pathways for mammalian COS production have yet to be identified.[13-15]

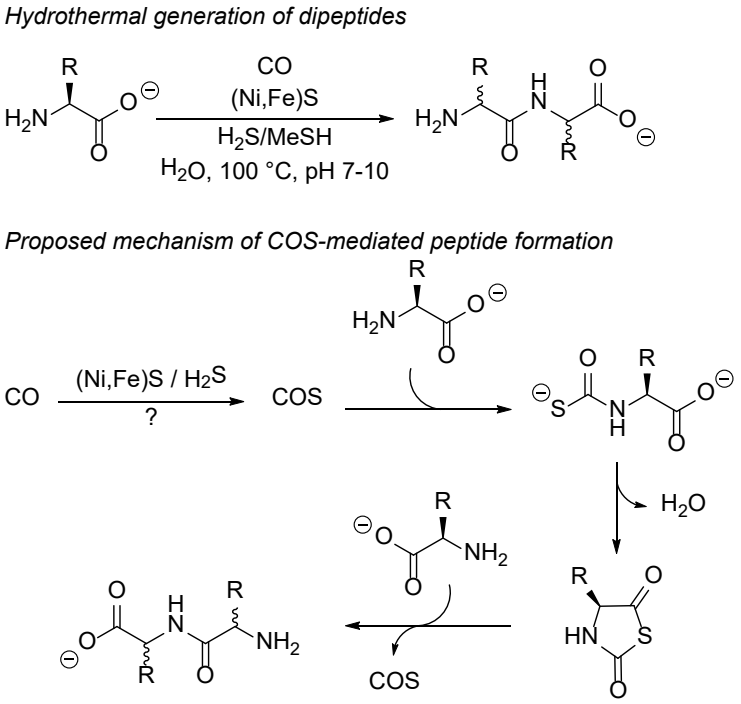

Figure 1.1 Hydrothermal generation of dipeptides in the presence of CO, (Ni,Fe)S, and H_2S/MeSH. COS generation serves as a key intermediate.

COS is converted to H_2S by a variety of enzymes with varying efficiency. These enzymes include CS_2 hydrolase, nitrogenase, CO dehydrogenase, ribulose-1,5-bisphosphate carboxylase (Rubisco), and carbonic anhydrase (CA).[16-20] Although CS_2 hydrolase has the greatest catalytic efficiency for COS hydrolysis (8.2×10^7 M^{-1} s^{-1}), this enzyme is isolated from acidophilic and

thermophilic archaea extremophiles and is not likely to contribute significantly to global COS hydrolysis nor COS conversion to H_2S in common terrestrial organisms.[16] CA, on the other hand, has a relatively high catalytic efficiency of COS hydrolysis (2.2 x 10^4 M^{-1} s^{-1}) and is widely distributed throughout cells.[17] The primary function of CA is to regulate biological pH by hydrolyzing CO_2 (k_{cat}/K_M = ~8 x 10^7 M^{-1} s^{-1}),[21] however, the widespread localization of CA paired with its relatively high catalytic efficiency suggests it could be a significant contributor to endogenous COS consumption. Although these two factors are convenient for COS delivery in biological milieu to produce H_2S, they complicate direct biological investigations into the role of COS independent to that of H_2S. For example, in toxicological investigations of COS on rats, Chengelis and Neal reported pretreatment of rats with acetazolamide (AAA), a known CA inhibitor, resulted in reduced blood levels of H_2S and subsequently reduced the toxicity of COS, suggesting at least some of the toxicity observed from COS comes from CA-mediated H_2S generation.[22]

1.3 COS-based H_2S delivery

The widespread localization of CA paired with its relatively high catalytic efficiently toward COS hydrolysis motivated the use of COS in H_2S donor development. As an alternative to producing H_2S directly, COS delivery can leverage already known biocompatible decarboxylation reactions, many of which can be activated by or tuned to specific analytes or environments. For example, self-immolative carbamates rely on cascade decarboxylation reactions and have been used previously as highly tunable methods for the controlled release of small molecules. These prodrugs are activated in the presence of specific analytes or environments to release CO_2, a quinone methide, and the desired payload. By simply replacing one oxygen atom with a sulfur

allows for these decarboxylation reactions to be tuned to release COS instead of CO_2 and serve as COS-based H_2S donors (Figure 1.2).

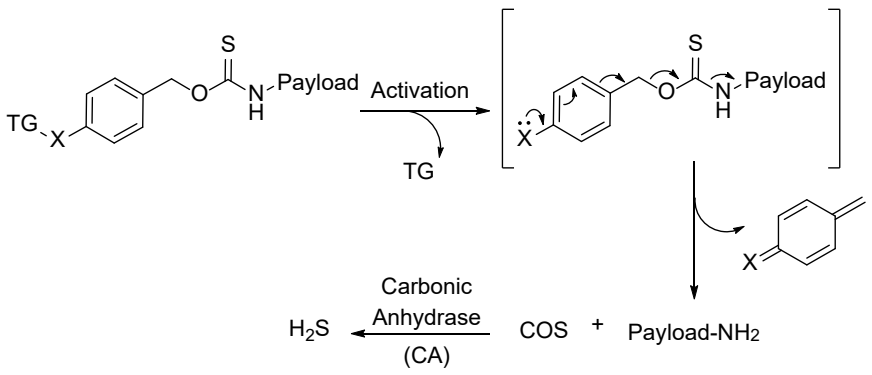

Figure 1.2 Self-immolation cascade reaction of caged thiocarbamates. Deprotection of a triggering group (TG) initiates decomposition to release COS which is rapidly hydrolyzed in the presence of carbonic anhydrase (CA) to produce H_2S.

The first application of the self-immolative thiocarbamate system described in Figure 1.2 was used to address the challenge of analyte consumption in activity based H_2S detection strategies. A common approach to develop activity-based H_2S-selective fluorescent probes is the use of H_2S-mediated azide reduction to produce a fluorescent amine. This reaction, however, consumes H_2S and could perturb cellular homeostasis or impact biological outcomes. To overcome these limitations, we developed an analyte replacement probe for H_2S that yields both a fluorescent turn-on response and COS/H_2S release to replace the consumed H_2S for probe activation (Figure 1.3).[23] A model thiocarbamate containing an azide triggering group was used to confirm biocompatibility by demonstrating H_2S production in whole mouse blood upon azide reduction using *tris*(2-carboxyethyl)phosphine (TCEP). Addition of AAA to inhibit CA resulted in decreased H_2S production, which confirmed that CA is required to convert the released COS to H_2S. Having confirmed the H_2S donating capabilities of the thiocarbamate scaffold, the H_2S-selective analyte

replacement probe (MeRho-TCA) was prepared by functionalizing a quenched methyl rhodol fluorophore with a *p*-azidobenzylthiocarbamate. Reduction of the azide triggering group by H_2S, initiates decomposition to release COS/H_2S and the methyl rhodol payload to generate a 65-fold fluorescent turn-on response with excellent selectivity over other reactive sulfur, oxygen, and nitrogen species. One limitation to this approach is that the fluorescence response is not directly proportional to the initial H_2S concentration because the probe releases COS/H_2S upon reaction with H_2S. Furthermore, complete azide reduction requires two equivalents of H_2S, which suggests that only one-half of the consumed H_2S is replaced. Despite these drawbacks, this work provided an important foundation for further expansion of COS-based H_2S donors. More recently, this azide-reduction triggering approach has been expanded to include polymeric donors.[24] Since this initial report of COS-based H_2S delivery, the available library of COS-based H_2S donors has expanded significantly to include donors activated by a wide variety of stimuli and conditions.

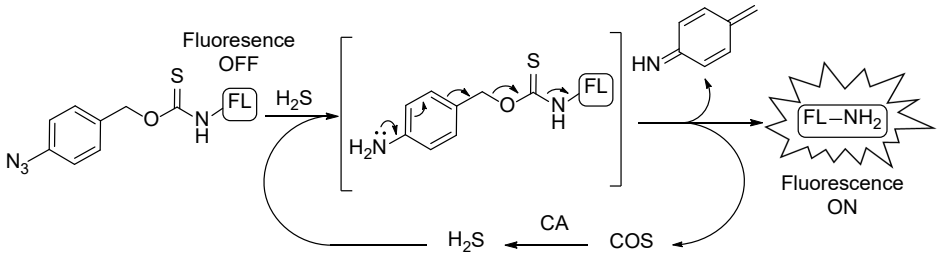

Figure 1.3 Analyte-replacement H_2S probe mechanism of COS/H_2S release with concomitant turn-on fluorescence.

1.3.1 Stimuli responsive COS/H_2S donors

The first application of caged thiocarbamates as stimulus-responsive COS/H_2S donors used a boronate ester trigger (Peroxy-TCM-1) to develop donors that were responsive to reactive oxygen species ROS.[25] In the presence of ROS, the boronate ester triggering group is converted to

a phenol, which initiates self-immolative decomposition to produce COS/H_2S (Figure 1.4). Using ROS as a stimulus for H_2S delivery not only localizes COS/H_2S where it can protect against ROS, but also combines the ROS scavenging abilities of boronate esters with cytoprotective effects of H_2S. Using the ROS-activated Peroxy-TCM-1, H_2O_2-dependent release of COS/H_2S was demonstrated in the presence of CA using an H_2S selective electrode. No COS/H_2S release was observed with the carbamate and triggerless control compounds confirming the thiocarbamate and boronate trigger are critical for COS/H_2S release. Furthermore, COS/H_2S release was confirmed in live cell environments. Incubation of HeLa cells with a fluorescent H_2S probe (HSN2) and Peroxy-TCM-1 resulted in a turn-on response when treated with exogenous H_2O_2. An increase in fluorescence was also observed when Raw 264.7 cells were treated with phorbol myristate acetate (PMA) to increase endogenous ROS levels in the presence of Peroxy-TCM-1 and the H_2S-responsive fluorescent probe HSN2. Furthermore, the pre-treatment of HeLa cells with the ROS-activated donor provided significant cytoprotective effects against exogenous H_2O_2.

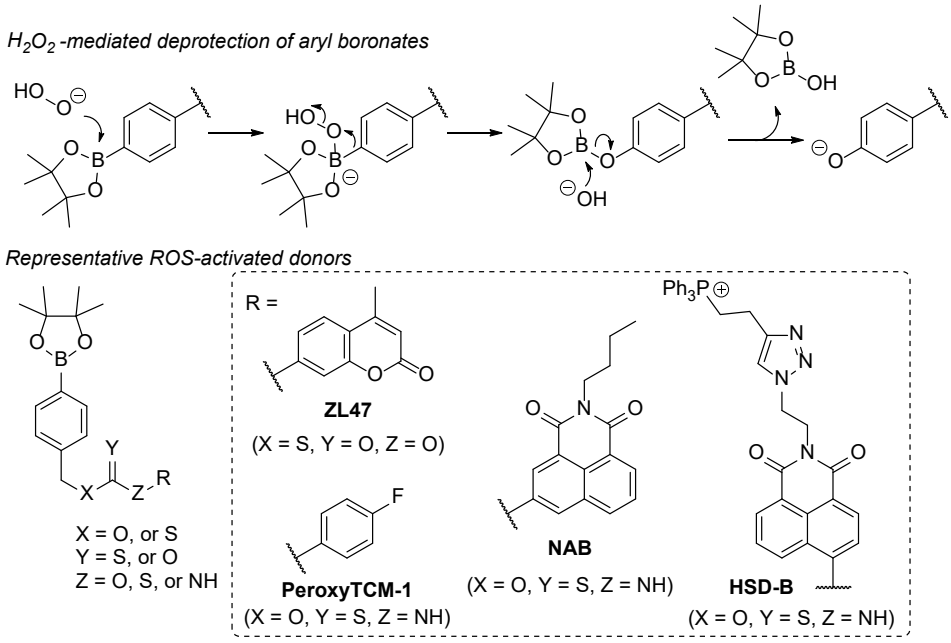

Figure 1.4 Mechanism of ROS-activation of aryl boronates and representative ROS-activated COS/H_2S donors.

The ROS-activated donor scaffold has served as useful platform for studying the self-immolative COS/H_2S donor system. Since the initial report, a variety of isomeric cores (*O*-alkyl and *S*-alkyl thiocarbamates/thiocarbonates) and a variety of payloads (electron donating and electron withdrawing) have been incorporated with the ROS-activated scaffold to study release kinetics.[26-27] Overall, the second order rate constant (k_2) for COS/H_2S delivery from *O*-alkyl thiocarbamates is over an order of magnitude greater than *S*-alkyl thiocarbamates (k_2 = 1.16 $M^{-1}s^{-1}$ compared to 0.16 $M^{-1}s^{-1}$). This difference was attributed to the greater ground state stability of the *S*-alkyl isomer due to enhanced resonance stabilization in the amide moiety of the thiocarbamate. Incorporating electron withdrawing groups (EWG) were hypothesized to accelerate COS/H_2S release and electron donating groups (EDG) were predicted to slow COS/H_2S release. This trend, however, was not observed uniformly across *O*-alkyl donors suggesting the acidification of the thiocarbamate NH proton could be interfering with COS release. For *S*-alkyl thiocarbamates, Chakrapani and co-workers reported the rate of COS/H_2S release could be altered predictably by modulating the pK_a of the thiocarbamate NH. Aniline-based derivatives with lower pK_a values (4.75–5.43) resulted in faster H_2S release compared to derivatives with higher pK_a values (8.36–10.53). This work also contributed a novel ROS-activated H_2S-releasing nonsteroidal anti-inflammatory drug (NSAID) based on mesalamine, which could have additional potential applications for H_2S delivery. The general approach of using an ROS-trigger to deliver COS/H_2S has also been used for the development of fluorescent COS/H_2S donors,[28-30] which are covered in more detail in section 1.3.6.

1.3.2 Bio-orthogonal donor activation

Bio-orthogonal activation strategies have also been used to develop COS/H_2S donors. For example, the click-and-release COS/H_2S donor (TCO-1) was developed that uses an inverse-electron demand Diels-Alder (IEDDA) reaction between a thiocarbamate-functionalized *trans*-cyclooctene and tetrazine.[31] The IEDDA reaction between these coupling partners produces a dihydropyridazine that spontaneously tautomerizes then deprotonates and rearomatizes to release COS/H_2S (Figure 1.5). This bio-orthogonal approach remained viable in both diluted sheep and bovine blood without the need for exogenous CA addition, which confirms that endogenous CA levels are sufficient for COS conversion to H_2S. Although this work demonstrated preliminary biological compatibility, further investigations are needed to improve upon the efficiency and rate of COS release in more complex environments.

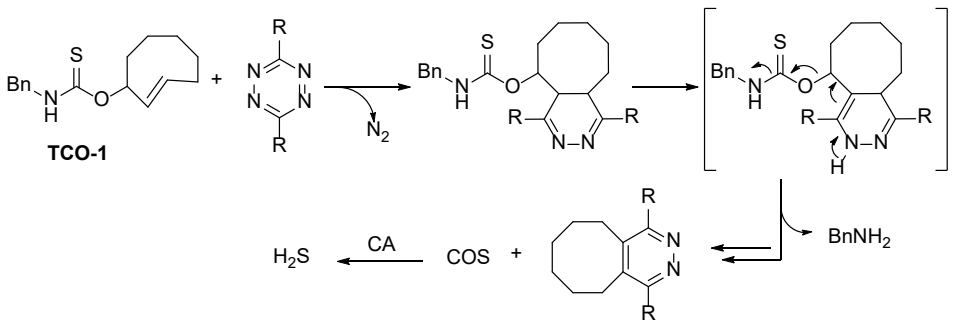

Figure 1.5 Click-and-release mechanism of TCO-1 to produce COS/H_2S.

Expanding the COS/H_2S donors that are activated by bio-orthogonal stimuli, a number of groups have reported photoactivated COS/H_2S donors. In the initial report, our group demonstrated the compatibility of using a photocleavable *o*-nitrobenzyl group to develop COS/H_2S donors.[32] Irradiation with UV light (λ = 365 nm) results in *o*-nitrobenzyl group cleavage by a Norrish type II mechanism to produce COS and an aniline byproduct (Figure 1.6). Consistent with previous findings, the photocleavage and rate of COS/H_2S release increases when electron-donating

substituents are added to the *o*-nitrobenzyl group. Gou and coworkers provided an additional photolabile COS/H_2S donor using the *o*-nitrobenzyl photolabile group and a napthalimide payload (Nap-Sul-ONB) to enable real-time tracking of COS release, which is covered in more detail in section 1.3.6.[33] Although these *o*-nitrobenzyl containing photoactivatable COS/H_2S donors demonstrate an on-demand approach to H_2S release, the requirement of UV light for activation significantly reduces the biocompatibility.

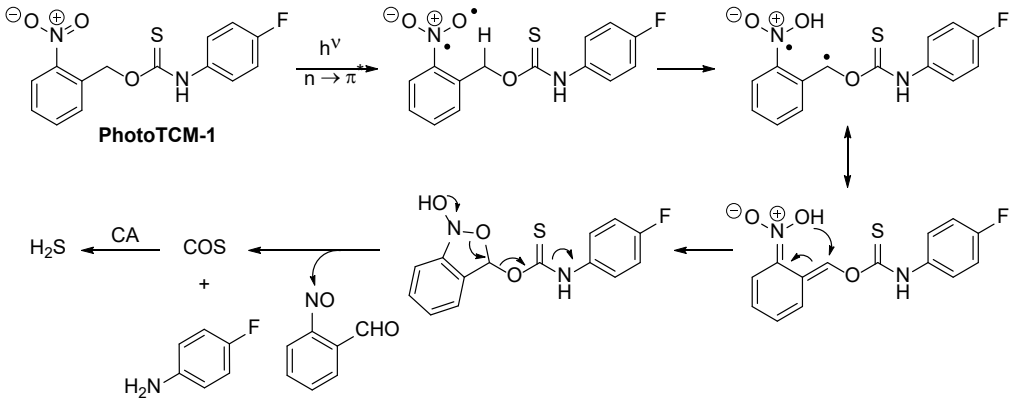

Figure 1.6 Light-activated COS/H_2S release of PhotoTCM-1.

Expanding the palette of light-activated COS/H_2S donors, Chakrapani and co-workers developed the visible light activated BODIPY COS/H_2S donor BODIPY-TCM (Figure 1.7).[34] The BODIPY-based photolabile group is cleaved by 470 nm light via a photoinduced electron transfer process, which then initiates COS release through a self-immolative decomposition. To evaluate the cell viability during photocleavage of BODIPY-TCM, HeLa cells were incubated with BODIPY-TCM and exposed to 470 nm light for 5 minutes. No cytotoxicity was observed demonstrating this compound and the light exposure is not cytotoxic and can be applied to cell-based applications. To expand photoactivatable COS/H_2S donors to longer-wavelength platforms, Klán and coworkers reported a NIR-activated donor compatible with the tissue-transparent region

(600-900 nm) with altering the substitution of the thiocarbamate in the BODIPY system to the *meso*-position (meso-Methyl-S-TCM).[35] To increase solubility, the fluorine atoms of the BF_2 motif were substituted with polyethylene glycol (PEG) chains. Further installment of a PEG-substituted styryl units to the BODIPY core shifted the absorption to the NIR region due to the extended π-conjugation. Irradiation of the resulting NIR-activated donor with 700 nm light in HepG2 cells treated with an H_2S-selective fluorescent probe results in a significant increase in fluorescence intensity compared to the control. Collectively, this donor demonstrates potential for on-demand delivery of H_2S to deep-tissue.

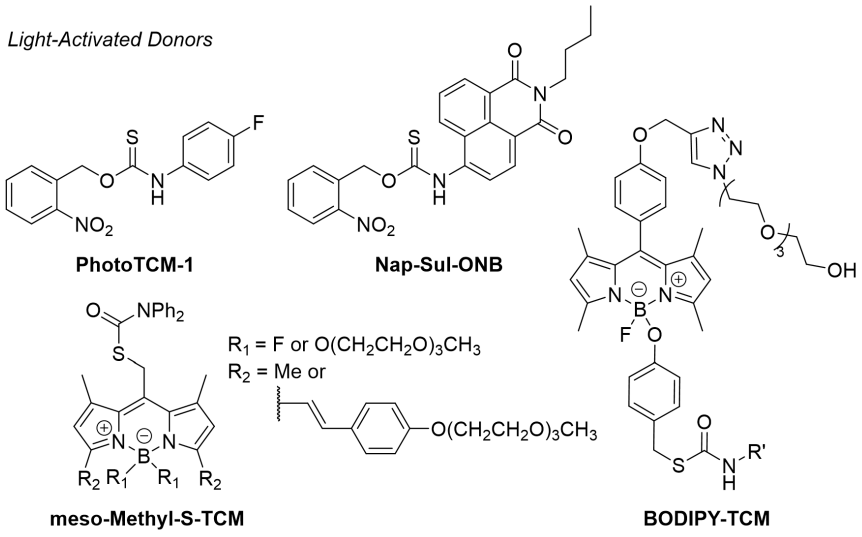

Figure 1.7 Representative light-activated COS-based H_2S donors.

1.3.3 Donors activated by nucleophiles

N-Thiocarboxyanhydrides (NTAs) are one of the first classes of COS-based H_2S donors and the first COS donor platform to avoid generation of electrophilic byproducts.[36] Matson and co-workers demonstrated that this class of donors is ring-opened upon nucleophilic attack of biological amines to release COS (Figure 1.8). H_2S production from NTAs (10 μM) was confirmed

in PBS buffer in the presence of glycine (1 mM) and CA (300 nM) using an H_2S-selective electrode. In the absence of CA, no H_2S generation was observed, confirming the necessity of CA in generating H_2S from COS. In subsequent work aimed at providing potential COS/H_2S releasing materials for localized H_2S delivery, the NTA donor platform was incorporated in a norbornene-based monomer and was successfully polymerized via ring-opening metathesis. The water soluble NTA functionalized co-polymer (polyNTA1, Figure 1.8) showed a rapid initial release followed by a plateau after 2 h with sustained release for 20 h. This extended release could serve beneficial for therapeutic delivery of H_2S in biological applications. Expanding the available COS/H_2S donating materials, the NTA scaffold was coupled with a series of functional groups used in bioconjugation and polymer chemistry including azides, alkynes, alkenes, and norbornenes (Figure 1.8).[37] The functionalized NTAs were successfully conjugated to azides and alkynes, alkenes, and thiols using copper-catalyzed azide-alkyne cycloaddition (CuAAC), olefin cross metathesis, and radical thiol-ene reactions. Polymer-NTA conjugates showed some variation of H_2S release rates with the NTA functionalized poly(acryloyl morpholine) polymer peaking in H_2S release at 20 min whereas the NTA polyethylene glycol polymer peaks in H_2S concentration around 2 h. Despite this variation, both polymeric donors show a gradual return to baseline H_2S concentrations, suggesting the polymer conjugates provide sustained release of H_2S. Collectively, this work highlights the versatility of the NTA scaffold to be incorporated in a variety of materials that provide sustained and localized H_2S release.

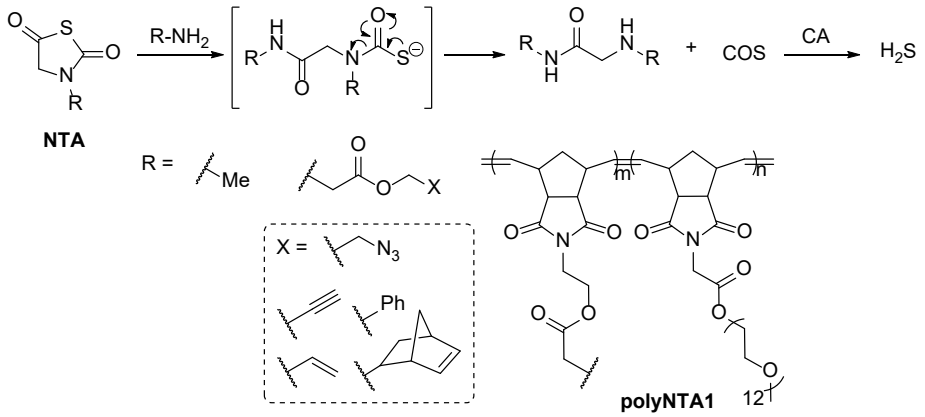

Figure 1.8 Example NTA-based COS/H_2S donors and the associated mechanism of release.

Adding to the amine-based nucleophile activation of NTAs, a number of different strategies have been developed that rely on thiol activation for COS/H_2S release. For example, our lab reported the cysteine-selective self-immolative COS/H_2S donor (OA-CysTCM) that uses the previously established cyclization between cysteine and acrylates commonly used to develop cysteine-selective probes.[38-39] With an acrylate group in the trigger position, nucleophilic attack by cysteine followed by a cyclization with the pendant amine uncages COS from OA-CysTCM (Figure 1.9), which also imparts selectivity for cysteine over other biological thiols. The COS/H_2S release was further confirmed in biological environments with bEnd.3 cells and an H_2S-selective fluorescent probe.

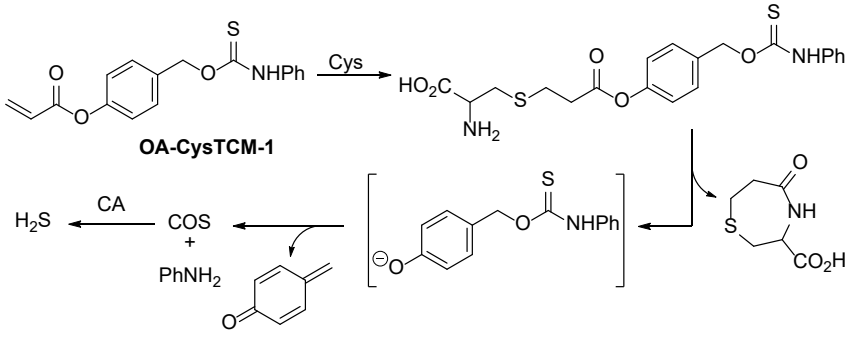

Figure 1.9 Cysteine-selective activation of OA-CysTCM-1.

Cyclic sulfenyl thiocarbamates (sulfenylTCMs) have also been demonstrated to release COS/H_2S upon reaction with thiols.[40] We demonstrated that sulfenylTCMs are stable in aqueous solution until activated by biological thiols to produce COS and an iminodisulfide intermediate (Figure 1.10). Further reaction of the iminodisulfide with thiols produces either a thioamide and H_2S or a thioamide and a persulfide which can further react with thiols to produce H_2S. Thioamides are one of the simplest direct-releasing H_2S donor motifs and have been coupled with pharmaceuticals like NSAIDs to help reduce GI damage.[41] Despite their accessibility, the mechanism of H_2S release from thioamides is not fully established and generally results in low H_2S releasing efficiencies (1-2%). Because sulfenylTCMs generate a thioamide upon reaction with thiols, we developed the donor YZ-597 that release both COS/H_2S and the previously developed H_2S-releasing thiobenzamide naproxen derivative (ATB-346) upon reaction with thiols. Compared to ATB-346, YZ-597 demonstrated significantly more efficient H_2S release (90%) whereas ATB-346 only produced baseline levels. This enhanced efficiency was also demonstrated in live cell imaging with a strong fluorescent signal resulting from treatment of HeLa cells with YZ-597 and the H_2S-selective probe (SF7-AM).

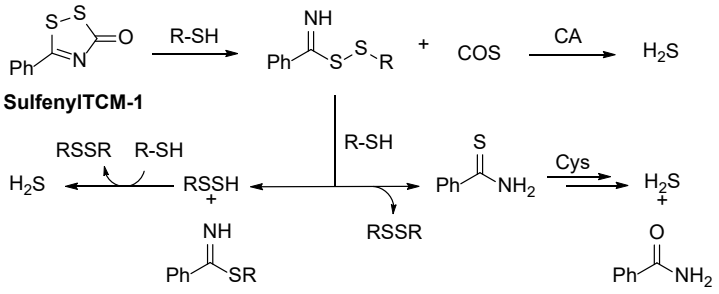

Figure 1.10 Proposed COS/H_2S release pathways from SulfenylTCM donors.

Similar to the sulfenylTCM and NTA scaffolds, the cyclic dithiasuccinoyl (DTS) group can also react with nucleophiles, in this case thiols, to release COS/H_2S without producing

electrophilic byproducts.[42] DTS groups have been previously used as protecting groups for amines in peptide synthesis[43] and its application to COS/H_2S delivery was reported independently by our group and Ji and co-workers.[44] This class of donors was hypothesized to have increased H_2S-releasing efficiency compared to other cyclic donor motifs because it reacts with thiols to uncage two equivalents of COS with an amine byproduct (Figure 1.11). As expected, the aryl DTS donors containing electron withdrawing groups released 2 equivalents of H_2S in the presence of cysteine (20 equiv.) and CA (25 μg/mL). Conversely, alkyl DTS donors resulted in significantly slower rates of H_2S release. We postulated that inductive donation of the alkyl amines likely stabilizes the thiocarbamic intermediate to decrease COS/H_2S-releasing kinetics.

Expanded mechanistic work by Ji and co-workers provided further insights into the COS and H_2S release from DTS-containing donors.[44] Notably, it was found that phenyl DTS, as well as other electron-withdrawing donors, produced a considerable amount of H_2S in the absence of CA, which indicated an alternative pathway for direct H_2S release (Figure 1.11). To investigate the role of electronic contributions to COS/H_2S or direct H_2S release, a series of differently substituted DTS-based donors were developed which led to mechanistic bifurcation shown in Path A and Path B in Figure 1.11. For DTS motifs with EWGs, the carbonyl carbon of the perthiocarbamate intermediate becomes sufficiently electrophilic such that it can be attacked by a thiol to generate a subsequent persulfide intermediate, which can further react with thiols to produce H_2S (Path B in Figure 1.11). An additional byproduct is observed by LC-MS for electron withdrawing DTS donors which matches the thiocarbamate formed in Path B, supporting the direct-releasing H_2S mechanism. For alkyl or electron donating donors, attack by thiol occurs primarily at the disulfide motif in the perthiocarbamate intermediate, rather than at the carbonyl carbon, which results in COS release exclusively (Path A in Figure 1.11). This exclusive COS release from alkyl or electron

donating donors is confirmed from H_2S-release experiments in the absence of CA resulting in no H_2S production. In addition to providing mechanistic insights to the DTS scaffold, Ji and co-workers also investigated the biocompatibility of the DTS motif. BV2 microglia cells treated with the H_2S-responsive probe HSip-1 and either phenyl or methyl DTS resulted in a significant fluorescent enhancement, even at low 2.5 μM concentrations of the donors. Furthermore, 1 and 2.5 μM levels of phenyl DTS provided dose-dependent anti-inflammatory effects, as indicated by the suppression of LPS-induced TNF-α production. These results not only confirm the biocompatibility of the DTS motif, but additionally reveal significant efficiency in delivering H_2S in biological milieu.

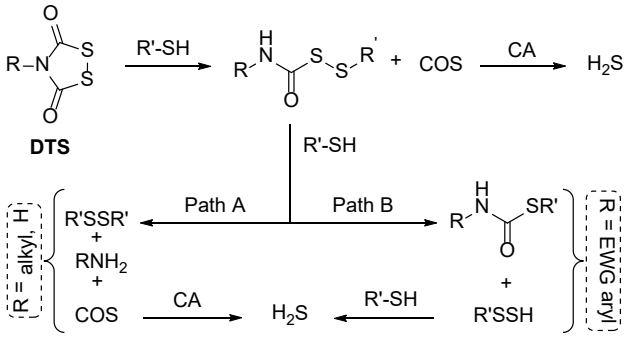

Figure 1.11 DTS mechanism of COS/H_2S release with alternative direct H_2S release pathway for alkyl groups.

Although 1,2,4-thiadiazolidin-3,5-diones have been previously reported as cysteine-activated direct H_2S releasing donors, the reported production of H_2S (<6.5% efficiency) compared to the observed biological activity (vasodilatory effects observed as low as 10 nM) suggests that other reactive sulfur species or release mechanisms could be at play.[45] Initially, the proposed mechanism of H_2S production was thiol-initiated ring opening of the thiadiazolidindione followed by a subsequent thiol addition into the resulting disulfide and hydrolysis of the thiocarbamate

(Figure 1.12). An alternative mechanism is that the thiocarbamate intermediate could dethiocarboxylate to produce COS, which would not be detected by amperometric measurements in the absence of CA but could result in H_2S production within biological environments. This proposed pathway is also consistent with previously established chemistry of thiocarbamate intermediates in COS-based donors and could explain the low H_2S levels initially reported.

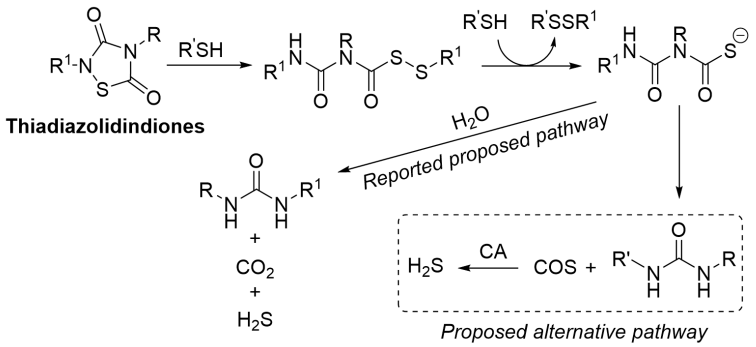

Figure 1.12 Proposed alternative pathway for COS-based H_2S release from 1,2,4-thiadiazolidin-3,5-diones.

Acyclic perthiocarbamate derivatives are an additional class of thiol-activated COS/H_2S donors. Toscano and co-workers demonstrated *N*-alkyl perthiocarbamates function as tunable platforms for persulfide and/or COS release.[46] Deprotonation of the ammonium produces an amine that cyclizes to release a persulfide and a urea byproduct in the absence of thiols (Figure 1.13). Varying the substituents on the perthiocarbamates altered the half-lives of persulfide release (1.4 to 484 min) which were measured using an electrophilic trap to quantify the persulfide. Longer-lived persulfide precursors also resulted in COS release generated through thiol attack of the perthiocarbamate to generate a thiocarbamate intermediate followed by dethiocarboxylation. This COS release pathway, however, is minor with persulfide releasing efficiency ranging from 82-94%. The donor platform demonstrated biocompatibility and cytoprotective effects upon

pretreatment of H9c2 cells with the perthiocarbamates prior to H_2O_2 exposure. Additionally, the donors provided cardioprotective effects in myocardial ischemic/reperfusion injury model which highlights the beneficial effects of combined persulfide and COS/H_2S delivery.

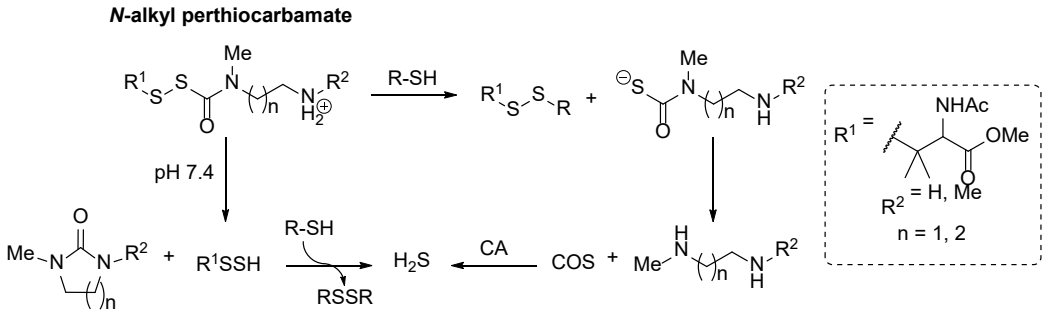

Figure 1.13 Persulfide and COS releasing pathways of *N*-alkyl perthiocarbamates.

1.3.4 Enzyme-activated donors

Enzyme-mediated bond cleavage is a widely used approach in prodrug activation. For example, enzyme-activated prodrug therapy has been used as an effective cancer treatment to localize non-toxic prodrugs to tumors where enzymes within the tumor microenvironment can subsequently convert the prodrugs into highly toxic drugs.[47] In addition to being a useful delivery strategy, this approach also uses physiologically relevant stimuli while avoiding the consumption of biological nucleophiles that could perturb cellular homeostasis. Enzyme-activated H_2S delivery was first reported by Wang and co-workers in 2016 by developing H_2S donors that were initiated by esterase-mediated cleavage.[48] The following year, both Chakrapini and co-workers[49] and our group[50] independently reported esterase-activated COS-based H_2S donors using the self-immolative thiocarbamate platform. Esterase is expressed in most tissue types allowing for activation throughout various cells and organs. Another benefit of esterase-activated donors is that the rate of COS/H_2S release can be tuned by modifying the ester trigger group.

Chakrapani and co-workers developed a series of *S*-alkyl thiocarbamates and *S*-alkyl thiocarbonates with a *t*-butyl ester linked to the scaffold via an extended methylenedioxy linker (Figure 1.14, a).[49] In this work, they provide a library of aryl and benzyl payloads with various substituents and measure H_2S production using danzyl azide, an H_2S-sensitive fluorogenic dye. The rate of COS/H_2S release in the presence of porcine liver esterase (PLE, 1 U/mL) and CA was similar in magnitude across the different payloads (R = 4-NO_2Ph, Ph or CH_2Ph) for thiocarbonate cores (k_{obs} = 6.5 – 7.0 x 10^{-4} s^{-1}). The thiocarbamate cores with aryl payloads (R = 4-NO_2Ph and Ph) had comparable rates to the thiocarbonates, however, the thiocarbamate core with a benzylic payload demonstrated a slower rate of H_2S release compared to the other compounds. HPLC analysis revealed a longer lived intermediate, potentially the thiocarbamate ion, suggesting the *S*-alkyl thiocarbamate scaffold could modulate H_2S release through stereoelectronic effects on the NH. Moreover, the esterase-activated donors showed H_2S production in MCF-7 human cancer cells using an H_2S-selective fluorogenic probe (NBD-Fluorescein) and showed no significant cytotoxicity up to 25 μM, demonstrating the biocompatibility of the donor platform.

Our group reported the *t*-butyl ester *O*-alkyl thiocarbamate Esterase-TCM-OA which released COS/H_2S in the presence of PLE and CA (k_{obs} = 1.6 x 10^{-3} s^{-1}).[50] Interestingly, treatment of human lung epithelial (BEAS2B) cells with low concentrations of this donor (10 μM) resulted in nearly complete cell death. Furthermore, the same concentrations of the carbamate and triggerless control compounds or Na_2S showed no cytotoxicity. We hypothesized this unexpected toxicity could be from a buildup of COS caused by the rapid release of COS from the donor. Because small ester hydrolysis is likely faster than COS hydrolysis (up to 5.8 × 10^5 M^{-1} s^{-1} compared to 2.2 × 10^4 M^{-1} s^{-1} for bovine CA II), a buildup of COS could be causing direct toxic effects. In a follow-up study to investigate this hypothesis, we prepared a library of donors with

varying sizes of ester groups to alter the rate of COS release.[51] We found that the rate of release directly correlated with cytotoxicity in HeLa cells (Figure 1.14, b). Although it is still unclear whether the cytotoxicity of these compounds was from direct COS effects or localization of COS/H_2S, this work demonstrated slower releasing esterase-activated donors were non-toxic and could be used to deliver COS/H_2S to live cells.

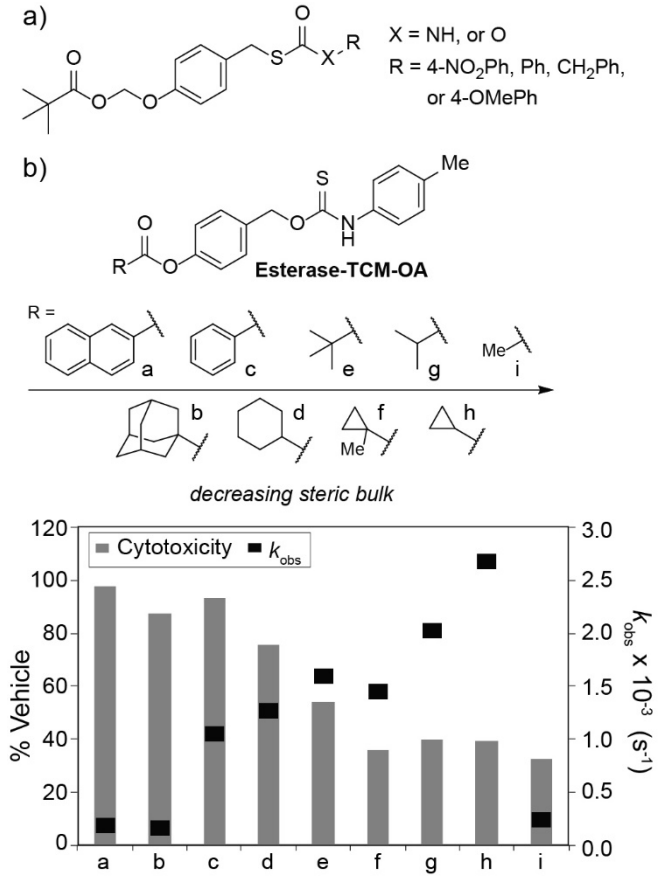

Figure 1.14 a) *t*-Butyl esterase donors with a methylenedioxy linker. b) Correlation between rate of COS/H_2S release and cytotoxicity in esterase thiocarbamates.

Expanding away from ester cleavage, Chakrapani and coworkers also developed a COS/H_2S donor activated by NAD(P)H quinoneoxidoreductase 1 (NQO1).[52] NQO1 is a two-electron reducing cytosolic enzyme that reduces quinones to hydroquinones and is predominantly

expressed under oxidative stress. The increased expression of NQO1 in oxidative environments makes it an ideal target for COS/H_2S delivery because H_2S should provide protective effects in such environments. The NQO1-activated donors contain a quinone triggering group linked to a thiocarbamate scaffold via an ethyl ester. Reduction of the quinone produces a hydroxyquinone that cyclizes and deprotects the caged thiocarbamate (Figure 1.15). The thiocarbamate intermediate subsequently undergoes self-immolative cascade to release COS which is converted to H_2S in the presence of CA. The persulfidation activity of the NQO1-activated donors was investigated in human colon adenocarcinoma (DLD-1) cells where NQO1 is overexpressed. DLD-1 cells were treated with the NQO1 donors (10 μM) for 1 h followed by treatment of methyl sulfonylbenzathiazole and CN-BOT to trap and fluorescently tag persulfides, respectively. Protein persulfidation from the NQO1 donors was confirmed with a significant enhancement in fluorescence intensity compared to the untreated control. Furthermore, this platform was coupled with mesalamine (a drug used to treat colitis) which demonstrated cytoprotective effects against oxidative stress in DLD-1 cells whereas mesalamine alone was not found to be as effective.

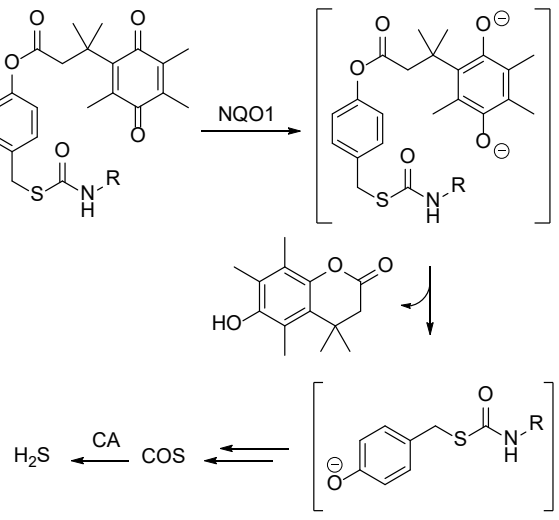

Figure 1.15 NQO1-mediated COS/H_2S release of NQO1 donors.

1.3.5 pH-Activated donors

The use of acidic conditions as a stimulus to initiate H_2S release has recently gained attention to treat myocardial ischemia reperfusion injury and suppress tumor growth, both of which typically occur in mildly acidic environments. Xian and co-workers developed an acid-activated direct H_2S releasing donor (JK-1) that demonstrated significant therapeutic effects towards treatment of ischemic injury.[53] To further establish control over H_2S release within specific mildly acidic environments, we developed a COS-based acid-labile donor (*S*-pHTCM) that releases within a specific pH window.[54] An acid-labile imine triggering group was appended to the caged thiocarbamate where under acidic conditions, imine hydrolysis is catalyzed to initiate self-immolative decomposition and COS/H_2S release. Although acidic conditions increase the rate and efficiency of COS/H_2S release compared to neutral and basic pH, strongly acidic conditions protonate the aniline intermediate and decrease COS/H_2S production (Figure 1.16). Collectively, COS/H_2S release peaked within a window of pH based on the pK_a of the iminium (pK_a ~ 5-7) and anilinium (pK_a ~ 4.6) ions shown in Figure 1.16, confirming the preference of COS/H_2S release in mildly acidic environments. This donor further establishes control in localizing H_2S release in mildly acidic environments and could serve as a useful strategy in the design of orally administered hydrolysis-based H_2S donor motifs.

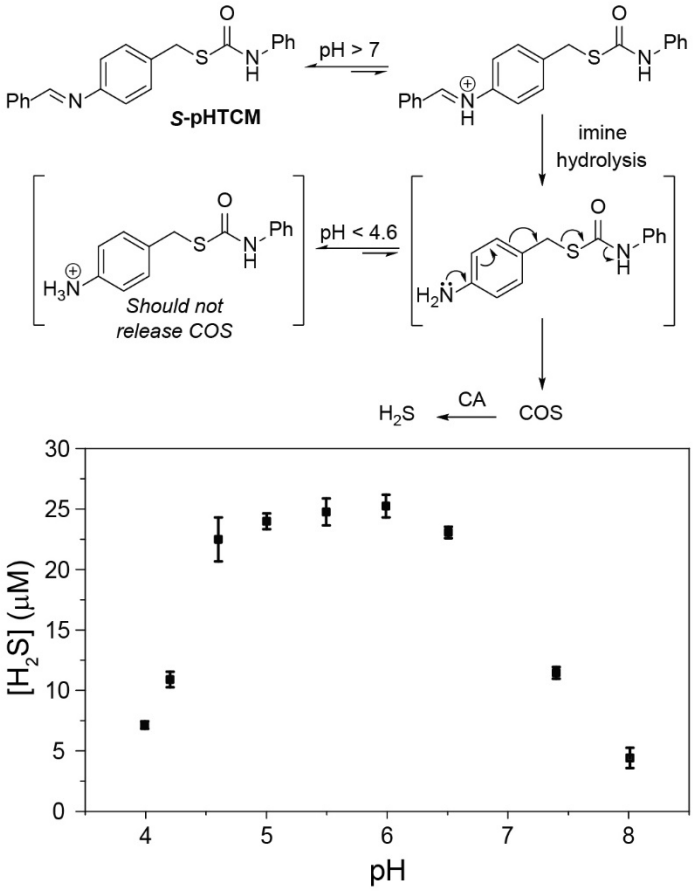

Figure 1.16 Proposed mechanism of pH-dependent release of *S*-pHTCM and pH curve of H_2S concentration at 5 h.

Another class of pH-dependent COS/H_2S donors include γ-ketothiocarbamates (γ-KetoTCM),[55] which are activated under basic conditions. This release mechanism proceeds through an enol intermediate, which subsequently undergoes ß-elimination to release COS/H_2S without any electrophilic byproducts (Figure 1.17). Furthermore, the donor contains a *p*-nitroaniline (PNA) payload to produce a turn-on colorimetric response (λ_{max} = 381 nm) for real-time monitoring of COS release via UV/Vis spectroscopy. The rate constant obtained from fitting the absorbance of PNA (k_{obs} = 8.6 ± 0.9 x 10^{-4} s^{-1}) matched the rate observed when measuring H_2S production (k_{obs} = 8.1 ± 0.3 x 10^{-4} s^{-1}), which confirmed that the colorimetric response directly correlates with H_2S production. The rate of COS/H_2S release demonstrated pH-dependence with

the fastest rate of COS/H_2S release observed at pH 8.0 ($k_{rel.}$ = 2.79) and the slowest rate of COS/H_2S release observed at pH 6.0 ($k_{rel.}$ = 0.084). Consistent with previous reports of bovine serum albumin (BSA)-catalyzed ß-elimination reactions, the rate of PNA formation was significantly faster in the presence BSA (5 mg/mL) and suggests that COS/H_2S release may be faster in biological environments. This highlights the ability of γ-KetoTCM as a colorimetric donor to evaluate donor release in complex biological systems and observe differences between *in vitro* and *in vivo* donor behavior. The γ-KetoTCM donor additionally demonstrated H_2S delivery in HeLa cells as visualized with an H_2S-selective fluorescent probe (SF7-AM) and exhibited anti-inflammatory effects by decreasing lipopolysaccharide (LPS)-induced NO_2^- formation in Raw 264.7 cells.

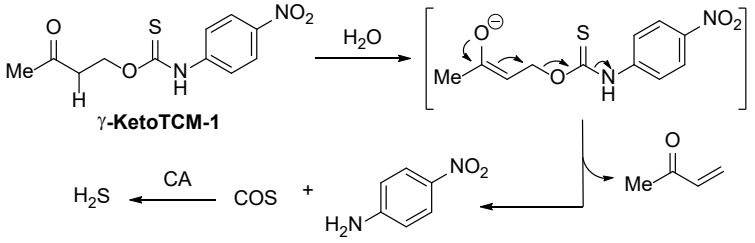

Figure 1.17 Mechanism of COS/H_2S release from γ-KetoTCM-1.

1.3.6 Fluorescent donors

One limitation of many H_2S donors is the inability to monitor release dynamics in complex environments without measuring, and subsequently consuming, the delivered H_2S. One approach to overcome these limitations is to develop H_2S donors that provide a fluorescent response upon H_2S delivery, and therefore allow for direct monitoring of H_2S release in complex environments. As an early example of this approach, we developed a turn-on fluorescent COS/H_2S based on a thiol-activated sulfenyl thiocarbonate motif.[56] The resulting donor (FLD-1) is not fluorescent until exposed to thiols, which subsequently cleave each sulfenyl thiocarbonate motifs to release COS

and fluorescein (Figure 1.18). Furthermore, this system does not produce electrophilic byproducts, which is a limitation in several self-immolative thiocarbamate donors. The COS/H_2S production from FLD-1 and concomitant fluorescent turn-on response was evaluated in the presence of excess cysteine (10 equiv) in PBS (pH 7.4, 10 mM) with CA (25 μg/mL). Cysteine activation of FLD-1 resulted in a 500-fold turn-on response that correlated directly to H_2S concentrations observed by the MBA. The donor platform was evaluated in HeLa cells where a fluorescence signal of the uncaged fluorescein was observed and H_2S production was further confirmed with the H_2S-selective fluorescent probe C7-Az. This donor also demonstrated significant biological activity where pre-treatment of RAW 264.7 cells with FLD-1 protected against lipopolysaccharide-induced inflammation.

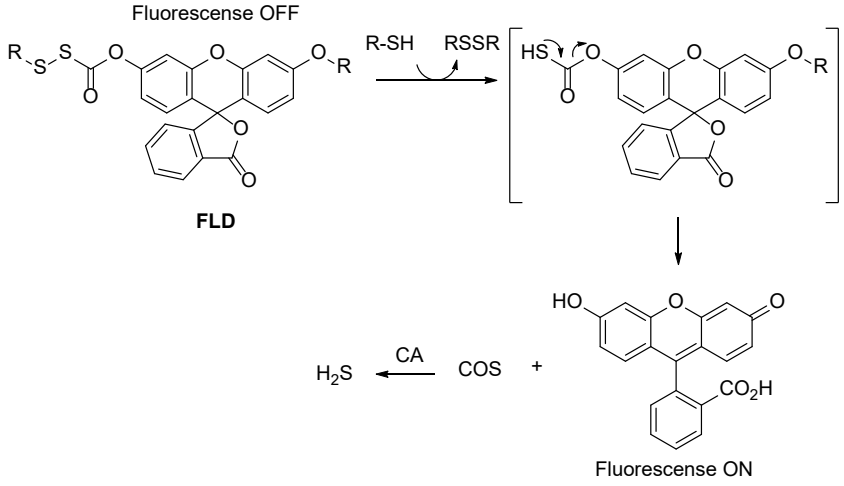

Figure 1.18 COS/H_2S release and simultaneous turn on fluorescence of FLD in the presence of thiols.

Expanding on fluorescent donor strategies, Ma and co-workers developed an ROS-activated COS/H_2S donor with a naphthalimide payload to produce a stimulus responsive donor with real-time tracking (NAB, Figure 1.19).[30] The ROS-activated fluorescent donor exhibits a weak fluorescence when excited at 405 nm. Upon exposure to ROS, self-immolative

decomposition of NAB releases COS with a 3-amino-*N*-butyl-1,8-naphthalimide that exhibits a strong fluorescence emission peak at 577 nm (λ_{ex} = 405 nm). To confirm H_2S delivery in cells and evaluate protective effects of NAB towards inflammation, Raw 264.7 cells were pre-treated with an ROS-inducing agent (PMA) followed by treatment with NAB (10 μM). The fluorescence intensity increased in cells treated with both PMA and NAB compared to the control. NAB additionally recovered decreased cell viability of PMA treated cells and showed ROS scavenging capacity observed via monitoring intracellular ROS change with an ROS-sensitive dye (CRDR).

He and co-workers expanded from this approach by tethering a mitochondrially-targeted triphenylphosphonium group to the naphthalimide fluorescent payload to localize COS/H_2S release to the mitochondria, which is a common site of ROS production.[29] The resulting donor (HSD-B, Figure1.19) is inherently fluorescent with a fluorescence maximum at 475 nm (λ_{ex} = 380 nm), but in the presence of H_2O_2, the emission peak of HSD-B decreases with concomitant growth of an emission peak at 540 nm corresponding to the uncaged naphthalimide (HSD-G). In H9c2 myocardial cells, the fluorescence of unreacted donor overlapped with the mitochondrially tracking dye, Mito-Tracker Red, demonstrating localization in the mitochondria. Treatment of H9c2 myocardial cells with Rosup (15/50 μg/mL) to increase endogenous ROS levels resulted in an increase in the uncaged HSD-G fluorescence intensity and a decrease in HSD-B intensity. An H_2S-selective probe (Cy-NO_2) further confirmed H_2S production only in the presence of Rosup. Notably, HSD-B demonstrated protective effects against myocardial ischemia reperfusion injury, elevating cell viability in a hypoxia/reoxygenation-induced injury model by nearly 40% with only 2 μM of the donor.

As an additional example of a fluorescent ROS-activated donor, Lukesh and co-workers appended a 7-hydroxy-4-methylcoumarin to a boronate *S*-alkyl thiocarbonate scaffold (ZL47,

Figure 1.19).[28] Upon exposure to H_2O_2, a greater than 70-fold increase in fluorescence intensity was observed, which correlated linearly with increasing H_2O_2 concentrations. Furthermore, this donor showed an increase in fluorescence intensity when imaged in live HeLa cells, suggesting its potential to image and alleviate oxidative stress in live cells. In addition to the ROS-activated fluorescent donor scaffolds, Gou and coworkers developed a photolabile *o*-nitrobenzyl thiocarbamate donor with a naphthalamide payload (Nap-Sul-ONB, Figure 1.19) to provide signal feedback upon photoinitiated uncaging of COS.[33] Although cytotoxic effects are typically observed with UV light exposure, a turn-on response of Nap-Sul-ONB was successfully imaged in live MCF-7 cancer cells upon irradiation with 365 nm light for 2 minutes. Moreover, Nap-Sul-ONB provided antioxidative and cytoprotective effects against endogenous ROS.

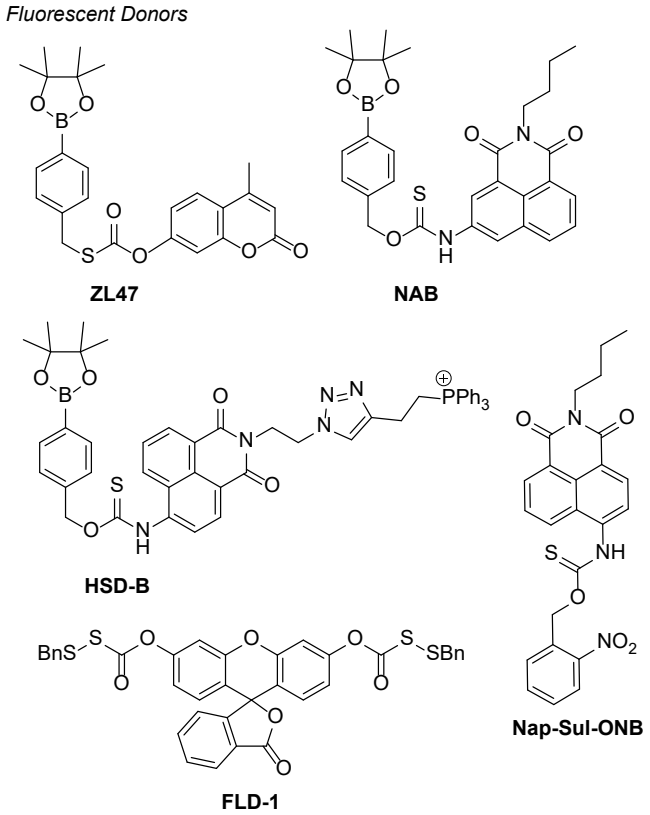

Figure 1.19 Fluorescent COS-based H_2S donors.

1.4 Conclusions and Outlook

Since the discovery that COS could act as an indirect source of H_2S, the palette of available H_2S donors has grown substantially. The donors highlighted in this chapter increase the efficiency of previous direct H_2S-releasing donors, provide synthetically accessible donors that can be integrated readily with drugs and fluorophores, and afford a great deal of tunability to develop donors that are activated in specific biological environments. One limitation with some of these scaffolds is the generation of electrophilic byproducts. Specifically, the electrophilic quinone/iminoquinone methide byproduct from the self-immolative thiocarbamate scaffold is likely scavenged by water but could result in unwanted side reactions in biological settings. Despite this drawback, several COS/H_2S donors lack electrophilic byproducts while still retaining a great deal of tunability and have recently been developed.

Another limitation of the COS/H_2S donor platform is the difficulty to delineate COS versus H_2S effects. The abundance of CA in combination with its rapid hydrolysis activity suggests that most released COS is converted to H_2S, but in certain examples where the rate of COS release is competitive with the rate of CA hydrolysis, this may not be the case. The direct study of COS cellular effects is quite challenging due to the widespread expression of CA, its roles in regulating pH, and its various isoforms. CA knock-out and inhibition studies alter cellular CO_2/HCO_3^- equilibria and buffering capacity, which further complicates attribution of observed outcomes with COS effects directly. Furthermore, the CA isoforms expressed commonly in mammalian cells have different sensitivities toward common CA inhibitors, which further complicates broad CA inhibition investigations. Lastly, there are few biological regions without CA because of its critical role in regulating pH.

To complement the available tools for COS/H_2S delivery, additional methods for COS measurement in complex environments are needed. Such systems could allow for determination of whether COS buildup was occurring from different classes of COS/H_2S donors. As an early effort toward developing chemical tools for COS detection, we recently demonstrated that a benzobisimidazolium salt (TBBI) could function as a responsive probe for COS that provided different responses for COS, CO_2, and CS_2, albeit still requiring organic solution.[57]

In summary, the strategy of indirect delivery of H_2S via COS has expanded the library of chemical tools to probe the chemical biology of H_2S in various biological settings. Ongoing work to provide tools that localize H_2S delivery to specific biological targets can help with harnessing the therapeutic potential of H_2S. My efforts towards improving the localization of H_2S delivery using COS donors are outlined in Chapters 2, 3, and 6.

CHAPTER II

DEVELOPMENT OF ACID-MEDIATED H_2S/COS DONORS THAT RESPOND TO A SPECIFIC PH WINDOW

This chapter includes previously published and co-authored material from Gilbert, A.K.; Zhao, Y.; Otteson, C.E.; Pluth, M.D. Development of Acid-Mediated H_2S/COS Donors That Respond to a Specific pH Window. *J. Org. Chem.* **2019**, *84* (22), 14469-14475. This manuscript was written by Annie K. Gilbert with editorial assistance by Professor Michael D. Pluth. The project in this chapter was conceived by Yu Zhao, and the experimental work was performed by Annie K. Gilbert and Claire E. Otteson.

2.1 Introduction

Hydrogen sulfide (H_2S) is an important biological signaling molecule and the most recent addition to the gasotransmitter family alongside nitric oxide and carbon monoxide.[1] Endogenous H_2S production is primarily attributed to four main enzymes including cystathionine β-synthase (CBS), cystathionine γ-lyase (CSE), 3-mercaptopyruvate sulfur transferase, and cysteine aminotransferase through cysteine and homocysteine catabolism. H_2S can also be generated through nonenzymatic pathways such as the thiol-mediated release of H_2S from allium- and garlic-derived polysulfides.[58] Once generated, H_2S is involved in different physiological processes, including K_{ATP} channel activation[59] as well as antioxidant and antiapoptotic signaling.[60] In efforts to modulate H_2S levels in different systems, most studies have used inorganic sulfide salts, such as sodium sulfide (Na_2S) and sodium hydrosulfide (NaSH), as exogenous H_2S sources. Although

these sulfide sources increase endogenous H_2S levels, the large and immediate dose can result in unwanted toxicity and sulfide oxidation.[61] To better understand and leverage H_2S levels in various biological systems, a variety of chemical tools have been developed in the last decade and include CSE and CBS inhibitors, H_2S donors, and activity-based H_2S probes for H_2S detection.[62-64]

Of the wide array of available H_2S donors, one common strategy to engineer H_2S release is to leverage water- or acid-mediated hydrolysis. For example, GYY4137 is one of the most widely used synthetic H_2S donors and releases H_2S slowly upon hydrolysis in the water at physiological pH (Figure 2.1a).[65] Similarly, deprotection of certain thioacetals[66-67] generates an unstable *gem*-dithiol intermediate that is hydrolyzed through an acid-mediated mechanism to release H_2S. In more recent examples, JK donors, which are based on the phosphorothioate core of GYY4137, were developed and designed to undergo an intramolecular cyclization upon protonation of the P–S moiety.[53] Highlighting potential applications of pH-activated donors, the JK family of donors showed cytoprotective effects in cell models of oxidative damage and cardioprotective effects in an in vivo mouse model of myocardial ischemia-reperfusion injury. More broadly, mildly acidic pH environments are found during ischemia injury, within the extracellular environment of cancerous cells, and in certain subcellular compartments, such as the lysosome. These acidic environments when taken in combination with the prior work showing the beneficial effects of H_2S in myocardial ischemia-reperfusion injury[53] and the ability to induce cell cycle arrest to suppress tumor growth[68] suggest the potential application for acid-activated H_2S donors. Aligned with these potential opportunities, a key need remains developing chemistry that enables access to donors that can be activated in specific pH ranges rather than just at increasing rates at more acidic pH. Such a strategy could be useful in developing design strategies for oral administration of hydrolysis-based H_2S donor motifs.

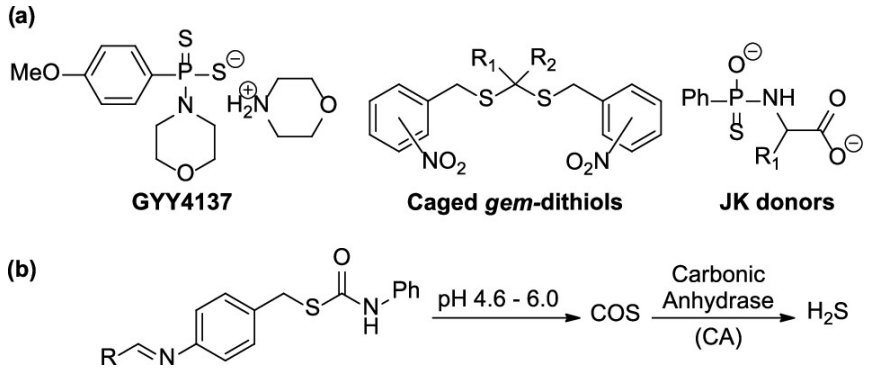

Figure 2.1 (a) Representative examples of current acid labile H_2S donors. (b) Design of pH-dependent carbonyl sulfide (COS)/H_2S release from caged thiocarbamate scaffolds.

To address this challenge, we viewed that triggerable caged thiocarbamates could be modified to develop donor motifs activated within a specific pH range. Caged thiocarbamates have recently emerged as a highly tunable class of donors that undergo a triggered, self-immolative elimination to release carbonyl sulfide (COS), which is rapidly hydrolyzed to H_2S by the ubiquitous enzyme carbonic anhydrase (CA).[5, 23, 36] Examples of triggers employed within this scaffold include reactive oxygen species,[25-27] esterases,[49-51] light,[32, 34-35] and cysteine.[38] We envisioned that using a pH-sensitive group, such as an imine, as the trigger could be used to develop acid-triggered COS/H_2S donors (Figure 2.1b). Here, we demonstrate that the use of an imine trigger, when coupled to the mechanism of 1,6-elimination required in the self-immolative thiocarbamates, provides donors that respond within a specific pH window. This new class of donors improves on the pH activation specificity of current acid-labile donors by providing H_2S delivery within a specific pH range. We expect this pH activation specificity will be useful in different applications requiring compound stability in strongly acidic or basic environments prior to H_2S release.

2.2 Results and Discussion

2.2.1 Donor Design

To develop donor motifs that are activated within a specific pH range, we chose to use an imine as the acid-sensitive trigger because imines are readily hydrolyzed under acidic conditions and have been used previously to initiate the 1,6-benzyl elimination of carbamate-containing prodrugs.[69] In our designed system, imine cleavage would generate a *p*-aminobenzylcarbamothioate intermediate, which would undergo a subsequent 1,6-elimination to release COS (Figure 2.2). Although imine hydrolysis is acid-mediated, if the solution is too acidic, then the resultant aniline intermediate will be protonated, which will inhibit the 1,6-elimination and should decrease the rate of COS release. Similarly, the imine should be stable under basic conditions and not release COS. Combining these parameters, we expected that the efficiency of the imine-based donor would peak at pH values between the pK_a of the iminium (pK_a ~ 5–7) and anilinium ion (pK_a ~ 4.6). In contrast to other available acid- or hydrolysis-based donors, this would result in a pH window for activation rather than a direct dependence of the release rate with pH.

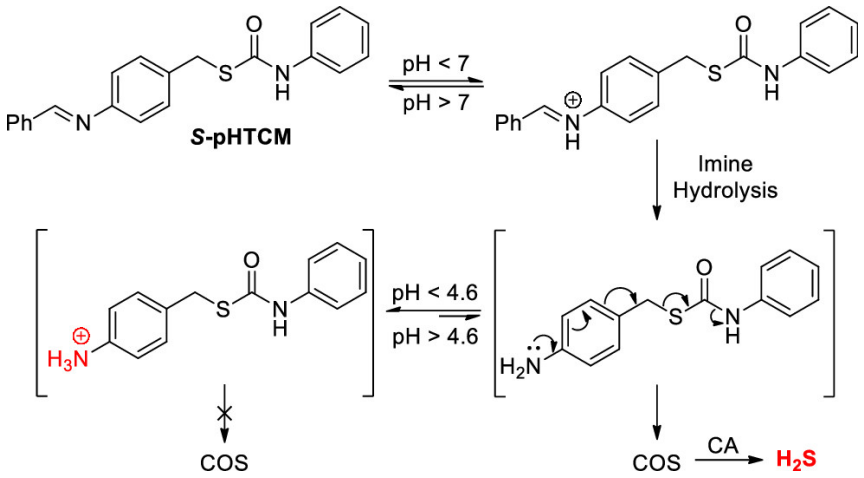

Figure 2.2 Proposed pH-dependent COS/H_2S-Release pathway: basic conditions decrease the rate of imine hydrolysis; strongly acidic conditions protonate the aniline intermediate and prevent COS release.

2.2.2 Synthesis

To test our hypothesis that the acid-triggered thiocarbamate donors undergo a pH-dependent release, we prepared a pH-sensitive imine-containing thiocarbamate donor. Treatment of 4-aminobenzyl alcohol with benzaldehyde in the presence of acetic acid formed 4-(benzylideneamino)benzyl alcohol, which was coupled with phenyl isothiocyanate in the presence of sodium hydride to obtain the *O*-alkyl thiocarbamate isomer (Figure 2.3a). Although analogous *O*-alkyl thiocarbamate donors have been prepared and are stable under ambient conditions, we found that the *O*-alkyl thiocarbamate with the imine trigger isomerized to the *S*-alkyl pH-sensitive thiocarbamate (**S-pHTCM**) isomer both in the solution and also in the solid state (Appendix A, Figure A.1). Thione–thiol isomerization is well known to occur in thiocarbamates via the Newman–Kwart rearrangement[70-71] but typically requires high temperatures or catalysts.[72-73] Similarly, benzylic Newman–Kwart rearrangements have recently been reported to occur at elevated temperatures.[74] We hypothesize that the electron-donating imine

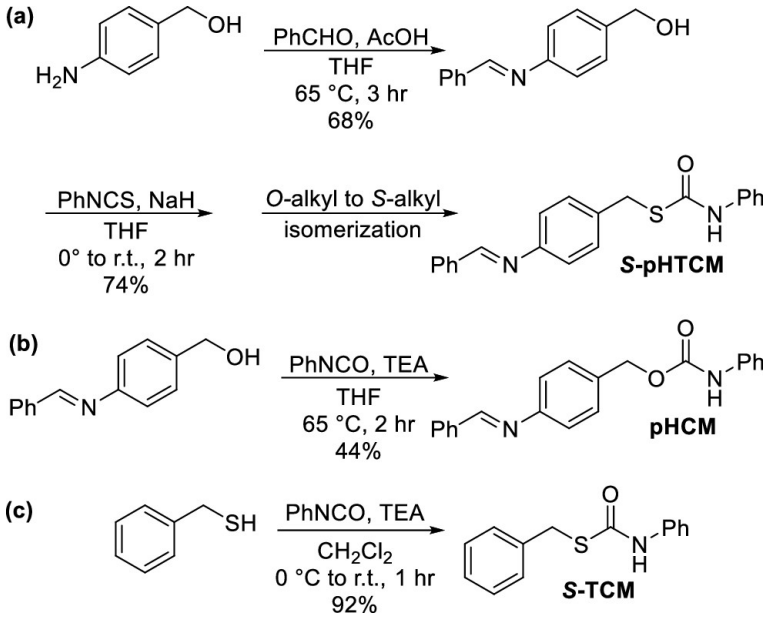

Figure 2.3 (a) Synthetic scheme for acid-triggered thiocarbamate COS/H_2S Donor (S-pHTCM), (b) carbamate control compound (pHCM), and (c) triggerless control compound (S-TCM).

substituent aids in the stabilization of the benzylic carbocation intermediate formed in the thiocarbamate rearrangement and, thus, may facilitate this isomerization under more mild conditions.

In addition to **S-pHTCM**, the corresponding pH-sensitive carbamate (**pHCM**) and triggerless *S*-alkyl thiocarbamate (**S-TCM**) were prepared as control compounds to confirm that the COS/H_2S release is triggered by imine hydrolysis of the thiocarbamate. In contrast to the model thiocarbamate, **pHCM** should undergo the same imine hydrolysis to release CO_2 instead of COS while generating the same byproducts as **S-pHTCM**. In the absence of the imine trigger, **S-TCM** is not expected to decompose and release COS.

2.2.3 Measurement of H_2S-Release

To evaluate COS/H_2S release from this series of compounds, we used the colorimetric methylene blue (MB) assay.(34) We measured COS/H_2S release from **S-pHTCM** (50 μM) across a range of pH values (4.0–8.0) in the presence of CA (25 μg/mL) at 37 °C. We confirmed CA activity at pH 5.5 using a *p*-nitrophenyl acetate assay (see Figure A.2). To span this range of pH, we used sodium citrate-buffered and phosphate-buffered saline (PBS) solutions. We observed no buffer dependence when evaluating H_2S release from **S-pHTCM** in citrate and PBS buffer at pH 6.0, as shown in Figure A.3. Consistent with our expectations, we observed more efficient COS/H_2S release in weakly acidic conditions from pH 4.6 to 6.5 than from pH values outside of this range (Figure 2.4). The rates of H_2S release have a similar pH dependence, but because the rate-limiting step of the reaction may change as a function of pH and not all of the H_2S release curves peaked at the same levels, we chose to measure H_2S concentration at 5 h for these investigations (Figure A.4). Further supporting our hypothesis, we found that the inflection points

of the pH response curve (4.3 and 7.3) matched the expected pK_a values of the iminium and the anilinium ions (Figure A.5). Taken together, these data support the mechanism of COS/H_2S release outlined in Figure 2.2.

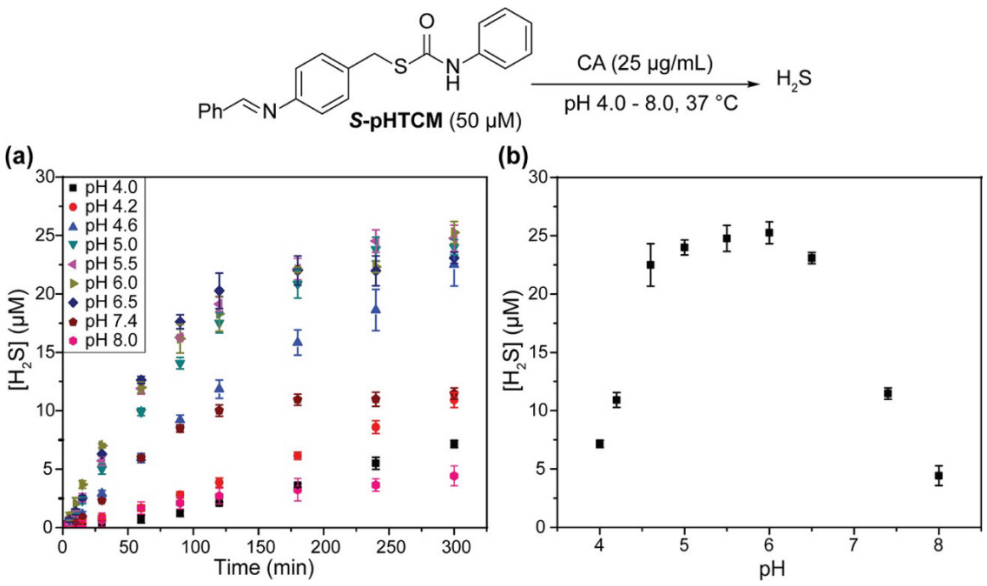

Figure 2.4 (a) COS/H_2S release from S-pHTCM (50 μM) at pH 4.0–8.0 containing CA (25 μg/mL). (b) pH curve of H_2S concentration at 5 h. Experiments were performed in quadruplicate with results expressed as mean ± standard deviation (SD) (n = 4).

To confirm that H_2S release from **S-pHTCM** requires both imine hydrolysis and the thiocarbamate moiety, we measured the H_2S release from the **pHCM** and **S-TCM** control compounds at pH 5.5. Under identical conditions, as those for **S-pHTCM**, we failed to observe H_2S generation from either **pHCM** or **S-TCM** (Figure 2.5). In the absence of CA, **S-pHTCM** showed a significantly reduced rate of H_2S release (Figure A.6). To further support the proposed release mechanism, we monitored the reaction by high-performance liquid chromatography (HPLC) analysis (Figures A.7). Consistent with the proposed 1,6-elimination mechanism, we observed benzaldehyde, aniline, and 4-aminobenzyl alcohol during the course of the reaction (Figure 2.6).

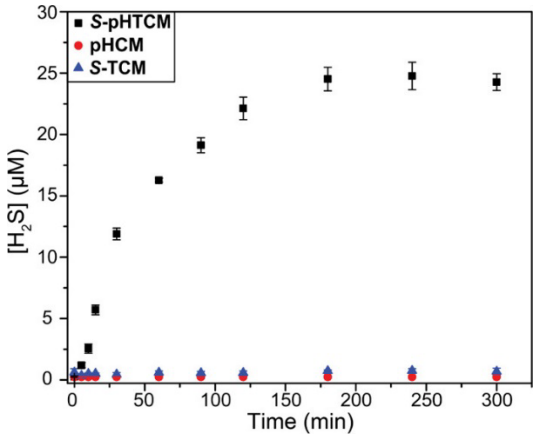

Figure 2.5 H_2S release from **S-pHTCM**, triggerless (**S-TCM**), and carbamate (**pHCM**) control compounds (50 μM) in citrate buffer (10 mM, pH 5.5) containing CA (25 μg/mL) at 37 °C. Experiments were performed in quadruplicate with results expressed as mean ± SD (n = 4).

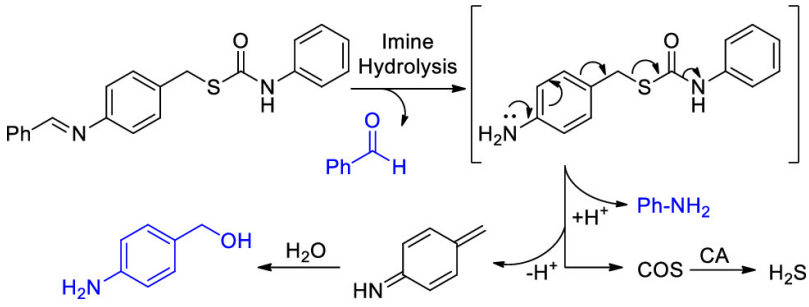

Figure 2.6. Proposed mechanism of acid-triggered COS/H_2S release from caged-thiocarbamate donors with byproducts of self-immolation.

We next investigated the tolerance of the acid-mediated cleavage and self-immolation to the presence of different biological nucleophiles by measuring H_2S release from **S-pHTCM** at pH 5.5 in the presence of different analytes. We did not observe a significant change in the donor efficiency in the presence of 250 μM of glutathione (GSH), Cys, Lys, Ser, Hcy, Gly, or GSSG, which demonstrates the compatibility of our approach with common nucleophiles and reactive species (Figure 2.7). In the presence of higher levels of GSH (5 mM), however, we did observe modest inhibition. We do not view this as a significant problem, however, because about 90% of GSH is localized in the cytosol, about 10% is localized in the mitochondria and the endoplasmic

reticulum, leaving negligible GSH levels in acidic cellular compartments.[75] To further investigate whether this observed inhibition was observed at physiological pH values, we repeated the measurement at pH 7.4 in the presence of 5 mM GSH and did not observe a significant difference in efficiency in the absence or presence of GSH (Figure A.8). These data suggest that high concentrations of GSH should not interfere with the application of this triggering motif in normal cellular environments.

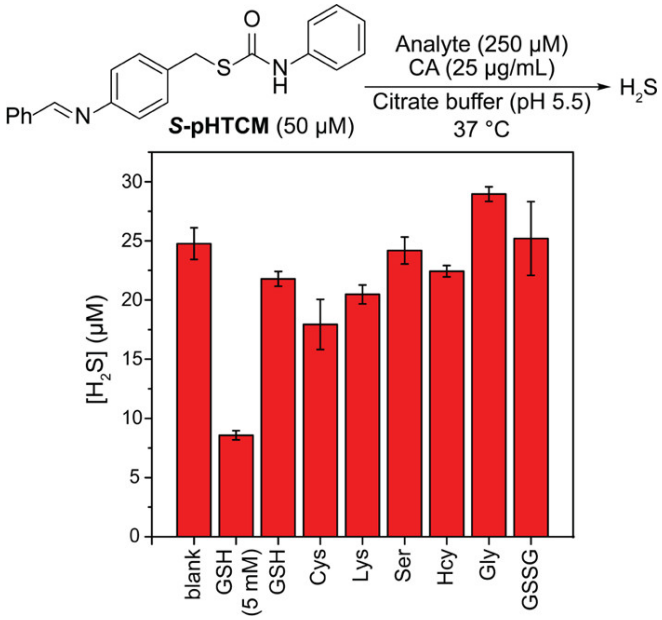

Figure 2.7 COS/H_2S release at 5 h from **S-pHTCM** (50 μM) in citrate (pH 5.5) in the presence of CA (25 μg/mL) and various analytes (250 μM unless otherwise noted): no analyte, GSH (5 mM), GSH, Cys, Lys, Ser, Hcy, Gly, and GSSG. Experiments were performed in triplicate with results expressed as mean ± SD (n = 3).

Although our primary goal was to develop chemistry that enabled donor response within a specific pH range, we also wanted to demonstrate the feasibility of appending the developed motif to commonly used subcellular targeting groups that direct compounds to acidic subcellular compartments. To demonstrate this compatibility, we prepared a thiocarbamate donor (**Lyso-pHTCM**), as well as the associated control compounds (**Lyso-pHCM** and **Lyso-TCM**), with an aminoethyl–morpholine group, which has been used previously to direct compounds to the

lysosome. We measured the H_2S release efficiency from the compounds and found that **Lyso-pHTCM** showed a 33% H_2S release efficiency over 5 h and that the control compounds did not release H_2S (Figure 2.8). Although beyond the scope of the present investigations, we anticipate that these compounds may be of use in investigating the role of lysosomal H_2S delivery in various contexts.

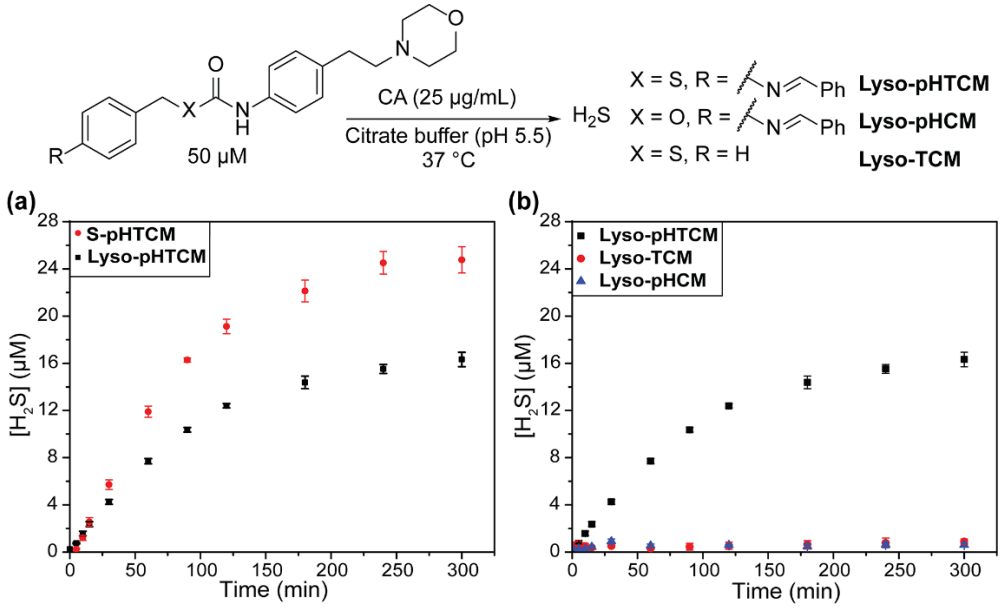

Figure 2.8 (a) H_2S release comparison of **Lyso-pHTCM** and **S-pHTCM**. (b) H_2S release from **Lyso-pHTCM** and related control compounds. All experiments performed in quadruplicate in citrate buffer (pH 5.5, 10 mM) containing CA (25 μg/mL) at 37 °C. Results expressed as a mean ± SD (n = 4).

2.3 Conclusions

Based on the broad utility of hydrolysis- and acid-sensitive H_2S donors, we developed a new strategy that enables for the efficiency of H_2S release to be tuned to specific pH ranges. This response profile is in contrast to currently available acid-mediated H_2S donor motifs. By including an acid-sensitive imine group on a caged thiocarbamate, we demonstrated that the acid-mediated imine hydrolysis in combination with inhibitory protonation of aniline product after hydrolysis

resulted in an operative pH response range of 4.6–6.5. The imine-based donor also shows good tolerance to a wide array of biological nucleophiles at physiologically relevant concentrations. We also demonstrated the modularity of our approach by attaching a common lysosomal targeting group to the donor motif and revealed that H_2S release is still efficient in this targeted construct. Overall, we anticipate that this approach will provide new opportunities to tune donor motifs to respond to specific pH windows associated with subcellular organelles and that the developed chemistry will enable specific pH windows to be targeted to other acidic microenvironments.

2.4 Experimental Details

Materials and Methods.

Reagents were purchased from Sigma-Aldrich, Tokyo Chemical Industry (TCI), Fisher Scientific, and VWR. Column chromatography was performed with 230–400 mesh silica gel. Deuterated solvents were purchased from Cambridge Isotope Laboratories. ^{1}H and $^{13}C\{^{1}H\}$ NMR spectra were recorded on a Bruker 500 MHz or Varian Inova 500 MHz instrument. Chemical shifts are reported relative to residual protic solvent resonances. Air-free experimental procedures were performed in an Innovative Atmospheres N_2-filled glovebox or using Schlenk technique. UV–vis spectra were acquired on an Agilent Cary 60 UV–vis spectrometer. Mass spectrometric data was acquired by the University of Illinois, Urbana Champaign MS Facility or on a Xevo Waters ESI LC/MS instrument.

General Procedure for H_2S Detection

In a N_2-filled glovebox, scintillation vials with septa caps were filled with 20 mL of degassed buffer (citrate/PBS, pH 4.0–8.0, 10 mM). All stock solutions were prepared in the glovebox with

degassed solvents. The 10 mM donor stock solution was prepared in dimethyl sulfoxide (DMSO), and a 10 mg/mL carbonic anhydrase (CA) stock solution was prepared in Millipore H_2O. Each scintillation was charged with 50 μL of the CA stock solution to achieve a final concentration of 25 μg/mL. The solutions were thermally equilibrated to 37 °C while stirring for 20 min. During this time, methylene blue cocktail solutions (0.3 mL) were prepared in 1.5 mL disposable cuvettes. The methylene blue cocktail solutions contained 60 μL of 1% (w/v) $Zn(OAc)_2$, 120 μL of 30 mM $FeCl_3$ in 1.2 M HCl, and 120 μL of 20 mM *N*,*N*-dimethyl-*p*-phenylene diamine in 7.2 M HCl. To each solution, 100 μL of the 10 mM donor stock solution was added to reach a final concentration of 50 μM. Immediately after donor addition at $t = 0$ min, a 0.3 mL reaction aliquot was removed and added to a methylene blue cocktail solution. This process was repeated at 5, 10, 15, 30, 60, 90, 120, 180, 240, and 300 min time points. The reaction aliquots added to the methylene blue cocktail solutions were mixed thoroughly and incubated for 1 h at room temperature in the dark, after which the absorbance values at 670 nm were measured.

MB Assay Calibration Curve

The methylene blue cocktail solution (0.5 mL) and PBS pH 7.4 buffer (0.5 mL) were added to 1.5 mL disposable cuvettes. A NaSH stock solution (100 mM) was prepared in degassed Millipore H_2O under an inert atmosphere and diluted to 1 mM. Immediately after dilution, aliquots of the NaSH stock solution were added to the methylene blue solutions to reach final concentrations of 10, 20, 30, 40, and 50 μM. The solutions were mixed and incubated at room temperature for 1 h, after which the absorbance values at 670 nm were measured.

Syntheses

4-(Benzylideneamino)benzyl Alcohol

4-Aminobenzyl alcohol (0.50 g, 4.1 mmol) and benzaldehyde (0.82 mL, 8.2 mmol) were added to anhydrous tetrahydrofuran (THF) (15 mL) in the presence of $MgSO_4$ (∼1 g). Glacial AcOH was then added dropwise (∼4 drops), and the resultant reaction mixture was refluxed for 2 h. The reaction was then quenched with a solution of saturated $NaHCO_3$ (30 mL) and extracted with EtOAc (3 × 15 mL). The organic layers were combined, washed with deionized H_2O (30 mL) and brine (30 mL), and dried over $MgSO_4$. The drying agent was removed by filtration, and the organic solvent was removed under reduced pressure. The product was isolated and purified by column chromatography using EtOAc/hexanes (10–100% gradient; 5% NEt_3) to yield a yellow solid (343 mg, 68% yield). ^{1}H NMR (500 MHz, DMSO-d_6) δ: 8.63 (s, 1 H), 8.02–7.87 (m, 2 H), 7.59–7.48 (m, 3 H), 7.36 (d, J = 8.2 Hz, 2 H), 7.24 (d, J = 8.2 Hz, 2 H), 5.18 (t, J = 5.7 Hz, 1 H), 4.51 (d, J = 5.7 Hz, 2 H).^{13}C{^{1}H} NMR (126 MHz, DMSO-d_6) δ: 160.1, 149.9, 140.5, 136.1, 131.4, 128.8, 128.6, 127.3, 120.8, 62.6. HRMS (ASAP TOF) (m/z): $[M + H]^+$ cacld for $C_{14}H_{14}NO$, 212.1075; found, 212.1090.

4-(Benzylideneamino)benzyl Phenylcarbamate (pHCM)

4-(Benzylideneamino)benzyl alcohol (61 mg, 0.28 mmol) and phenyl isocyanate (31 μL, 0.28 mmol) were added to anhydrous THF (15 mL). The reaction mixture was cooled to 0 °C before the addition of NEt_3 (0.50 mL, 3.6 mmol), after which the reaction mixture was refluxed for 2 h. The reaction was quenched with brine (30 mL) and extracted with EtOAc (3 × 15 mL). The organic layers were combined, washed with deionized H_2O (30 mL) and brine (30 mL), and dried over $MgSO_4$. The drying agent was removed by filtration, and the solvent was removed under reduced

pressure. The crude mixture was purified by column chromatography with EtOAc/hexane (4–34% gradient; 5% NEt_3) to afford the product as a white solid (41 mg, 44%). ^{1}H NMR (500 MHz, DMSO-d_6) δ: 9.76 (s, 1 H), 8.63 (s, 1 H), 7.94 (dd, J = 7.3, 2.2 Hz, 2 H), 7.63–7.37 (m, 7 H), 7.37–7.20 (m, 4 H), 6.99 (t, J = 7.4 Hz, 1 H), 5.17 (s, 2 H). ^{13}C{^{1}H} NMR (126 MHz, DMSO-d_6) δ: 161.0, 153.4, 151.3, 139.1, 136.0, 134.3, 131.6, 129.3, 128.8, 128.8, 128.7, 122.4, 121.1, 118.2, 65.5. HRMS (ES + TOF) (*m*/*z*): $[M + H]^+$ cacld for $C_{21}H_{19}N_2O_2$, 331.1447; found, 331.1435.

S-Benzyl Phenylcarbamothioate (S-TCM)

Benzyl mercaptan (61 µL, 0.52 mmol) and phenyl isocyanate (58 µL, 0.51 mmol) were combined in anhydrous THF (15 mL). The reaction mixture was cooled to 0 °C before adding NEt_3 (0.1 mL), after which the reaction was stirred at room temperature for 1 h. The reaction was then quenched with brine (30 mL) and extracted with EtOAc (3 × 15 mL). The organic layers were combined and dried over $MgSO_4$. The organic layer was filtered, and the solvent was removed under reduced pressure. The product was isolated by column chromatography using EtOAc/hexane (4–34% gradient; 5% NEt_3) to afford the product as a white solid (120 mg, 92% yield). ^{1}H NMR (500 MHz, DMSO-d_6) δ: 10.33 (s, 1 H), 7.55–7.46 (m, 2 H), 7.39–7.20 (m, 7 H), 7.05 (t, J = 7.4 Hz, 1 H), 4.15 (s, 2 H). ^{13}C{^{1}H} NMR (126 MHz, DMSO-d_6) δ: 164.3, 138.9, 138.7, 128.9, 128.7, 128.4, 127.0, 123.4, 119.0, 32.9. HRMS (ASAP TOF) (*m*/*z*): $[M + H]^+$ cacld for $C_{14}H_{14}NOS$, 244.0796; found, 244.0791.

4-(2-Aminoethyl)morpholine Phenyl Isothiocyanate

4-(2-Morpholinoethyl) aniline (61 mg, 0.30 mmol) was added to anhydrous CH_2Cl_2 (20 mL). The reaction mixture was cooled to 0 °C, then a solution of 1,1′-thiocarbonyldiimidazole (53 mg, 0.30

mmol) in anhydrous CH_2Cl_2 (5 mL) was added dropwise. The reaction was stirred at room temperature for 2 h, after which the solvent was removed under reduced pressure. The crude mixture was purified by column chromatography with MeOH/CH_2Cl_2 (2–20% gradient) and isolated as a yellow oil (180 mg, 86% yield). ^{1}H NMR (500 MHz, $CDCl_3$) δ 7.22–7.11 (m, 4 H), 3.73 (t, *J* = 4.6 Hz, 4 H), 2.79 (dd, *J* = 9.7, 6.3 Hz, 2 H), 2.57 (dd, *J* = 9.6, 6.4 Hz, 2 H), 2.50 (t, *J* = 4.6 Hz, 4 H). ^{13}C{^{1}H} NMR (126 MHz, $CDCl_3$) δ 140.0, 135.0, 130.0, 129.3, 125.9, 67.1, 60.5, 53.8, 33.1. HRMS (ASAP TOF) (*m*/*z*): $[M + H]^+$ cacld for $C_{13}H_{17}N_2OS$, 249.1062; found, 249.1078.

S-4-(Benzylideneamino)benzyl(4-(2-morpholinoethyl)phenyl) Carbamothioate (Lyso-pHTCM)

4-(Benzylideneamino)benzyl alcohol (100 mg, 0.473 mmol) and morpholine isothiocyanate (118 mg, 0.473 mmol) were added to anhydrous THF (20 mL). The reaction mixture was cooled to 0 °C before the addition of NaH (18 mg, 0.75 mmol) and then stirred for 10 h at room temperature. The solvent was removed under reduced pressure. The crude mixture was purified by column chromatography with EtOAc/hexane (8–66% gradient; 5% NEt_3) to afford the product as a white solid that isomerizes from the *O*-alkyl to *S*-alkyl isomer over 4 days (77 mg, 36%).^{1}H NMR (500 MHz, DMSO-d_6) δ: 10.26 (s, 1 H), 8.61 (s, 1 H), 7.95–7.89 (m, 2 H), 7.56–7.48 (m, 3 H), 7.43–7.37 (m, 4 H), 7.22 (d, 2 H), 7.15 (d, 2 H), 4.17 (s, 2 H), 3.56 (d, *J* = 5.0 Hz, 4 H), 2.67 (t, *J* = 7.7 Hz, 2 H), 2.46 (t, 1 H), 2.40 (s, 4 H). ^{13}C{^{1}H} NMR (126 MHz, DMSO-d_6) δ: 164.6, 161.0, 150.7, 137.3, 137.1, 136.5, 136.0, 132.0, 130.1, 129.5, 129.3, 129.1, 121.6, 119.6, 66.7, 60.5, 53.7, 33.1, 32.3. HRMS (ES + TOF) (*m*/*z*): $[M + H]^+$ cacld for $C_{27}H_{30}N_3O_2S$, 460.2059; found, 460.2076.

S-4-(Benzylideneamino)benzyl(4-(2-morpholinoethyl)phenyl) Carbamate (Lyso-pHCM)

4-(2-Morpholinoethyl) aniline (61 mg, 0.30 mmol) and triphosgene (41 mg, 0.36 mmol) were combined in anhydrous CH_2Cl_2 (15 mL). The reaction was cooled to 0 °C and NEt_3 (0.2 mL, 5 equiv) was added. After stirring at 0 °C for 2 h, the reaction mixture was purged with N_2 before adding a solution of phenyl imine benzyl alcohol (74 mg, 0.35 mmol) in anhydrous CH_2Cl_2 (5 mL) dropwise. The reaction was stirred at room temperature for 2 h, after which the solvent was removed under reduced pressure. The crude mixture was purified by column chromatography with EtOAc/hexane (12–100% gradient; 5% NEt_3) to yield the product as a white solid (70.1 mg, 54% yield). ^{1}H NMR (500 MHz, DMSO-d_6) δ: 9.66 (s, 1 H), 8.63 (s, 1 H), 7.98–7.90 (m, 2 H), 7.57–7.50 (m, 3 H), 7.50–7.44 (m, 2 H), 7.37 (d, J = 8.1 Hz, 2 H), 7.33–7.26 (m, 2 H), 7.17–7.09 (m, 2 H), 5.15 (s, 2 H), 3.56 (t, J = 4.7 Hz, 4 H), 2.66 (dd, J = 9.3, 6.4 Hz, 2 H), 2.46 (dd, J = 9.2, 6.5 Hz, 2 H), 2.40 (s, 4 H). ^{13}C{^{1}H} NMR (126 MHz, DMSO-d_6) δ: 160.9, 153.4, 151.2, 136.9, 135.9, 134.4, 134.3, 131.6, 129.2, 128.9, 128.8, 128.7, 121.0, 118.2, 66.2, 65.4, 60.2, 53.3, 31.8. HRMS (ASAP_TOF) (*m*/*z*): $[M + H]^+$ cacld for $C_{27}H_{30}N_3O_3$, 444.2287; found, 444.2282.

S-Benzyl(4-(2-morpholinoethyl)phenyl) Carbamothioate (Lyso-TCM)

4-(2-Morpholinoethyl) aniline (61 mg, 0.29 mmol) and triphosgene (41 mg, 0.35 mmol) were combined in anhydrous CH_2Cl_2 (15 mL). The reaction mixture was cooled to 0 °C and NEt_3 (0.20 mL, 1.5 mmol) was added. The reaction mixture was warmed from 0 °C to room temperature and stirred overnight, after which it was purged with N_2 before adding benzyl mercaptan (41 μL, 0.35 mmol) dropwise. The reaction mixture was stirred at room temperature for 10 h. The solvent was removed under reduced pressure, and the product was purified by column chromatography with MeOH/CH_2Cl_2 2–20% gradient to afford the product as a yellow solid (41 mg, 39% yield). ^{1}H

NMR (500 MHz, DMSO-d_6) δ 10.25 (s, 1 H), 7.43–7.28 (m, 6 H), 7.27–7.21 (m, 1 H), 7.18–7.12 (m, 2 H), 4.14 (s, 2 H), 3.56 (t, J = 4.7 Hz, 4 H), 2.67 (t, 2 H), 2.47 (t, J = 8.0 Hz, 1 H), 2.40 (s, 4 H). ^{13}C: NMR (126 MHz, DMSO-d_6) δ: 164.6, 139.3, 137.3, 129.5, 129.2, 128.9, 127.4, 119.5, 66.7, 60.5, 55.4, 53.7, 40.5, 33.4, 32.3. HRMS (ES+ TOF) (m/z): $[M + H]^+$ cacld for $C_{20}H_{25}N_2O_2S$, 357.1637; found, 357.1641.

CHAPTER III

SUBCELLULAR H_2S DELIVERY VIA SMALL MOLECULE DONORS

This chapter includes unpublished and co-authored material. The content included in this chapter was written by Annie K. Gilbert with editorial assistance by Professor Michael D. Pluth. The project in this chapter was conceived by Annie K. Gilbert with insight from Professor Michael D. Pluth. The experimental work was performed by Annie K Gilbert.

3.1 Introduction

Trillions of cells make up our body and provide vital functions in maintaining our health. Each cell is a complex system with specific roles carried out by various compartments within the cell called organelles. For example, the endoplasmic reticulum (ER) is essential for the assembly of proteins; the Golgi apparatus packages these proteins and transports them; the lysosome digests cellular waste; and the mitochondria provide energy to exert these functions. Malfunction of any of these organelles can result in disease. Mitochondrial dysfunction and resulting oxidative stress are linked to a variety of diseases such as Parkinson's disease,[76] type 2 diabetes,[77] and cardiovascular diseases.[78] Unfolded protein buildup results in ER stress, which can lead to neurological diseases like Alzheimer's disease and amyotrophic lateral sclerosis (ALS).[79] The Golgi apparatus is additionally involved in neurological diseases where Golgi fragmentation has been observed in neurons of patients with Alzheimer's disease, ALS, and Creutzfeldt-Jakob disease.[80] This relationship between organelle dysfunction and disease motivates the development

of therapeutics that can help resolve specific organelle stress and aid in the treatment of these diseases.

One such potential therapeutic includes hydrogen sulfide (H_2S), an endogenously produced gaseous signaling molecule with important roles in regulating organelle function and stress. H_2S regulates mitochondrial biogenesis and oxidative stress,[81] attenuates ER stress in a variety of disease states,[82] and protects against Golgi stress by regulating intracellular Ca^{2+} levels.[83] Several of these effects are initiated through persulfidation of cysteine residues on proteins, which are unlikely the direct activity of H_2S alone but rather from persulfides generated by H_2S from oxidized thiols that can subsequently undergo transpersulfidation.[84] Nevertheless, the proximity of H_2S production to result in specific persulfidation activity must be important as both H_2S and persulfides are highly reactive. Subcellular production of H_2S is moderated by three main enzymes including cystathionine λ-lyase (CSE) and cystathionine β-synthase (CBS), which are generally localized in the cytosol, and 3-mercaptopyruvate sulfur transferase (3-MST), which is localized in the mitochondria. There is evidence that CBS and CSE are not confined to the cytosol but rather localize in various organelles under certain conditions. For example, CBS has been shown to accumulate in the mitochondria in liver ischemia,[85] and both CBS and CSE can be transported to the nucleus upon modification by small ubiquitin-like modifier (SUMO) proteins.[86] Localization of these enzymes could be Nature's way of directing H_2S to the site of therapeutic need while reducing off-target effects. Developing chemical tools that can mimic this enzymatic localization of H_2S production could be one way to better understand subcellular roles of H_2S and investigate potential therapeutic effects of subcellular H_2S delivery.

Current strategies to investigate subcellular roles of H_2S include the use of chemical probes to visualize H_2S distribution,[87-93] regulation of CSE expression, and administration of exogenous

sources of H_2S. Inorganic sulfide salts are often used as exogenous sources of H_2S, but these salts produce a large bolus of H_2S upon dissolving in water. This uncontrolled release is a challenge for investigating subcellular H_2S effects as large amounts of these salts are required to observe any physiological effects and excess H_2S can lead to different biological outcomes due to off-target effects. To address these challenges of H_2S delivery, small molecule donors have been developed to control the rate of H_2S release and localization of H_2S delivery.[6] H_2S donors can be tuned to react with specific analytes or environments at the site of therapeutic interest to produce H_2S or contain targeting groups to help localize delivery. Few organelle-targeted H_2S donors have been developed, all of which target H_2S delivery to either the mitochondria or the lysosome (Figure 3.1a).[29, 54, 94-96] AP39, a mitochondria-targeted H_2S donor, exhibits significantly higher potency in promoting antioxidant and cytoprotective effects than non-targeted donors.[94] The high efficiency of AP39 has made it an attractive donor to investigate therapeutic effects of H_2S. For example, AP39 has demonstrated promising therapeutic effects in ischemia injury, with AP39 treatment resulting in protection against myocardial reperfusion injury, and neuroprotective activity in brain ischemia models.[97-98] Additionally, AP39 has demonstrated protective roles in Alzheimer's disease (AD) where AP39 attenuated special memory deficits and inhibited brain atrophy in a mice AD model.[99] All these conditions heavily involve mitochondrial function and reactive oxygen species production, which suggests the mitochondria-targeting feature of AP39 could be important in promoting these therapeutic effects. Despite evidence of other subcellular roles of H_2S, the expansion of targeted H_2S delivery to other organelles remains largely absent.

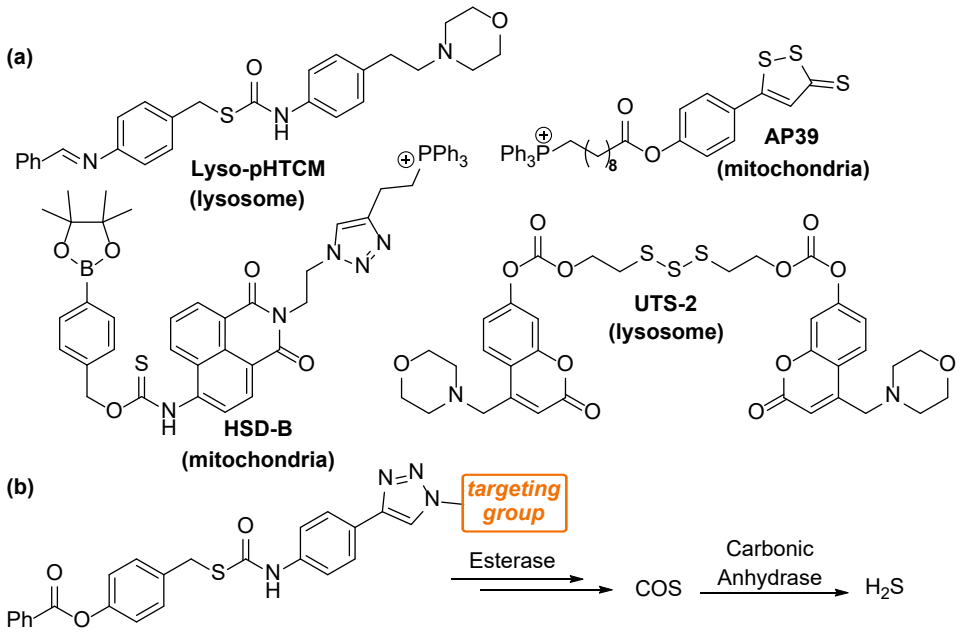

Figure 3.1 (a) Current library of organelle-targeted donors with targeted organelle indicated below. (b) Targeted delivery of carbonyl sulfide (COS)/H_2S via esterase-activated caged thiocarbamates.

To address this key unmet need, we developed a library of organelle targeted H_2S donors using a caged thiocarbamate scaffold. Caged thiocarbamates (TCMs) are highly tunable H_2S donors that undergo an activatable 1,6-elimination to release carbonyl sulfide (COS), which is rapidly hydrolyzed by the ubiquitous enzyme carbonic anhydrase (CA) to produce H_2S.[7] Within the last decade, several examples of TCMs have been developed including those activated by light,[32] cysteine,[38] mildly acidic environments,[54] reactive oxygen species,[25] and esterases.[49-50] Here, we appended known organelle-targeted groups onto the esterase-activated TCM scaffold to localize H_2S delivery within specific subcellular regions (Figure 3.1b), providing a set of chemical tools to investigate subcellular H_2S effects. Due to the reactivity of H_2S, we hypothesized that targeting H_2S delivery within the cell to the area of therapeutic need would significantly enhance the efficacy of small molecule H_2S donors in resolving organelle stress.

3.2 Results and Discussion.

3.2.1 Donor Design

To investigate the effects of subcellular H_2S delivery, we prepared a library of organelle-targeted caged thiocarbamate COS/H_2S donors. The caged thiocarbamate (TCM) scaffold is highly tunable and modular, which allows simple attachment of targeting groups. We selected an esterase-activated thiocarbamate due to the widespread distribution of esterase throughout the cell that enables activation of COS/H_2S in diverse cellular environments. Although early work on esterase-activated thiocarbamates demonstrated a high degree of cytotoxicity, possibly due to the direct impacts of COS release, follow-up work demonstrated this cytotoxicity could be decreased by increasing the ester steric bulk and as a result, decreasing the rate of esterase hydrolysis and COS/H_2S release.[50-51] Furthermore, this work confirmed the slower-releasing donors could be used for cell-based experiments. With this in mind, we selected the phenyl ester thiocarbamate scaffold because of its low cytotoxicity yet moderate release rate.

To localize H_2S delivery to the mitochondria, lysosome, endoplasmic reticulum (ER), and Golgi Apparatus, we appended known organelle targeting groups onto the thiocarbamate scaffold using click chemistry. Using click chemistry has the added benefit of generating a triazole linkage between the donor and targeting group, which is more resistant to cleavage than the commonly-used ester linkage in AP39. We used the well-established triphenylphosphonium and morpholine groups to target the mitochondria and lysosome, respectively. We used the *p*-toluenesulfonamide group, which binds potassium ATP channels on the membrane of the ER to target the ER.[91] Lastly, we used a phenylsulfonamide group to target the Golgi apparatus due to its affinity for cyclo-oxygenase-2, which is maximally present in the Golgi apparatus of cancerous cells.[90, 100] Both of

the sulfonamide-based targeting groups have been shown to localize small molecule probes to these corresponding organelles in previous reports.[90-91, 100]

3.2.2 Synthesis

To prepare the donors, we first synthesized 4-ethynl aryl isothiocyanate (**2**) via treatment of 4-ethynyl aniline with 1,1'-thiocarbonyldiimidazole. The thiocarbamate alkyne coupling partner (**TCM alkyne**) was prepared by coupling 4-(hydroxylmethyl)phenyl benzoate (**1**) and **2** in the presence of DBU (Figure 3.2). Azides of the organelle-targeted groups were prepared according to literature procedures.[101-105] The azide targeting groups were appended to the **TCM alkyne** using a copper catalyzed azide-alkyne cycloaddition reaction with copper sulfate and sodium ascorbate in the presence of tris((1-benzyl-4-triazolyl)methyl)amine (TBTA). The copper catalyzed click reaction was challenging to find suitable conditions due to sulfur incorporation that can lead to copper coordination. Additionally, each targeted donor had varying levels of polarity

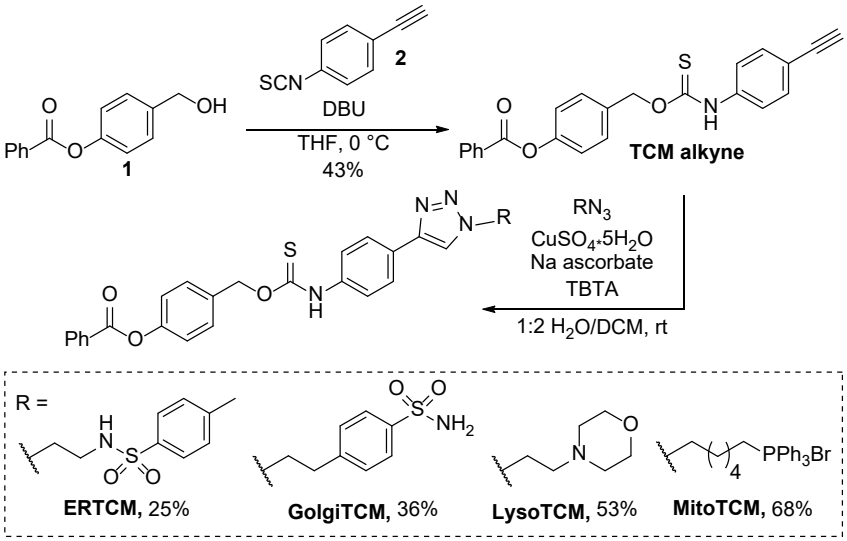

Figure 3.2 Synthesis of organelle-targeted COS/H_2S donor molecules.

that made purification from the TBTA ligand challenging. To address these challenges, several click reaction conditions were screened, and adjustments were made to donor reactions where TBTA was difficult to separate from the product.

3.2.3 Measurement of H_2S-Release

After preparing the library of organelle-targeted H_2S donors, we next evaluated COS/H_2S release in the presence of porcine liver esterase (PLE) and carbonic anhydrase (CA) using an H_2S-selective electrode to confirm that the targeting functionalizations did not prohibit H_2S release. For each targeted donor, we measured the H_2S release using the TCM (50 μM) in PBS (10 mM, pH 7.4) containing PLE (5 U mL^{-1}), and CA (25 μg mL^{-1}) under nitrogen over the course of 60 min. All targeted donors exhibited H_2S production in the presence of both CA and PLE (Figure 3.3). Over the course of 60 min, we observed 9 – 30 % efficiency of the donor, with some variations based on donor functionalization. In particular, the sulfonamide based TCMs (**ERTCM** and **GolgiTCM**) exhibited lower efficiencies of H_2S release compared to **MitoTCM** and **LysoTCM**. We hypothesized this decrease in H_2S production could be from potential coordination of the targeting group to the Zn(II) site in CA since some sulfonamides are known inhibitors of CA. Despite this decreased efficiency, we still observe modest H_2S release from both donors and evaluated H_2S production in cells with all the targeted TCMs.

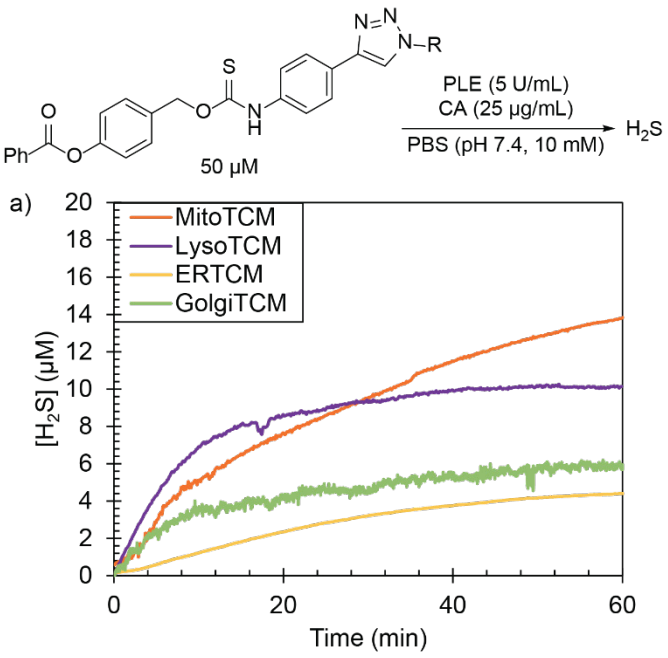

b)

Donor	k_{obs} x10^{-4} (s^{-1})
MitoTCM	4.4 ± 0.9
LysoTCM	16 ± 5
GolgiTCM	16 ± 5
ERTCM	6.2 ± 0.3

Figure 3.3 a) COS/H_2S release from organelle targeted TCMs (50 µM) in the presence of PLE (5 U mL^{-1}) and CA (25 µg mL^{-1}) in PBS (10 mM, pH 7.4) using an H_2S-selective electrode. Experiments were performed in triplicate, and release curves are expressed as the mean (n = 3). b) Rates of COS/H_2S release reported as pseudo 1st-order rate constants (k_{obs}) with results expressed as mean ± S.E. (n = 3).

3.2.4 Live-Cell Imaging of Localized H_2S Delivery

We next evaluated the localization of H_2S delivery using live-cell fluorescent imaging. To visualize H_2S production within the cell, we prepared the following organelle-targeted H_2S-responsive fluorescent probes to visualize H_2S production: Mito-HS,[93] Na-H_2S-ER,[91] Lyso-AFP,[92] and Golgi-NH,[90] which target the mitochondria, ER, lysosome, and Golgi apparatus, respectively (Figure 3.4). Although the earlier cell imaging with the mitochondrially-targeted H_2S donor AP39 were performed with a non-targeted coumarin-azide fluorescent probe, we wanted to ensure that

probes were localized directly to organelles being investigated. We selected organelle-targeted fluorescent H_2S probes to monitor intracellular H_2S production because H_2S is membrane permeable and could disperse throughout the cell once produced if not trapped in the local area of delivery. Furthermore, non-targeted H_2S probes could diffuse throughout the cell after reacting with H_2S, making it difficult to discern if H_2S delivery was localized. With the targeted probes in hand, we next imaged each targeted TCM in the presence of an organelle-targeted probe and commercial organelle-targeted dye.

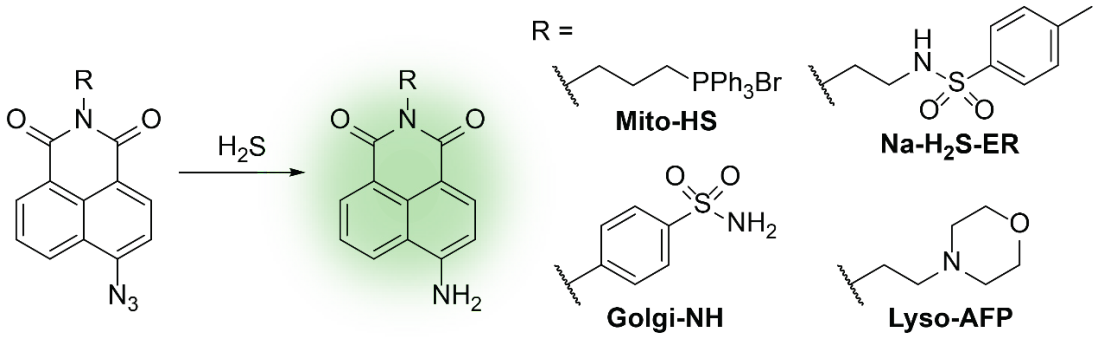

Figure 3.4 Selected organelle-targeted H_2S-responsive fluorescent probes.

HeLa cells were first incubated with a probe (Mito-HS, Lyso-AFP, Na-H_2S-ER, or Golgi-NH) and an organelle marker dye (MitoTracker™, LysoTracker™, ER-Tracker™, or BODIPY™ TR Ceramide) for 30 min. After washing with PBS (pH 7.4, 10 mM), cells were incubated for 1 hour with targeted TCM (**MitoTCM**, **LysoTCM**, **ERTCM**, or **GolgiTCM**) or the non-targeted control compound **TCM alkyne**. As shown in Figure 3.5, a bright fluorescent response indicating H_2S production was observed with only 200 nM of targeted TCM, whereas the vehicle treatment had minimal fluorescence (Figure 3.6a). Notably, these results support that organelle targeted delivery allows for a significantly lower donor concentration required to produce a visible turn-on response when compared to previously reported cell imaging experiments of non-targeted small

molecule H_2S donors (50-100 μM).[25, 38, 40, 49, 51, 55-56] Furthermore, the fluorescent response for each targeted donor overlapped with commercial organelle-targeted dyes, and the calculated Pearson's coefficients (**MitoTCM**/Mito-HS/MitoTracker™: 0.96, **LysoTCM**/Lyso-AFP/LysoTracker™: 0.94, **ERTCM**/Na-H_2S-ER/ERTracker™: 0.95, **GolgiTCM**/Golgi-NH/BODIPY™ TR Ceramide: 0.92) matched the literature values for the corresponding organelle-targeted probes (Figure 3.5).

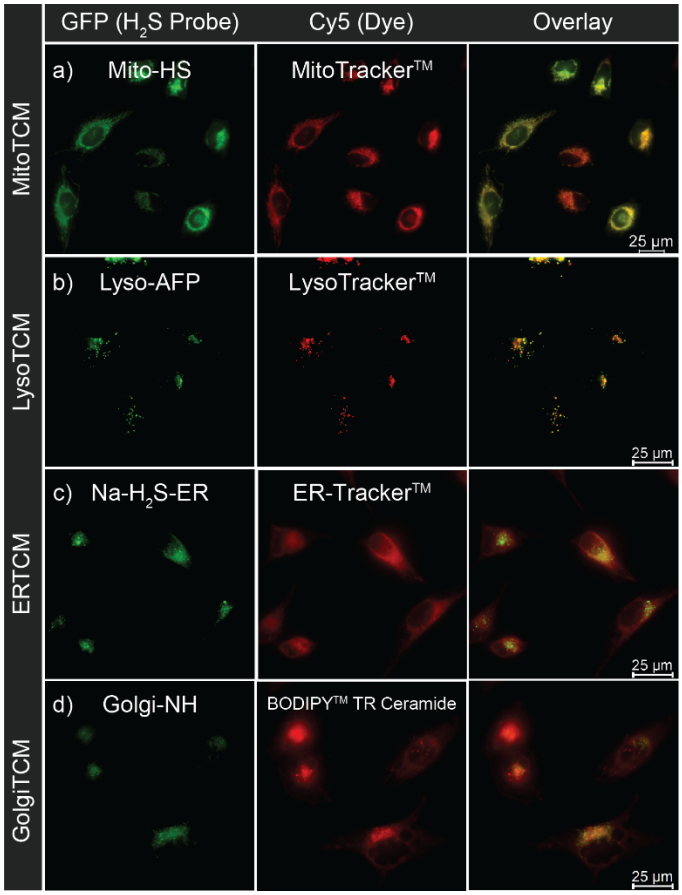

Figure 3.5 Live-cell imaging of localized H_2S production in HeLa cells. (a) Mitochondria-localized H_2S delivery from **MitoTCM** (200 nM) in the presence of Mito-HS (10 μM) and MitoTracker™ (50 nM). (b) Lysosome-localized H_2S delivery from **LysoTCM** (200 nM) in the presence of Lyso-AFP (10 μM) and LysoTracker™ (50 nM). (c) ER-localized H_2S delivery from **ERTCM** (200 nM) in the presence of Na-H_2S-ER (10 μM) and ER-Tracker™ (1 μM). (d) Golgi-localized H_2S delivery from **GolgiTCM** (200 nM) in the presence of Golgi-NH (5 μM) and BODIPY™ TR Ceramide (2 μg/mL).

To confirm that the observed turn-on fluorescent response was due to the organelle-targeting character of the TCMs, we imaged the **TCM alkyne** donor alongside the targeted TCMs as a non-targeted control compound. Interestingly, **TCM alkyne** resulted in significantly lower fluorescence in all targeted TCMs except **LysoTCM** at the same concentrations (Figure 3.6). Although this observation corroborates our hypothesis that appending directing groups onto the H_2S donor scaffold enables localization of H_2S delivery, it also suggests that non-targeted TCMs (and potentially other small molecule H_2S donors) may also accumulate in the lysosome. The lysosome is mildly acidic (pH 4.5 – 5.5) which would result in ~99% of hydrogen sulfide produced within the lysosome to be in its diprotic and gaseous form (H_2S vs HS^-). H_2S is membrane permeable and would likely diffuse readily outside of the lysosome and throughout the cell, which would explain the unconfined fluorescence response typically observed with non-targeted donors.

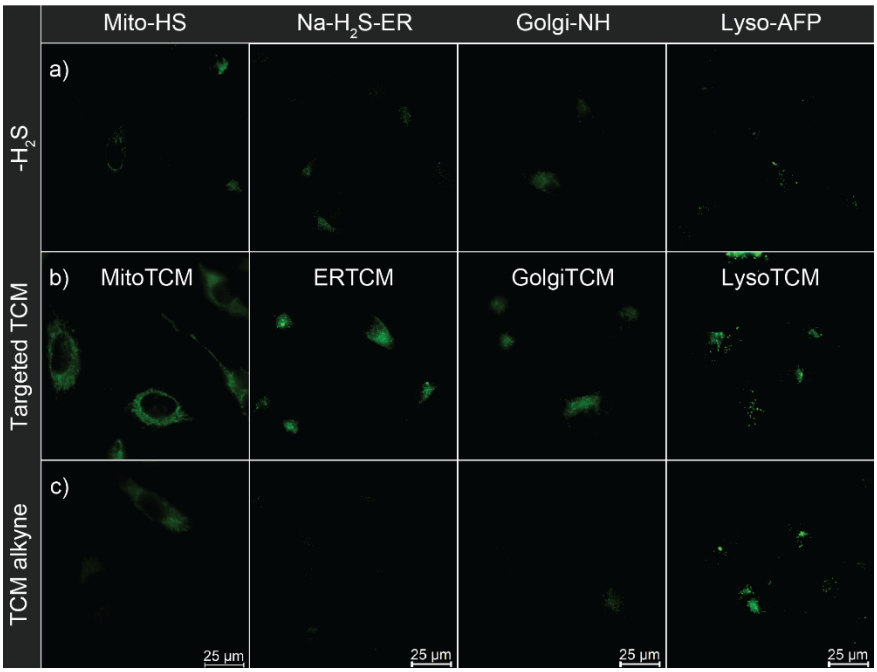

Figure 3.6 Fluorescent turn-on response of targeted H_2S probes in the presence of targeted TCMs compared to non-targeted control (**TCM alkyne**). HeLa cells were treated with probe (5 µM Mito-HS, 10 µM Na-H_2S-ER, 5 µM Golgi-NH, or 10 µM Lyso-AFP) and (a) No exogenous H_2S (b) Targeted TCM (200 nM), or (c) **TCM alkyne** (200 nM).

This finding could also explain the higher concentrations required to observe cellular H_2S production and to produce physiological effects with non-targeted H_2S donors.

In a separate cell imaging experiment, we also compared the response of the mitochondrially-targeted H_2S fluorescent probe, Mito-HS, in the presence of **MitoTCM**, AP39 (a known mitochondrially-targeted H_2S donor), and **ERTCM** (Figure 3.7). Whereas **MitoTCM** and AP39 had comparable fluorescence responses as both mitochondrially-targeted H_2S donors, we observed minimal fluorescence of Mito-HS in the presence of **ERTCM**. This diminished fluorescence in the presence of **ERTCM** further demonstrates the specificity of H_2S delivery with the targeted TCMs as H_2S production is enhanced only in the designated region of interest.

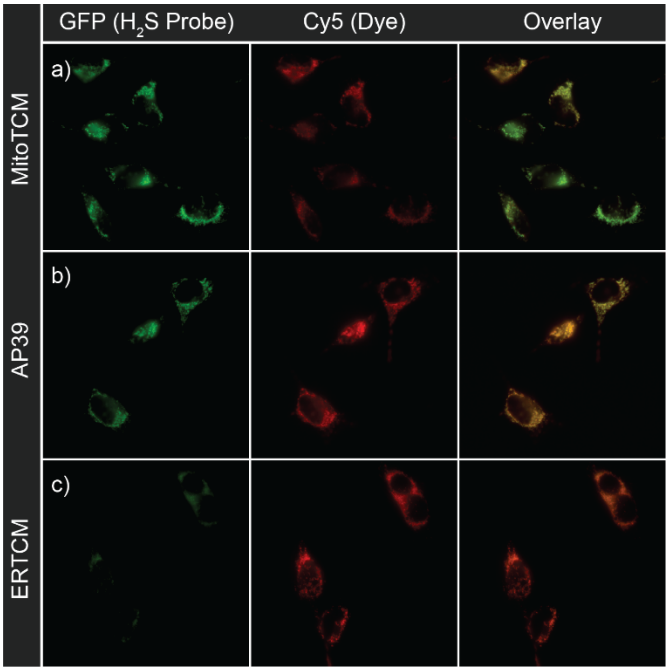

Figure 3.7 Live-cell imaging of 200 nM (a) **MitoTCM** (b) AP39 and (c) **ERTCM** in the presence of Mito-HS (10 μM) and MitoTracker™ (50 nM).

3.3 Conclusions and outlook

We prepared the first library of organelle targeted H_2S donors to provide tools to investigate subcellular effects of H_2S. These donors are readily prepared using click chemistry to append the various targeting groups onto an esterase-activated TCM scaffold. Appending directing groups onto TCMs enabled subcellular localization of H_2S delivery, which was observed through live-cell fluorescent imaging and localizations were confirmed with targeted H_2S-responsive probes. We unexpectantly observed lysosomal localization of H_2S with non-targeted TCM donors. This could explain the higher concentrations required to produce physiological effects with non-targeted donors, further highlighting the importance of targeting H_2S delivery. We anticipate this class of targeted TCMs will enable future studies of H_2S activity within specific organelles and provide new opportunities to investigate therapeutic effects of H_2S in diseases associated with specific organelle stress.

3.4 Experimental Section

Methods and Materials

Reagents were purchased from Sigma-Aldrich, Tokyo Chemical Industry (TCI), Fisher Scientific, Combi-Blocks, and VWR and used directly as received. Silica gel (SiliaFlash F60, Silicycle, 230−400 mesh) and preparatory TLC plates (SiliaPlate Prep TLC, Silicycle, 1000 μm thickness) was used for column chromatography. Deuterated solvents were purchased from Cambridge Isotope Laboratories (Tewksbury, Massachusetts, USA). ^{1}H, $^{31}P\{H\}$, and $^{13}C\{H\}$ NMR spectra were recorded on Bruker 500 MHz and 600 MHz NMR instruments. Chemical shifts are reported in ppm relative to residual protic solvent resonances for ^{1}H and $^{13}C\{H\}$ NMR spectra. Mass

spectrometric measurements were performed by the University of Illinois, Urbana Champaign MS facility or on Xevo Waters ESI LC/MS instrument. H_2S electrode data were acquired with a World Precision Instruments (WPI) ISO-H2S-2 sensor connected to a TBR4100 Free Radical Analyzer or a Unisense H_2S Microsensor Sulf-100 connected to a Unisense Microsensor Multimeter. All air-free manipulations were performed under an inert atmosphere using standard Schlenk techniques or an Innovative Atmospheres N_2-filled glovebox.

H_2S Electrode Materials and Methods

Phosphate buffered saline (PBS) tablets (1X, CalBioChem) were used to make buffered solutions (PBS, 140 mM NaCl, 3 mM KCl, 10 mM phosphate, pH 7.4) in Millipore water. Buffer solutions were sparged with N_2 and stored in an N_2-filled glovebox. Carbonic anhydrase (CA) from bovine erythrocytes (≥3,500 W/A units/mg) and porcine liver esterase (PLE, ≥15 U/mg) was obtained from Sigma-Aldrich. A 10 mg/mL CA stock solution and a 1000 U/mL PLE stock solution was prepared in deoxygenated buffer (PBS, 10 mM, pH 7.4) in a glovebox immediately prior to use. Thiocarbamate stock solutions were prepared in an N_2-filled glovebox in DMSO and stored at −25 °C until immediately before use.

General Procedure for H_2S Electrode Experiments

Scintillation vials containing 20.0 mL of phosphate buffer (10 mM, pH 7.4) were prepared in an N_2-filled glovebox. The CA stock solution (50 μL, 25 μg/mL) and PLE stock solution (100 μL, 5 U/mL) were injected into the vials. Outside of the glove box, the WPI/Unisense electrode was inserted into the vial with a split-top septum. The measured current was allowed to equilibrate before starting the experiment. With moderate stirring, the thiocarbamate stock solution (100 μL, 50 μM) was injected and H_2S release was monitored using the electrode.

Cell Imaging

HeLa cells (ATCC CCL-2) were cultured in Dulbecco's modified Eagle's medium (DMEM) supplemented with 10% fetal bovine serum (FBS) and 1% penicillin/streptomycin at 37 °C under 5% CO_2. Poly-D-lysine coated glass-bottom imaging dishes (MatTek) were seeded with HeLa cells at 10,000 cells/cm^2 overnight. The cells were then washed and incubated with an H_2S-responsive fluorescent probe (Mito-HS, Lyso-AFP, Na-H_2S-ER, or Golgi-NH) and a commercial organelle-targeted dye (MitoTracker, LysoTracker, ER-Tracker, or BODIPY TR Ceramide) in FBS-free DMEM for 30 min. Cells were then washed with PBS and incubated with either a targeted TCM (**MitoTCM**, **LysoTCM**, **ERTCM**, or **GolgiTCM**), **TCM alkyne**, or vehicle (DMSO, 0.5%) in FBS-free DMEM for 60 min prior to being washed with PBS and imaged in FluoroBrite DMEM. Imaging was performed in replicate on a Leica DMi8 fluorescent microscope using DIC for bright field imaging and CY5 and GFP filter cubes for fluorescence imaging. Image workup was done in LAS X and Pearson's Coefficients were calculated in FIJI.[106]

Synthesis

1-Ethynyl-4-isothiocyanatobenzene (2)

4-Ethynylaniline (0.50 g, 4.3 mmol, 1.0 equiv) was dissolved in anhydrous CH_2Cl_2 (20 mL). The reaction was cooled to 0 °C, and then a solution of 1,1′-thiocarbonyldiimidazole (0.761 g, 4.27 mmol, 1.0 equiv) in CH_2Cl_2 (5 mL) was added dropwise. The reaction mixture was stirred at 0 °C for 1 h, warmed to room temperature, and stirred for an additional 1 h. The crude reaction mixture was evaporated and purified by column chromatography (12-100% EtOAc/Hexanes) to isolate a white solid (0.585 g, 86%). ^{1}H NMR (600 MHz, $CDCl_3$) δ: 7.46 (d, J = 8.6 Hz, 2H), 7.17 (d, J = 8.5 Hz, 2H), 3.16 (s, 1H). ^{13}C{H} NMR (151 MHz, $CDCl_3$) δ: 137.1, 133.5, 131.8, 125.9, 121.3, 82.6, 79.3. HRMS (ES+ TOF) (m/z): $[M]^+$ calc'd for C_9H_5NS 159.01427; found 159.01439.

TCM alkyne

4-(Benzoyloxy)benzenemethanol (**1**) (201 mg, 0.876 mmol, 1.0 equiv) and **2** (146 mg, 0.920 mmol 1.05 equiv) were combined in anhydrous THF (10 mL) under N_2. The reaction mixture was cooled to 0 °C before adding DBU (148 µL, 0.964 mmol, 1.10 equiv). The reaction mixture was warmed to room temperature and stirred for 4 h. The reaction was quenched with brine (10 mL) and extracted with EtOAc (3 × 10 mL). The combined organic layers were dried over anhydrous $MgSO_4$, filtered, evaporated, and purified by silica column chromatography (2-32% EtOAc/Hexanes) to obtain the product as a white solid (157 mg, 46%). ^{1}H NMR (500 MHz, DMSO-d_6, 60 °C) δ: 11.25 (s, 1H), 8.14 (d, J = 6.8 Hz, 1H), 7.75 (t, J = 7.4 Hz, 1H), 7.62 (t, J = 7.8 Hz, 2H), 7.56 (d, J = 8.3 Hz, 2H), 7.44 (d, J = 8.3 Hz, 2H), 7.33 (d, J = 8.5 Hz, 2H), 5.61 (s, 2H), 4.03 (s, 1H). ^{13}C{H} NMR (126 MHz, DMSO, 60 °C) δ: 187.0, 164.3, 150.3, 138.4, 133.7, 133.2, 131.8, 129.5, 129.3, 128.8, 128.7, 121.8, 121.7, 117.7, 83.0, 80.0, 70.5. TOF MS (ASAP+) (m/z): $[M + H]^+$ calc'd for $C_{23}H_{18}NO_3S$, 388.1007; found, 388.1015.

Azide Targeting Groups

MitoN$_3$ was prepared according to previous reports.[101-102]

(6-Bromohexyl)triphenylphosphonium bromide. 1,6-Dibromohexane (0.94 mL, 6.1 mmol, 1.0 equiv) and triphenylphosphonium bromide (0.532 g, 2.03 mmol, 0.33 equiv) were combined in MeCN (35 mL) and refluxed for 12 h. After cooling to room temperature, the solvent was evaporated, and the crude mixture was dissolved in DI water (10 mL) and extracted with EtOAc (3 x 20 mL). The crude product was purified by column chromatography (10% MeOH/CH_2Cl_2) to afford a white powder (1.07 g, 34%). ^{1}H NMR (500 MHz, DMSO-d_6) δ: 7.90 (m, 3H), 7.83 – 7.72 (m, 12H), 3.62 – 3.51 (m, 2H), 3.49 (t, J = 6.7 Hz, 2H), 1.74 (p, J = 6.8 Hz, 2H), 1.62 – 1.44 (m, 4H), 1.39 (m, 2H). ^{13}C{H} NMR (126 MHz, DMSO-d_6) δ: 134.9 (d, J = 2.9 Hz), 133.6 (d, J =

10.1 Hz), 130.2 (d, J = 12.3 Hz), 118.5 (d, J = 85.8 Hz), 34.9, 31.8, 28.9 (d, J = 16.8 Hz), 26.7, 21.6 (d, J = 4.2 Hz), 20.2 (d, J = 50.0 Hz). ^{31}P{H} NMR (202 MHz, DMSO-d_6) δ: 24.03.

(6-Azidohexyl)triphenylphosphonium bromide. (4-bromobutyl)triphenylphosphonium bromide (0.5 g, 1 mmol) was dissolved in EtOH/H_2O (1:1, 1.2 mL). NaN_3 (77 mg, 1.2 mmol, 1.2 equiv) was added, and the reaction mixture was shielded from light and heated to 100 °C overnight. The reaction mixture was cooled to room temperature, and the solvent was evaporated. The crude product was purified by column chromatography (10% MeOH/CH_2Cl_2) to afford a white solid (0.438 mg, 95%). ^{1}H NMR (600 MHz, $CDCl_3$) δ: 7.91 – 7.82 (m, 6H), 7.82 – 7.76 (m, 3H), 7.70 (m, 6H), 3.94 – 3.85 (m, 2H), 3.24 (t, J = 6.7 Hz, 2H), 1.72 (m, 2H), 1.63 (h, J = 8.1 Hz, 2H), 1.54 (m, 4H), 1.39 (m, 2H). ^{13}C{H} NMR (151 MHz, $CDCl_3$) δ: 135.1 (d, J = 3.0 Hz), 133.9 (d, J = 10.0 Hz), 130.6 (d, J = 12.6 Hz), 118.6 (d, J = 85.8 Hz), 51.3, 29.9 (d, J = 16.3 Hz), 28.6, 26.5, 22.8 (d, J = 49.7 Hz), 22.8 (d, J = 4.5 Hz). ^{31}P{H} NMR (202 MHz, $CDCl_3$) δ: 19.66.

LysoN$_3$ was prepared according to the reported procedures.[103]

Trifluoromethanesulfonyl azide (TfN_3). NaN_3 (1.17 g, 18.0 mmol, 6.0 equiv) was added to water (3 mL) and CH_2Cl_2 (1.1 mL) and cooled to 0 °C. Once cooled, Tf_2O (0.5 mL, 3 mmol, 1.0 equiv) was added dropwise over 5 minutes to the reaction solution and stirred for an additional 2 h at 0 °C. The organic phase was separated, and the aqueous phase was extracted with CH_2Cl_2 (3 mL). The combined organic layers were washed with saturated aqueous $NaHCO_3$ (10 mL) and reserved for the next step.

4-(2-Azidoethyl)morpholine. 4-(2-Aminoethyl)morpholine (130 mg, 1.00 mmol, 1.0 equiv) was dissolved in CH_2Cl_2 (0.7 mL) and cooled to 0 °C. NEt_3 (0.42 mL, 3.0 mmol, 3.0 equiv) and a solution of $CuSO_4$•$5H_2O$ (13 mg, 0.050 mmol, 0.05 equiv) in water (0.17 mL) was added to the reaction mixture. The reserved solution of TfN_3 was added dropwise followed by addition of

MeOH (0.7 mL). The reaction mixture was stirred at room temperature overnight, then quenched with saturated aqueous $NaHCO_3$ (10 mL), and extracted with CH_2Cl_2 (3 x 10 mL). The combined organic layers were washed with brine, dried over $MgSO_4$, and purified by column chromatography (5% MeOH/CH_2Cl_2). The product was isolated as a yellow solid (146 mg, 94%). ^{1}H NMR (500 MHz, $CDCl_3$) δ: 3.73 (t, *J* = 4.7 Hz, 4H), 3.37 (t, *J* = 6.0 Hz, 2H), 2.61 (t, *J* = 6.0 Hz, 2H), 2.52 (t, *J* = 4.6 Hz, 4H). ^{13}C{H} NMR (126 MHz, $CDCl_3$) δ: 66.7, 57.6, 53.6, 47.9.

ERN$_3$ was prepared according to the modified reported procedure.[104]

2-Chloroethaneamine HCl (0.40 g, 3.5 mmol, 1.0 equiv) was dissolved in water (4 mL). NaN_3 (0.682 g, 10.5 mmol, 3.0 equiv) was added, and then the reaction mixture was heated to 80 °C for 24 h. The reaction mixture was basified with NaOH (1 M) and then extracted with CH_2Cl_2 (3 x 2 mL). Sulfonyl chloride (0.667 g, 3.50 mmol, 1.0 equiv) was then added to the combined organic layers at room temperature. The resultant reaction mixture was stirred for 3 h, concentrated under vacuum, and purified by column chromatography (25% EtOAc/Hexanes). The product was isolated as a clear oil (0.301 g, 35%). ^{1}H NMR (500 MHz, $CDCl_3$) δ: 7.76 (d, *J* = 8.3 Hz, 2H), 7.32 (d, *J* = 8.0 Hz, 2H), 4.96 (t, *J* = 6.5 Hz, 1H), 3.40 (t, *J* = 5.7 Hz, 2H), 3.11 (q, *J* = 6.0 Hz, 2H), 2.43 (s, 3H). ^{13}C{H} NMR (126 MHz, $CDCl_3$) δ: 144.0, 136.9, 130.0, 127.2, 51.0, 42.5, 21.7.

GolgiN$_3$ was prepared according to the reported procedures.[103, 105]

4-(2-Azidoethyl)-benzenesulfonamide. TfN_3 was freshly prepared according to the procedure above. 4-(2-Aminoethyl)benzenesulfonamide (201 mg, 1.00 mmol, 1.0 equiv) was dissolved in CH_2Cl_2 (3 mL) and MeOH (6 mL). The reaction mixture was cooled to 0 °C and then $CuSO_4$•$5H_2O$ (13 mg, 0.050 mmol, 0.05 equiv) was added. The freshly prepared TfN_3 was then added dropwise. The reaction mixture was stirred at room temperature for 16 h, and then the solvents were removed under vacuum. The crude product was redissolved in EtOAc, washed with brine, and dried over

$MgSO_4$. The filtered and evaporated crude product was purified by column chromatography (10% MeOH/CH_2Cl_2). The product was isolated as a pale-yellow solid (177 mg, 78%). ^{1}H NMR (500 MHz, DMSO-d_6) δ: 7.76 (d, J = 7.9 Hz, 2H), 7.47 (d, J = 7.9 Hz, 2H), 3.62 (t, J = 7.1 Hz, 2H), 2.93 (t, J = 7.1 Hz, 2H). ^{13}C{H} NMR (126 MHz, DMSO-d_6) δ: 142.6, 142.4, 129.3, 125.7, 51.1, 34.1.

General Procedure for the Synthesis of Targeted Thiocarbamates

The **TCM alkyne** (1.0 equiv), azide coupling partner (1.08 equiv), and TBTA (1.0 equiv) were dissolved in CH_2Cl_2 (2.6 mL). An aqueous solution of sodium ascorbate (2.0 equiv) and $CuSO_4$•$5H_2O$ (2.0 equiv) was prepared and mixed thoroughly to generate an orange suspension containing copper (I) catalytic species. The copper (I) solution was added to the CH_2Cl_2 reaction mixture, and the resultant mixture was shielded from light and stirred vigorously at room temperature for 1 h. Water (10 mL) was then added, and the mixture was extracted with CH_2Cl_2 (3 x 10 mL). The combined organic phases were dried over $MgSO_4$, filtered, and evaporated under reduced pressure. The reaction was then purified by column chromatography.

MitoTCM was prepared with MitoN_3 and TCM alkyne according to the general procedure above and purified by column chromatography (10% MeOH/DCM) to isolate a white solid (13 mg, 68%). ^{1}H NMR (600 MHz, DMSO-d_6) δ: 11.21 (s, 1H), 8.46 (s, 1H), 8.14 (d, J = 6.6 Hz, 2H), 7.97 – 7.85 (m, 3H), 7.85 – 7.70 (m, 17H), 7.62 (t, J = 7.8 Hz, 2H), 7.58 (d, J = 8.1 Hz, 2H), 7.34 (d, J = 8.3 Hz, 2H), 5.62 (s, 2H), 4.36 (t, J = 7.0 Hz, 2H), 3.62 – 3.38 (m, 2H), 1.83 (p, J = 7.1 Hz, 2H), 1.53 (m, 4H), 1.41 – 1.22 (m, 2H). ^{13}C{H} NMR (151 MHz, DMSO-d_6) δ: 187.0, 164.3, 150.3, 145.6, 134.6 (d, J = 3.2 Hz), 133.8, 133.3 (d, J = 10.2 Hz), 130.0 (d, J = 12.3 Hz), 129.5, 129.3, 128.8, 128.7 (d, J = 2.9 Hz), 128.4, 125.9, 125.1, 122.5, 121.7, 120.8, 118.6, 118.1, 49.1, 48.3, 28.9 (d, J = 3.3 Hz), 24.7, 21.4 (d, J = 4.3 Hz), 20.3 (d, J = 50.1 Hz). ^{31}P{H} NMR (202 MHz,

DMSO) δ: 24.0. HRMS (ES+ TOF) (m/z): $[M]^+$ calcd for $C_{47}H_{44}N_4O_3SP$ 775.2872; found 775.2850.

LysoTCM was prepared with $LysoN_3$ and TCM alkyne according to the general procedure above with the following modifications: the reaction was run in the absence of TBTA for 16 h at room temperature. The reaction was worked up according to the generalized procedure above and purified by column chromatography (5% MeOH/CH_2Cl_2) to isolate a white solid (13 mg, 53%). ^{1}H NMR (600 MHz, DMSO-d_6) δ: 11.19 (s, 1H), 8.46 (s, 1H), 8.14 (d, J = 6.7 Hz, 2H), 7.80 (d, J = 7.9 Hz, 2H), 7.75 (t, J = 7.4 Hz, 1H), 7.61 (t, J = 7.8 Hz, 2H), 7.58 (d, J = 8.1 Hz, 2H), 7.33 (d, J = 8.5 Hz, 2H), 5.62 (s, 2H), 4.51 (t, J = 6.3 Hz, 2H), 3.68 – 3.48 (m, 4H), 2.81 (t, J = 6.4 Hz, 2H), 2.45 (t, J = 4.6 Hz, 4H). ^{13}C{^{1}H} NMR (151 MHz, DMSO) δ: 187.0, 164.3, 150.3, 145.5, 137.4, 133.8, 133.4, 129.5, 129.3, 128.8, 128.7, 127.4, 125.2, 122.5, 121.7, 121.2, 70.4, 65.9, 57.1, 52.8, 46.6. HRMS (ES+ TOF) (m/z): $[M+H]^+$ calcd for $C_{29}H_{30}N_5O_4S$ 544.2019; found 544.2014.

ERTCM was prepared with ERN_3 and TCM alkyne according to the general procedure above and purified by column chromatography (10% MeOH/DCM) to isolate a white solid (10 mg, 25%). ^{1}H NMR (600 MHz, DMSO-d_6) δ: 11.29 – 11.07 (m, 1H), 8.36 (s, 1H), 8.14 (d, J = 6.9 Hz, 2H), 7.83 – 7.69 (m, 5H), 7.69 – 7.59 (m, 5H), 7.58 (d, J = 8.2 Hz, 2H), 7.34 (d, J = 6.2 Hz, 4H), 5.62 (s, 2H), 4.44 (t, J = 6.1 Hz, 2H), 3.39 – 3.26 (m, 2H), 2.33 (s, 3H). ^{13}C{H} NMR (151 MHz, DMSO) δ: 205.9, 187.0, 164.3, 150.4, 145.6, 142.5, 137.3, 133.8, 133.4, 129.5, 129.4, 129.3, 128.8, 128.7, 127.3, 126.2, 125.2, 122.5, 121.7, 121.2, 49.2, 42.2, 30.3, 20.6. HRMS (ES+ TOF) (m/z): $[M+H]^+$ calcd for $C_{32}H_{30}N_5O_5S_2$ 628.1688; found 628.1688.

GolgiTCM was prepared with $GolgiN_3$ and TCM alkyne according to the general procedure above with the following modifications: the reaction was run in the absence of TBTA and sonicated for 1 h before stirring at room temperature overnight. The reaction was worked up according to the

generalized procedure above and purified by column chromatography (5% MeOH/CH_2Cl_2) to isolate a white solid (14 mg, 36%). ^{1}H NMR (600 MHz, DMSO-d_6) δ: 11.19 (s, 1H), 8.46 (s, 1H), 8.14 (d, J = 6.9 Hz, 2H), 7.90 – 7.69 (m, 6H), 7.66 – 7.59 (m, 5H), 7.41 (d, J = 8.3 Hz, 2H), 7.33 (d, J = 8.5 Hz, 2H), 7.17 (s, 2H), 5.61 (s, 2H), 4.70 (t, J = 7.1 Hz, 2H), 3.32 (t, J = 7.2 Hz, 2H). ^{13}C{^{1}H} NMR (151 MHz, DMSO) δ: 187.1, 164.3, 150.3, 145.6, 142.4, 141.5, 133.8, 133.3, 129.5, 129.3, 128.9, 128.7, 127.3, 126.3, 125.5, 125.2, 122.5, 122.1, 121.7, 120.8, 70.4, 49.9, 34.9. HRMS (ES+ TOF) (m/z): $[M+H]^+$ calcd for $C_{31}H_{28}N_5O_5S_2$ 614.1523; found 614.1532.

Mito-HS was prepared according to the reported procedure.[93]

4-Bromo-1,8-napthalic anhydride (0.50 g, 1.8 mmol, 1.0 equiv) was dissolved in DMF (7.2 mL), and then a suspension of NaN_3 (0.178 g, 2.70 mmol, 1.5 equiv) in water (0.3 mL) was added. The reaction mixture was stirred vigorously for 5 h at room temperature and then poured into ice water to precipitate the product. The product was filtered off as a yellow solid (0.378 g, 88%).

(3-Ammoniopropyl)triphenyl phosphonium bromide (60 mg, 0.15 mmol, 1.0 equiv) and 4-azido-1,8-naphtalic anhydride (36 mg, 0.15 mmol, 1.0 equiv) were combined in MeOH (7.5 mL) and NEt_3 (0.85 mL) was added. The reaction mixture was heated to reflux for 8 h, cooled to room temperature, and the solvents were removed under vacuum. The crude product was purified by column and then by using a preparatory TLC plate (10% MeOH/CH_2Cl_2) to yield 9.8 mg of product (11% yield). ^{1}H NMR (500 MHz, CD_3OD) δ 8.59 (d, J = 7.5 Hz, 1H), 8.57 (d, J = 8.0 Hz, 1H), 8.53 (d, J = 8.2 Hz, 1H), 7.93 – 7.69 (m, 19H), 7.67 (d, J = 8.0 Hz, 1H), 4.34 (t, J = 7.1 Hz, 2H), 3.70 – 3.53 (m, 2H), 2.15 (m, 2H).

Lyso-AFP was prepared according to the reported procedures.[89, 92]

4-Bromo-1,8-napthalic anhydride (120 mg, 0.43 mmol, 1.0 equiv) and 4-(2-aminoethyl)morpholine (57 μL, 0.434 mmol, 1.0 equiv) were combined in EtOH (15 mL) and

heated to reflux for 3 h. The reaction mixture was cooled to room temperature and filtered to afford a yellow solid (58 mg, 69%). The resulting product (LysoBr) was carried forward without further purification. LysoBr (60.0 mg, 0.154 mmol, 1.0 equiv) was dissolved in DMF (3 mL). A solution of NaN_3 (18 mg, 0.28 mmol, 1.8 equiv) in H_2O (0.5 mL) was added dropwise. The reaction mixture was stirred at 100 °C for 8 h, then quenched with H_2O (10 mL) and extracted into CH_2Cl_2 (3 x 20 mL). The combined organic layers were washed with a 5% LiCl solution in H_2O (5 x 20 mL) and brine (1 x 20 mL), then dried over $MgSO_4$, filtered, and evaporated. The crude product was purified by column chromatography (5% MeOH/CH_2Cl_2) to isolate a yellow solid (13 mg, 23%). ^{1}H NMR (500 MHz, $CDCl_3$) δ: 8.64 (d, *J* = 7.3 Hz, 1H), 8.59 (d, *J* = 7.7 Hz, 1H), 8.46 (d, *J* = 8.4 Hz, 1H), 7.75 (t, *J* = 7.9 Hz, 1H), 7.48 (d, *J* = 8.1 Hz, 1H), 4.34 (t, *J* = 7.0 Hz, 2H), 3.68 (t, *J* = 4.7 Hz, 4H), 2.70 (t, *J* = 7.0 Hz, 2H), 2.60 (s, 4H).

Na-H_2S-ER was prepared according to the reported procedures.[91, 107]

4-Bromo-1,8-napthalic anhydride (51.4 mg, 0.215 mmol, 1.0 equiv) and *N*-(2-aminoethyl)-4-methylbenzenesulfonamide (60 mg, 0.28 mmol, 1.3 equiv) were combined in EtOH (0.5 mL) and heated to reflux. The reaction mixture was stirred for 3 h, then cooled to room temperature, filtered, and dried to give a white solid (67 mg, 66% yield). The benzenesulfonamide (66.7 mg, 0.141 mmol, 1.0 equiv) was combined with NaN_3 (45.8 mg, 0.705 mmol, 5.0 equiv) in 3 mL of DMF and stirred at 50 °C for 8 h. Water (10 mL) was added, and the reaction mixture was extracted with CH_2Cl_2 (3 x 20 mL), washed with 5 % LiCl (4 x 20 mL) and brine (1 x 20 mL), dried over $MgSO_4$, filtered, and evaporated. The crude product was purified by column chromatography (3:1 EtOAc/Hex) to isolate a yellow solid (12 mg, 20%). ^{1}H NMR (500 MHz, DMSO-d_6) δ: 8.50 (d, *J* = 7.3 Hz, 1H), 8.45 (t, *J* = 8.4 Hz, 2H), 7.87 (t, *J* = 8.0 Hz, 1H), 7.77 (d, *J* = 8.1 Hz, 1H), 7.73 (t,

J = 6.3 Hz, 1H), 7.57 (d, *J* = 8.5 Hz, 2H), 7.22 (d, *J* = 7.9 Hz, 3H), 4.10 (t, *J* = 6.7 Hz, 3H), 3.08 (q, *J* = 6.5 Hz, 3H), 2.25 (s, 4H).

GolgiNH was prepared according to the reported procedures.[90]

4-Bromo-1,8-napthalic anhydride (478 mg, 2.00 mmol, 1.0 equiv) and sulfanilamide (344 mg, 2.00 mmol, 1.0 equiv) were dissolved in acetic acid (5 mL) and refluxed for 8 h. The reaction mixture was cooled to room temperature for 1 h, and the precipitate was filtered and dried to yield a grey solid (0.326 g, 38%). The crude product (GolgiBr) was carried over to the next step without further purification. GolgiBr (60.0 mg, 0.139 mmol, 1.0 equiv) and NaN_3 were dissolved in DMSO (3 mL) and stirred at 100 °C for 2 h. The reaction was quenched with H_2O and extracted into DCM (3 x 20 mL). The combined organic layers were washed with brine (20 mL), dried over $MgSO_4$, filtered, and evaporated. The crude product was purified by column chromatography (75% EtOAc/Hex) to yield (9 mg, 16%). ^{1}H NMR (500 MHz, DMSO-d_6) δ: 8.57 (d, *J* = 7.3 Hz, 1H), 8.55 – 8.50 (m, 2H), 7.97 (d, *J* = 8.5 Hz, 2H), 7.96 – 7.90 (m, 1H), 7.83 (d, *J* = 8.0 Hz, 1H), 7.62 (d, *J* = 8.5 Hz, 2H), 7.51 (s, 2H).

CHAPTER IV

ROLES OF REACTIVE SULFUR SPECIES IN BONE

This chapter includes unpublished and co-authored material. This content included in this chapter was written by either Annie K. Gilbert or Turner D. Newton, with editorial assistance from Professor Michael D. Pluth and Marian H. Hettiaratchi.

4.1 Introduction

Reactive oxygen species (ROS) are often viewed as detrimental to health, but these reactive species also play important signaling roles in different systems. For example, ROS have established roles in the cardiovascular, muscular, and immune systems. In the cardiovascular system, multiple redox pathways are involved in angiogenesis and vasodilation.[108] The muscular system relies on redox signaling for skeletal muscle regeneration and muscle cell activity regulation.[108] Furthermore, the lack of ROS-generating NADPH oxidase 2 (NOX2) in chronic granulomatous disease (CGD) leads to immunodeficiency in patients.[109] ROS are also critical for bone remodeling in processes associated with both bone strengthening and healing.[110] Looking farther down the chalcogens on the periodic table, reactive sulfur species (RSS) are intertwined with ROS, and recent work suggests that these chalcogens are involved in different components of bone regulation.

Many RSS are established to play important roles in biological processes, but hydrogen sulfide (H_2S) has garnered significant recognition in the past two decades. As a recent addition to the gasotransmitter family, H_2S is endogenously produced, membrane permeable, and active at physiologically relevant concentrations. Moreover, many of its biological effects can be mimicked

by exogenously applied H_2S sources.[111] H_2S is produced by three main enzymes including cystathionine γ-lyase (CSE), cystathionine β-synthase (CBS), and 3-mercaptopyruvate sulfurtransferase (3-MST). These enzymes are localized throughout various organ systems and cell types with CBS primarily localized in the brain, CSE in the liver and cardiovascular system, and 3-MST in the mitochondria.[112] As evidenced by the diverse localization of these enzymes, H_2S plays a wide variety of important physiological roles throughout the body. For example, H_2S provides neuroprotection and cardioprotection, promotes vasodilation and angiogenesis, and has recently been found to regulate bone homeostasis.[1, 113] H_2S promotes bone formation through persulfidation of Ca^{2+} channels, which stimulates the differentiation of mesenchymal stem cells (MSCs) to bone-forming osteoblasts.[2] CBS and CSE expression are also closely correlated with the transition of human MSCs (hMSCs) towards the osteoblastic phenotype with CSE potentially serving as a novel marker of osteogenic differentiation.[114] Additionally, irregular H_2S levels have been correlated to certain bone diseases including osteoporosis, which has brought forth efforts to better understand the therapeutic potential and role of H_2S and other RSS in the skeletal system.[115-118]

Based on the role of RSS in oxidative stress and other processes involved in tissue regeneration, it is likely that RSS play key roles in hard tissue repair and homeostasis. This review summarizes recent work on the applications of RSS related to bone regeneration and highlights different methods, tools, and common sources of chalcogenides used in different investigations (summarized in Figure 4.4). We also identify future opportunities for delivery of RSS in biological environments relating to bone.

4.2 Role of RSS in Bone

4.2.1 Osteoporosis

ROS play critical roles in bone regulation and remodeling. For example, ROS upregulate receptor activator of nuclear factor κβ ligand (RANKL), which in turn increases osteoclastogenesis.[119-120] Continuous remodeling by osteoclasts and osteoblasts is necessary for maintaining healthy and strong bone, and ROS serve a vital role in this process. Excessive ROS, and consequently excessive osteoclast activity, can disrupt bone homeostasis, resulting in bone loss diseases like osteoporosis.[121] Osteoporosis is a prevalent bone disease primarily occurring in postmenopausal women and elderly men. The disease is characterized by low bone mineral density, which leads to increased risk of fracture. Common therapeutic strategies to treat osteoporosis include the use of amino-bisphosphonates. Bisphosphonates have a high affinity for bone, but the acidic pH caused by osteoclast resorption causes the dissociation of bisphosphonates from bone and subsequent internalization by osteoclasts. Once internalized, amino-bisphosphonates induce cell death in osteoclasts by inhibiting the mevalonate pathway.[122] Despite the success of bisphosphonates in decreasing bone resorption activity, extended use can suppress osteoblast activity, which has led to the decline of bisphosphonate therapies. Developing alternative strategies to restore balance in ROS-dependent pathways that regulate bone mineral density remains an unmet need.

H_2S has been shown to decrease osteoclast activity and differentiation and reduce bone resorption by decreasing ROS production (Figure 4.1). For example, Gambari et al. demonstrated that administration of sodium hydrosulfide (NaSH) as an exogenous H_2S source to CD11b+ human monocytes prevented osteoclast differentiation and function in a dose-dependent manner. The concentration range of NaSH (100 – 200 μM) that prevented osteoclastogenesis was not cytotoxic

to cells, but rather inhibited RANKL-induced ROS production by upregulating NRF2 protein expression.[123] Excess ROS in osteoporotic bone additionally impacts osteoblast proliferation and differentiation. Xu et al. showed that pretreatment of MC3T3-E1 osteoblastic cells with NaSH (100 μM) protected against H_2O_2 (400 μM)-induced cell injury through a MAPK-dependent mechanism.[124] Taken together, the ability of H_2S to inhibit osteoclast activity and differentiation, promote osteogenic differentiation, and protect osteoblasts against oxidative stress make it a potential target for future treatment for osteoporosis.[125]

Early work aimed at combining current therapeutic strategies for osteoporosis with H_2S delivery included the development of the amino-bisphosphonate H_2S donor DM-22.[122] DM-22 combines alendronate, an established osteoporosis therapeutic, with an aryl isothiocyanate that releases H_2S in the presence of excess cysteine. Although DM-22 showed relatively low H_2S release efficiency (4% of total DM-22, measured using an H_2S electrode), it enhanced the mineralization of hMSCs under osteogenic stimulation after 21 days as evidenced by the increased Alizarin Red-S staining when compared to the vehicle treatment. In contrast, alendronate alone inhibited mineralization compared to the vehicle treatment and demonstrated dose-dependent cytotoxicity to hMSCs over 72 h. Despite enhancing the mineralization of hMSCs, DM-22 treatment resulted in a high variability of gene expression of osteogenic biomarkers, making it difficult to confirm the effects of DM-22 in promoting osteogenic differentiation in hMSCs. One of the main goals of combining H_2S delivery with currently used bisphosphonate osteoporosis therapeutics is to achieve both anabolic activity and anti-catabolic activity. Although the bone-forming activity of DM-22 is still unclear, DM-22 was able to retain the anti-resorptive activity of alendronate as observed through osteoclast activity assays (TRAP and PIT) at DM-22 levels that were previously determined as not cytotoxic to hMSCs (33 μM). Collectively, the enhanced

mineralization of hMSCs in the presence of DM-22 paired with the anti-resorptive effects of DM-22 demonstrate therapeutic potential for incorporation of H_2S delivery in current osteoporosis therapeutics. We anticipate H_2S donors with increased H_2S release efficiency could be more effective at promoting osteogenic differentiation at lower doses.

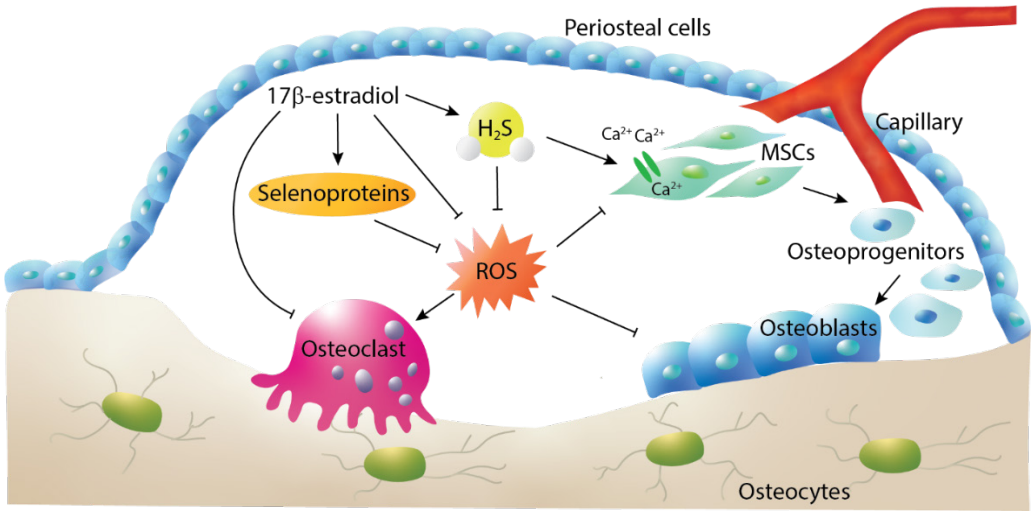

Figure 4.1 H_2S regulation of osteoclast and osteoblasts in a trabecular bone remodeling cavity. H_2S activates Ca^{2+} channels on MSCs to promote osteoblast production. H_2S also protects MSCs and osteoblasts against oxidative stress and decreases osteoclast generation and activity through ROS-dependent pathways. Estrogen levels have been associated with H_2S, suggesting that RSS may be important in pathways associated with estrogen-mediated regulation of bone.

4.2.2 Ovariectomy-Induced Bone Loss

Osteoporosis is predominately found in postmenopausal women because of the natural decline of estrogen production from the ovaries. Estrogen plays an important role in bone health in both women and men. For example, estrogen inhibits bone remodeling activation by osteocytes (cells embedded into formed bone), inhibits bone resorption by osteoclasts, and protects osteoblasts from apoptosis and oxidative stress (Figure 4.1).[126] Since ovaries are a major source of

estrogen, ovariectomy (ovx) osteoporosis models are useful to replicate postmenopausal osteoporosis.

To investigate the effects of estrogen deficiency on endogenous H_2S, Grassi et al. used an ovx-postmenopausal bone loss model in mice. Compared to sham-operated mice, ovx mice had lower serum H_2S levels by 65% and significantly reduced bone marrow levels of CBS and CSE.[127] Administration of the small molecule H_2S donor, GYY4137 (1 mg/mouse/day), normalized serum H_2S levels and completely prevented bone loss induced by ovariectomy. MSCs harvested from ovx and sham-operated mice showed that GYY4137 treatment promotes bone formation through activating Wnt signaling in MSCs. Further investigating the relationship between estrogen and H_2S, Grassi et al. treated human bone marrow stromal cells with 17β-estradiol (an estrogen steroid hormone) and showed upregulated levels of CBS and CSE. This work suggests that estrogen regulation of H_2S levels may be one mechanism by which estrogen stimulates bone formation, and consequently the restoration of H_2S levels could be potential approach for combating postmenopausal osteoporosis.

4.2.3 Hyperhomocysteinemia

Hyperhomocysteinemia (HHcy) is a condition characterized by elevated levels of homocysteine (>15 μM) caused by the dysfunction of enzymes associated with homocysteine (Hcy) metabolism.[128] HHcy not only influences Hcy levels, but CBS deficient patients also show decreased levels of plasma H_2S since CBS generates H_2S from Hcy and cysteine condensation.[2] A variety of different disease states and physiological conditions are associated with HHcy including lens dislocation, cardiovascular disease, Alzheimer's disease, schizophrenia, and osteoporosis.[129] HHcy-induced bone loss can be attributed to increased levels of intracellular ROS, which enhances osteoclast differentiation and activity while decreasing osteoblast activity.[130] Highlighting the role

of the transsulfuration pathway in HHcy (Figure 4.2), both Hcy buildup and depleted H_2S levels can lead to increased oxidative stress and excessive bone resorption through RANKL upregulation. Understanding the role of H_2S and other RSS in HHcy-induced bone loss may provide future opportunities for useful research models or potential therapeutic interventions.

A number of investigations have already highlighted the roles of H_2S in HHcy-induced bone loss. For example, Behera et al. fed mice a methionine enriched diet (1.2% methionine) to elevate Hcy levels and treated the HHcy mice with NaSH (10 mg/kg/day) daily through intraperitoneal injection.[131] In the absence of NaSH treatment, the HHcy mice showed decreased mRNA expressions of CBS and CSE, decreased CBS enzymatic activity, and lower H_2S levels than mice on a normal diet. Furthermore, mice induced with HHcy epigenetically upregulated RANKL and downregulated osteoprotegerin (a RANKL inhibitor), which increased osteoclastogenesis and osteoclast activity and led to osteoporotic phenotypes. Pre-treatment of mice with NaSH increased H_2S levels, resulted in upregulated CBS expression and activity, and prevented the HHcy-induced bone loss by enhancing osteogenesis and inhibiting osteoclastogenesis. In a follow-up study, heterozygous CBS knockout ($CBS^{+/-}$) mice were fed a high methionine diet to investigate whether H_2S alleviates HHcy-induced epigenetic changes that lead to bone loss.[132] HHcy-induced $CBS^{+/-}$ mice showed inhibited histone deacetylase 3 (HDAC3) activity, which causes inflammatory cytokine transcriptional activation in MSCs and increases osteoclastogenesis. The HHcy-induced $CBS^{+/-}$ mice also showed accelerated bone resorption, significantly lower bone mineral density, and reduced trabecular bone volume fraction compared to wild-type mice. H_2S supplementation by intraperitoneal NaSH injection (10 mg/kg/day) provided protection against these epigenetic alterations and inflammatory NF-κB signaling to prevent bone loss. In addition, NaSH administration led to persulfidation of runt-related

transcription factor 2 (RUNX2), which is a key transcription factor for osteoblast differentiation, and highlights the role of S-based posttranslational modifications in signaling pathways associated with bone regeneration.

Osteoblast function is also disrupted by elevated levels of Hcy, which results in mitochondrial oxidative damage and further exacerbates bone loss in HHcy. For example, Zhai et al. demonstrated that treatment of MC3T3-E1 osteoblastic cells with Hcy (50-300 μM) decreased osteoblast activity, resulted in a dose-dependent increase in ROS, and increased mitochondrial dysfunction.[133] Furthermore, treatment of MC3T3-E1 cells with 300 μM Hcy decreased H_2S levels

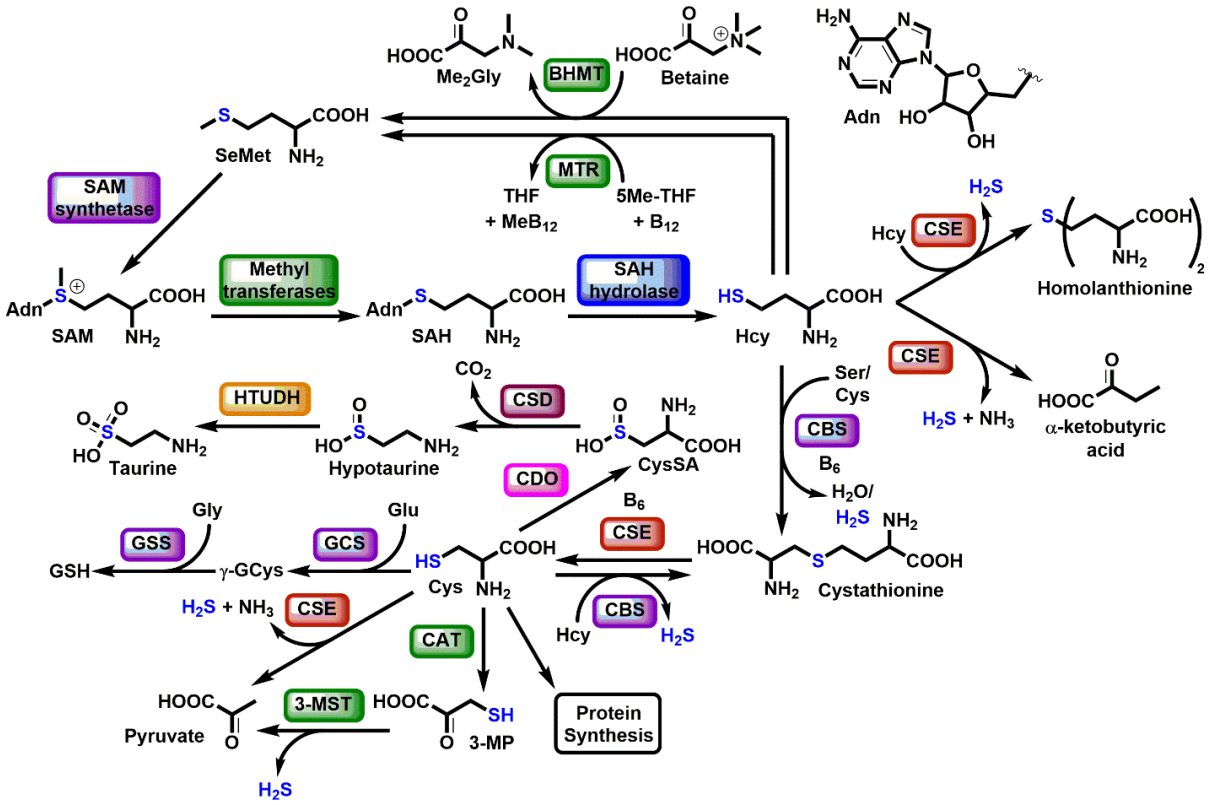

Figure 4.2 The transsulfuration pathway. Metabolites: SAM – *S*-adenosylmethionine, SAH – *S*-adenosylhomocysteine, CysSA – cysteine sulfinic acid, γ-GCys – γ-glutamylcysteine, 3-MP – 3-mercaptopyruvate. Enzymes: BHMT – betaine homocysteine *S*-methyltransferase, MTR – methionine synthase, CDO – cysteine dioxygenase, CSD – cysteine sulfinate decarboxylase, HTUDH – hypotaurine dehydrogenase, GCS – γ-glutamylcysteine synthetase, GSS – glutathione synthetase, CAT – cysteine aminotransferase.

and reduced CBS and CSE expression. Pretreatment with NaSH (30 μM) attenuated Hcy-induced mitochondrial toxicity in the MC3T3-E1 cells and reduced Hcy-induced apoptosis. Across these various models of HHcy, supplementation with NaSH successfully reversed osteoblast dysfunction and bone loss, suggesting that H_2S or related RSS may play an important role in mitigating HHcy effects.

4.2.4 Fracture Healing

Bone fractures are common injuries (~6 million occur annually in the United States) that often fully heal without significant scarring.[134] This efficient healing is due to the fracture repair model that can be broken down into four main phases.[135] In the first phase, a hematoma forms from bleeding within the fracture site. Inflammatory cells within the hematoma secrete cytokines and growth factors that recruit stem cells to the injury site and differentiate cells towards osteogenic fates. A soft fibrocartilage callus is formed by chondrocytes and fibroblasts in the second stage to provide mechanical support to the fracture and offer a scaffold for vascularization. The soft callus is gradually replaced with a hard callus in the third stage. The hard callus stage is where osteogenesis primarily occurs, and osteoblasts form a mineralized bone matrix that contains mineralized extracellular matrix tissue.[135] The final stage includes the remodeling of the hard callus into cortical and/or trabecular bone through osteoclast resorption and osteoblast anabolism, resulting in restored bone homeostasis. Although the fracture repair model is effective for healing most fractures, there can be complications due to factors such as age, underlying conditions, severity of injury that result in defect bone sites called nonunion.

According to the FDA, a nonunion is a fracture that persists for a minimum of nine months without signs of healing for three months. It is estimated that up to 10% of all fractures proceed to nonunion status.[136] Nonunions are classified into four categories: hypertrophic, atrophic,

oligotrophic, or septic nonunion.[136] Each category differs in the extent of callus formation, blood supply, stability, and infection, which provides information on whether biological stimulation, fixation, or antibiotics are necessary. If biological stimulation is required, treatment strategies include the use of a bone graft or the delivery of FDA-approved recombinant human bone morphogenic protein 2 (BMP-2).

BMP-2 is naturally secreted by cells during fracture healing to recruit osteoprogenitor cells and induce osteogenic differentiation. The clinical use of BMP-2 can result in numerous complications. Typically, BMP-2 is loaded up in a porous scaffold which is embedded in the defect site. Large doses of BMP-2 are required to produce a therapeutic effect; however, a surplus of BMP-2 can also lead to inflammation and abnormal bone growth into soft tissues surrounding the defect region.[137] Rapid clearance of protein therapeutics from the tissue requires the use of large quantities of BMP-2, which significantly increases the cost and decreases the safety profile of treatment.[138] Controlling the release of BMP-2 from these scaffolds has recently emerged as effective strategy to decrease ectopic bone growth and reduce the amount of BMP-2 required to promote defect healing.[139]

Analogous to BMP-2, physiologically sufficient levels of H_2S have also been shown to be important for bone formation and fracture healing. Endogenous H_2S production in osteoblasts is primarily attributed to CSE. To investigate the role of H_2S in osteoblast function and bone formation, Zheng et al. overexpressed CSE by transfection of recombinant adenovirus in pre-osteoblasts and implanted the adenovirus in a rat femur defect.[140] CSE overexpression in pre-osteoblasts increased osteoblast differentiation and maturation, resulting in upregulated BMP-2 and osteopontin expression, increased ALP activity, and increased calcium nodule formation. CSE overexpression additionally increased RUNX2 nuclear accumulation, DNA binding activity, and

transcription of its target genes. Using NaSH as an exogenous source of H_2S, Zheng et al. found that RUNX2 was persulfidated, and that persulfidated RUNX2 had increased binding to the osteocalcin promoter. Mutations at the two cysteine residue sites, C123 and C132, prevented persulfidation and DNA binding activity, suggesting that persulfidation of RUNX2 promotes its transactivation. Implantation of a gelatin sponge containing the CSE adenovirus in a rat bone fracture resulted in repair of the fracture lesion after 2 weeks. Less inflammatory cell infiltration and increased collagen secretion was observed after only 1 week when compared to the vehicle treatment. Collectively, this work suggests that H_2S promotes osteoblast differentiation and maturation through persulfidation of RUNX2 to enhance bone healing. Furthermore, the anti-inflammatory effects observed after 1 week of fracture healing suggest that H_2S may provide a variety of important regenerative effects throughout the healing process.

The dynamic therapeutic potential of H_2S in fracture healing has been recently highlighted by Gambari et al. who hypothesized that exogenous H_2S delivery through both early and late stages of healing could be beneficial (Figure 4.3).[116] In early stages, H_2S could aid in regulating inflammation and restoring vasculature in the injury site. In later stages, H_2S promotion of osteoblast differentiation and decrease of osteoclast differentiation and activity could also aid defect bone healing.[116] The effects of exogenous H_2S delivery in H_2S deficient mice has been investigated in the healing of mandibular defects.[141] CSE knockout ($CSE^{-/-}$) inhibited osteogenic differentiation of bone marrow MSCs and suppressed defect healing, whereas intraperitoneal injection of GYY4137 (1 mg/kg) reversed these effects by regulating expression and activity of ALP and RUNX2. Administration of GYY4137 has also been shown to promote bone formation in unfavorable osteogenic environments such as distraction osteogenesis (bone lengthening) in rabbits (intravenous injection of 50 mg/kg twice per day) and in microgravity (intraperitoneal

injection of 25 mg/kg/day).[142-143] These examples highlight the opportunity for treatment of bone defects in more nontraditional bone fracture cases.

To control the delivery of potential therapeutic agents in bone, researchers have developed a number of scaffolds that can be embedded into the defect site and serve as a vehicle for chemical compounds while simultaneously breaking down as the bone heals. For example, the common H_2S donor GYY4137 has been embedded in a silk fibroin scaffold which, when applied to hMSCs, resulted in enhanced osteogenic differentiation observed through increased mineralization and upregulation of osteogenic biomarkers.[144-145]

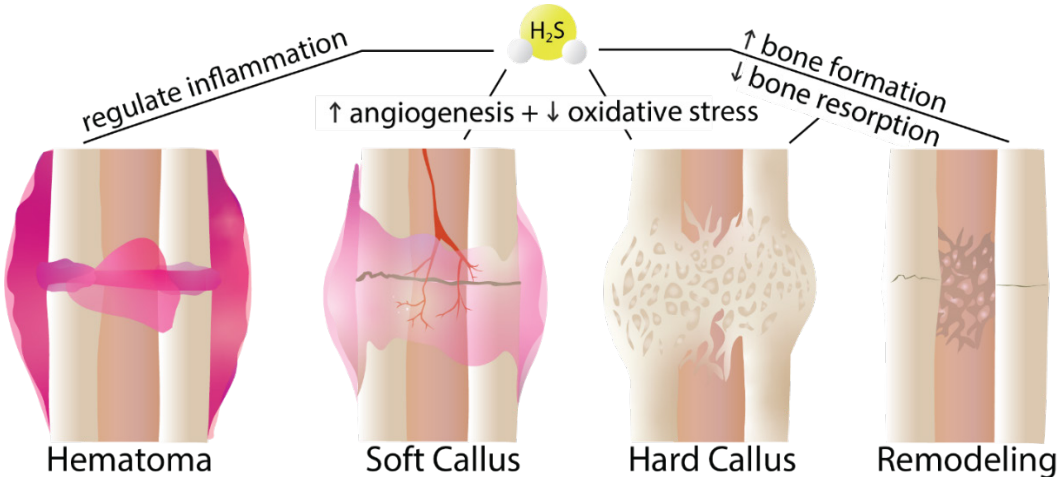

Figure 4.3 Potential therapeutic roles of H_2S throughout the four stages of the bone healing.

4.3 Future Outlook

4.3.1 Sources of RSS

The investigations of RSS highlighted above set the groundwork for future investigations into the importance of RSS in bone. As this area of research continues to expand, new chemical tools for investigating RSS are needed. For example, most prior work on H_2S in bone, which is

summarized in Figure 4.4, has utilized NaSH or GYY4137 as H_2S sources. NaSH is an exogenous H_2S source that rapidly releases a large dose of H_2S upon administration. Much of the produced H_2S is immediately volatilized or oxidized, which makes it difficult to determine actual H_2S concentrations, especially over longer time periods, and adds uncertainty to the proposed therapeutic levels of H_2S. As an alternative to NaSH administration, other researchers have used GYY4137, which is one of the first and most widely used controlled-releasing molecular H_2S donors to date. H_2S release from GYY4137 relies on hydrolysis and is relatively inefficient. In addition, GYY4137 is often sold as a dichloromethane complex. Dichloromethane is metabolized to form carbon monoxide, which is another important gasotransmitter with similar biological effects as H_2S, and could potentially contribute to the observed effects by GYY4137.[146] DM-22, a bisphosphonate isothiocyanate, was developed as an H_2S donor with a high affinity to bone, however, isothiocyanates are also inefficient H_2S sources that require cysteine to release H_2S.[122] Looking to other sources of RSS, Gambari et al. also recently demonstrated an increase in mineralization and increase in expression of certain osteogenic biomarkers after treatment of hMSCs with sulfurous thermal water.[147] Despite these findings, it remains unclear which specific contents of the thermal water were contributing to the observed results.

The palette of tools for H_2S research has greatly expanded since the development of GYY4137 in 2008. Small molecular H_2S donors activated in response to hydrolysis, endogenous species, photoactivation, and biorthogonal chemistry have been developed.[6-7] Based on available technologies, there is now a significant opportunity to tune H_2S release to respond to biological stimuli specific to bone or even within specific stages of the bone healing process. Donors that release H_2S in response to ROS and mildly acidic conditions (both of which are naturally occurring in bone healing environments)[148] have already been developed.[25, 53-54] Applying such donors in

therapeutic scaffolds and developing other H_2S donors that can target specific stages of bone healing could lead to more efficient therapeutic strategies for treating bone defects and diseases.

Exogenous source of H_2S	Observed effects	Year
$H_2S_{(g)}$	Prevents bone cancer pain in rats[149]	2018
NaSH	Decreases osteoclast differentiation[123]	2014
	Alleviates HHcy-induced bone loss[131-132]	2018
	Attenuates HHcy-induced mitochondrial oxidative damage in osteoblasts[133]	2019
NaSH and GYY4137	Protects osteoblasts against oxidative damage[124, 150]	2011, 2017
	Activates Ca^{2+} channels to promote osteogenic differentiation[2]	2014
	Increases osteoblast activity to promote bone fracture healing[151]	2017
GYY4137	Exhibits anti-cancer effects towards an osteosarcoma cell line[152]	2011
	Accelerates bone formation in mandibular distraction osteogenesis[142]	2015
	Rescues bone loss induced by estrogen deficiency[127]	2016
	Promotes osteoclastogenesis in mechanical loading model[153]	2018
	H_2S-releasing scaffold promotes osteogenic differentiation of hMSCs[145]	2019
	Decreases bone loss induced by modeled microgravity[143]	2019
	Promotes mandibular defect healing[141]	2020
Other	H_2S-releasing bisphosphonate (DM-22) decreases osteoclast function and stimulates mineralization with hMSCs undergoing osteogenic differentiation[122]	2017
	Sulfurous thermal water increases H_2S levels in hMSCs and increases mineralization and expression of some osteogenic biomarkers[147]	2020

Figure 4.4 Sources of H_2S used to study H_2S in bone regeneration and their observed effects.

4.3.2 Conclusion

The investigation of RSS in bone is still an emerging field, but significant research contributions that demonstrate important roles for RSS in regulating bone homeostasis have

already been reported. Building from this recent progress, we expect that this area is poised for the development and application of chemical tools specifically designed to control the delivery of RSS in environments relevant to bone homeostasis and regeneration. These future investigations will lay the foundation for expanding our knowledge and therapeutic potential of the roles of RSS in this important research and clinical area. My efforts towards applying previously developed H_2S donors to bone regeneration and developing novel H_2S donors designed for bone healing applications are described in Chapters 5-6.

CHAPTER V

APPLICATION OF SMALL MOLECULE H_2S DONORS TOWARDS BONE HEALING

This chapter includes unpublished and co-authored material written by me. The experimental work was done by me with assistance from Ireland D. Johnson and Spencer Siegel. The project was conceptualized by me with Professor Marian H. Hettiaratchi and Professor Michael D. Pluth.

5.1 Introduction

Hydrogen sulfide (H_2S) is an endogenously produced, gaseous signaling molecule, and has been recently recognized as an important regulator of bone homeostasis.[115] H_2S promotes osteogenic differentiation of mesenchymal stem cells (MSCs) by activating Ca^{2+} TRP channels, which results in the formation of bone-forming osteoblasts.[2] The expression of the H_2S-producing enzymes, cystathionine γ-lyase (CSE) and cystathionine β-synthase (CBS) are also correlated with the transition of human MSCs (hMSCs) towards osteoblastic phenotypes.[114] CBS is primarily expressed in hMSCs whereas H_2S production in osteoblasts is mainly attributed to CSE. In addition to stimulating bone-formation activity, H_2S decreases bone-resorbing osteoclast activity and formation through decreasing ROS levels.[154] These direct effects of H_2S on bone combined with other regenerative effects of H_2S, including its ability to promote angiogenesis and regulate inflammation,[1] make it an ideal therapeutic target for bone healing applications.[116]

Despite the therapeutic potential of H_2S, the high reactivity and gaseous state of H_2S make it challenging to study. To control the delivery of H_2S to biological environments, researchers have developed H_2S-releasing small molecules, often referred to as H_2S donors.[6] GYY4137 is the first

water-soluble H_2S donor and one of the most widely used H_2S donors to date (Figure 5.1a).[65] The phosphorothioate undergoes hydrolysis to produce H_2S that mimics the slow, sustained release of endogenous H_2S production. GYY4137 has been used to study the therapeutic roles of H_2S in estrogen-deficient osteoporosis models and fracture healing.[127, 141, 143, 155] In these studies, GYY4137 was injected into the test subject (mouse or rabbit) resulting in no specificity of localization of H_2S delivery. To help localize H_2S delivery at sites of tissue injury, Raggio et al. developed a silk fibroin scaffold loaded with GYY4137. Dose-dependent H_2S release was observed from the scaffold and cytocompatibility of the scaffold was confirmed with hMSCs and embryonic mouse fibroblasts (NIH/3T3 cells).[144] In subsequent work, Gambari et al. showed that hMSCs seeded on the silk fibroin GYY4137-loaded scaffolds exhibited early mineralization and upregulation of osteogenic biomarkers under osteogenic stimulation.[156] These results are promising, however, large concentrations of GYY4137 are required to produce these effects which could additionally result in off-target effects in vivo. Furthermore, the osteogenic potential of the byproduct of GYY4137 has not been investigated to delineate the direct effects of H_2S, which is essential for understanding the therapeutic roles of H_2S within bone healing applications.[62]

Since the development of GYY4137, several other small molecule H_2S donors have been developed, including donors that differ in activation, release kinetics, byproducts, and payloads.[6-7] These differences between donors have led to some inconsistencies in observed biological effects of H_2S. For example, the osteoinductivity of both GYY4137 and an aryl isothiocyanate bisphosphonate H_2S donor (DM-22) have been investigated in hMSCs.[122, 156] GYY4137 promoted enhanced mineralization of hMSCs and upregulation of osteogenic biomarkers as early as 7 days of osteogenic stimulation. DM-22 on the other hand, enhanced the mineralization of hMSCs after 21 days of osteogenic stimulation, and lacked significant upregulation of osteogenic biomarkers

observed with GYY4137. To clearly understand these differences, further work directly comparing the two H_2S donors is necessary. A key need remains in analyzing biological effects from different sources of H_2S to understand how these different donor features could contribute to downstream H_2S effects. In the process, we can determine what chemical tools will have maximal therapeutic effects in the application of these H_2S sources to certain diseases.

Here, we investigated the potential therapeutic application of *N*-acetylcysteine tetrasulfide ($NACS_4$) toward bone regeneration. $NACS_4$ is a thiol-activated tetrasulfide H_2S donor that releases 2 equivalents of H_2S through a persulfide-dependent pathway (Figure 5.1a).[157] We hypothesized that this scaffold could be immobilized and retained in an alginate hydrogel biomaterial through non-covalent interactions with the *N*-acetylcysteine backbone. Furthermore, the persulfide-based release pathway of $NACS_4$ could result in efficient persulfidation of Ca^{2+} TRP channels from transpersulfidation of *N*-acetylcysteine persulfide or indirect persulfide production from H_2S (Figure 5.1b). To investigate the potential therapeutic application of $NACS_4$ to bone defect healing, we show the incorporation of $NACS_4$ into a hydrogel biomaterial and investigate the effects of $NACS_4$ on the osteogenic differentiation of hMSCs.

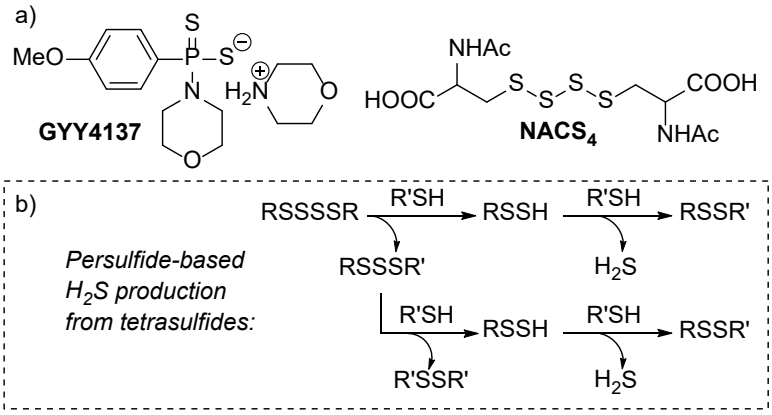

Figure 5.1 a) Representative H_2S donors. b) One pathway of H_2S production from tetrasulfides.

5. 2 Results and Discussion

5.2.1 Preparation and analysis of $NACS_4$-loaded alginate hydrogels

Alginate hydrogels have been established as biocompatible scaffolds to deliver proteins and therapeutics to bone defect sites.[158] Alginate is a polysaccharide that contains homopolymeric blocks of β-D-mannuronate and α-L-guluronate residues. In the presence of calcium, alginate forms "egg-box" cross-linking structures around the divalent cation, which results in gelation. These mild crosslinking conditions are attractive for H_2S donor incorporation into the hydrogel scaffold as several H_2S donors can degrade in crosslinking conditions that require UV light or nucleophiles. Furthermore, we hypothesized that $NACS_4$ could be retained in the alginate hydrogels without covalent modification due to non-covalent hydrogen bonding interactions between the *N*-acetylcysteine backbone and the polysaccharides.

To test our hypothesis that $NACS_4$ could be retained in alginate hydrogel scaffolds, we prepared $NACS_4$-loaded gels and analyzed the supernatant of the gels over time. $NACS_4$ was prepared according to literature procedures.[157] To prepare the hydrogels, alginate was reconstituted in DMEM to obtain a 3% (w/w) solution. $NACS_4$ (100 mM, DMSO) was added to DMEM (3% DMSO) and was mixed with the alginate solution between two interlocked syringes (final $NACS_4$ concentration = 1 mM). Calcium sulfate (0.21 g/mL) was added at a ratio of 25:1 and the solution was rapidly mixed. The alginate solution was allowed to gel in the syringes overnight at 4 °C. The following day, the gels were injected into vials and centrifuged down to obtain a pellet. The gels were purged briefly with N_2 before a layer of degassed PBS (10 mM, pH 7.4) was added. At varying time points, the entire layer of supernatant was replaced, and the removed layer was added to an air-free 10 mM glutathione (GSH) PBS solution. After 24 h of incubation, the concentration of H_2S in the GSH reaction solution was measured using the methylene blue assay. As shown in

Figure 5.2, a small amount of $NACS_4$ is released from the gel over 2 days of incubation. After 7 days, the stability of the $NACS_4$ embedded in the gel was determined by adding GSH and measuring H_2S production directly from the gel. H_2S production was observed over 3 days after thiol addition, which totaled to 54% of H_2S observed with free $NACS_4$ in the presence of 10 mM GSH (positive control). These results show that $NACS_4$ is retained in the alginate hydrogel and is stable within the hydrogel for at least 7 days.

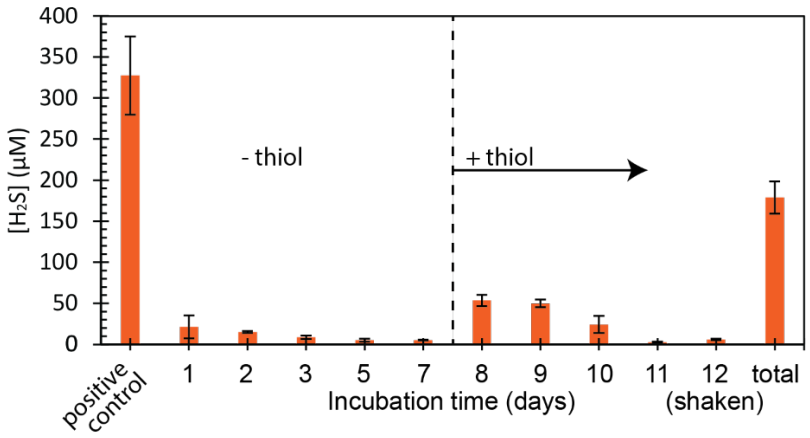

Figure 5.2 Stability of $NACS_4$ and diffusion from alginate hydrogels. Minimal $NACS_4$ was diffused out of the alginate hydrogels over 7 days. Upon thiol addition, however, significant H_2S production was observed over 3 days and amounted to about 54% of the positive control in total over the 10 days. Between each measurement, the entire supernatant was replaced to observe only fresh H_2S production from the gels. Results are expressed as mean ±SD (n=3).

We next evaluated direct H_2S production from the $NACS_4$-loaded alginate hydrogels. The gels were prepared according to the same procedure above. After purging the gels briefly with N_2, degassed PBS (10 mM, pH 7.4) supplemented with GSH (10 mM) was added directly to the gels. Over 5 days, H_2S production was measured using the methylene blue assay. The entire supernatant was removed and replaced with each measurement to observe only fresh H_2S production in subsequent measurements. We observed a large amount of H_2S production in the $NACS_4$-loaded gels after 1 day of incubation with thiol. In comparison to the donor release experiment, we

observed 40% more H_2S production from the gels after 1 day of incubation (Figure 5.3, Thiol addition at day 0) compared to the total H_2S production from $NACS_4$ release (Figure 5.3, Released $NACS_4$ H_2S production day 0-7) combined with H_2S production after thiol addition at day 7 (Figure 5.3, Thiol addition day 7). Despite this difference in H_2S production after 1 day of incubation with thiol, we observed similar H_2S production from the gels from days 2-5. This suggests that some loosely bound $NACS_4$ degrades over the 7 days, however, a consistent amount of $NACS_4$ is retained and stable within the gel after 7 days.

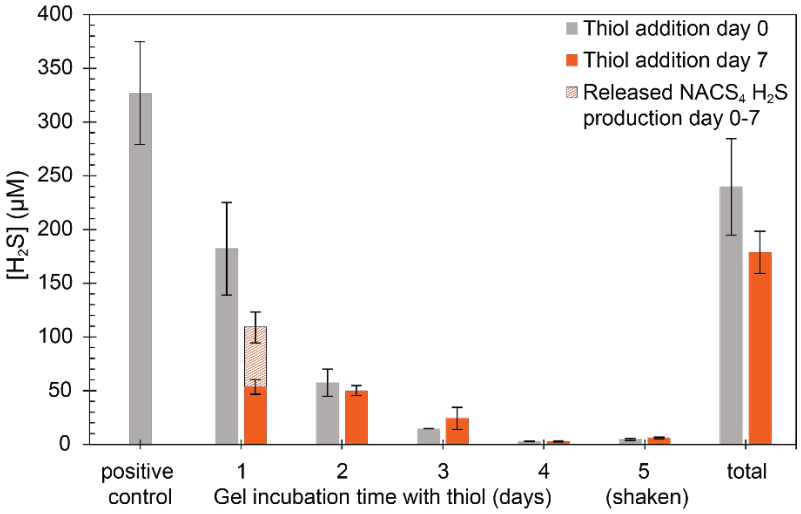

Figure 5.3 H_2S production from $NACS_4$-loaded alginate hydrogels after addition of GSH (10 mM in PBS) at day 0 and after 7 days. Between each measurement, the entire supernatant was replaced to observe only fresh H_2S production from the gels. Results are expressed at mean ±SD (n=3).

Having confirmed that $NACS_4$ is retained in alginate hydrogels and that it is accessible to thiols, we next investigated the difference in H_2S release kinetics between free and hydrogel-bound $NACS_4$. H_2S production from free $NACS_4$ was measured using the methylene blue assay. $NACS_4$ (25 μM) was dissolved in PBS (pH 7.4, 10 mM) containing GSH (1.5 mM, 60 equiv) and reaction aliquots were removed at designated time points for 90 min (Appendix C, Figure C.1). To observe only H_2S production from bound $NACS_4$, the $NACS_4$-loaded gels were soaked in buffer for one

week with the buffer replaced daily. After 7 days, PBS containing GSH (60 equiv) was added to the $NACS_4$-loaded gel and continuous H_2S production was monitored using an H_2S selective electrode (Figure C.2). Substantially slower H_2S production was observed with the hydrogel-bound $NACS_4$. Plots of the H_2S concentrations versus time for both the free and hydrogel-bound $NACS_4$ fit the first-order rate equation, and the fits were used to obtain pseudo first-order rate constants (k_{obs}). The k_{obs} for the hydrogel-bound $NACS_4$ H_2S production was 5 orders of magnitude lower than the free $NACS_4$ (Free: $k_{obs} = 7.13 \times 10^{-4}$ s^{-1} versus Bound: $k_{obs} = 7.84 \times 10^{-9}$ s^{-1}). The difference corresponds to a release half-life of ~16 minutes for the free $NACS_4$ and ~25 hours for the bound $NACS_4$. The slowed production of H_2S in the $NACS_4$-loaded hydrogels demonstrates the potential for these scaffolds in delivering H_2S through multiple days of bone healing.

Overall, these experiments suggest a significant amount of $NACS_4$ is retained within the alginate hydrogels, and the $NACS_4$ embedded within the alginate hydrogels is stable and accessible to thiol. Furthermore, the gels drastically slow H_2S production from $NACS_4$, which is desirable for investigating effects of H_2S delivery through stages of bone defect healing. Although $NACS_4$ demonstrates compatibility in alginate hydrogel scaffolds, the therapeutic benefit of $NACS_4$ towards bone healing needs to be investigated in vitro before applying the scaffold to an in vivo bone defect model.

5.2.2 Osteogenic Differentiation Experiments

To investigate the therapeutic potential of $NACS_4$ in promoting bone healing, we first tested the cytotoxicity of $NACS_4$ towards hMSCs (RoosterBio, bone-marrow derived). hMSCs were treated with varying concentrations of $NACS_4$ (10, 25, 50, and 100 μM) for 24 h and cell viability was analyzed using the Cell Counting Kit-8 (CCK-8) Assay. No significant cytotoxicity was observed from $NACS_4$ treatment up to 100 μM (Figure C.3). We next investigated the effect

of $NACS_4$ on the osteogenic differentiation of hMSCs. Cells were seeded in 48-well plates at 5 x 10^4 cells/cm^2. The day after seeding, the cells were treated with osteogenic medium (Lonza hMSC Osteogenic Differentiation Medium BulletKit™) supplemented with either DMSO (0.5%, vehicle), $NACS_4$ (10, 25, or 50 µM), GYY4137 (50 µM), and NAC (50 µM). The medium was replaced twice per week until 21 days of culture. On day 7, 14, and 21, we performed Alizarin Red S (ARS) staining and collected cell lysates and samples to analyze alkaline phosphatase (ALP) activity, RNA, and calcium deposition.

Over 21 days, we saw no significant differences in mineralization with both the ARS staining (Figure 5.4a) and calcium concentrations (measured using the calcium Arsenazo III

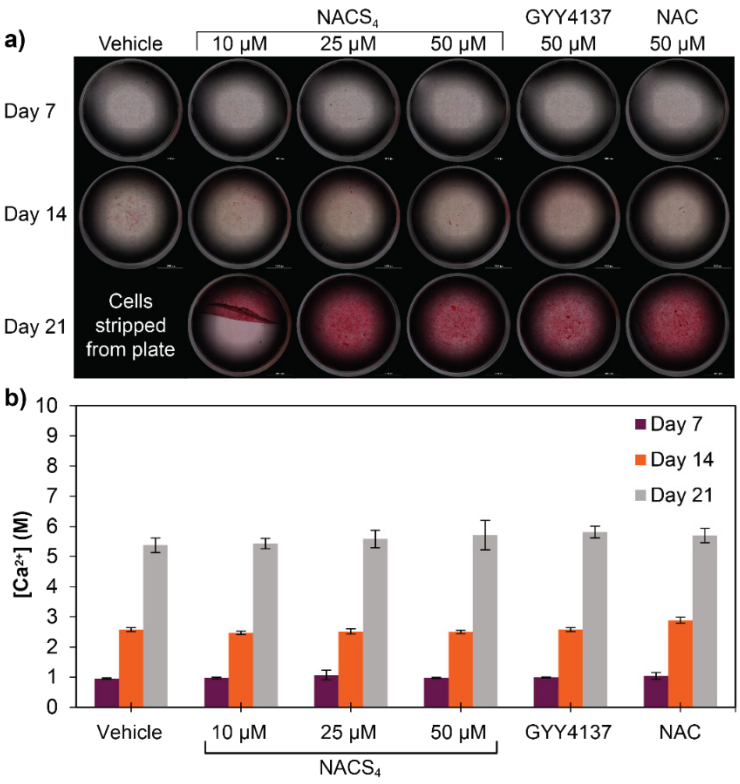

Figure 5.4 $NACS_4$ treatment does not increase mineralization by hMSCs. a) Colored bright field 4x montages of fixed and ARS stained-hMSCs after 7, 14, and 21 days of treatment. All vehicle trials were stripped from the plate before workup at day 21. Only partially stripped cells remained in the $NACS_4$ (10 µM) treatment by day 21. b) Calcium content of samples collected at 7, 14, and 21 days analyzed using the calcium Arsenazo reagent. Results are expressed as a mean ±SD (n=4).

reagent) (Figure 5.4b). Several cells at the day 21 timepoint were stripped from the plate, including all vehicle treatments and all but two partial sheets of cells with the 10 μM $NACS_4$ treatments. Despite the loss of these samples, we were still able to quantify calcium deposition in both the vehicle and 10 μM $NACS_4$-treated cells, which showed no significant differences with the other treatments.

To investigate the expression of the early osteogenic differentiation biomarker, ALP, we used the colorimetric ALP activity assay. ALP-catalyzed *p*-nitrophenol formation from *p*-nitrophenyl phosphate was measured in cell lysates and normalized to dsDNA content (Figure 5.5). Once again, we observed no significant differences in ALP activity in $NACS_4$-treated hMSCs compared to the vehicle treatment (Figure 5.5a). The only significant differences we observed were increased ALP expression in GYY4137 (50 μM) after 7 days of treatment compared to the vehicle treatment (Figure 5.5b). This result corroborates previous results that GYY4137 promotes early osteogenic differentiation of hMSCs. Collectively, these initial results suggest that $NACS_4$ does not enhance the osteogeogenic differentitation of hMSCs. One hypothesis is that potential differences in cell permeability of $NACS_4$ compared to GYY4137 could lead to less persulfidation of Ca^{2+} TRP channels on the plasma membrane. This could be one method to target bone-formation activity of H_2S versus other endogenous effects like angiogenesis and anti-inflammation. Further investigations of H_2S donor cell permeability are necessary, as H_2S is membrane permeable and current work has focused on H_2S detection within cells.

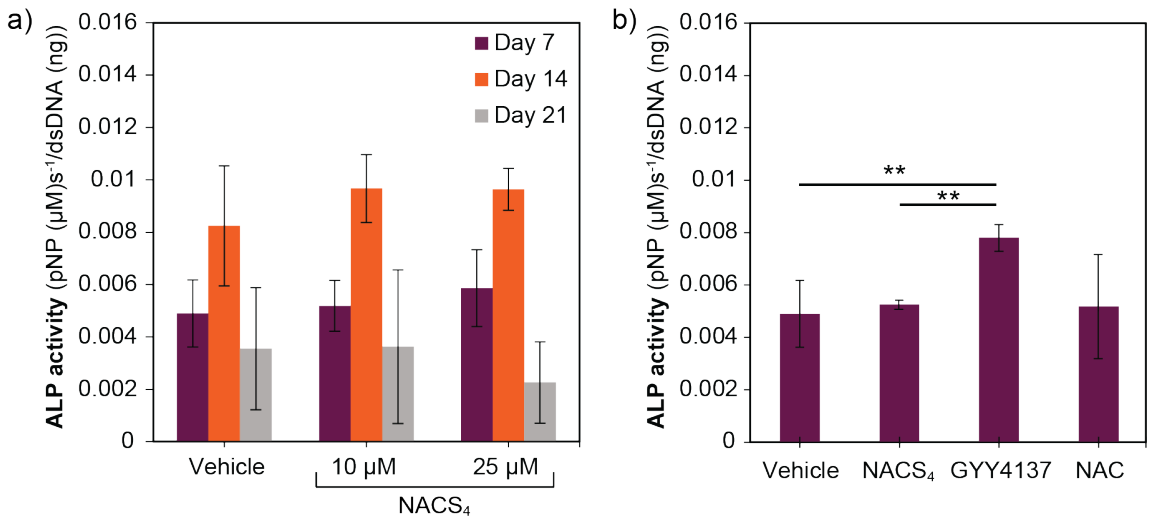

Figure 5.5 ALP activity of a) cell lysates from vehicle and $NACS_4$ treatments over 7, 14, and 21 days of treatment and b) cell lysates from vehicle and 50 μM treatments of $NACS_4$, GYY4137, and NAC at day 7 (***$p < 0.01$ as indicated).

5.3 Conclusions and perspective

The current chemical toolset available to study the therapeutic deilvery of H_2S is expansive, and leaves an important area of research in analyzing different H_2S-releasing small molecules in biological applications. In this work, we demonstrated successful incorporation of $NACS_4$ into alginate hydrogels for implantation into bone defects. With these scaffolds, we demonstrated non-covalent retainment of $NACS_4$, accessiblity of $NACS_4$ to thiol activation, and stability within the hydrogels. Moreover, H_2S production in the presence of thiols was significantly slowed in the hydrogel-bound $NACS_4$ compared to free $NACS_4$. Although we did not observe enhanced osteogenic differentation in hMSCs treated with $NACS_4$, ongoing work to investigate other beneficial effects of $NACS_4$ within bone healing applications are underway. We anticipate the release profile of $NACS_4$ could result in anti-inflammatory and pro-angiogensis effects early in the bone healing process and could complement the osteoinductive properties of GYY4137.

5.4 Experimental Section

Synthesis of *N*-acetylcysteine tetrasulfide ($NACS_4$)

The synthesis of $NACS_4$ was prepared according to the literature procedure.[157] *N*-Acetylcysteine (201 mg, 1.23 mmol, 1.0 equiv) was added to dry THF (20 mL). Pyridine (99 µL, 1.2 mmol, 1.0 equiv) was added, and the reaction was cooled to -78 °C under N_2. S_2Cl_2 (59 µL, 0.74 mmol, 0.6 equiv) was slowly added dropwise and the reaction mixture was stirred at -78 °C for 2.5 h. Immediately after warming to room temperature, the reaction mixture was quenched with DI H_2O (30 mL) and acidified with 3 M HCl. The product was extracted into CH_2Cl_2 (3 x 20 mL) and washed with DI H_2O (20 mL) and brine (20 mL). The combined organic layers were dried over $MgSO_4$, filtered, and evaporated under reduced pressure to afford pure product (177 mg, 74%). ^{1}H NMR (500 MHz, DMSO-d_6) δ: 12.96 (s, 1H), 8.34 (m, 2H), 4.55 (m, 2H), 3.41 (m, 2H), 3.15 (m, 2H), 1.86 (s, 3H). ^{13}C NMR (126 MHz, DMSO) δ: 171.74, 171.65, 169.41, 169.38, 51.32, 51.17, 22.37.

Preparation of $NACS_4$-loaded hydrogels

An alginate solution (3% w/w) in DMEM was prepared and set for 20 h at 0 – 5 °C. Alginate hydrogels were prepared by first mixing 3% alginate solution, DMEM supplemented with either DMSO (1%) or $NACS_4$ (1 mM) between two interlocked syringes. $CaSO_4$ (0.21 g/mL) was added and rapidly mixed between the two syringes for 5 min then set for 20 h at 0 – 5 °C. The gel was injected into 4 mL vials with septa caps and centrifuged down (3 x 20 s @ 1000 rpm) to form an even pellet.

Donor/H_2S release measurement materials

Phosphate buffered saline (PBS) tablets (1x, CalBioChem) were used to prepare PBS buffered solutions (140 mM NaCl, 3 mM KCl, 10 mM phosphate, pH 7.4) in DI water. The buffered solutions were sparged with N_2 and stored in an N_2-filled glovebox. $NACS_4$ stock solutions were prepared in DMSO and prepared fresh before preparation of hydrogels. Glutathione stock solutions in PBS were freshly prepared in an N_2-filled glovebox immediately before use.

$NACS_4$ release from alginate hydrogels

Hydrogels prepared with $NACS_4$ (1 mM) according to the procedure described above were purged with N_2 briefly and a layer of degassed PBS (3.0 mL, pH 7,4. 10 mM) was added. After 24 h of incubation, the entire PBS layer was removed and added to a separate vial containing degassed PBS (17 mL, pH 7.4, 10 mM) supplemented with glutathione (GSH, 10 mM). The PBS layer was replaced on the gel and H_2S produced from the thiol-containing reaction solution was measured using the methylene blue assay after 24 h incubation. This was repeated at 2, 3, 5, and 7 days of incubation. A control sample was prepared (positive control) containing the maximum concentration of $NACS_4$ (168 μM) in PBS (20 mL, pH 7.4, 10 mM) with GSH (10 mM). The positive control sample was incubated for 24 h then the H_2S concentration from the reaction was measured using the methylene blue assay.

To assess the stability of $NACS_4$ in the gel after 7 days of incubation, degassed PBS supplemented with GSH (10 mM) was added directly to the gel. After 24 hours of incubation, H_2S produced from the gel was measured using the methylene blue assay. The entire PBS layer was replaced with fresh, degassed PBS supplemented with GSH (10 mM) then incubated for another 24 h. This

process was repeated 3 more times to yield time points at day 1, 2, 3, and 4. After day 4, the gel was shaken up and the H_2S content was measured.

H_2S production from $NACS_4$-loaded alginate hydrogels

Hydrogels prepared with $NACS_4$ (1 mM) according to the procedure described above were purged with N_2 briefly and a layer of degassed PBS (3.0 mL, pH 7,4. 10 mM) supplemented with GSH (10 mM) was added. After 24 hours of incubation, an aliquot of the gel suspension (0.3 mL) was removed and analyzed for H_2S concentration using the methylene blue assay. The entire GSH-containing PBS layer was removed and replaced with freshly prepared PBS supplemented with 10 mM GSH. H_2S production was monitored every 24 h according to the procedure above for x days.

General procedure for measuring H_2S via methylene blue assay (MBA)

Immediately prior to aliquot measurement, 0.3 mL methylene blue cocktail solutions were prepared in disposable 1.5 mL cuvettes for each sample and one blank. The methylene blue cocktail solution contained: 120 µL of 30 mM $FeCl_3$ in 1.2 M HCl, 120 µL of 20 mM *N,N*-dimethyl-*p*-phenylene diamine in 7.2 M HCl, and 60 µL of 1% (w/v) $Zn(OAc)_2$. A blank sample was prepared by adding 0.3 mL of PBS (10 mM, pH 7.4) supplemented with GSH (10 mM) to one methylene blue cocktail solution. Sample aliquots were added to the remaining methylene blue cocktails and all the samples and blank were mixed. After 1 h incubation at room temperature and shielded from light, the absorbance was measured at 670 nm.

MBA calibration curve

Solutions containing 0.5 mL of the methylene blue cocktail and 0.5 mL of PBS supplemented with 10 mM GSH were freshly prepared in disposable 1.5 mL cuvettes. A 100 mM NaSH stock solution (in PBS) was prepared under inert conditions and diluted to 1 mM. Immediately after preparing

the NaSH stock solution, 10, 20, 30, 40, and 50 µL of the NaSH 1 mM stock was added to the 1 mL methylene blue cocktail solutions for final concentrations of 10, 20, 30, 40, and 50 µM. The solutions were mixed, then incubated at room temperature shielded from light. After 1 h, the absorbances at 670 nm were measured.

Cytotoxicity assay

Bone marrow-derived human mesenchymal stem cells (RoosterBio) were cultured in Dulbecco's modified Eagle's medium (DMEM) supplemented with 10% fetal bovine serum (FBS) and 1% penicillin/streptomycin at 37 °C under 5% CO_2. Cells were seeded at 5,000 cells/well in a 96-well plate overnight, then washed and incubated in FBS-free DMEM containing vehicle (0.5% DMSO) or $NACS_4$ (10, 25, 50, and 100 µM) for 16 h. The cells were then washed with PBS and a CCK-8 solution (10% in FBS-free DMEM) was added to each well. The cells were incubated for 2 h at 37 °C under 5% CO_2. The absorbance at 450 nm was measured using a microplate reader, and the cell viability was measured and normalized to the vehicle group.

hMSCs osteogenic differentiation

hMSCs at PDL 15 were expanded and seeded in 48 well plates at $5x10^4$ cells/cm^2 in α-MEM 10% FBS. The day after seeding, the cells were treated with osteogenic medium (Lonza hMSC Osteogenic Differentiation Medium BulletKit™) supplemented with either DMSO (0.5%), $NACS_4$ (10, 25, 50 µM), GYY4137 (50 µM), or *N*-acetyl cysteine (50 µM). The medium was replaced twice per week with stocks of the supplements prepared fresh before each treatment. After 7, 14, and 21 days of treatment, 2 x 48 well plates were worked up as follows: 4 wells per treatment were either fixed and stained with Alizarin Red S (AR-S), lysed with CelLytic™ MT Cell Lysis

Reagent, lysed with RNA lysis buffer, or treated with acetic acid (1 M) for analyzing calcium concentration. Detailed procedures for ARS staining and calcium sample collection are below.

ARS staining of hMSCs

Cells were washed with calcium-free PBS and fixed with PFA (4% in PBS) for 45 min. The cells were then washed with DI H_2O (2 x 0.2 mL) then treated with freshly prepared AR-S (40 mM, pH 4.1 – 4.2) for 45 min. The cells were washed with DI H_2O (4x) then DI H_2O was added for imaging. The stained cells were imaged on a BioTek Lionheart FX Automated Microscope using the colored bright field channel. Montages of each well were collected at 4x magnification and stitched together using the Gen5 software.

Calcium Assay

Cells were washed with calcium-free PBS and treated with acetic acid (1 M, 200 µL). The cells were incubated in acetic acid for 16 h at 4 °C. The digested samples were collected in microfuge tubes and stored at -20 °C. Calcium standards were prepared from $CaCl_2$ (10 mM in 1 M acetic acid) with 6 serial dilutions in acetic acid (1 M). 25 µL of each standard and sample was pipetted into a clear 96-well plate. Calcium reagent (Arsenazo III, Point Scientific, 300 µL) was added to each well, and the samples were mixed briefly using a pipette. The absorbance at 650 nm was measured using a plate reader.

Alkaline phosphatase activity assay

A buffer solution containing a 1:1:1 ratio of 2-amino-2-methyl-1-propanol (1.5 M), *p*-nitrophenylphosphate (20 mM), and Mg_2Cl_2 hexahydrate (10 mM) was prepared. Standards of *p*-nitrophenol were prepared containing CelLytic Lysis buffer (250 µL), *p*-nitrophenol (0, 1, 2.5, 5, 10, 20, 30, 40, 50 µL), and enough buffer solution to achieve a final volume of 500 µL. Each

standard was vortexed then 100 μL of each standard was pipetted into separate wells on a 96 well plate. Each cell lysate sample was vortexed and 50 μL of each sample was pipetted into separate wells on the 96 well plate. Buffer solution (50 μL) was added to each cell lysate sample and the plate was incubated at 37 °C for 5 – 15 min. NaOH (1M, 100 μL) was added to each standard and sample wells to quench the reaction. The absorbance at 405 nm was measured using a plate reader. A calibration curve was plotted using the standards and the concentration of *p*-nitrophenol formed was calculated from each of the samples. The dsDNA content of each cell lysate sample was quantified using a QuantiFluor dsDNA System kit (Promega), and ALP activity was normalized to dsDNA concentration.

CHAPTER VI

ALKALINE PHOSPHATE-ACTIVATED COS/H_2S DONORS

This chapter includes unpublished and co-authored material written by me. The experimental work was done by me or Mia Ramos. The project was conceptualized by me with insight from Professor Michael D. Pluth.

6.1 Introduction

Bone fracture healing involves a series of coordinated steps that are facilitated by signaling from cells, proteins, and small molecules. One small molecule that has recently emerged as a potential signaling molecule in bone healing includes hydrogen sulfide (H_2S). H_2S is biological signaling molecule that is endogenously produced by three main enzymes: cystathionine γ-lyase (CSE), cystathionine β-synthase (CBS), and 3-mercaptopyruvate sulfur transferase (3-MST).[159] H_2S promotes a variety of physiological effects including angiogenesis, anti-inflammation, and antioxidant effects.[1] More recently, H_2S has been found to have important roles in promoting bone formation and decreasing bone resorption.[115-116] H_2S promotes bone formation through activating calcium TRP channels on mesenchymal stem cells (MSCs) to stimulate osteogenic differentiation.[2] Bone resorption by osteoclasts is mediated by reactive oxygen species which are decreased in the presence of H_2S.[154, 160]

H_2S has also been shown to have an important role in bone defect healing. In a mandibular defect model, CSE knockout ($CSE^{-/-}$) mice experienced suppressed defect healing and inhibition of osteogenic differentiation of bone marrow MSCs.[141] H_2S supplementation reversed these effects and promoted the upregulation of alkaline phosphatase (ALP) and runt-related transcription factor 2 (RUNX2), both of which are biomarkers for osteogenic differentiation. In a separate study, CSE was overexpressed in a rat femoral bone defect by implanting a gelatin sponge containing a CSE

adenovirus.[140] Compared to the vehicle treatment, the overexpression of CSE resulted in significantly enhanced bone healing, resulting in full bridging of the fracture sites within 2 weeks. Furthermore, the overexpressed CSE treatment resulted in less inflammatory cell infiltration and increased collagen secretion compared to the vehicle after only 1 week. This suggests that H_2S delivery could be important through multiple stages of bone healing to help regulate inflammation, callus formation, and later support bone formation.

Gambari et al. recently highlighted the dynamic therapeutic potential of H_2S throughout various stages of the fracture healing process.[116] Early administration of exogenous H_2S could aid in the regulation of inflammation and angiogenesis. Later stages of bone healing could benefit from H_2S delivery to promote osteoblast formation and to decrease osteoclast activity and formation. One significant challenge in studying the therapeutic potential of H_2S throughout fracture healing is controlling its delivery. H_2S is a gaseous and highly reactive small molecule that can have very different biological outcomes depending on the concentration, rate of production, and localization of delivery. Small molecule H_2S donors have been developed to help control the rate and localization of H_2S delivery in biological environments.[6] One particularly tunable class of H_2S donors includes caged thiocarbamates (TCMs).[7] Upon activation, TCMs undergo a 1,6-elimination reaction to produce COS, which is rapidly hydrolyzed to H_2S by the ubiquitous enzyme carbonic anhydrase (CA). TCMs activated by light,[32] reactive oxygen species,[25] cysteine,[161] acidic conditions,[54] and esterases[49-51] have been developed. Currently, there is significant opportunity in developing H_2S donors activated by specific analytes and biological stimuli within bone healing environments to target H_2S delivery to various stages of bone healing.

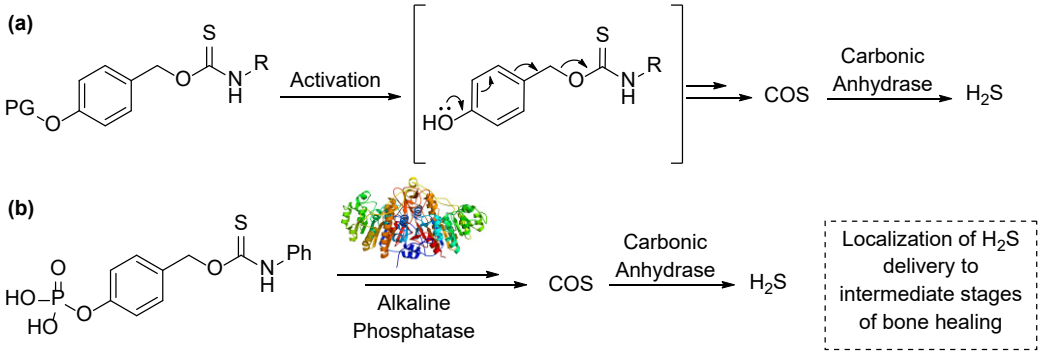

Figure 6.1 a) Mechanism of TCM 1,6-elimination to produce COS, which is rapidly hydrolyzed by carbonic anhydrase to produce H_2S (PG = protecting group). b) Proposed ALP-activated COS/H_2S donors.

Addressing this key unmet need, we developed an ALP-activated H_2S donor utilizing the TCM platform. ALP is an enzyme that catalyzes phosphomonoester hydrolysis at elevated pH (8-10) and is upregulated in early stages of fracture healing.[162] ALP is expressed throughout various tissues including in intestinal, liver, bone, and kidney tissues.[163] Bone specific ALP (BAP) is expressed by differentiated osteoblasts and plays an important role in the generating inorganic phosphate, which is used by osteoblasts to form bone mineral (hydroxyapatite, $Ca_{10}(PO_4)_6(OH)_2$).[164] BAP expression and activity is upregulated in fracture healing and peaks around 10-14 days.[165] Because of this early upregulation, ALP is often used as a biomarker for osteogenic differentiation. We hypothesized that utilizing ALP as an activator for H_2S production would enable targeted H_2S delivery to intermediate stages of bone healing and provide meaningful information of where and when H_2S delivery is beneficial in the fracture healing process.

6.2 Results and Discussion

6.2.1 Synthesis of a model ALP-activated carbamate

ALP activation has been utilized in carbamate-based prodrugs and probes, where dephosphorylation results in a 1,6-elimination to release a payload, quinone methide, and CO_2.[166-170] In these examples, alkyl groups are used to protect the phosphate through the carbamate synthesis. These protecting groups are removed in the final step of the synthesis with base, acid, or bromotrimethylsilane (TMSBr). One significant challenge with the TCM donors is that they can readily isomerize or decompose in various conditions, including acidic or basic conditions. To address this challenge, we envisioned the use of photolabile 2-nitrobenzyl groups to protect the phosphate through the donor synthesis. Previous work has demonstrated the compatibility of TCMs with UV light exposure in an *o*-nitrobenzyl protected TCM.[32] Furthermore, this reaction pathway could provide a dual stimuli H_2S donor to further enable temporal control over H_2S delivery.

To assess this synthetic route, we first prepared a photolabile ALP-activated carbamate (**PL-ALPCM)**. Carbamates are generally more stable than TCMs and serve as useful control compounds that undergo the same elimination mechanism and produce the same byproducts as TCMs but produce CO_2 instead of COS. **ALPCM** was prepared from treatment of excess phosphoryl chloride with TBS protected benzyl alcohol in the presence of triethylamine at -78 °C. The crude product was reacted with excess 2-nitrobenzyl alcohol and deprotected in the presence of Amberlyst-15 to produce the photolabile benzyl alcohol (**PL-BnOH**). Subsequent reaction of **PL-BnOH** with phenyl isocyanate resulted the formation of **PL-ALPCM**.

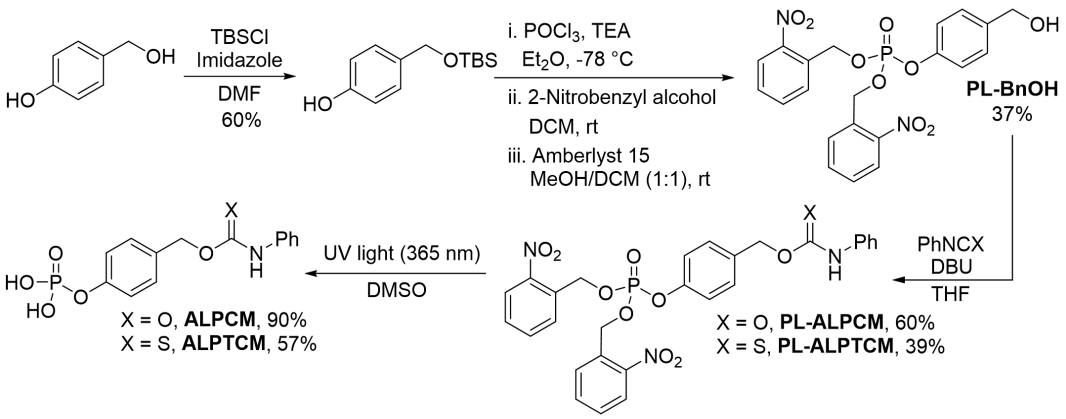

Figure 6.2 ALP-activated thiocarbamate and carbamate synthetic routes.

6.2.2 Photo-uncaging and ALP-catalyzed dephosphorylation

We next investigated photo-uncaging conditions for the removal of the photolabile protecting groups. Deprotection of **PL-ALPCM** in DMSO (20 mM) under UV light (365 nm) was monitored using ^{31}P NMR spectroscopy (Figure 6.3a). After 48 h, we observed complete conversion to the deprotected product (**ALPCM**) as shown in the ^{31}P NMR shift from -6.8 to -6.2 ppm. To confirm the stability of TCMs with this duration of UV light exposure, we prepared a control sample of a model TCM (Appendix D, Figure D.1) and exposed it to UV light alongside the **ALPCM** sample. We did not observe isomerization or degradation of the model TCM over 24 h, indicating the TCM should be stable in these conditions. After the deprotection, the **ALPCM** reaction mixture was diluted with water and lyophilized to afford a crude solid. **ALPCM** was precipitated in DCM to afford clean product in great yields (90%). With clean **ALPCM** in hand, we next evaluated dephosphorylation catalyzed by ALP (5 µg/mL, 0.005 U/mL, from bovine intestinal mucosa) in carbamate/bicarbonate buffer (pH 9.8, 10 mM) using no-deuterium ^{31}P NMR spectroscopy. As shown in Figure 6.3b, we observed inorganic phosphate production after 3 h of incubation at room temperature, confirming ALP-catalyzed hydrolysis of **ALPCM**.

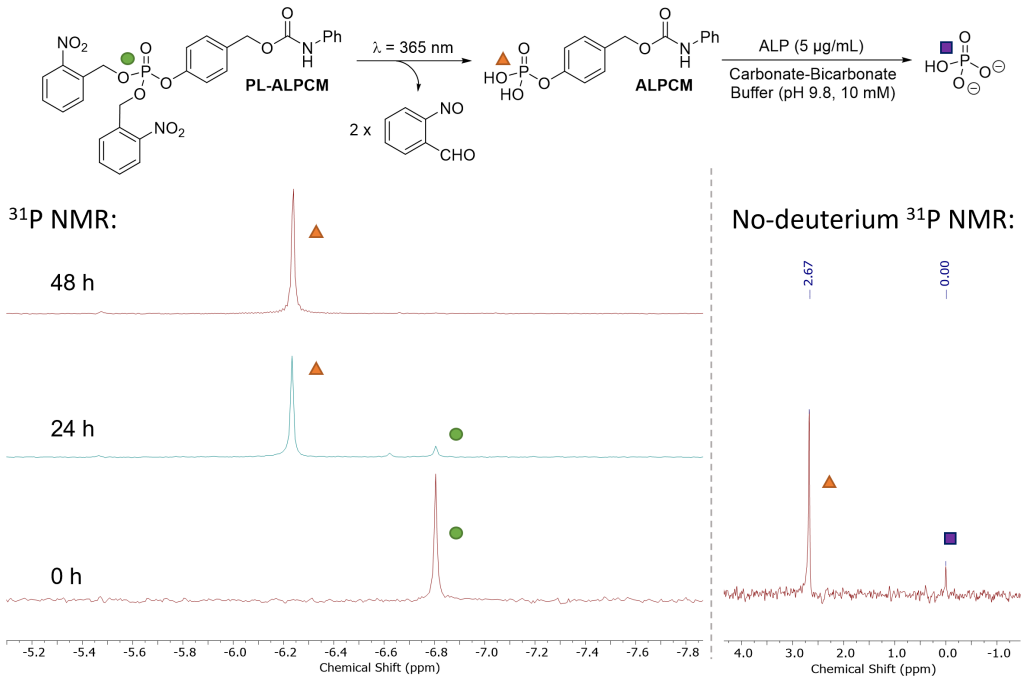

Figure 6.3 Photo-uncaging of **PL-ALPCM** and dephosphorylation of **ALPCM** by ALP. a) Photo-uncaging of **PL-ALPCM** (20 mM in DMSO-d_6) monitored by ^{31}P NMR spectroscopy. b) ALP-catalyzed hydrolysis activity of **ALPCM** (1 mM) in the presence of ALP (5 µg/mL, 0.05 U/mL) in Carbonate-Bicarbonate buffer (pH 9.8, 10 mM) monitored using no-deuterium ^{31}P NMR spectroscopy.

6.2.3 Synthesis and dual-stimuli H_2S release of PL-ALPTCM

Having shown successful ALP-activation of **ALPCM** and compatibility of TCMs with prolonged UV light exposure, we next prepared the photolabile ALP-activated TCM (**PL-ALPTCM**). As shown in Figure 6.2, **PL-ALPTCM** was prepared from treatment of **PL-BnOH** with phenyl isothiocyanate in the presence of DBU. **PL-ALPTCM** was deprotected using the same conditions as **PL-ALPCM** and was additionally monitored using ^{31}P NMR spectroscopy. Unlike the **ALPCM**, we saw complete conversion after only 24 h. The resulting product proved significantly more challenging to purify than **ALPCM**. Although the model TCM did not undergo isomerization with this duration of UV light exposure, we believe the identity of the triggering group could alter the stability of the TCM under these conditions and result in an isomerized S-

alkyl impurity which is challenging to separate from the O-alkyl isomer. Ongoing efforts to purify **ALPTCM** include using reverse phase preparatory TLC, high-performance liquid chromatography (HPLC), and recrystallization. Furthermore, we are working on tuning the deprotection conditions to avoid this potential isomerization.

We next investigated the potential of **PL-ALPTCM** as a dual stimuli H_2S donor that first undergoes photo-uncaging followed by ALP-catalyzed hydrolysis to produce COS/H_2S. For these experiments, H_2S production from **PL-ALPTCM** was monitored using an H_2S-selective electrode (WPI). The electrode was immersed in a quartz cuvette containing a solution of PBS (10 mM, pH 7.4) supplemented with ALP (0.5 U/L) and CA (25 μg/mL). Once the electrode had stabilized, **PL-ALPTCM** was injected into the reaction solution. To confirm uncaging of COS/H_2S requires both UV activation and ALP, we incubated the reaction for 45 min in the dark before turning on the UV light source (365 nm). As shown in Figure D.2, no H_2S production was observed until the reaction mixture was exposed to UV light. Despite these initial promising results, we discovered that the H_2S-electrode is sensitive to the UV light exposure, which resulted in significant and unpredictable drift of the signal over time (Figure D.4). To address the electrode light sensitivity, we exposed **PL-ALPTCM** (50 μM) to UV light for 24 h in the absence of the H_2S electrode, then added the enzymes and monitored H_2S production. Significant H_2S production was observed, however, the response fluctuated significantly throughout the data collection (Figure 6.4). We hypothesize that buildup of the nitrosobenzaldehyde byproduct could be interfering with the electrode response or enzyme activity. Based off previous work outlined in Chapter 5 of this dissertation, we anticipate that **PL-ALPTCM** could be embedded into an alginate hydrogel and retained in the gel after deprotection of the phosphate. The resulting nitrosobenzaldehyde

byproduct could then be diffused out of the gel to obtain a biomaterial with only the desired **ALPTCM**.

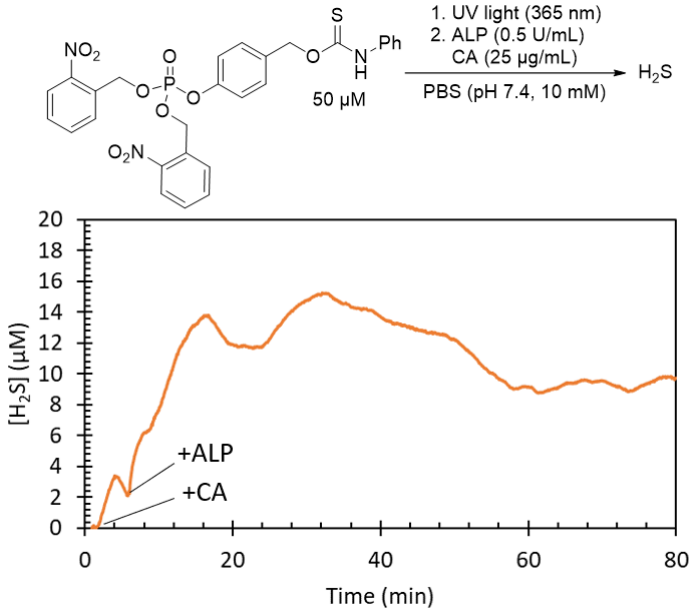

Figure 6.4 Dual stimuli H_2S release from **PL-ALPTCM** (50 μM) in the presence of UV light (365 nm) followed by addition of CA (25 μg/mL) and ALP (50 μg/mL) in PBS (pH 7.4, 10 mM). H_2S production was monitored using an H_2S-selective electrode (WPI).

6.3 Conclusions and Future Work

Current work shows that H_2S has important roles in regulating bone homeostasis, and that spatial and temporal control over H_2S delivery within bone healing environments could enable investigations of therapeutic effects of H_2S. ALP is upregulated throughout fracture healing and could serve as an activator for delivering H_2S to intermediate stages of bone healing. This work serves as progress towards the development of an ALP-activated COS/H_2S donor. To address current limitations in the synthesis of phosphate-containing TCMs, we utilized photolabile phosphate protecting groups. The carbamate control compounds, **PL-ALPCM** and **ALPCM**, exhibited successful photo-uncaging of the free phosphate and activation by ALP to produce

inorganic phosphate. The synthesis of **ALPTCM** proved much more challenging. We hypothesize that the prolonged UV exposure resulted in partial isomerization of the thiocarbamate to the S-alkyl despite no evidence of TCM breakdown or isomerization in control experiments. We investigated the potential of **PL-ALPTCM** as a dual stimuli H_2S donor, first exposing the donor to UV light, then adding ALP and CA. Although significant H_2S production was observed, the unstable response suggests that there is some interference with the resulting nitrosobenzaldehdye byproduct. We anticipate this donor system will have an affinity for alginate hydrogel materials based off previous work outlined in Chapter 5. Incorporation of **PL-ALPTCM** into alginate hydrogels followed by irradiation with light could provide **ALPTCM**-loaded biomaterials and facilitate investigations of H_2S delivery in bone defect models.

6.4 Experimental Section

TBS protected 4-hydroxybenzyl alcohol

4-Hydroxybenzyl alcohol (1.0 g, 8.0 mmol, 1.0 equiv) was dissolved in dry DMF (8 mL) and cooled to 0 °C. TBS chloride (1.2 g, 8.0 mmol, 1.0 equiv) and imidazole (2.74 g, 40.3 mmol, 5.0 equiv) were added, and the reaction mixture was stirred at room temperature for 1 h. The reaction mixture was quenched with water then extracted with EtOAc (3 x 20 mL). The combined organic layers were washed with a LiCl solution (5% in DI water, 5 x 10 mL), DI water (1 x 20 mL), and brine (1 x 20 mL). The organic layer was dried over Mg_2SO_4, filtered, and the solvent was removed under vacuum. The crude product was purified by column chromatography (25-50% EtOAc/Hexanes) to isolate the product as a clear liquid (1.14 g, 60%). ^{1}H NMR (500 MHz, $CDCl_3$) δ: 7.19 (d, J = 8.5 Hz, 2H), 6.79 (d, J = 8.5 Hz, 2H), 4.77 (s, 1H), 4.66 (s, 2H), 0.93 (s, 9H), 0.09 (s, 6H).

PL-BnOH

$POCl_3$ (0.245 mL, 2.62 mmol, 1.0 equiv) was dissolved in dry Et_2O (40 mL) and cooled to -78 °C. NEt_3 (0.365 mL, 2.62 mmol, 1.0 equiv) was added, and then a solution of TBS protected 4-hydroxybenzyl alcohol (0.50 g, 2.1, 0.8 equiv) in Et_2O (5 mL) was added dropwise. The reaction solution was stirred at -78 °C for 2 h. The reaction mixture was warmed to room temperature and the solvents were removed under vacuum. The crude reaction mixture was resuspended in CH_2Cl_2 (20 mL) and cooled to 0 °C. NEt_3 (1.83 mL, 13.1 mmol, 5 equiv) was added, and then 2-nitrobenzyl alcohol (2.00 g, 13.1 mmol, 5.0 equiv) was added. The reaction mixture was stirred for at room temperature and shielded from light. After 1 h, the solvent was removed under vacuum and the reaction mixture was purified by column chromatography (1:1 EtOAc/Hexanes) to obtain a crude mixture of TBS protected product and 2-nitrobenzyl alcohol. The crude product was resuspended in MeOH/DCM (1:1, 10 mL) and Amberlyst® 15 (0.792 g, 2.52 mmol, 1.2 equiv) was added. The reaction mixture was stirred for 16 h, then the Amberlyst® 15 was filtered out of the reaction mixture. The solvent was removed under vacuum and the crude product was purified by column chromatography (50-100% EtOAc/Hexanes) to isolate a pale yellow solid (0.365 g, 37%). ^{1}H NMR (500 MHz, DMSO-d_6) δ: 8.13 (dd, J = 8.2, 1.3 Hz, 2H), 7.78 (td, J = 7.6, 1.3 Hz, 2H), 7.68 (d, J = 7.9 Hz, 2H), 7.64 (td, J = 7.7, 1.5 Hz, 2H), 7.32 (d, J = 8.4 Hz, 2H), 7.18 (d, J = 7.4 Hz, 2H), 5.58 (d, J = 7.5 Hz, 4H), 5.21 (t, J = 5.7 Hz, 1H), 4.47 (d, J = 5.7 Hz, 2H). ^{13}C NMR (126 MHz, $CDCl_3$) δ: 149.6 (d, J = 6.9 Hz), 146.7, 138.6, 134.3, 132.0 (d, J = 8.2 Hz), 129.2, 128.6, 128.5, 125.2, 120.1 (d, J = 4.7 Hz), 66.9 (d, J = 4.5 Hz), 64.5. ^{31}P NMR (243 MHz, $CDCl_3$) δ: -6.04. HRMS (ES + TOF) (m/z): $[M+H]^+$ calc'd for $C_{21}H_{20}N_2O_9P$, 475.0912; found, 474.0906.

PL-ALPCM

PL-BnOH (100 mg, 0.2 mmol, 1.0 equiv) was dissolved in THF (10 mL) and cooled to 0 °C. Phenyl isocyanate (27 µL, 0.25 mmol, 1.2 equiv) was added, and then DBU (31 µL, 0.21 mmol, 1.0 equiv) was added. The reaction mixture was stirred at room temperature for 2 h. The solvent was removed under vacuum and the crude product was purified by column chromatography (75% EtOAc/Hexanes) to isolate a white solid (70 mg, 60%). ^{1}H NMR (500 MHz, DMSO-d_6) δ: 9.75 (s, 1H), 8.13 (d, J = 8.1 Hz, 2H), 7.77 (t, J = 7.6 Hz, 2H), 7.67 (d, J = 7.8 Hz, 2H), 7.62 (t, J = 7.8 Hz, 2H), 7.46 (d, J = 8.7 Hz, 4H), 7.33 – 7.21 (m, 4H), 6.99 (t, J = 7.4 Hz, 1H), 5.59 (d, J = 7.5 Hz, 4H), 5.13 (s, 2H). ^{13}C NMR (126 MHz, DMSO-d_6) δ: 153.3, 149.6 (d, J = 6.9 Hz), 146.8, 139.0, 134.3, 134.0, 131.2 (d, J = 8.2 Hz), 129.9, 129.6, 128.8, 128.8, 125.0, 122.5, 120.1 (d, J = 4.6 Hz), 118.2, 66.3 (d, J = 4.3 Hz), 65.0. ^{31}P NMR (202 MHz, DMSO) δ: -6.80. HRMS (ES + TOF) (m/z): $[M+Na]^+$ calc'd for $C_{28}H_{24}N_3O_{10}NaP$, 616.1092; found, 616.1097.

ALPCM

PL-ALPCM (10.9 mg, 0.018 mmol) was added to DMSO (3 mL) in a quartz cuvette which was exposed to 365 nm light. After 72 h, the DMSO was diluted with DI water and lyophilized to obtain a brown solid. The product was precipitated in CH_2Cl_2, filtered, and washed with CH_2Cl_2 to obtain the product as a brown solid (7.3 mg, 90%). ^{1}H NMR (500 MHz, DMSO-d_6) δ: 9.71 (s, 1H), 7.46 (d, J = 8.0 Hz, 2H), 7.40 (d, J = 8.2 Hz, 2H), 7.27 (t, J = 7.9 Hz, 2H), 7.17 (d, J = 8.2 Hz, 2H), 6.98 (t, J = 7.4 Hz, 1H), 5.10 (s, 2H). ^{13}C NMR (126 MHz, DMSO-d_6) δ: 153.34, 151.59, 139.06, 131.93, 129.59, 128.74, 122.41, 120.06 (d, J = 4.6 Hz), 118.16, 65.30. ^{31}P NMR (202 MHz, DMSO-d_6) δ -6.05.

PL-ALPTCM

PL-BnOH (60.0 mg, 0.127 mmol, 1.0 equiv) was dissolved in dry THF (6.5 mL) and cooled to 0 °C. Phenyl isothiocyanate (15.9 µL, 0.133 mmol, 1.05 equiv) was added and then DBU (18.9 µL, 0.127 mmol, 1.0 equiv) was added. The reaction mixture was stirred at room temperature for 4 h. The solvent was removed under vacuum and the crude product was purified by column chromatography (10% MeOH/DCM) to isolate the product as a pale-yellow solid (30 mg, 39%). ^{1}H NMR (500 MHz, DMSO-d_6) δ: 10.40 (s, 1H), 8.03 (m, 1H), 7.96 (d, J = 8.4 Hz, 1H), 7.79 (s, 1H), 7.68 (m, 1H), 7.57 – 7.39 (m, 4H), 7.26 (m, 6H), 7.14 – 6.95 (m, 2H), 6.74 (d, J = 7.7 Hz, 1H), 5.23 (s, 4H), 4.36 (s, 2H). ^{31}P NMR (243 MHz, DMSO) δ: -7.25. HRMS (ES+ TOF) (m/z): $[M+H]^+$ calc'd for $C_{28}H_{25}N_3O_9SP$, 610.1044; found, 610.1049.

ALPTCM

PL-ALPTCM (7.9 mg, 0.013 mmol) was added to DMSO (0.5 mL) in a quartz NMR tube which was exposed to 365 nm light. After 24 h, the reaction mixture was diluted with DI water and lyophilized to obtain a brown solid. The product was precipitated in CH_2Cl_2, filtered, and washed with CH_2Cl_2 to obtain the product as a brown solid (2.5 mg, 57%). ^{1}H NMR (600 MHz, DMSO-d_6, 60 °C) δ: 11.01 (s, 1H), 7.31 (d, J = 7.6 Hz, 3H), 7.20 (d, J = 8.1 Hz, 2H), 7.14 (dd, J = 13.6, 6.1 Hz, 4H), 5.47 (s, 2H). ^{31}P NMR (243 MHz, DMSO) δ -7.25.

CHAPTER VII

CONCLUDING REMARKS

Over the past couple of decades, several chemical tools have been developed to help understand the roles of H_2S in biology. These tools have enabled visualization of H_2S in biological environments, regulation of biological levels of H_2S, and control over exogenous H_2S delivery. Furthermore, the combination of these tools has revealed the therapeutic potential of H_2S. An important emerging research area aims to bridge the gap between biological discovery and therapeutic application.

In this dissertation, I outlined my contributions to this area by providing small molecule H_2S donors that target H_2S delivery to specific environments of therapeutic interest. Additionally, this work includes the application of current H_2S donors to regenerative applications. I have utilized two different mechanisms of targeted delivery: passive and active localization. In Chapters 2 and 6, I use a passive localization approach to develop COS-based H_2S donors that react in specific environments of therapeutic interest to produce H_2S. I developed H_2S donors that react with mildly acidic environments found in ischemic sites (Chapter 2) and developed H_2S donors that react with a biomarker for bone healing (Chapter 6). These approaches have limitations because both mildly acidic conditions and alkaline phosphatase are not only found in ischemic sites or bone healing environments, but also in other environments. However, when paired with a more active targeting approach (i.e., biomaterials), we could obtain highly selective localization of H_2S delivery in these respective applications. In Chapters 3 and 5, I use an active targeting approach with H_2S delivery. I appended organelle-targeting groups onto thiocarbamate COS/H_2S donors (Chapter 3) and developed biomaterials embedded with polysulfide H_2S donors (Chapter

5). These two projects provide exciting opportunities to study the subcellular delivery of H_2S and the therapeutic benefits of H_2S delivery in bone healing.

Lastly, an important area of therapeutic H_2S discovery includes screening through currently available H_2S sources to understand which types of donors could be beneficial for the treatment of certain diseases and conditions. Currently available H_2S donors differ in mechanism of activation, release kinetics, byproducts, payloads, and localization – all of which drastically alter biological outcomes of H_2S delivery. To better understand which tools could be beneficial for bone healing applications, I outlined my contributions with investigating a polysulfide-based H_2S donor, *N*-acetylcysteine tetrasulfide ($NACS_4$), for bone healing applications. H_2S delivery in bone healing environments is attractive because of the various regenerative roles of H_2S, including its ability to regulate inflammation, provide antioxidant effects, and promote angiogenesis and osteogenesis. Despite evidence of H_2S exerting these various physiological functions, it is unclear which sources of H_2S result in each of these biological effects. In this work outlined in Chapter 5, I discovered that $NACS_4$ does not significantly upregulate osteogenic differentiation of mesenchymal stem cells, which differs from other H_2S sources including sodium hydrosulfide and GYY4137. We are currently investigating other effects of $NACS_4$ to understand when and where the application of this small molecule could be beneficial in bone healing. Overall, this work demonstrates tremendous opportunity with utilizing previously developed H_2S donors to target specific biological effects.

APPENDIX A

SUPPLEMENTARY CONTENT FOR CHAPTER II

Appendix A is the supplementary appendix for Chapter II of this dissertation. It includes all spectra and experimental information relevant to the material in Chapter II.

Isomerization of O-alkyl to S-alkyl donors

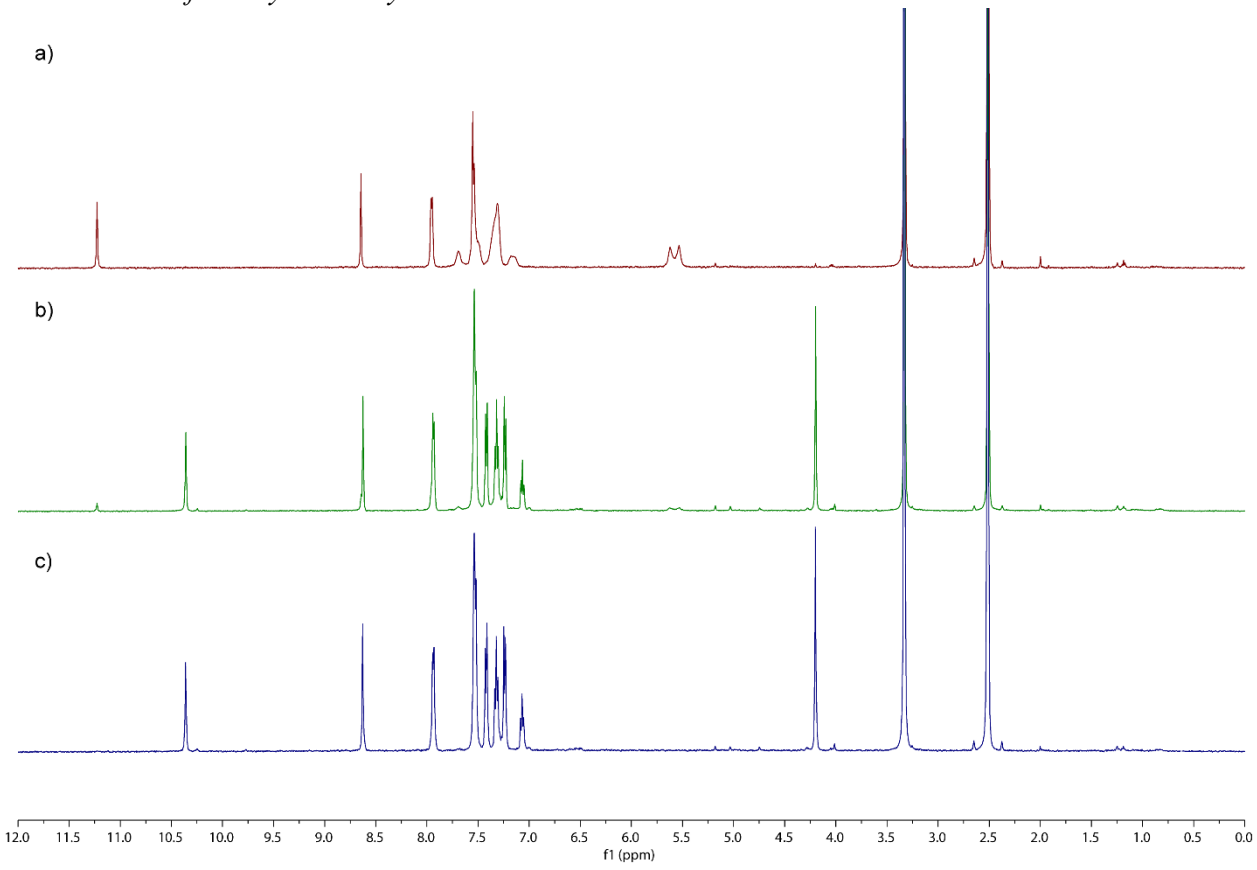

Figure A.1 Complete isomerization of ***S*-pHTCM** from the *O*-alkyl isomer (a, day 1) to a mixture of *O*-alkyl and *S*-alkyl isomer (b, day 2), and then to the *S*-alkyl isomer (c, day 3) in the solid state at room temperature.

Carbonic Anhydrase Activity at pH 5.5

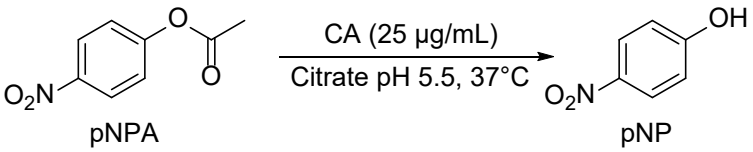

General Procedure for p-nitrophenyl acetate (pNPA) Assay: To 14.5 mL of citrate buffer (10 mM, pH 5.5), 37.5 µL of 10 mg/mL CA in Millipore water was added to achieve a final concentration of 25 µg/mL. The resultant solution was thermally equilibrated at 37 °C. To monitor the background hydrolysis of pNPA, a second 14.5 mL of citrate buffer without CA was also thermally equilibrated at 37 °C. During this time, 0.950 mL of a PBS buffer (100 mM, pH 8.0) solution containing 20 µM of acetazolamide, which is a well-known CA inhibitor, was added to 1.5 mL disposable cuvettes. After 20 min, 0.5 mL of 15 mM pNPA in ethanol was added to citrate buffer solution generate a 500 µM pNPA solution. At t = 0, 3, 5, 10, 15, 20, 25, 30, 60, 75, 90, 120 min, a 50 µL reaction aliquot was added to the PBS buffer solution. Immediately after addition, the absorbance values at 400 nm were measured.

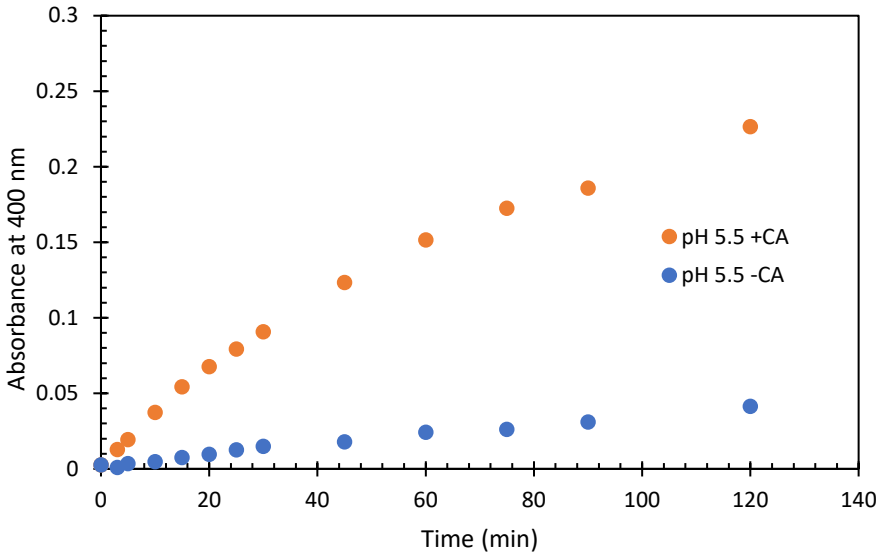

Figure A.2 CA activity evaluated through CA-mediated hydrolysis of pNPA to form pNP in citrate pH 5.5 buffer.

pH Dependence of Donor Activation

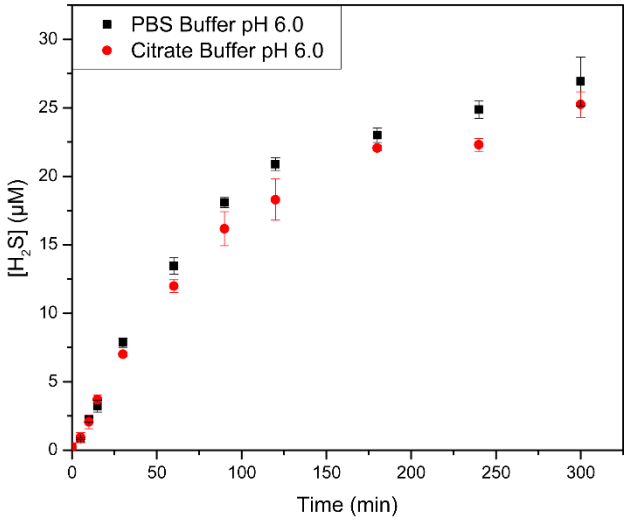

Figure A.3 H_2S-release of ***S*-pHTCM** at pH 6.0 in citrate and PBS buffer (10 mM) containing CA (25 μg/mL) at 37 °C. No significant effects of buffer identity were observed. Experiments were performed in quadruplicate with results expressed as mean ± S.D. (n = 4).

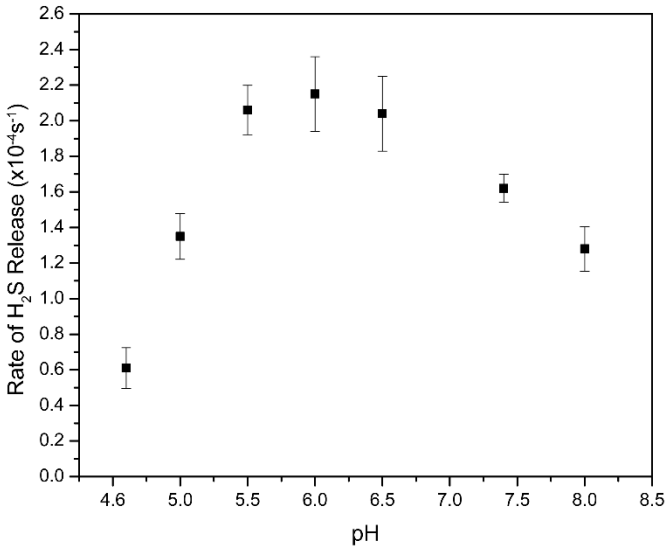

pH	Rate (x $10^{-4}s^{-1}$)
4.6	0.61
5.0	1.35
5.5	2.06
6.0	2.15
6.5	2.04
7.4	1.62
8.0	1.28

Figure A.4 Rate of COS/H_2S release from ***S*-pHTCM** (50 μM) at varying pH reported as pseudo 1st-order rate constants (k_{obs}). Conditions: 10 mM PBS/citrate buffer, pH 4.6-8.0, CA (25 μg/mL), 37 °C. Experiments were performed in quadruplicate with results expressed as mean ± S.D. (n =4).

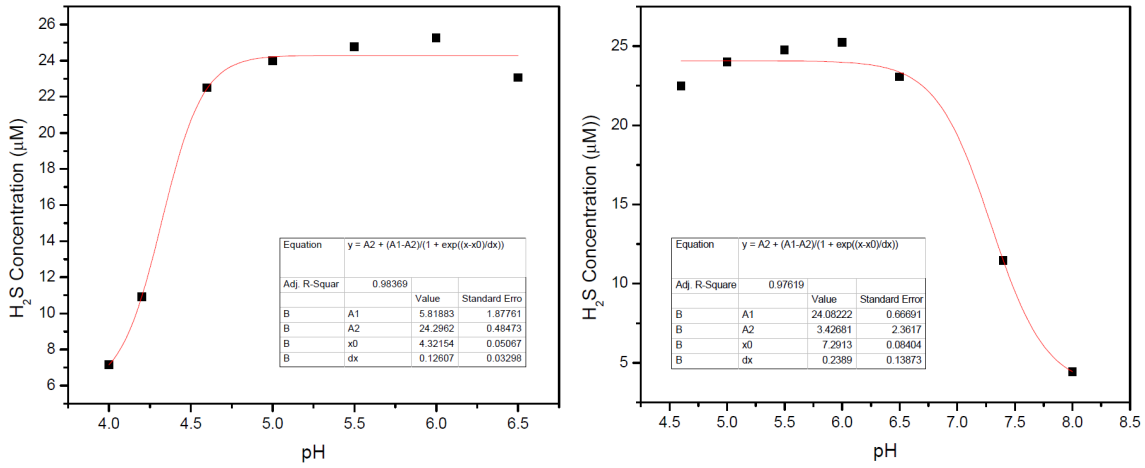

Figure A.5 Sigmoidal fits of H_2S concentration (μM) at t = 5 h across different pH values (10 mM PBS/citrate buffer, pH 4.6-8.0, CA (25 μg/mL), 37 °C).

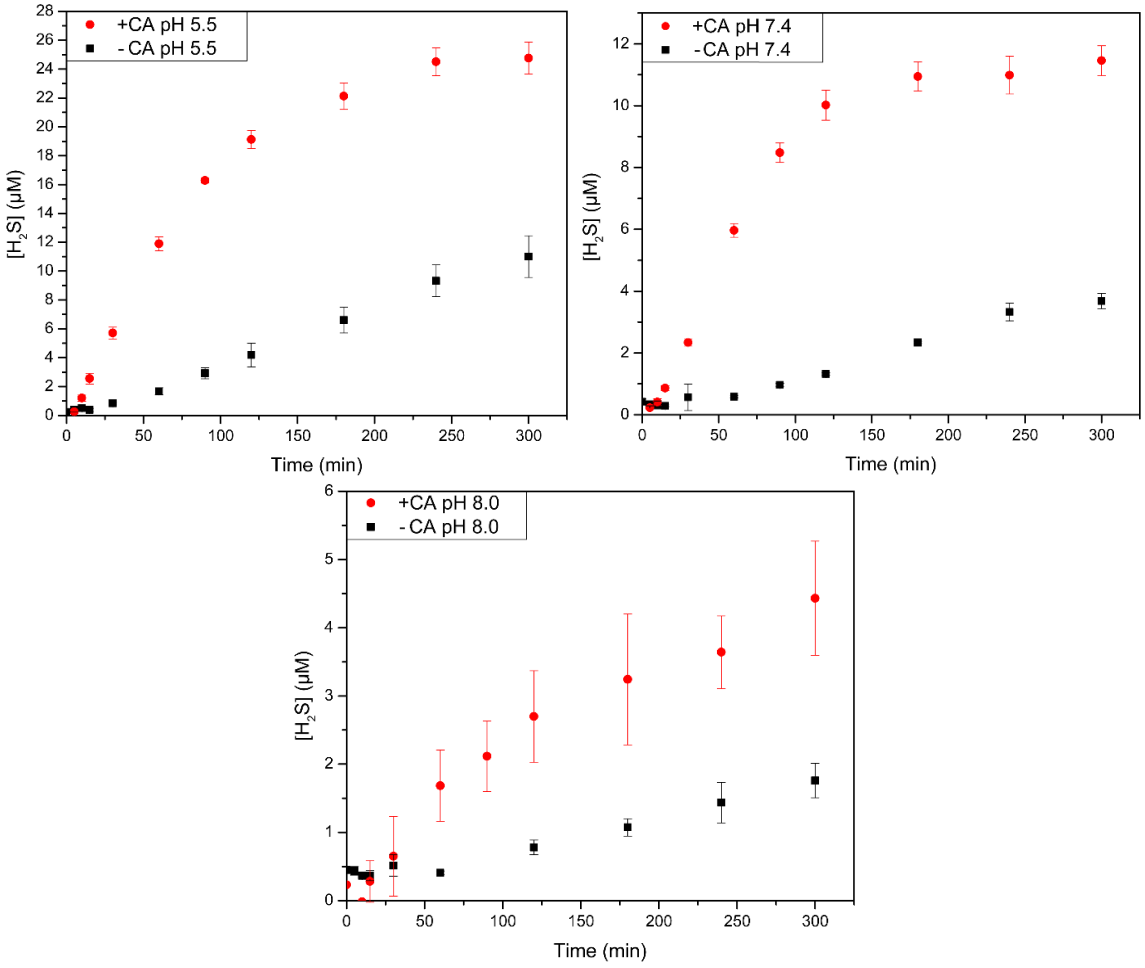

Figure A.6 H_2S release from ***S*-pHTCM** in citrate pH 5.5/PBS pH 7.4/PBS 8.0 (10 mM buffer) in the presence or absence of CA (25 μg/mL) at 37 °C. Experiments were performed in triplicate with results expressed as mean ± S.D. (n = 3).

HPLC Analysis of Release Pathway

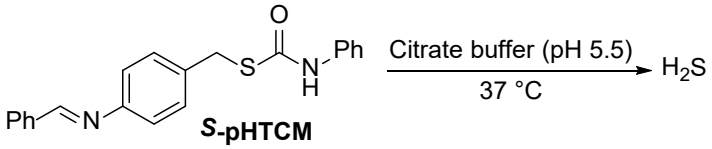

General conditions for HPLC Analysis: To 20 mL of citrate buffer (10 mM, pH 5.5), 100 µL of 10 mM ***S*-pHTCM** in DMSO was added to generate a 50 µM donor, which was stirred at 37 °C. After 5 h, a 1 mL reaction aliquot was filtered and analyzed by HPLC. An Agilent 1260 HPLC instrument with a Poroshell 120 EC-C18 4.6x100 mm column was used with products monitored at 230 nm. Solvent A: 95% H_2O, 5% MeOH, Solvent B: 100% MeCN. Gradient: 35% Solvent A/65% Solvent B for 2 min. Change to 100% Solvent B over 4 min and hold for 6.5 min. Change to 35% Solvent A/65% Solvent B over 0.5 min and hold for 4.5 min. Flow Rate: 0.5 mL/min, 2 µL injection.

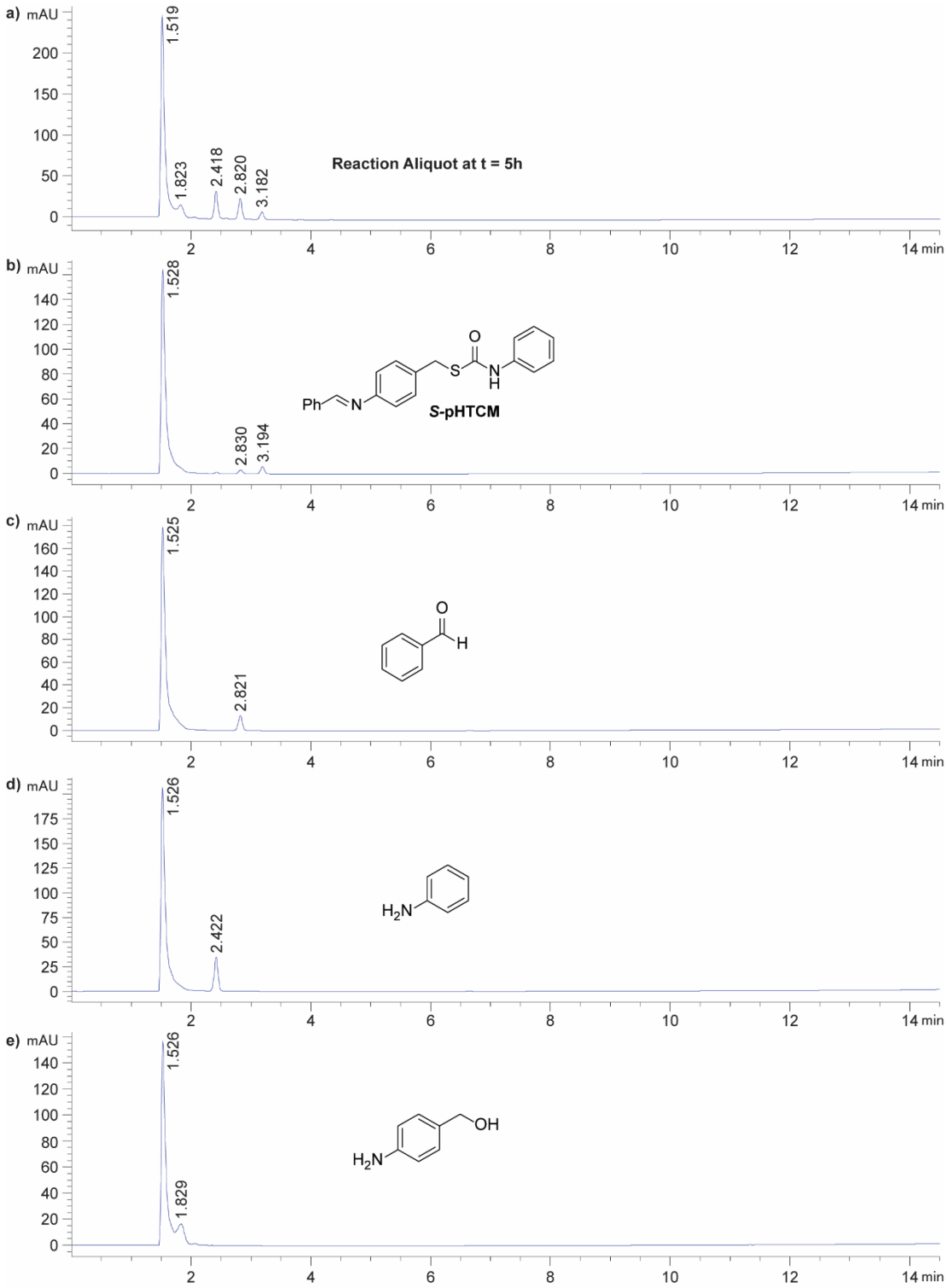

Figure A.7 (a) Reaction aliquot after 5 h. (b) ***S*-pHTCM**, (c) benzaldehyde standard, (d) aniline standard, (e) 4-aminobenzyl alcohol standard. The reaction aliquot contains 50 µM ***S*-pHTCM** in citrate buffer (10 mM, pH 5.5) at 37 °C. All other compounds analyzed at 50 µM in citrate buffer (10 mM, pH 5.5). The ***S*-pHTCM** trace contains a small amount of benzaldehyde from compound hydrolysis in the buffer within the time-frame of the measurement.

GSH Dependence at pH 7.4

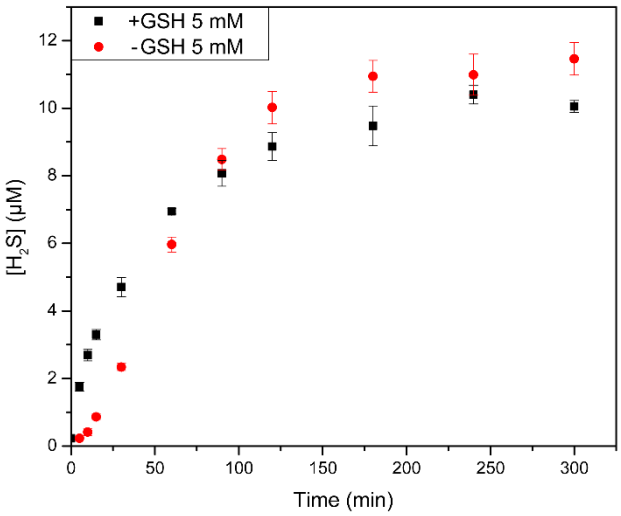

Figure A.8 H_2S release of ***S*-pHTCM** in PBS buffer (10 mM, pH 7.4) in the presence and absence of 5 mM GSH and CA (25 μg/mL) at 37 °C. Experiments were performed in quadruplicate with results expressed as mean ± S.D. (n = 4).

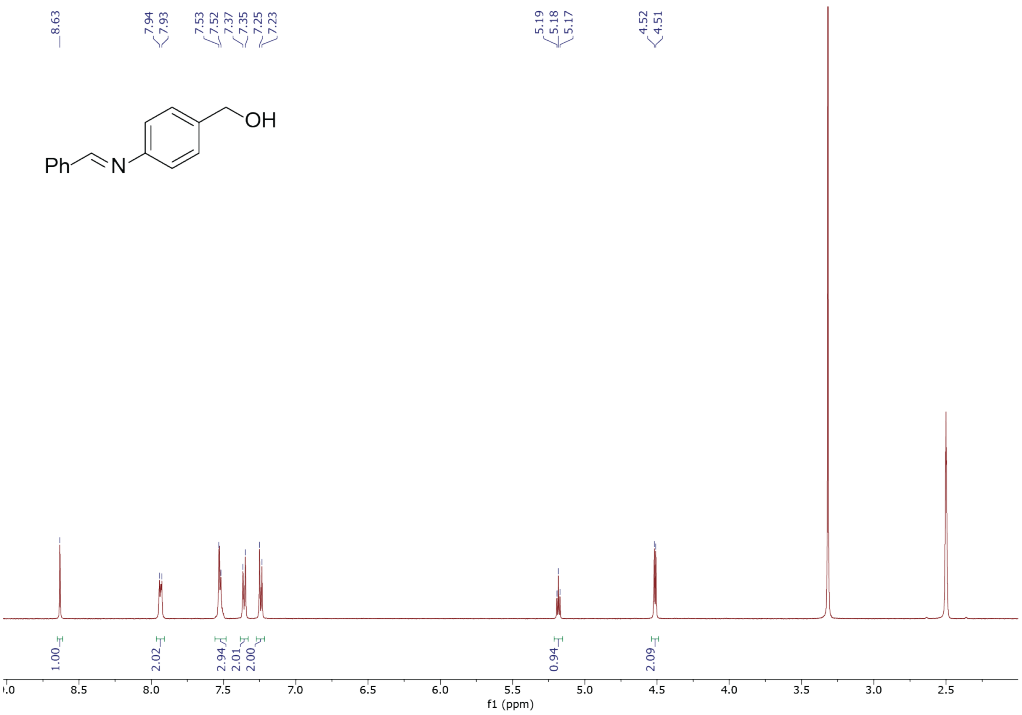

Figure A.9 ^{1}H (500 MHz, DMSO-d_6) NMR spectrum of 4-(benzylideneamino)benzyl alcohol.

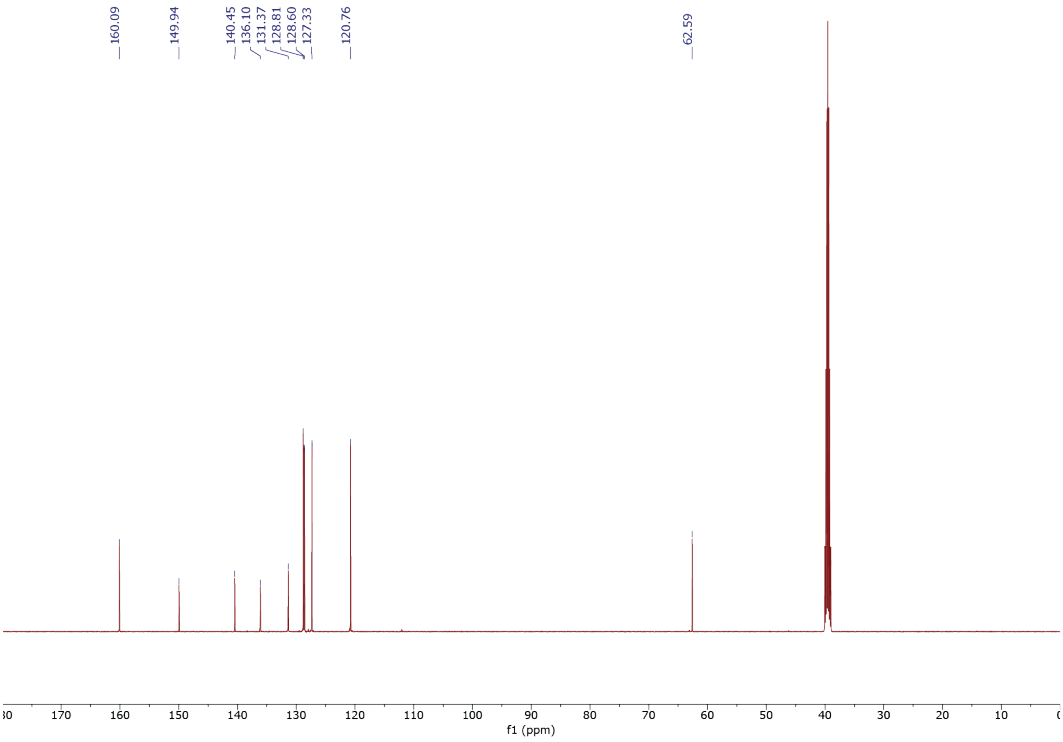

Figure A.10 ^{13}C{^{1}H} (126 MHz, DMSO-d_6) NMR spectrum of 4-(benzylideneamino)benzyl alcohol.

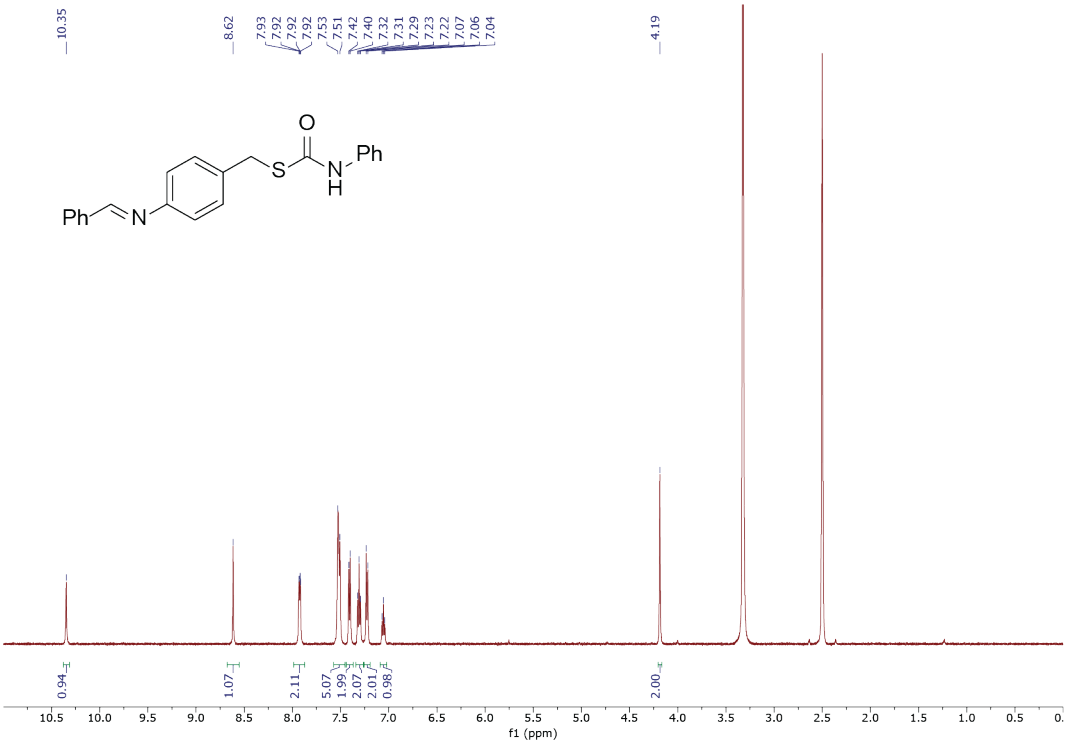

Figure A.11 ^{1}H (500 MHz, DMSO-d_6) NMR spectrum of ***S*-pHTCM**.

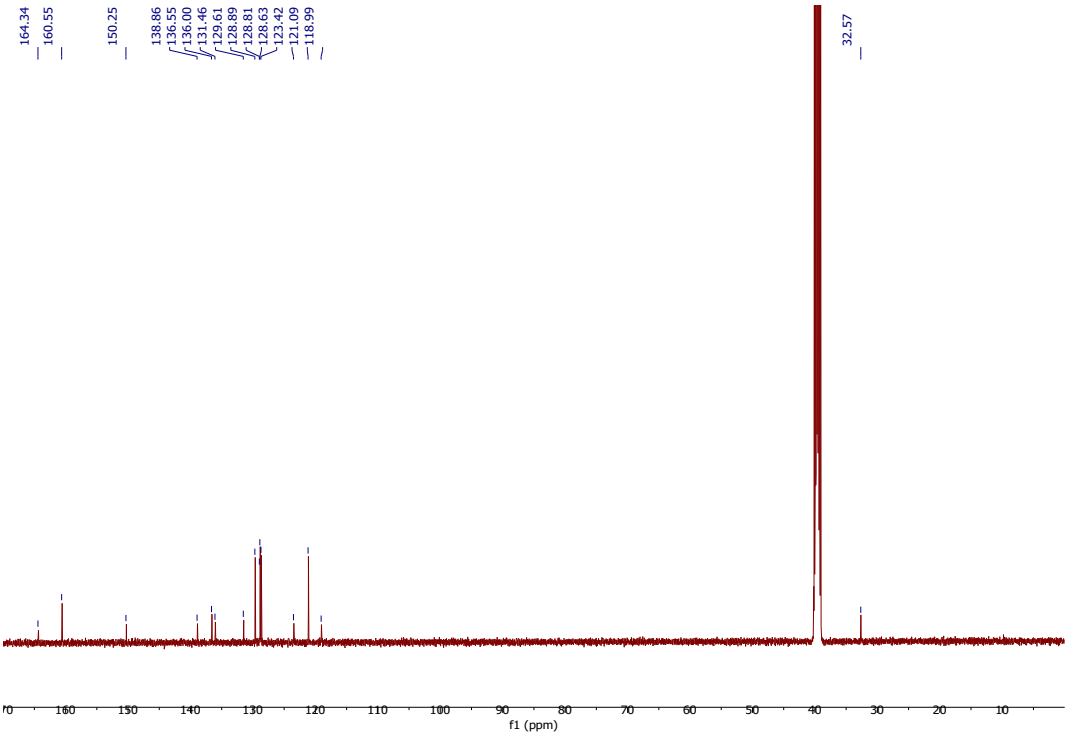

Figure A.12 ^{13}C{^{1}H} (126 MHz, DMSO-d_6) NMR spectrum of ***S*-pHTCM**.

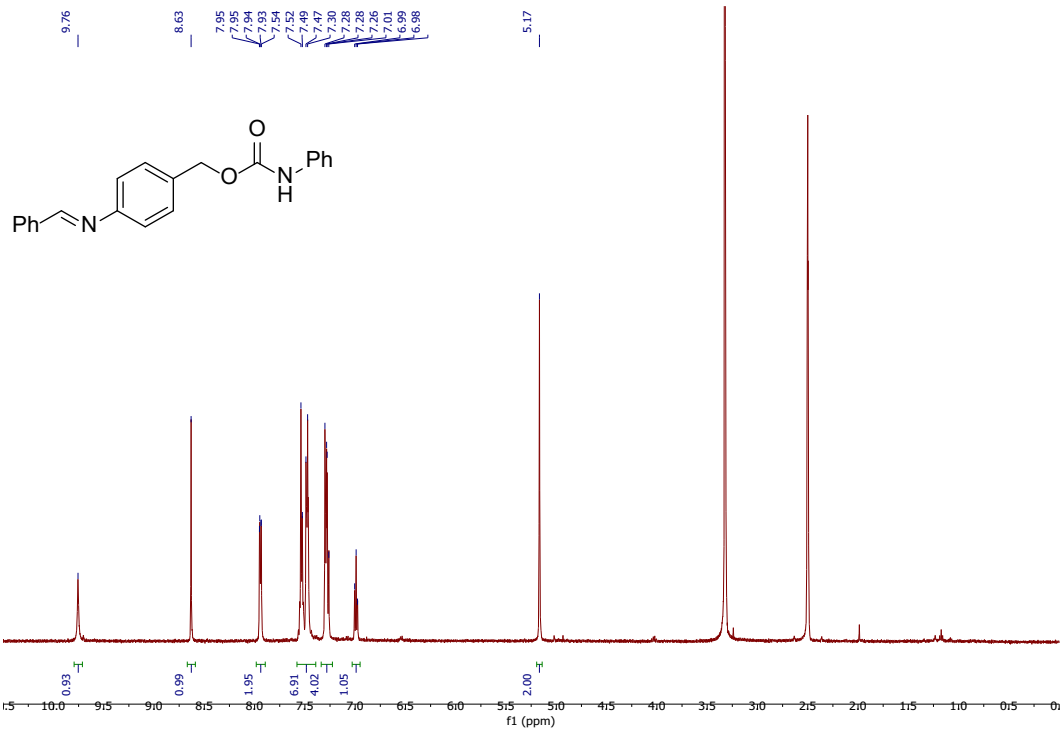

Figure A.13 ^{1}H (500 MHz, DMSO-d_6) NMR spectrum of **pHCM**.

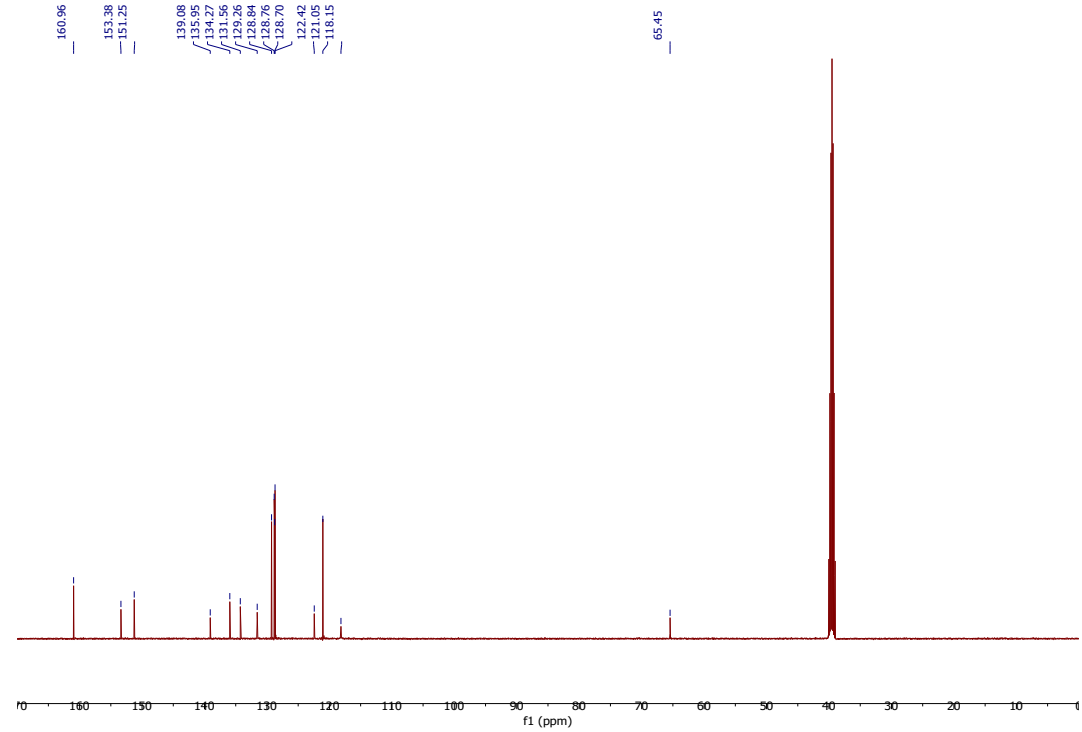

Figure A.14 ^{13}C{^{1}H} (126 MHz, DMSO-d_6) NMR spectrum of **pHCM**.

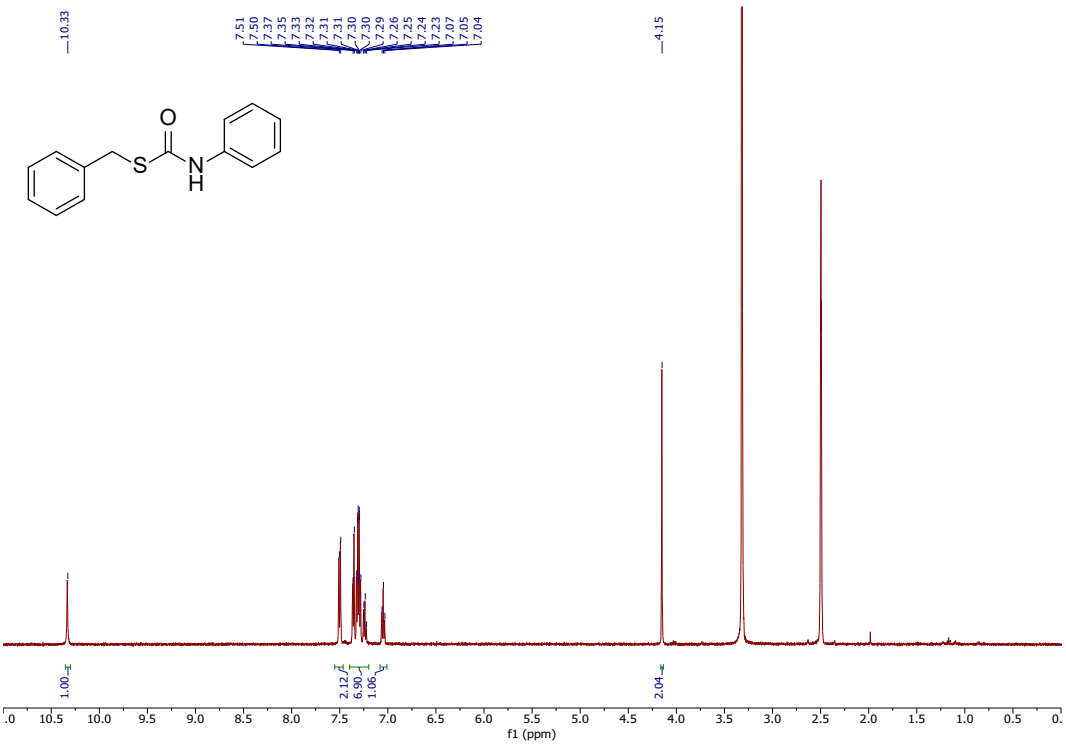

Figure A.15 ^{1}H (500 MHz, DMSO-d_6) NMR spectrum of ***S*-TCM**.

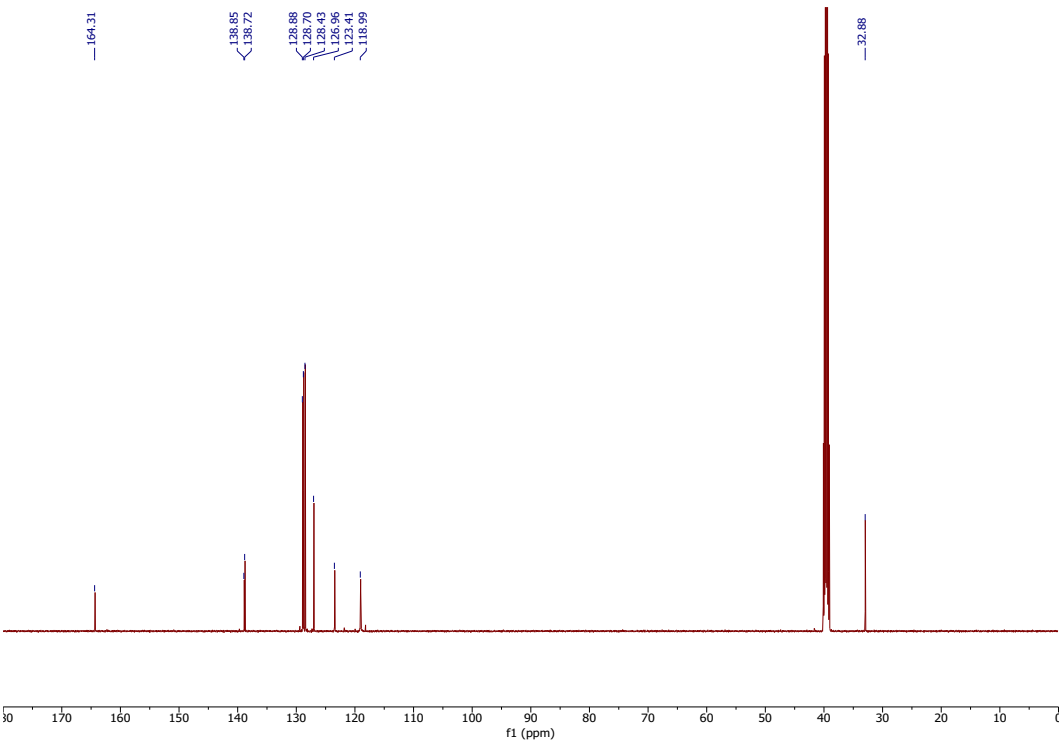

Figure A.16 ^{13}C{^{1}H} (126 MHz, DMSO-d_6) NMR spectrum of ***S*-TCM**.

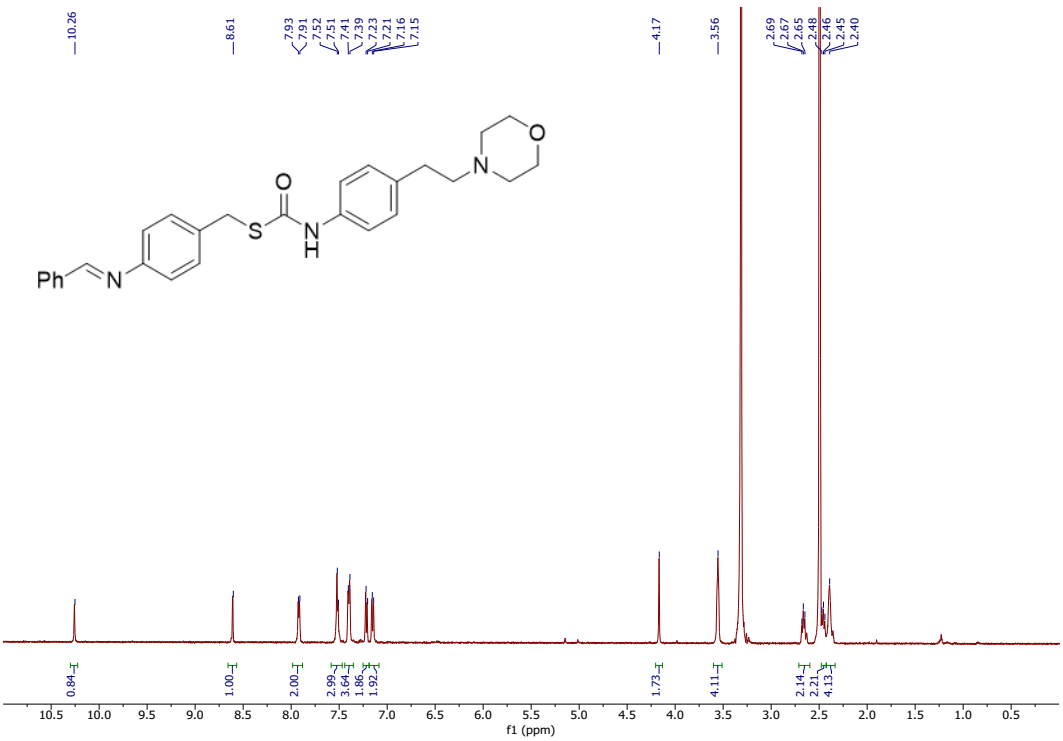

Figure A.17 ^{1}H (500 MHz, DMSO-d_6) NMR spectrum of **Lyso-pHTCM**.

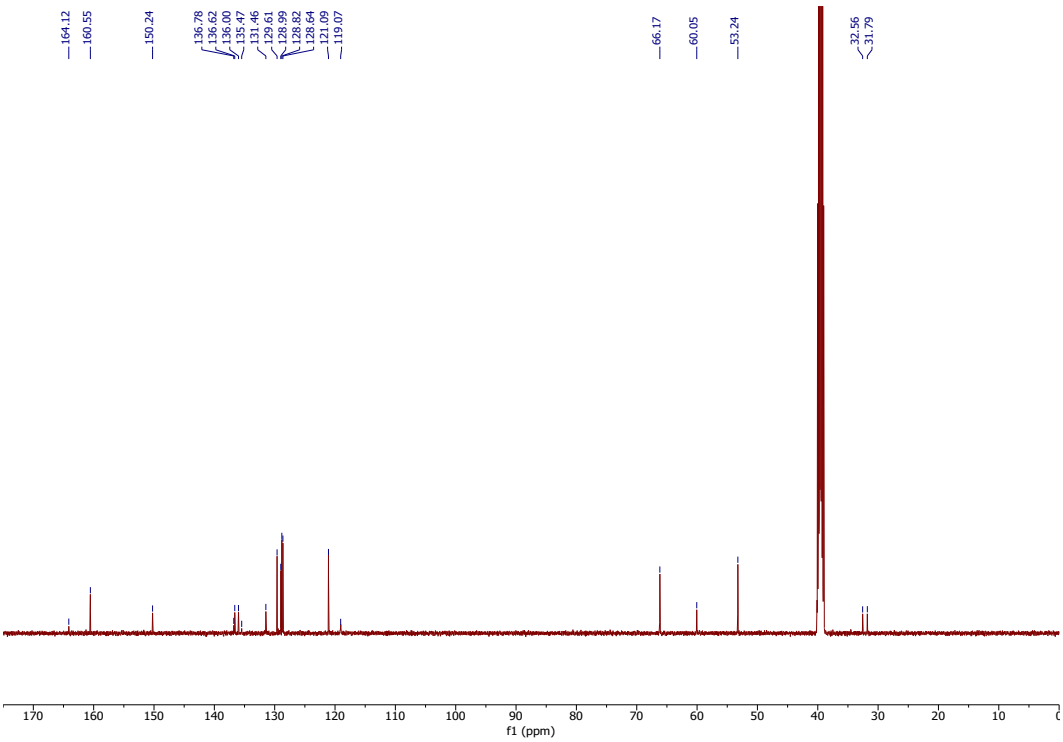

Figure A.18 ^{13}C{^{1}H} (126 MHz, DMSO-d_6) NMR spectrum of **Lyso-pHTCM**.

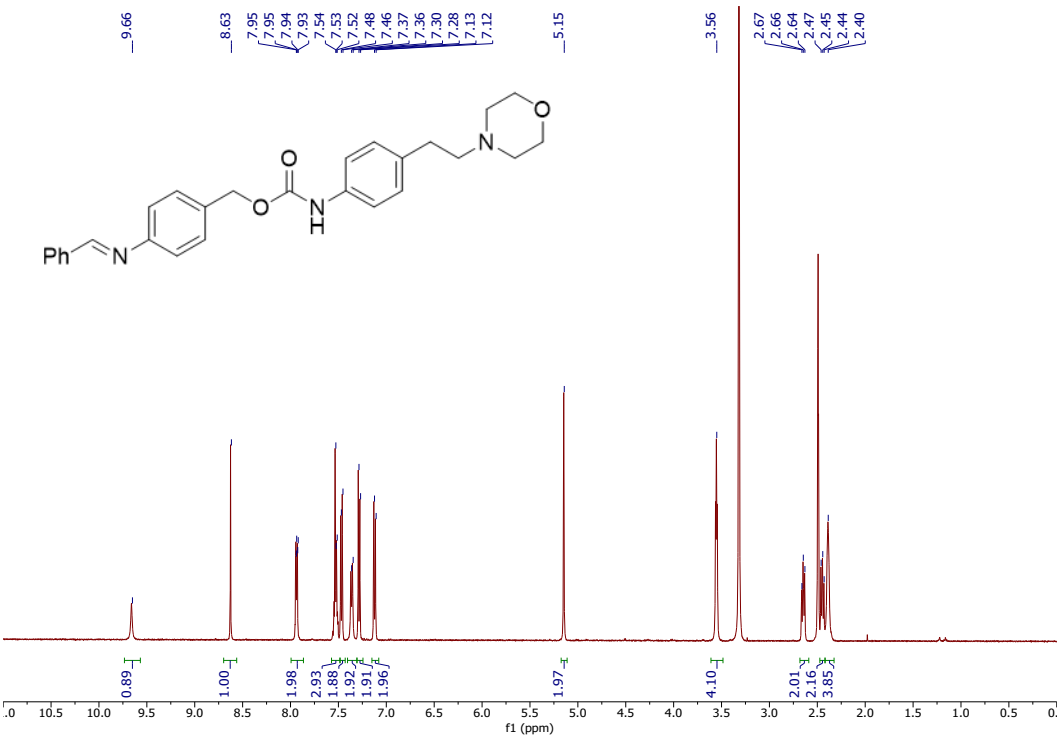

Figure A.19 ^{1}H (500 MHz, DMSO-d_6) NMR spectrum of **Lyso-pHCM**.

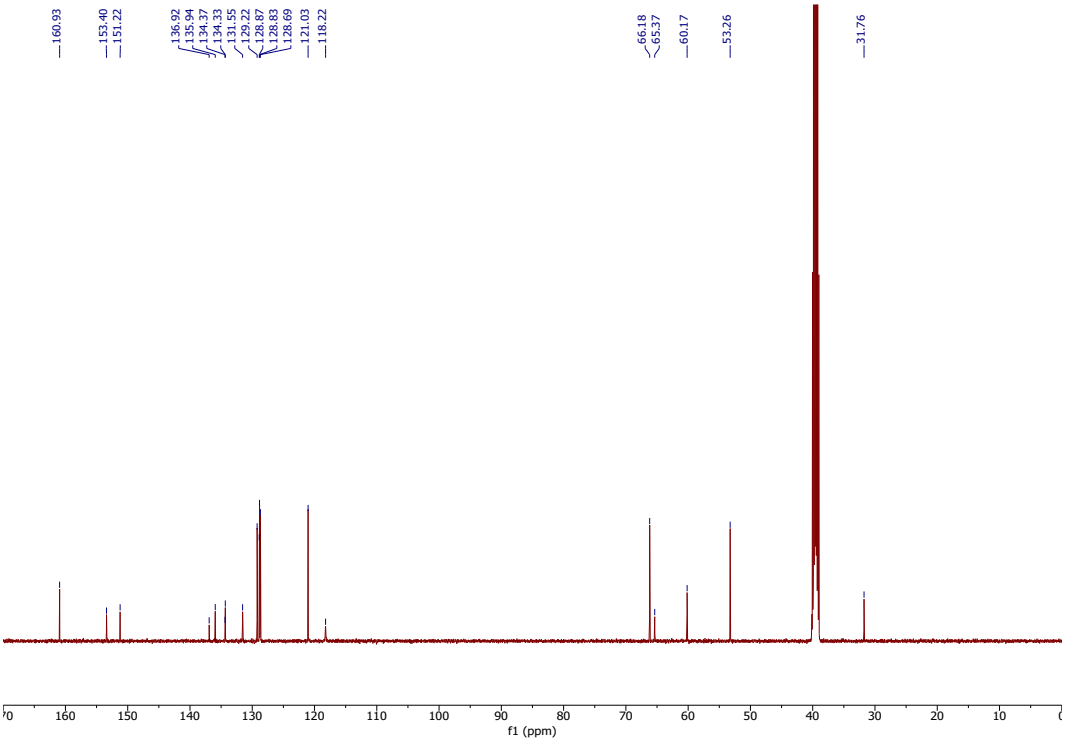

Figure A.20 ^{13}C{^{1}H} (126 MHz, DMSO-d_6) NMR spectrum of **Lyso-pHCM**.

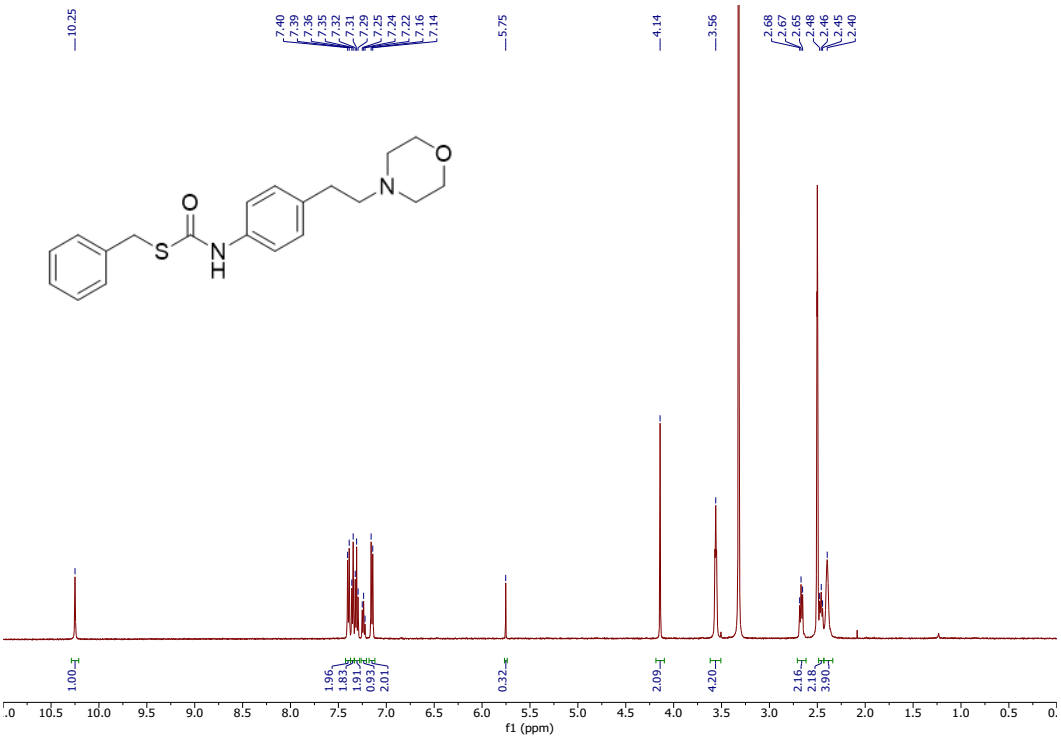

Figure A.21 ^{1}H (500 MHz, DMSO-d_6) NMR spectrum of **Lyso-TCM**.

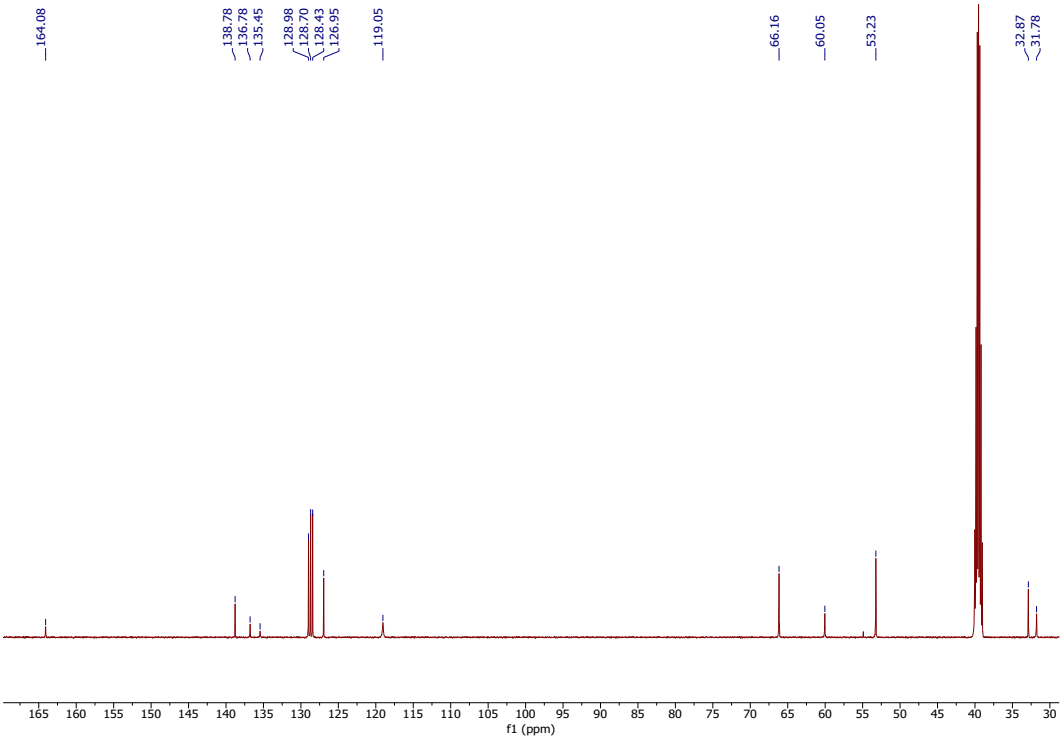

Figure A.22 ^{13}C{^{1}H} (126 MHz, DMSO-d_6) NMR spectrum of **Lyso-TCM**.

APPENDIX B

SUPPLEMENTARY CONTENT FOR CHAPTER III

Appendix B is the supplementary appendix for Chapter III of this dissertation. It includes all spectra relevant to the material in Chapter III.

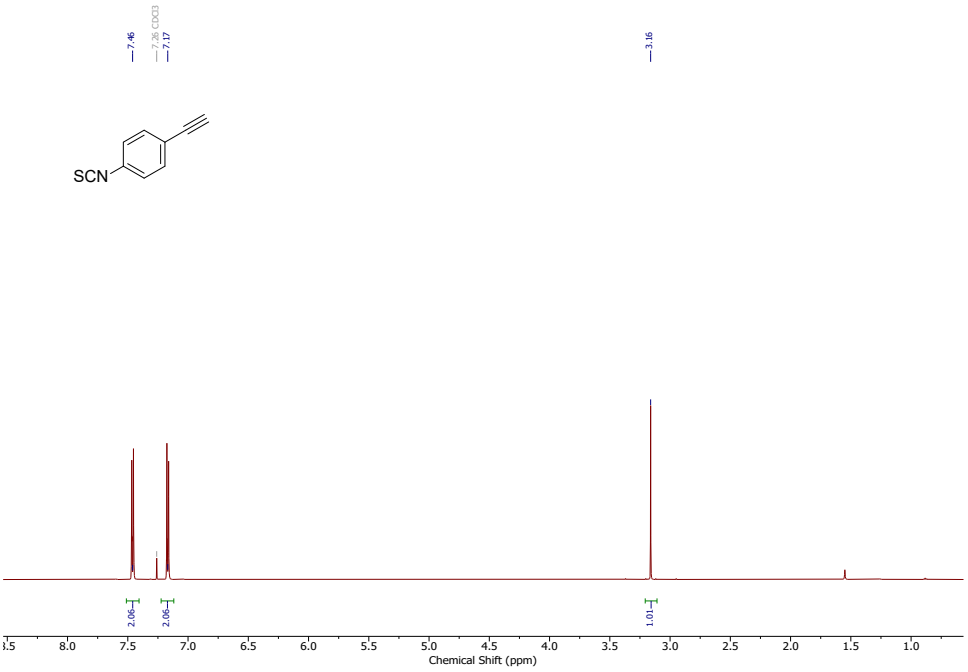

Figure B.1 ^{1}H NMR (600 MHz, $CDCl_3$) spectrum of 1-ethynyl-4-isothiocyanatobenzene.

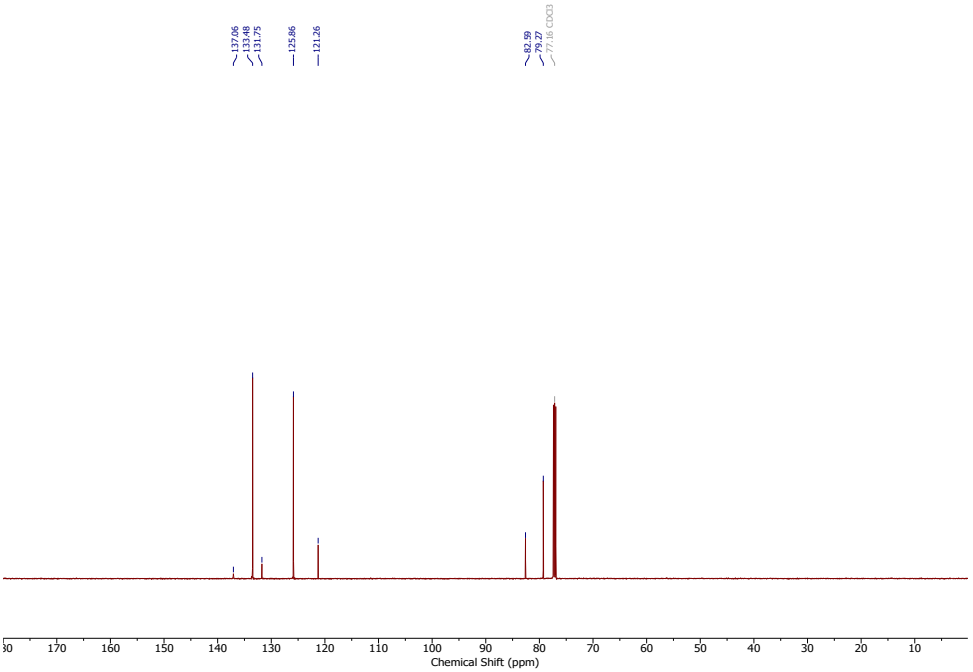

Figure B.2 $^{13}C\{H\}$ NMR (151 MHz, $CDCl_3$) spectrum of 1-ethynyl-4-isothiocyanatobenzene.

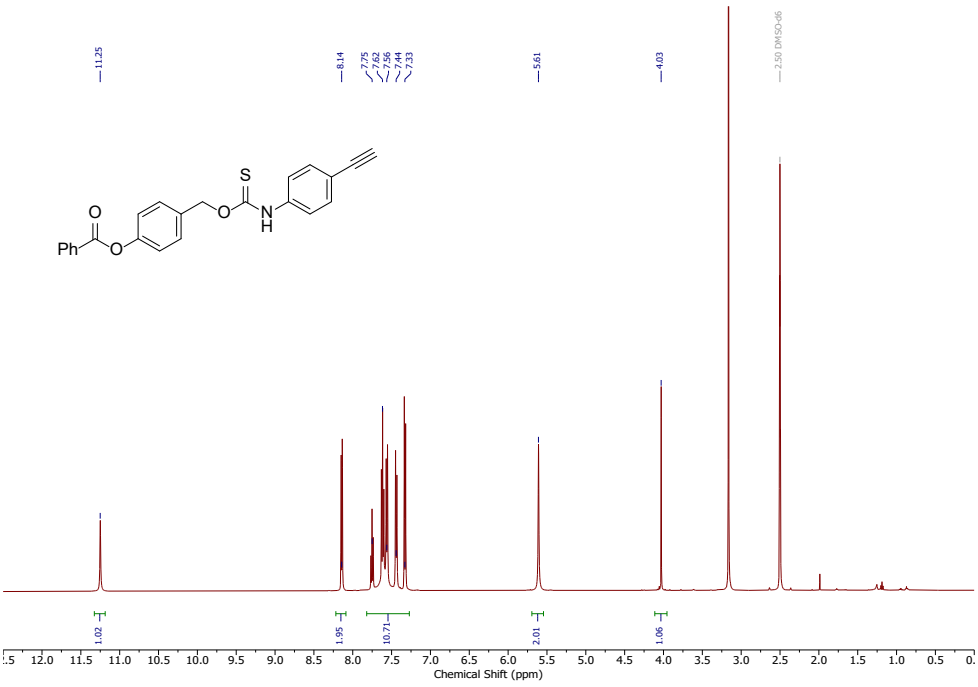

Figure B.3 ^{1}H NMR (500 MHz, DMSO-d_6, 60 °C) spectrum of **TCM alkyne**.

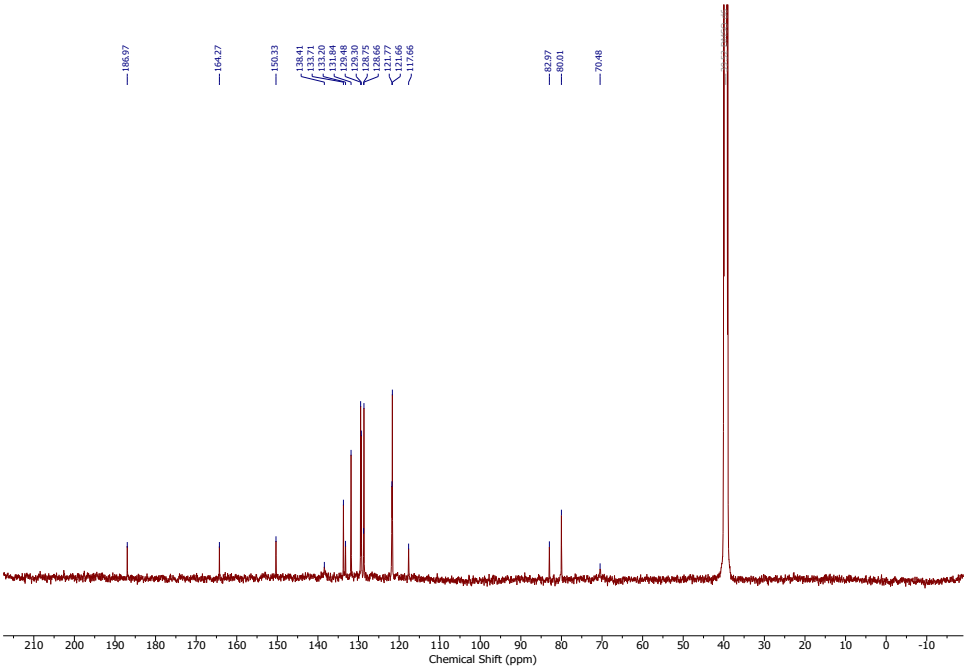

Figure B.4 $^{13}C\{H\}$ NMR (126 MHz, DMSO-d_6, 60 °C) spectrum of **TCM alkyne**.

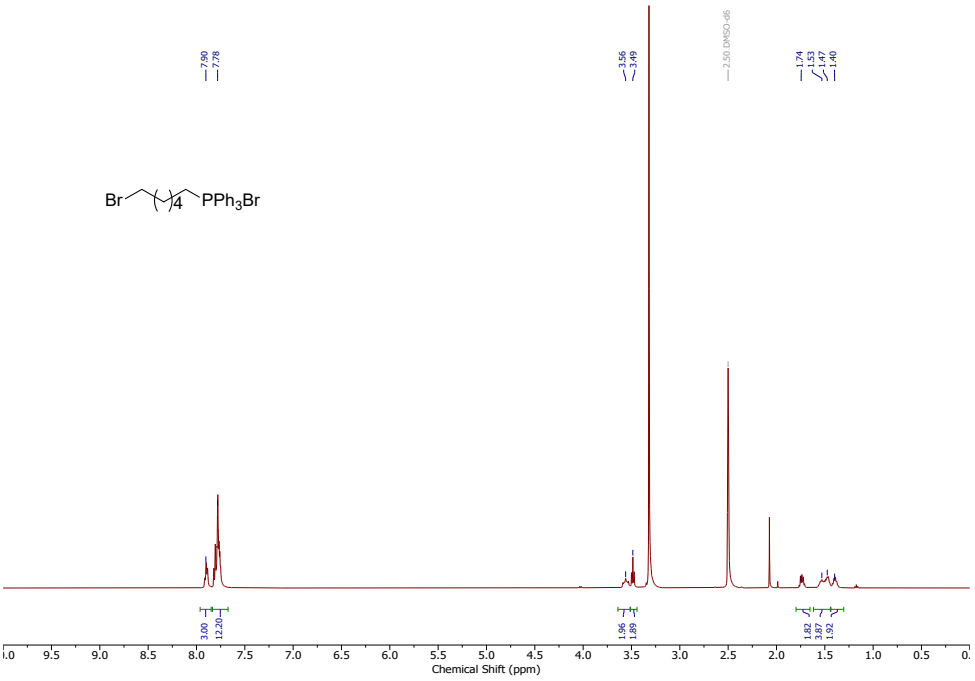

Figure B.5 ^{1}H NMR (500 MHz, DMSO-d_6) spectrum of (6-bromohexyl)triphenylphosphonium bromide.

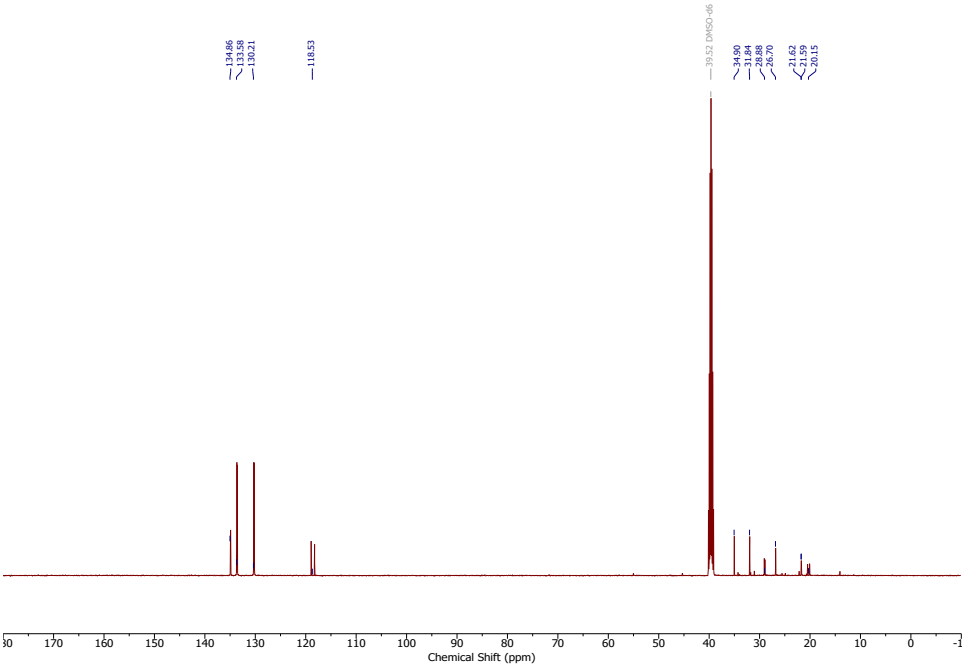

Figure B.6 $^{13}C\{H\}$ NMR (126 MHz, DMSO-d_6) spectrum of (6-bromohexyl) triphenylphosphonium bromide.

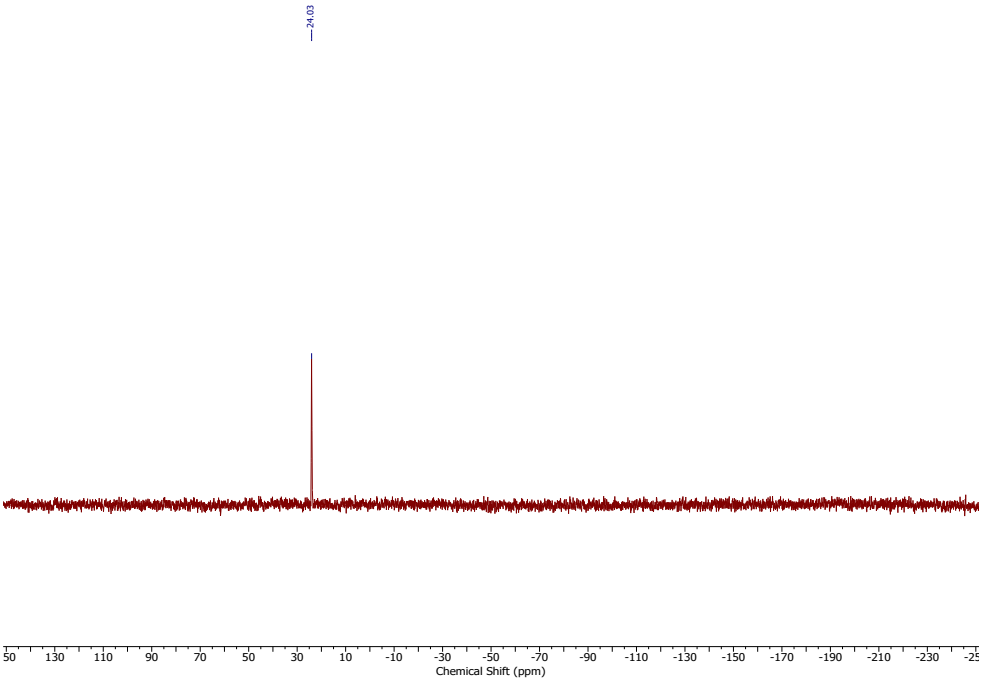

Figure B.7 $^{31}P\{H\}$ NMR (202 MHz, DMSO-d_6) spectrum of (6-bromohexyl) triphenylphosphonium bromide.

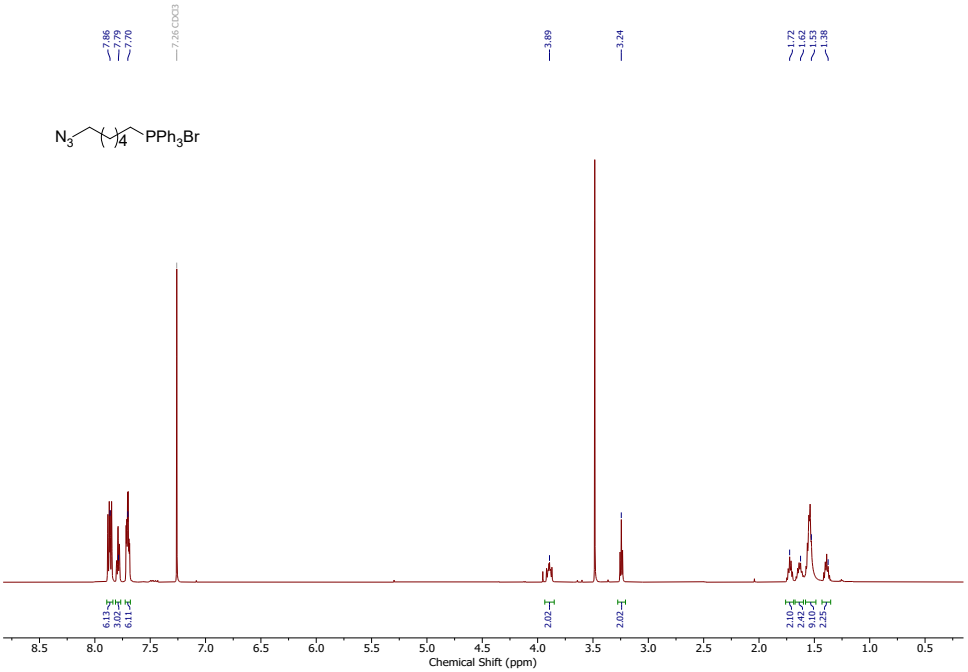

Figure B.8 ^{1}H NMR (500 MHz, DMSO-d_6) spectrum of (6-azidohexyl)triphenylphosphonium bromide.

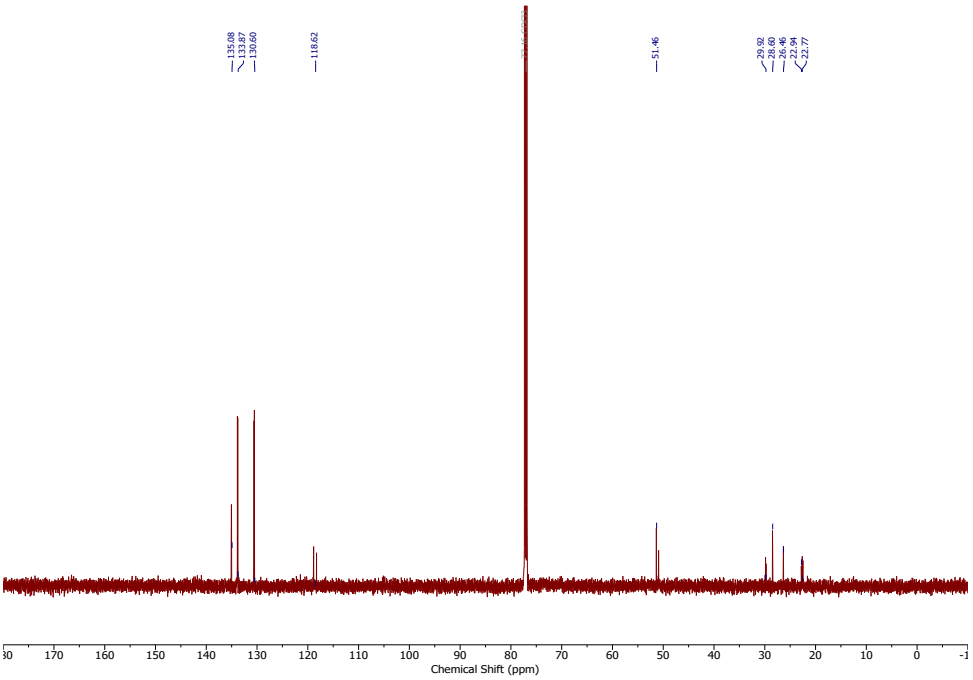

Figure B.9 ^{13}C{H} NMR (151 MHz, $CDCl_3$) spectrum of (6-azidohexyl)triphenylphosphonium bromide.

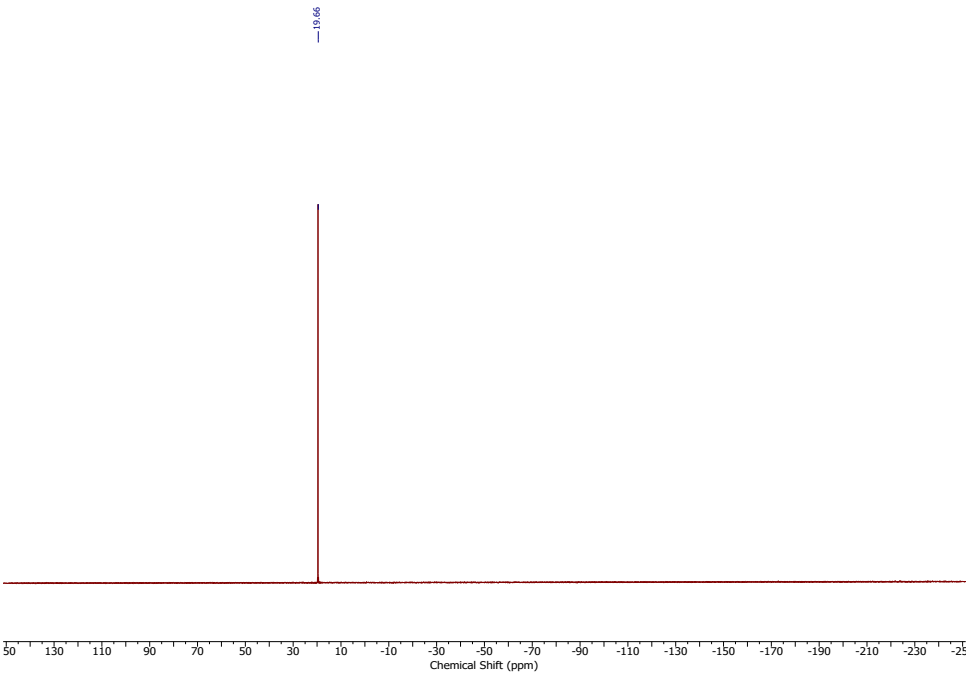

Figure B.10 $^{31}P\{H\}$ NMR (202 MHz, $CDCl_3$) spectrum of (6-azidohexyl)triphenylphosphonium bromide.

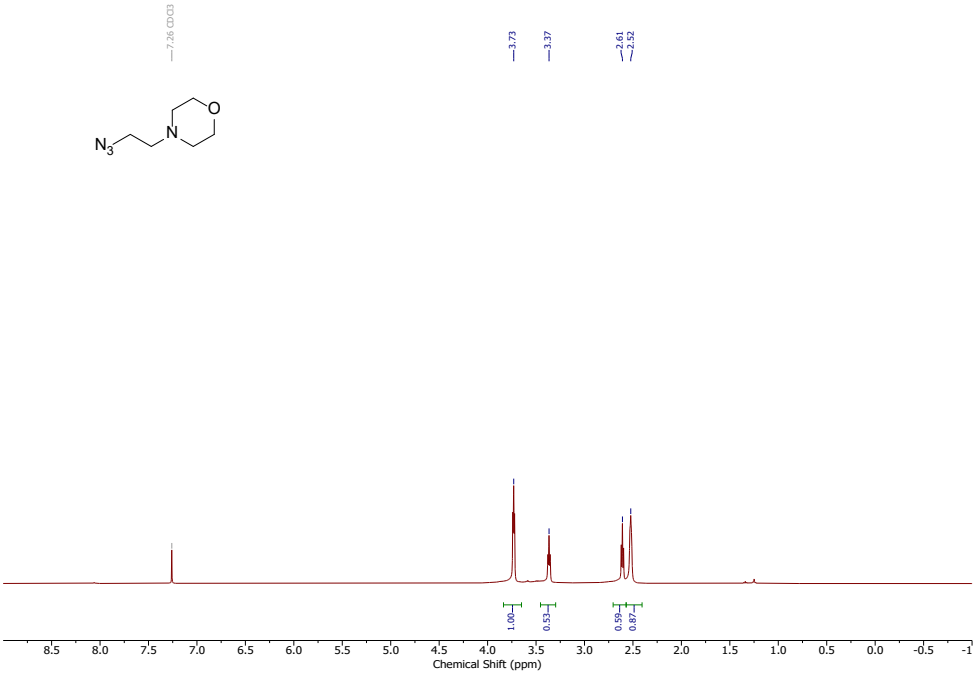

Figure B.11 ^{1}H NMR (500 MHz, $CDCl_3$) spectrum of 4-(2-azidoethyl)morpholine.

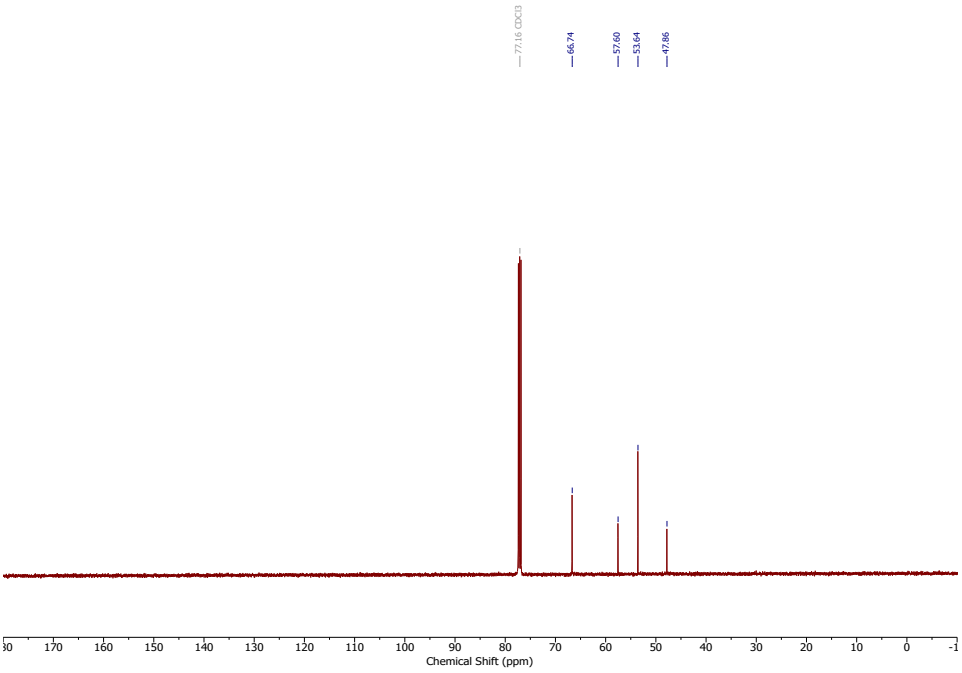

Figure B.12 $^{13}C\{H\}$ NMR (126 MHz, $CDCl_3$) spectrum of 4-(2-azidoethyl)morpholine.

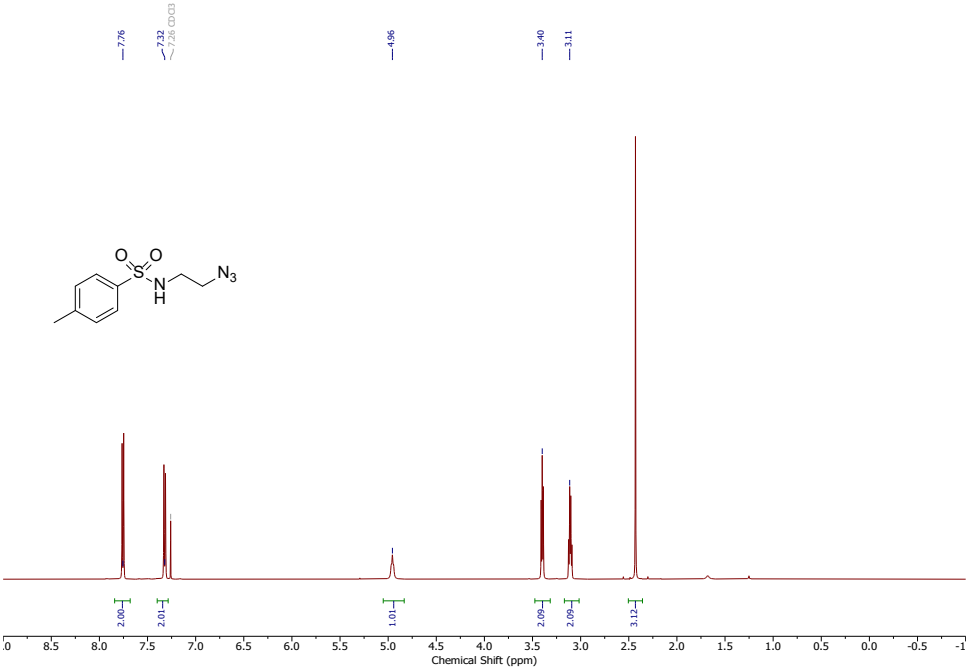

Figure B.13 ^{1}H NMR (500 MHz, $CDCl_3$) spectrum of *N*-(2-azidoethyl)-4-methylbenzenesulfonamide.

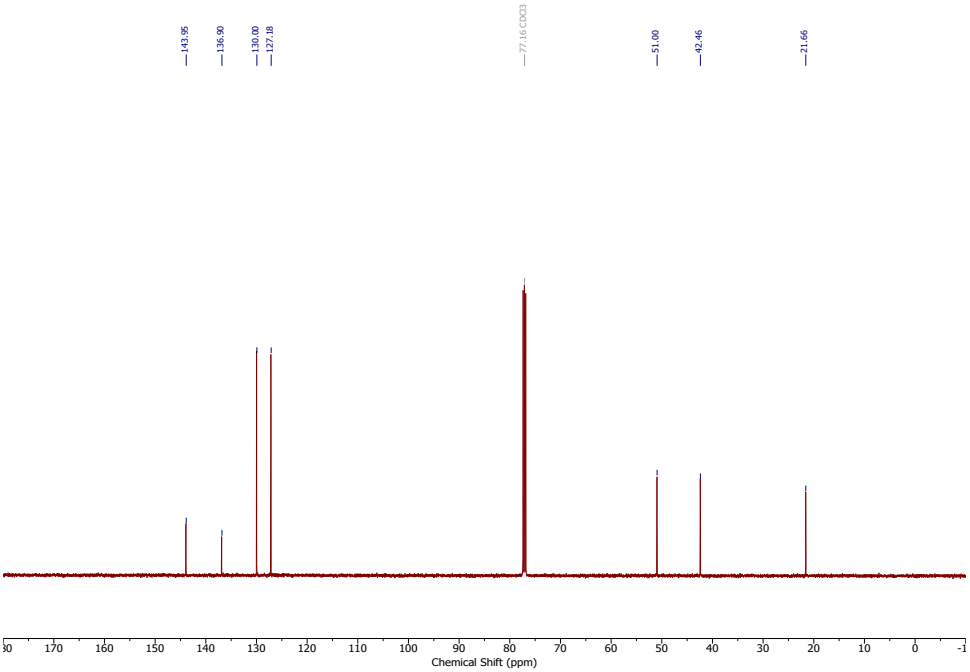

Figure B.14 $^{13}C\{H\}$ NMR (126 MHz, $CDCl_3$) spectrum of *N*-(2-azidoethyl)-4-methylbenzenesulfonamide.

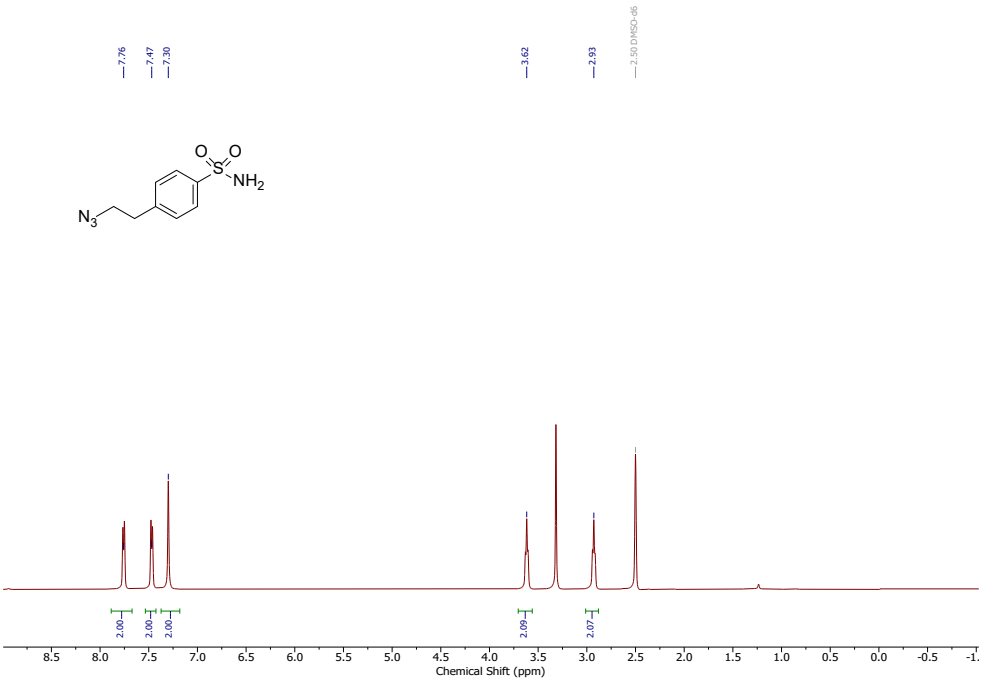

Figure B.15 ^{1}H NMR (500 MHz, $CDCl_3$) spectrum of 4-(2-azidoethyl)-benzenesulfonamide.

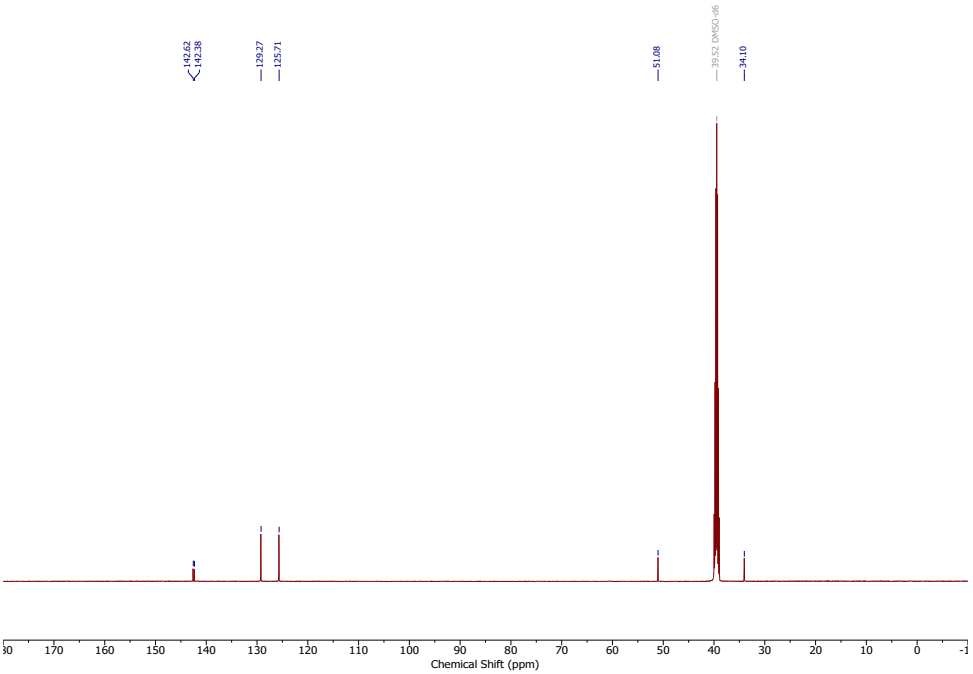

Figure B.16 $^{13}C\{H\}$ NMR (126 MHz, $CDCl_3$) spectrum of 4-(2-azidoethyl)-benzenesulfonamide.

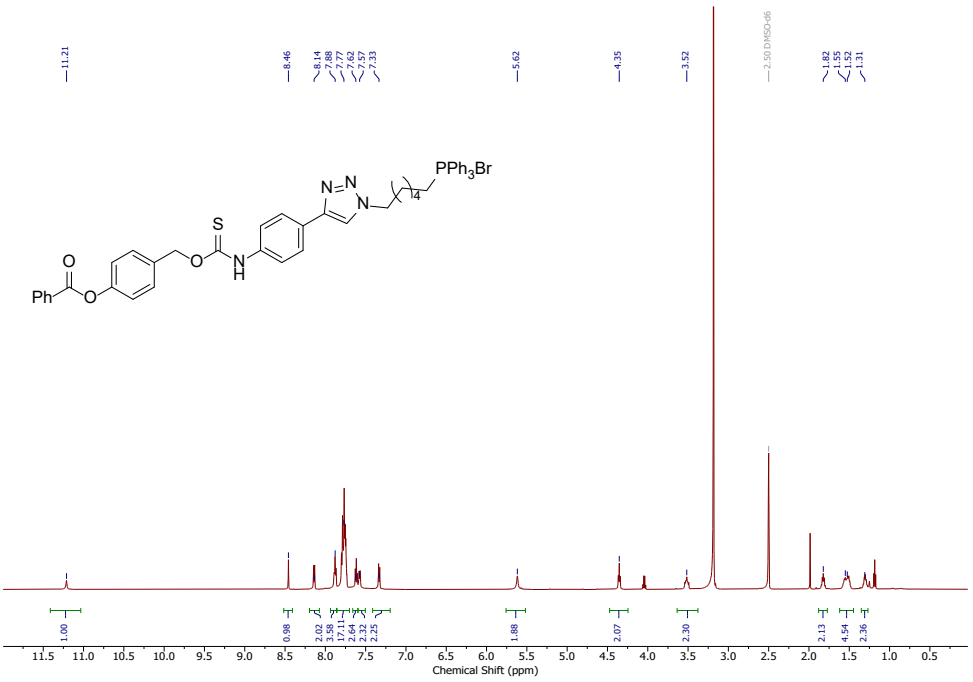

Figure B.17 ^{1}H NMR (600 MHz, DMSO-d_6, 60 °C) spectrum of **MitoTCM**.

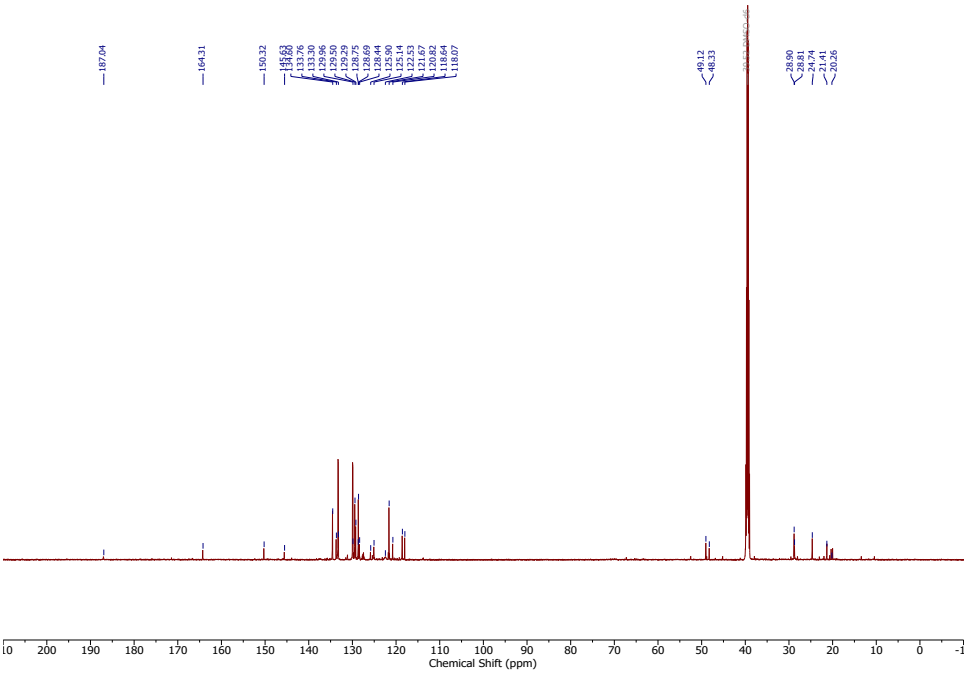

Figure B.18 ^{13}C NMR (126 MHz, DMSO-d_6, 60 °C) spectrum of **MitoTCM**.

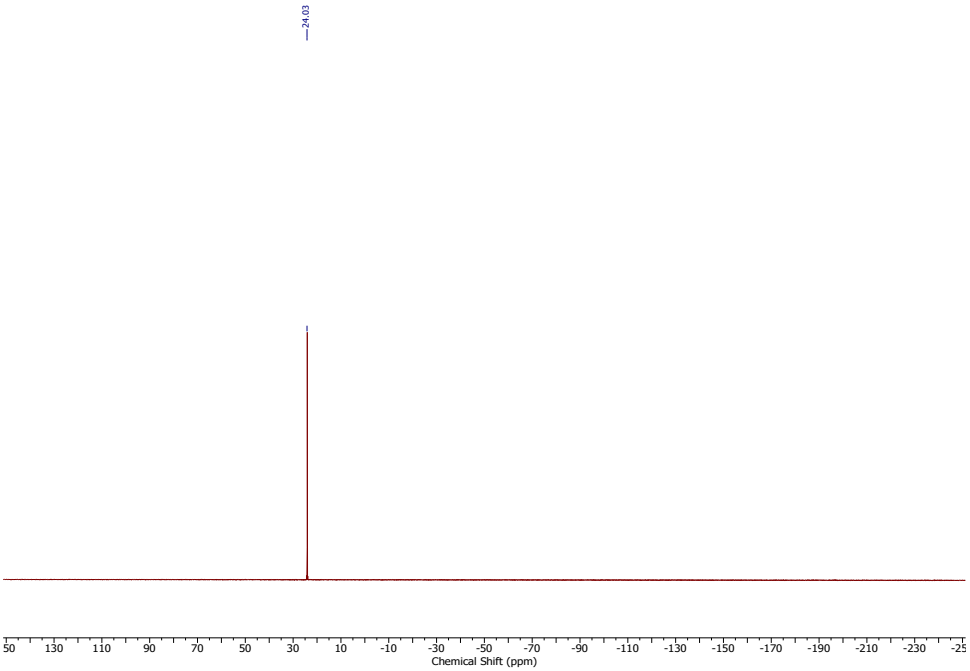

Figure B.19 ^{31}P{H} NMR (202 MHz, DMSO-d_6, 60 °C) spectrum of **MitoTCM**.

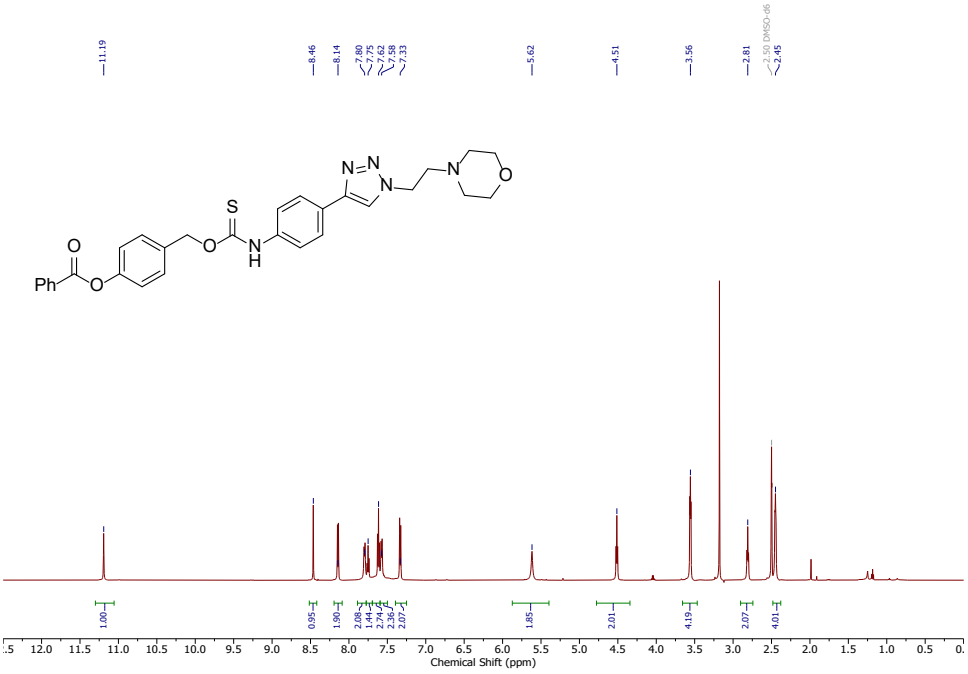

Figure B.20 ^{1}H NMR (600 MHz, DMSO-d_6, 60 °C) spectrum of **LysoTCM**.

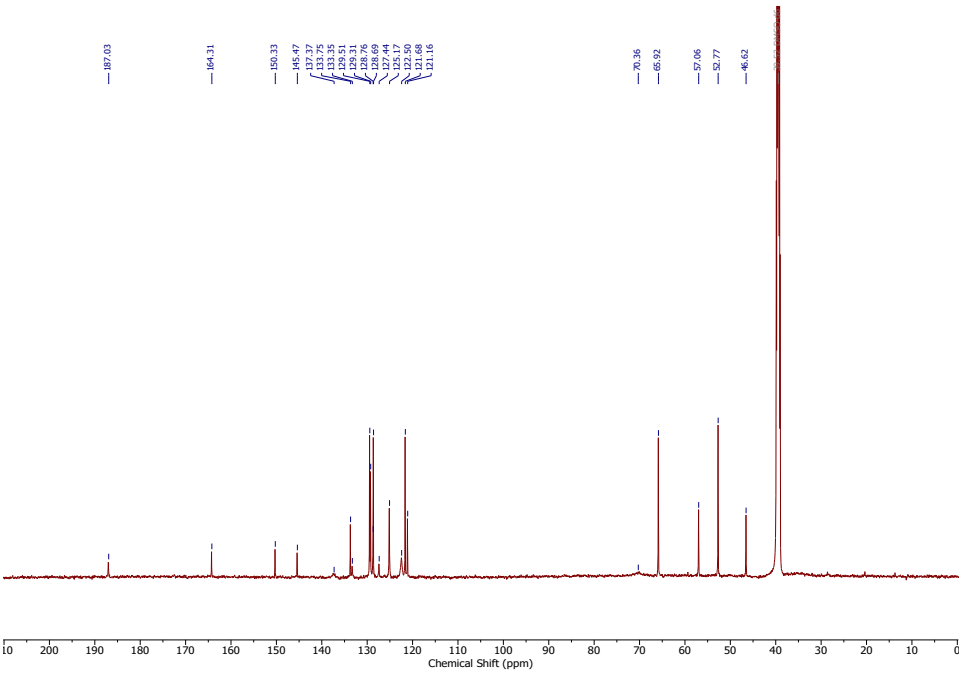

Figure B.21 ^{13}C{H} NMR (151 MHz, DMSO-d_6, 60 °C) spectrum of **LysoTCM**.

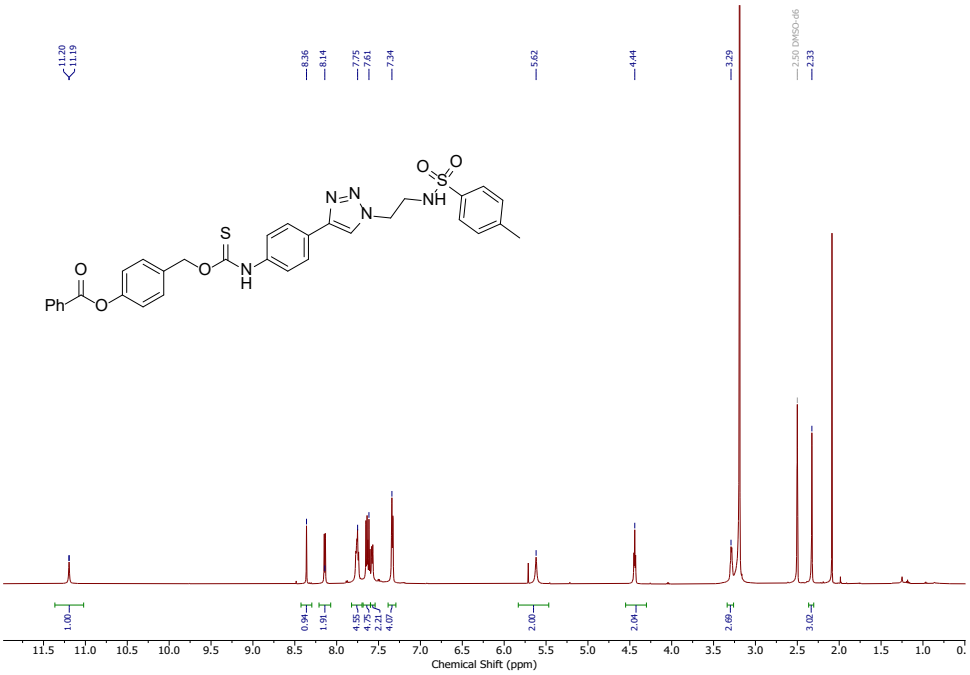

Figure B.22 ^{1}H NMR (600 MHz, DMSO-d_6, 60 °C) spectrum of **ERTCM**.

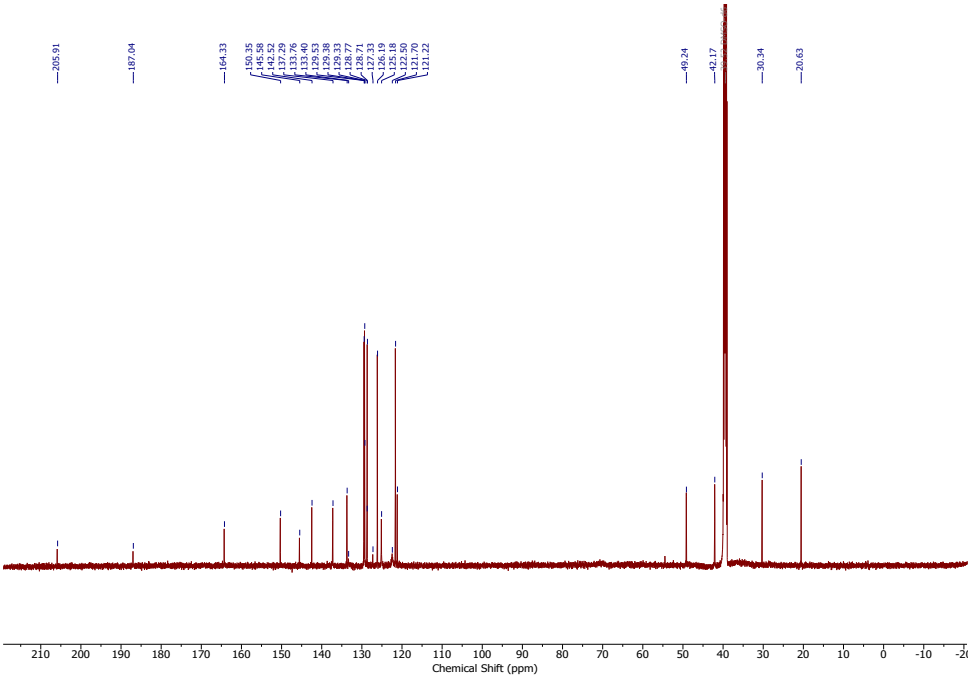

Figure B.23 ^{13}C{H} NMR (151 MHz, DMSO-d_6, 60 °C) spectrum of **ERTCM**.

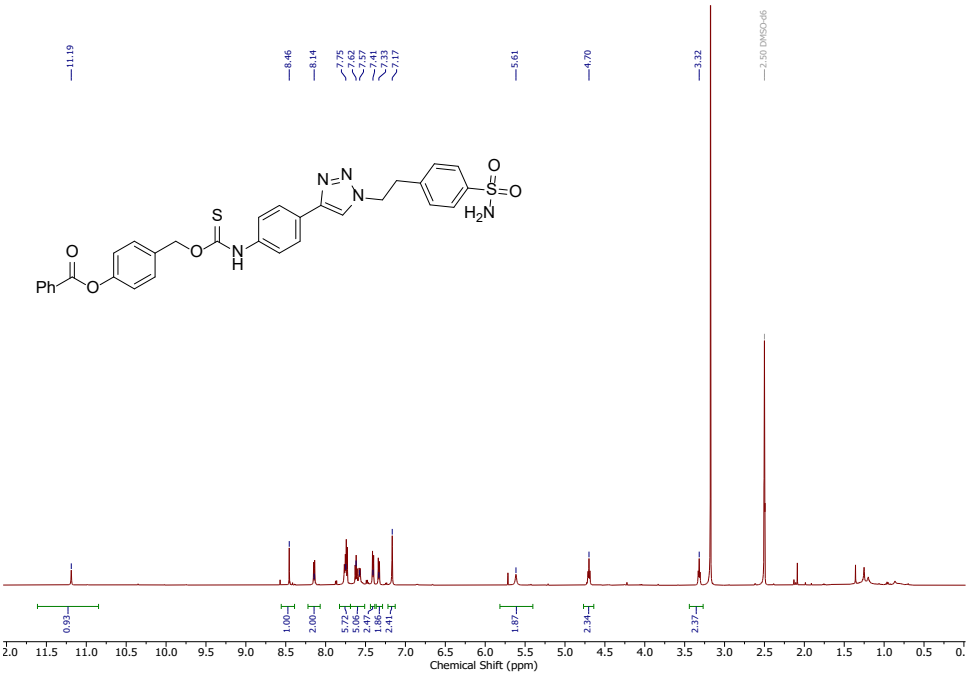

Figure B.24 ^{1}H NMR (600 MHz, DMSO-d_6, 60 °C) spectrum of **GolgiTCM**.

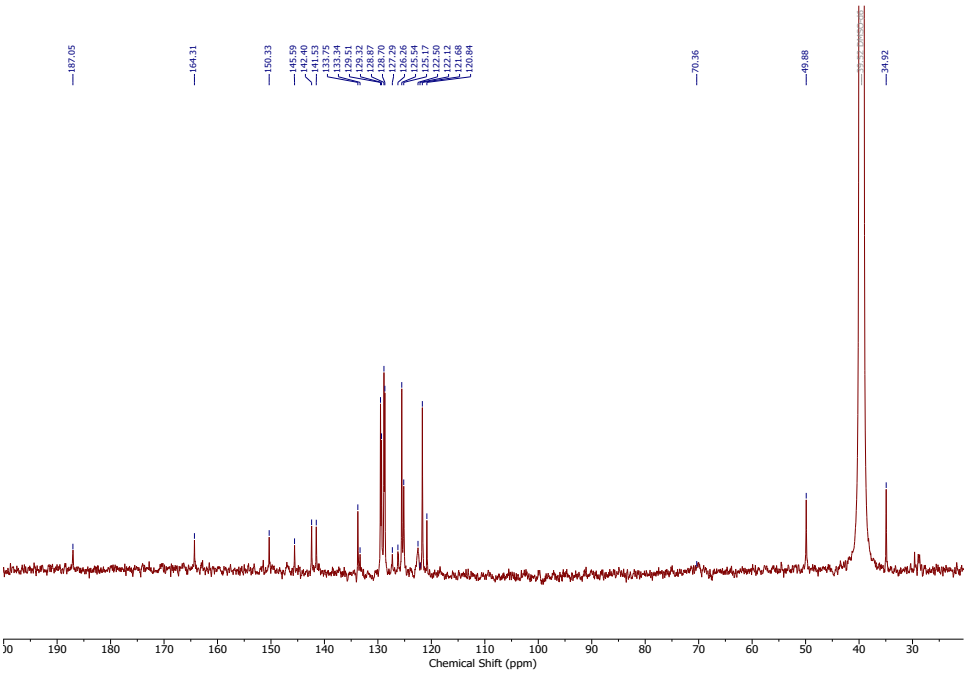

Figure B.25 ^{13}C{H} NMR (151 MHz, DMSO-d_6, 60 °C) spectrum of **GolgiTCM**.

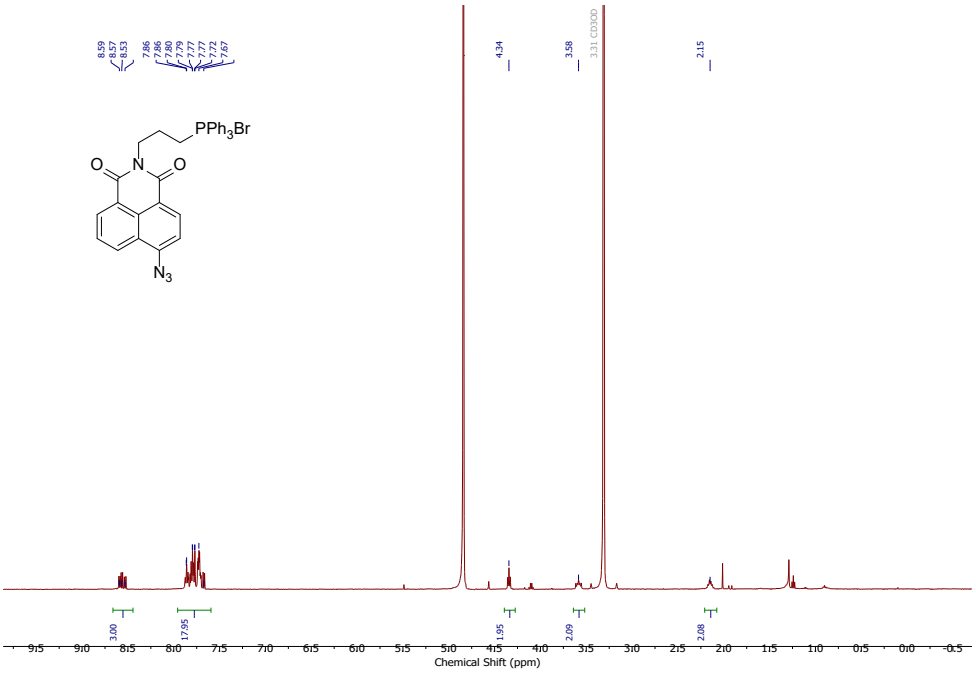

Figure B.26 ^{1}H NMR (500 MHz, CD_3OD) spectrum of Mito-HS.

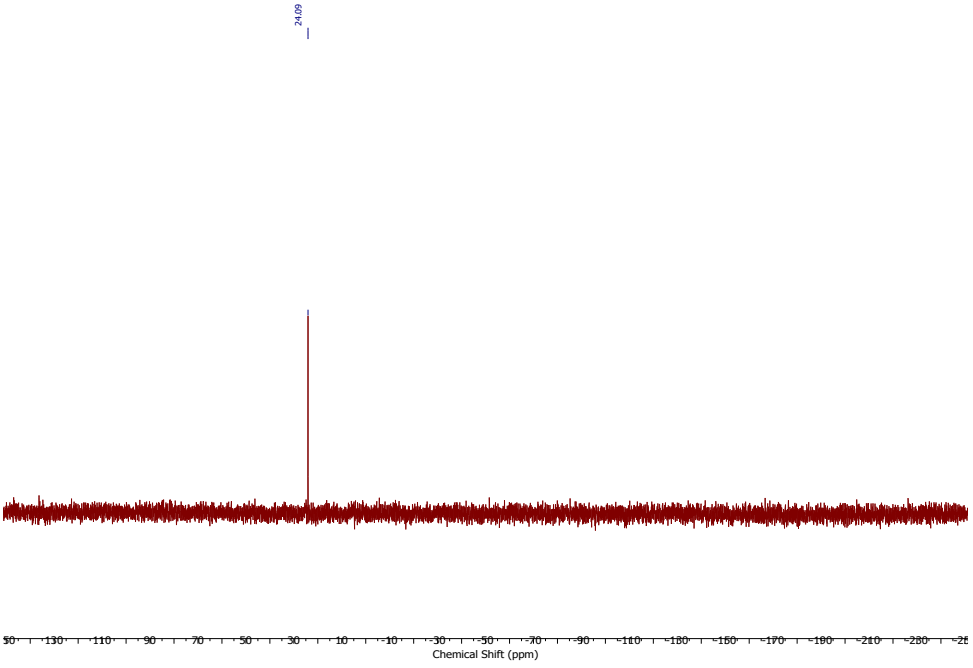

Figure B.27 ^{31}P NMR (202 MHz, CD_3OD) spectrum of Mito-HS.

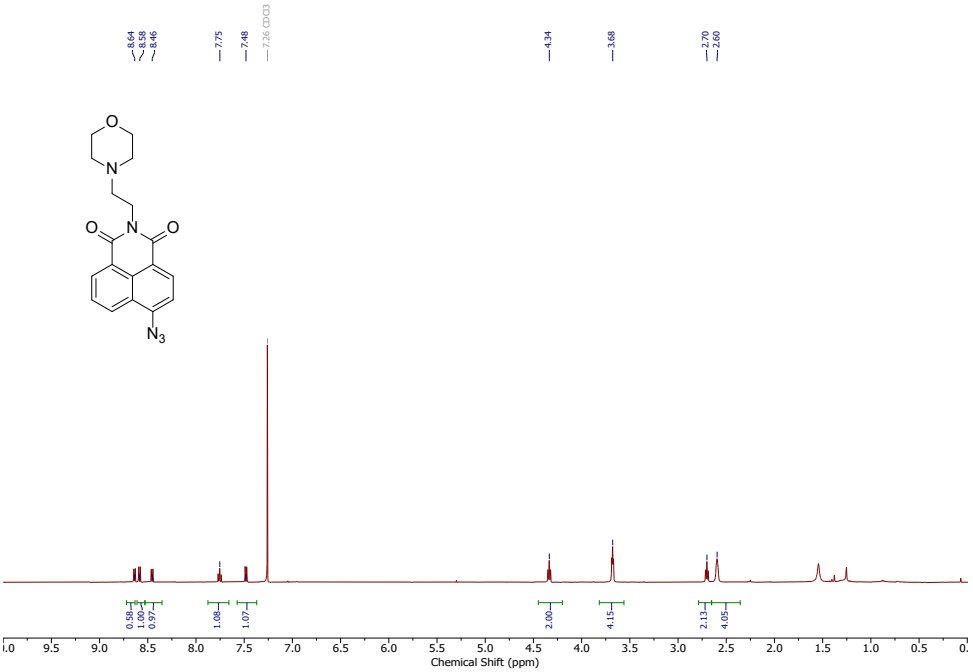

Figure B.28 ^{1}H NMR (500 MHz, $CDCl_3$) spectrum of Lyso-AFP.

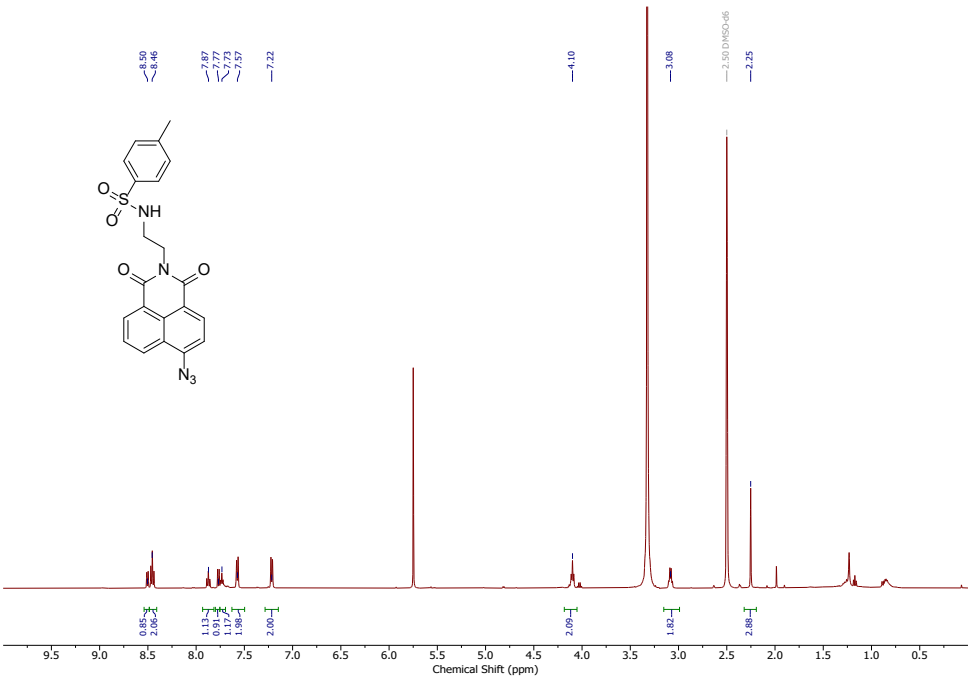

Figure B.29 ^{1}H NMR (500 MHz, DMSO-d_6) spectrum of Na-H_2S-ER.

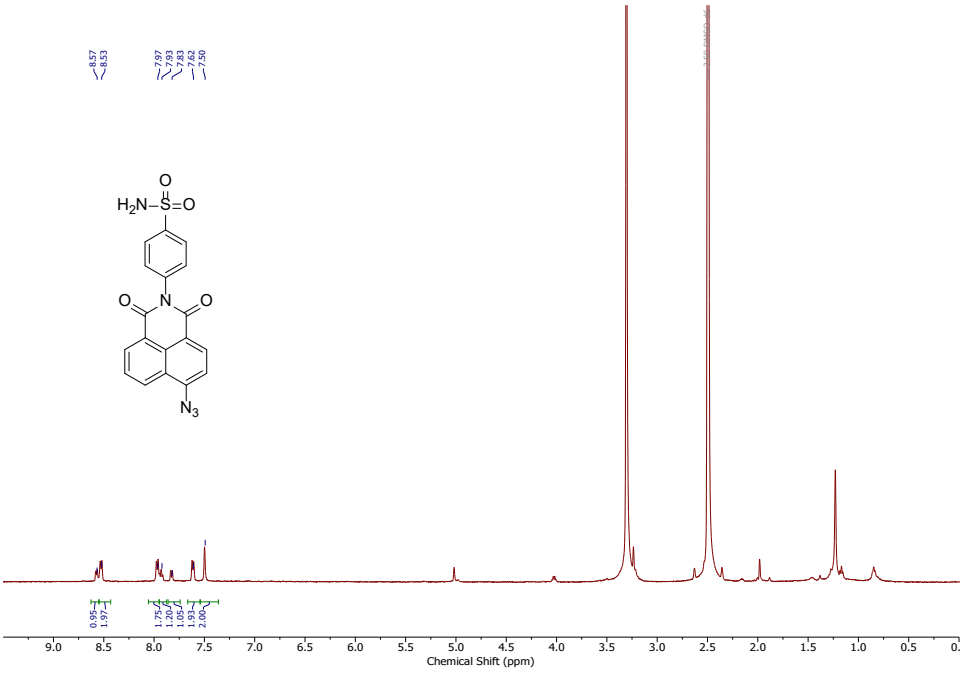

Figure B.30 ^{1}H NMR (500 MHz, DMSO-d_6) spectrum of Golgi-NH.

APPENDIX C

SUPPLEMENTARY CONTENT FOR CHAPTER V

Appendix C is the supplementary appendix for Chapter V of this dissertation. It includes all spectra and supplemental information relevant to the material in Chapter V.

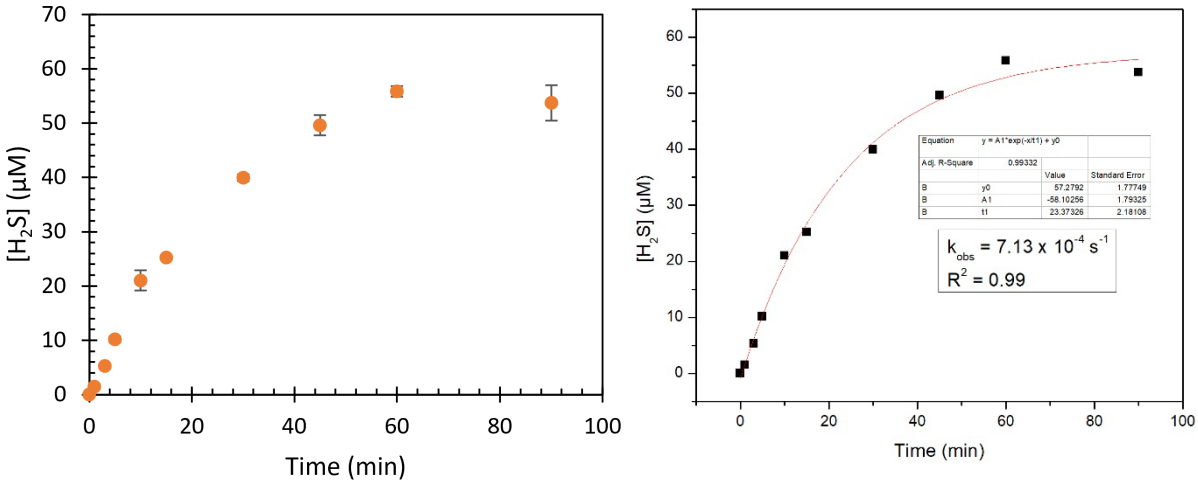

Figure C.1 H_2S release from free $NACS_4$ (25 μM) in the presence of glutathione (1.5 mM, 60 equiv) in PBS (pH 7.4, 10 mM). H_2S was measured using the methylene blue assay with results expressed as mean ± standard deviation (SD) (n = 3).

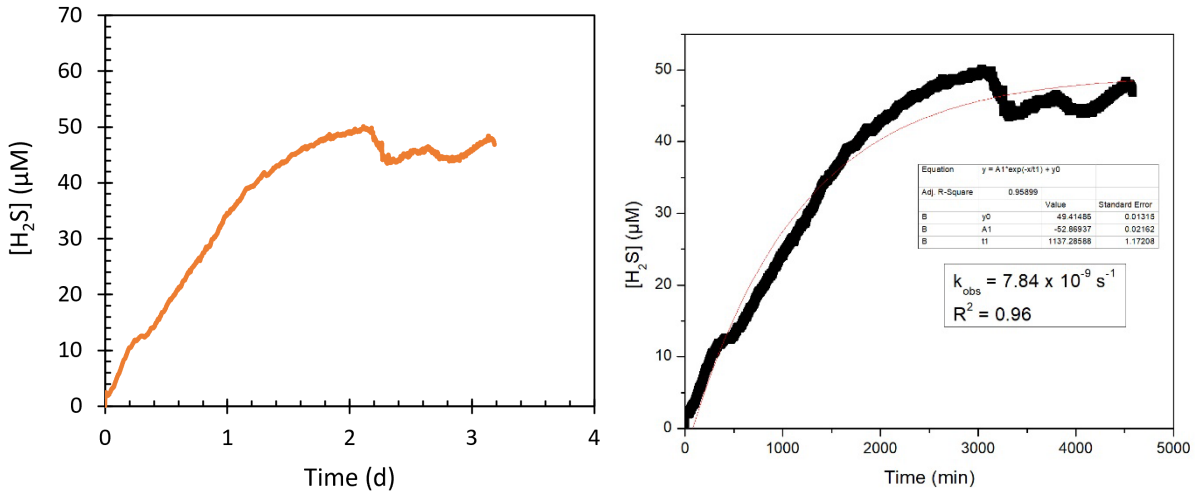

Figure C.2 H_2S release from hydrogel-bound $NACS_4$ in the presence of glutathione (10 mM) in PBS (pH 7.4, 10 mM). H_2S was measured using an H_2S-selective electrode (WPI).

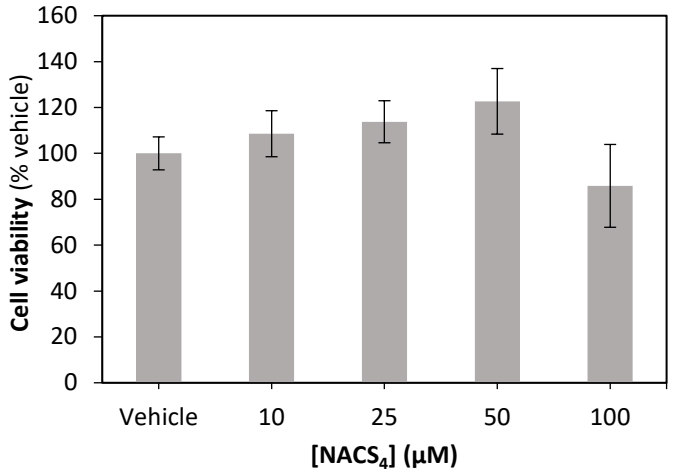

Figure C.3 Cytotoxicity of $NACS_4$ in hMSCs.

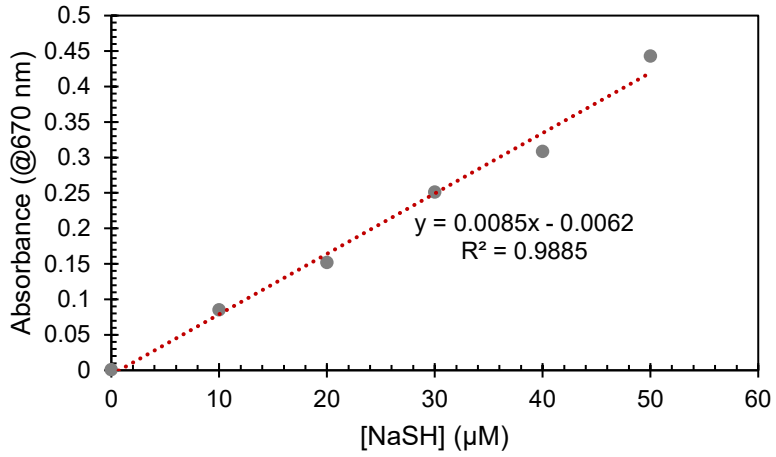

Figure C.4 MBA calibration curve generated using known concentrations of NaSH in the presence of 10 mM GSH.

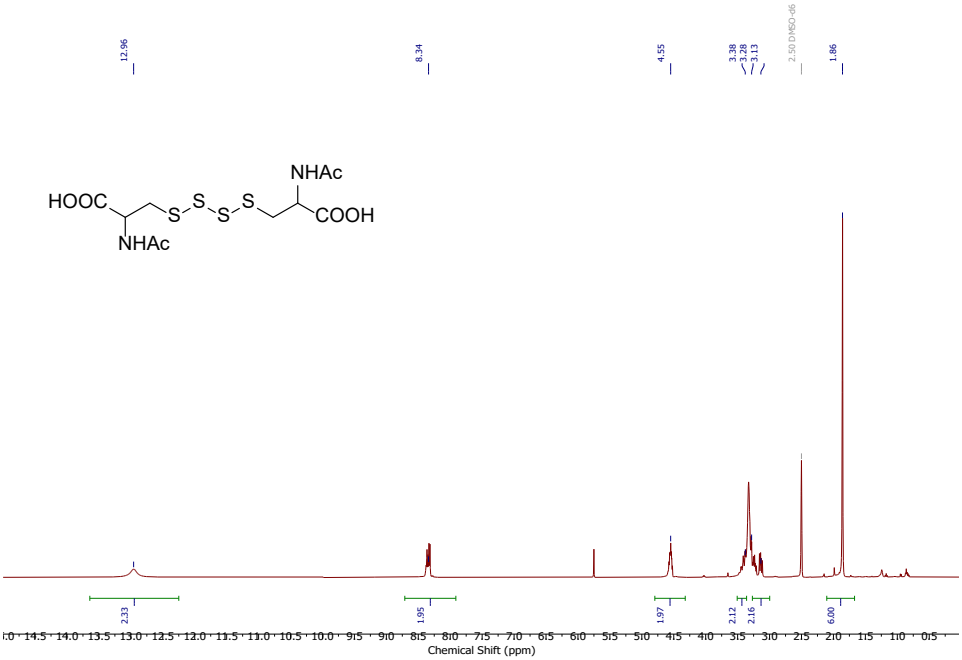

Figure C.5 ^{1}H NMR (500 MHz, DMSO-d_6) spectrum of **NACS$_4$**.

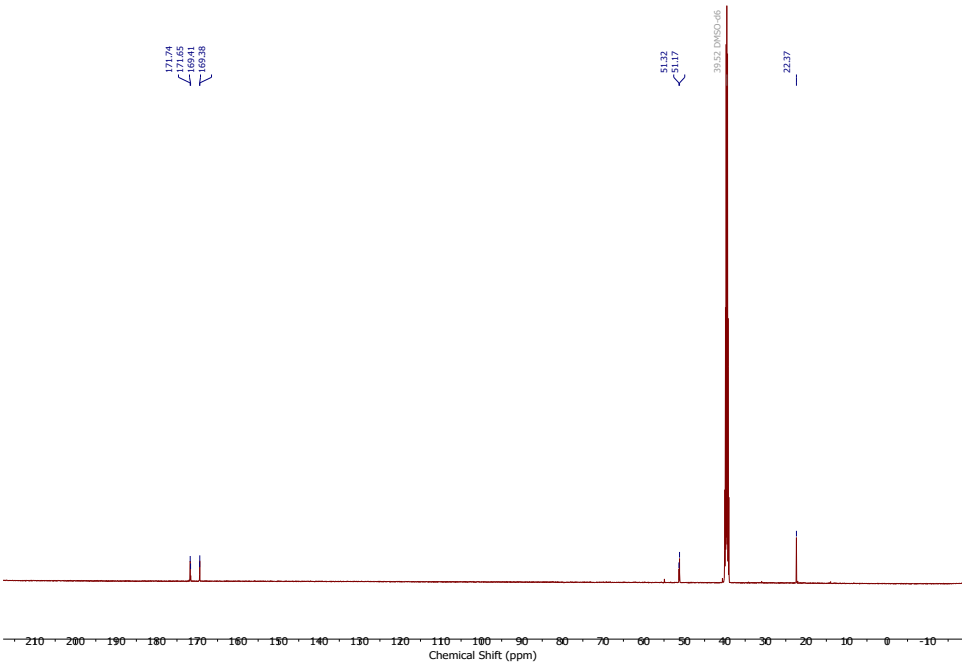

Figure C.6 ^{13}C NMR (126 MHz, DMSO-d_6) spectrum of **NACS$_4$**.

APPENDIX D

SUPPLEMENTARY CONTENT FOR CHAPTER V

Appendix D is the supplementary appendix for Chapter VI of this dissertation. It includes all spectra and supplemental information relevant to the material in Chapter VI.

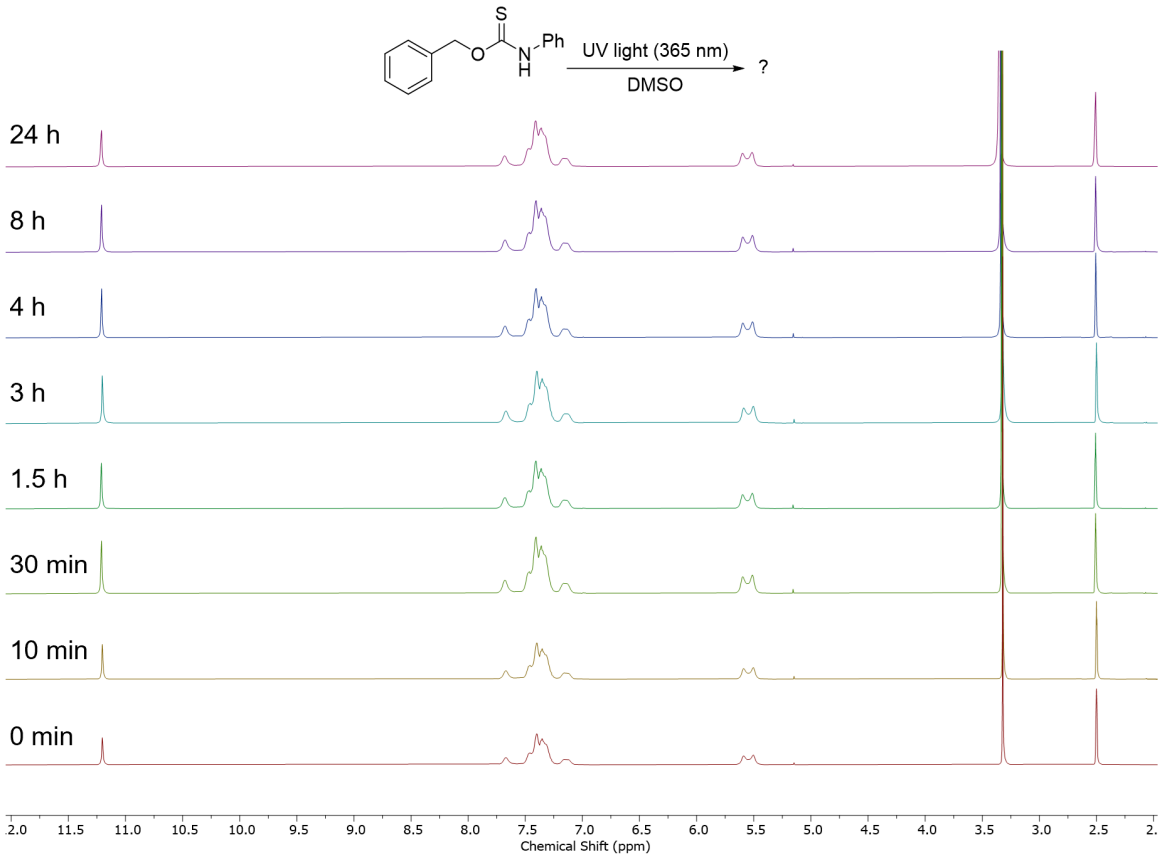

Figure D.1 Model TCM stability in DMSO in the presence of UV light (365 nm) over 24 h.

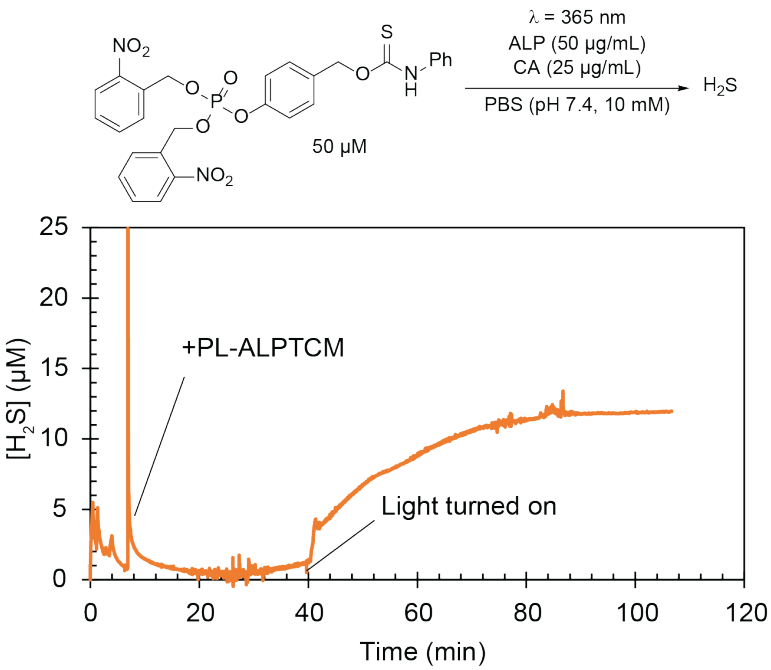

Figure D.2 Dual stimuli H_2S production in the presence of ALP (50 μg/mL, 0.5 U/mL) and CA (25 μg/mL) followed by UV light exposure (365 nm) starting at 45 min.

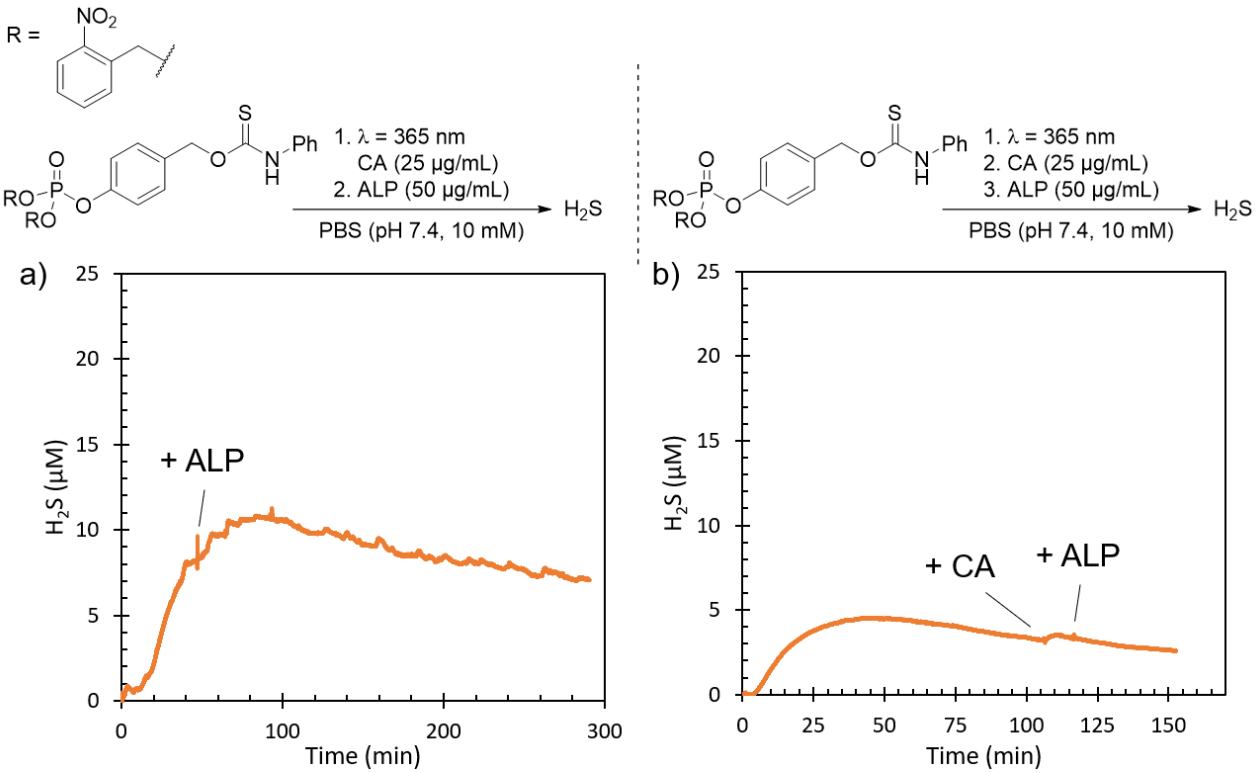

Figure D.3 H_2S-selective electrode sensitivity to UV light exposure. a) PL-ALPTCM (50 μM) in PBS (pH 7.4, 10 mM) with CA (25 μg/mL) and exposed to UV light (365 nm). ALP (50 μg/mL, 0.5 U/mL) was added after 50 min, resulting in minimal increase in response. b) PL-ALPTCM (50 μM) in PBS (pH 7.4, 10 mM) was exposed to UV light (365 nm). Both CA (25 μg/mL) and ALP (50 μg/mL, 0.5 U/mL) was added after 100 min. No increase in response was observed after enzyme additions.

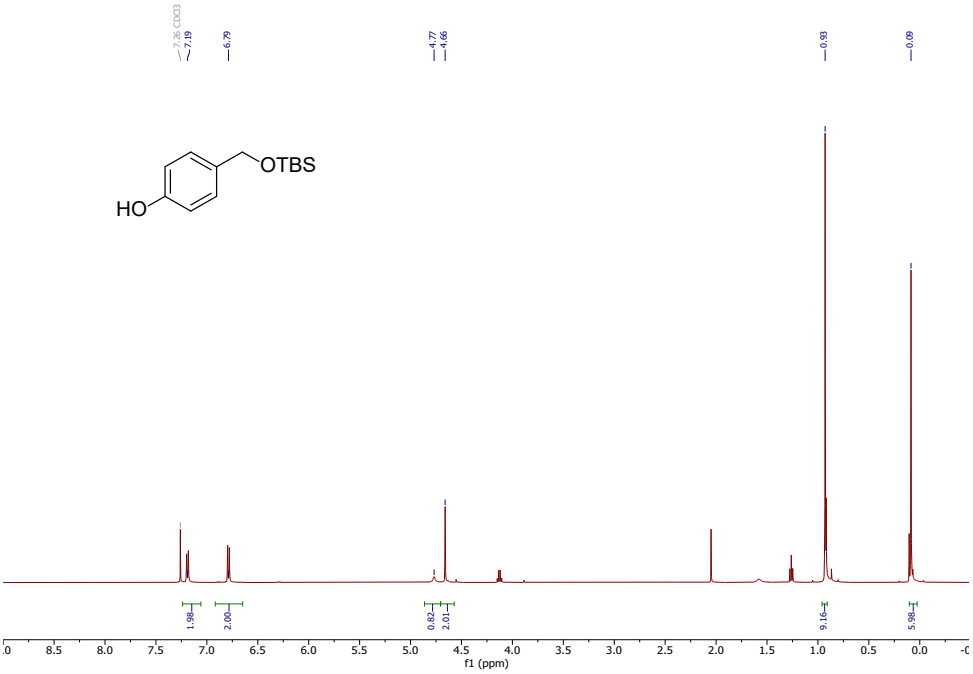

Figure D.4 ^{1}H NMR (500 MHz, $CDCl_3$) spectrum of TBS protected BnOH.

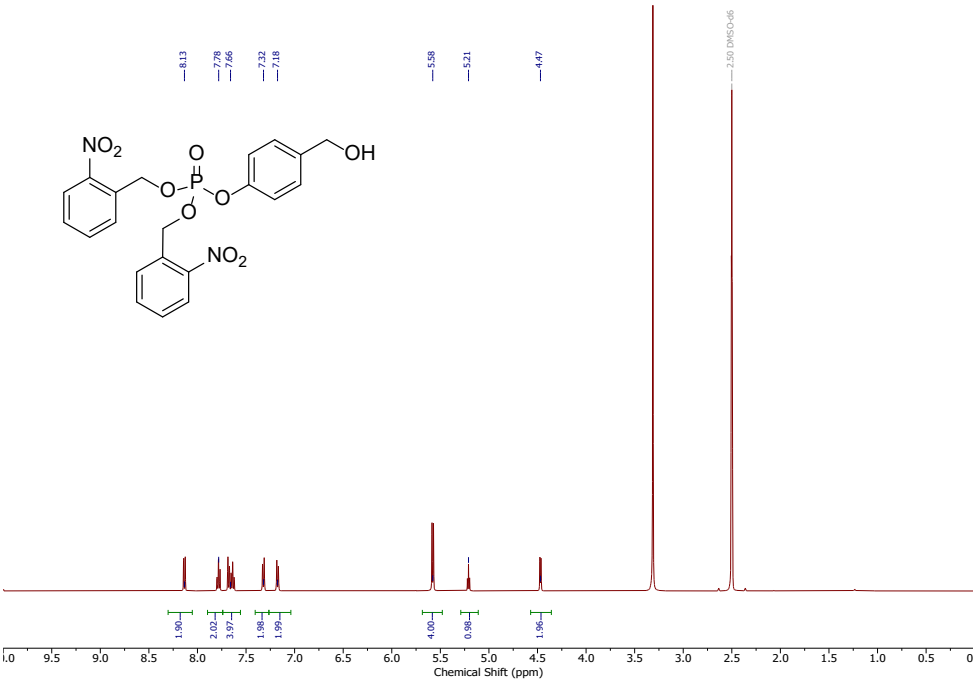

Figure D.5 ^{1}H NMR (500 MHz, DMSO) spectrum of **PL-BnOH**.

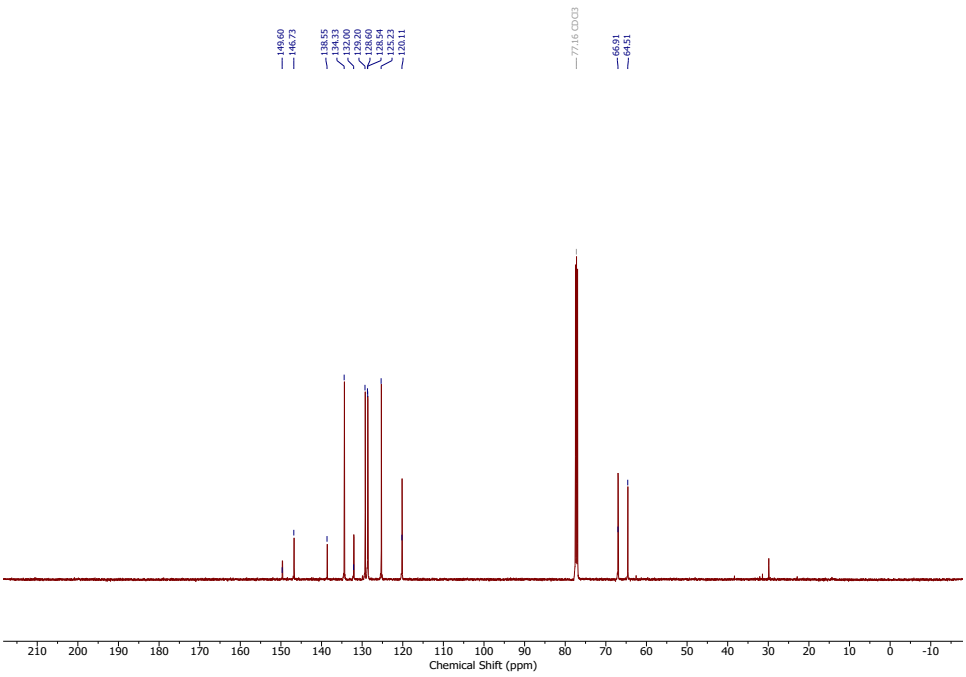

Figure D.6 $^{13}C\{H\}$ NMR (151 MHz, DMSO) spectrum of **PL-BnOH**.

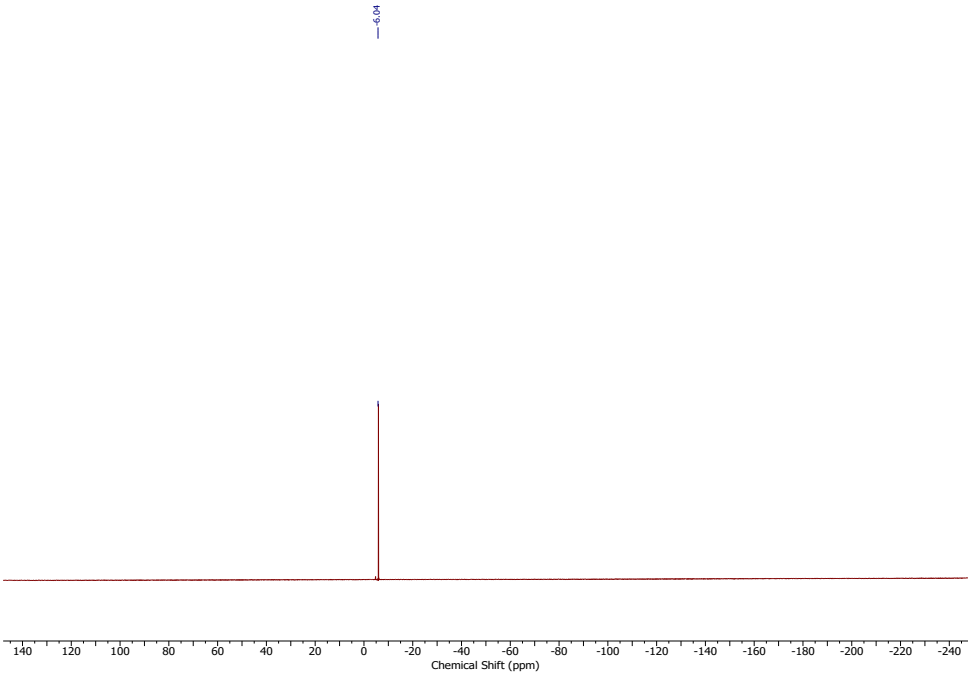

Figure D.7 ^{31}P NMR (243 MHz, $CDCl_3$) spectrum of **PL-BnOH**.

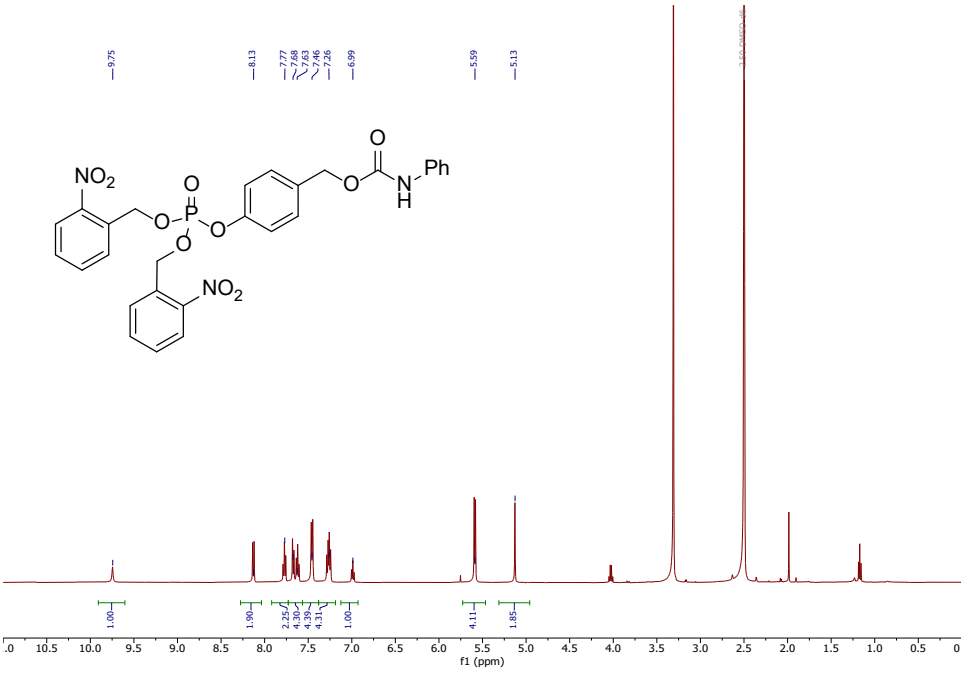

Figure D.8 ^{1}H NMR (500 MHz, DMSO) spectrum of **PL-ALPCM**.

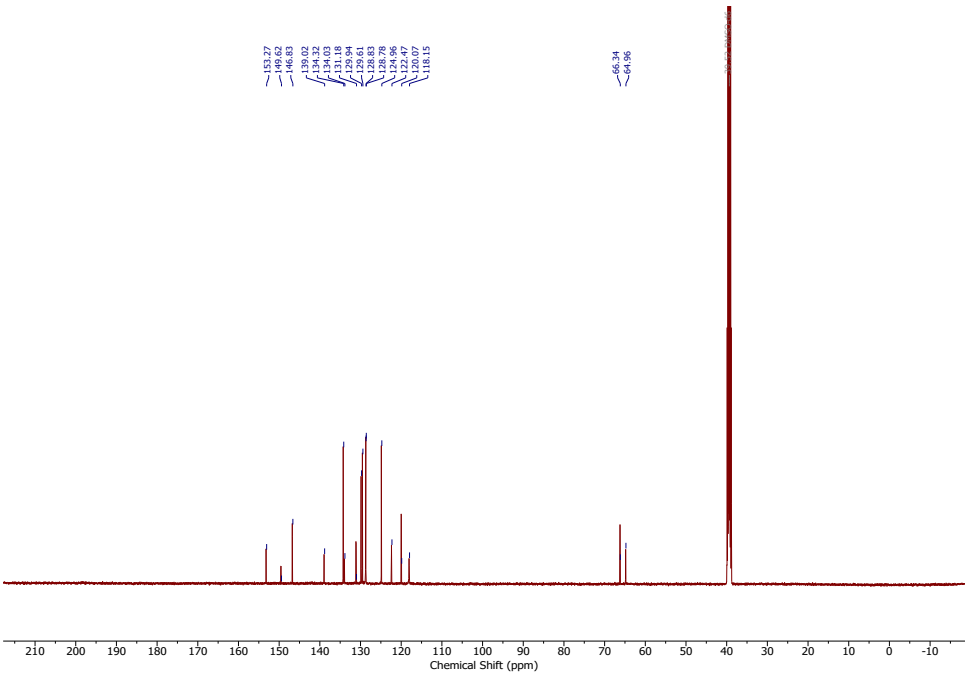

Figure D.9 ^{13}C{H} NMR (151 MHz, DMSO) spectrum of **PL-ALPCM**.

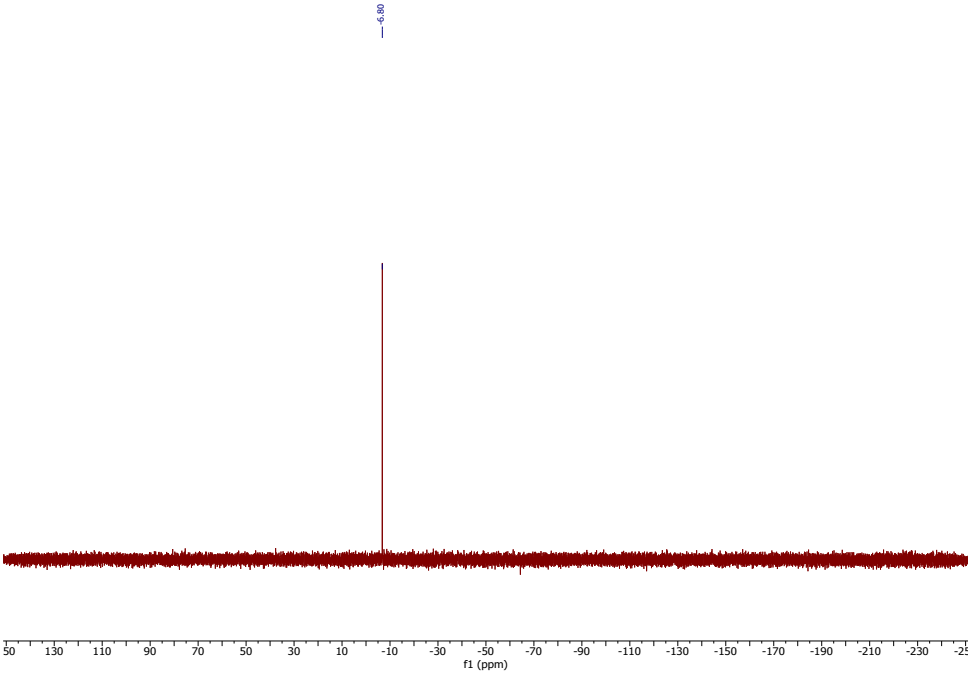

Figure D.10 ^{31}P NMR (202 MHz, DMSO) spectrum of **PL-ALPCM**.

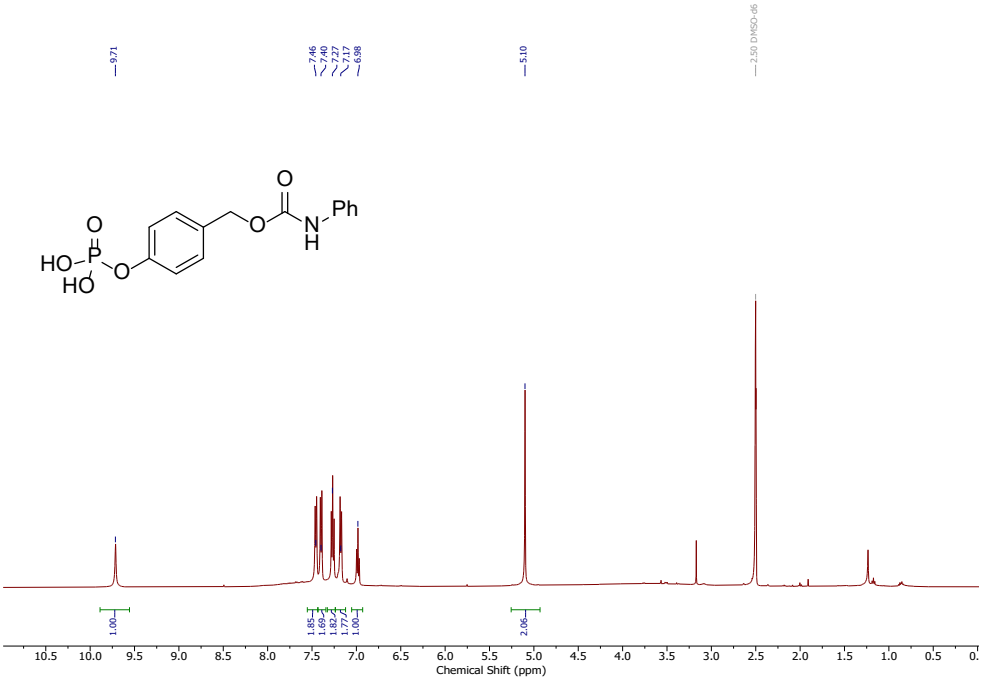

Figure D.11 ^{1}H NMR (500 MHz, DMSO) spectrum of **ALPCM**.

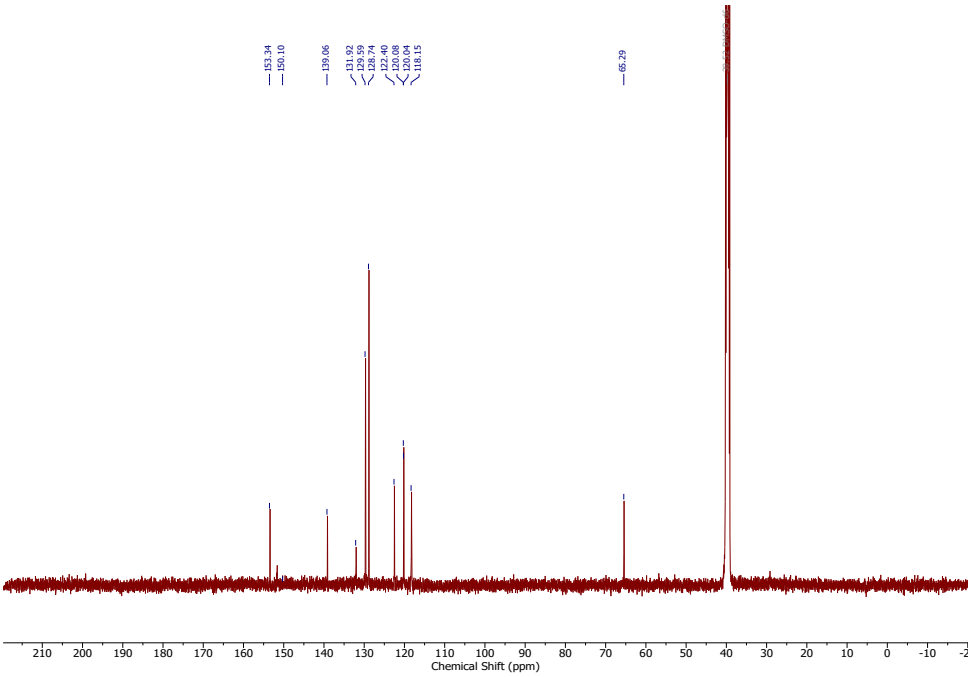

Figure D.12 $^{13}C\{H\}$ NMR (126 MHz, DMSO) spectrum of **ALPCM**.

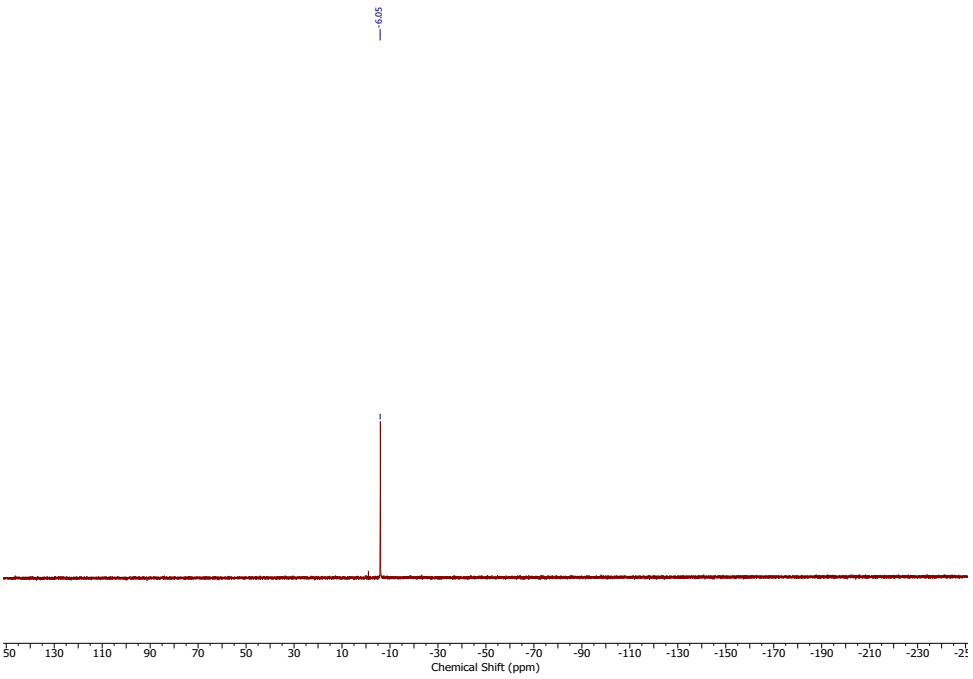

Figure D.13 ^{31}P NMR (243 MHz, DMSO) spectrum of **PL-ALPCM**.

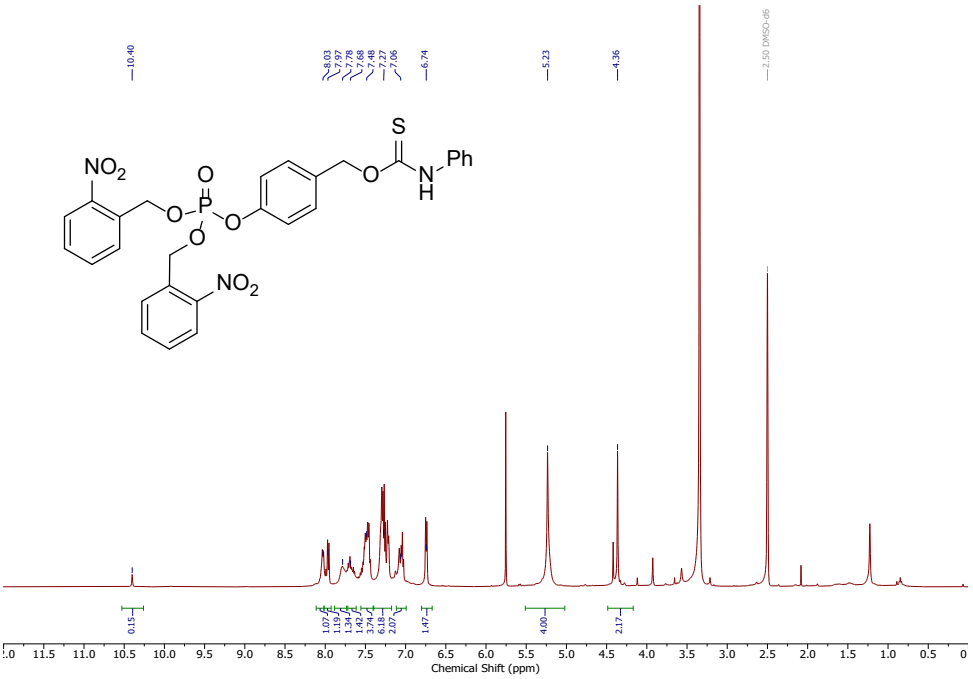

Figure D.14 ^{1}H NMR (500 MHz, DMSO) spectrum of **PL-ALPTCM**.

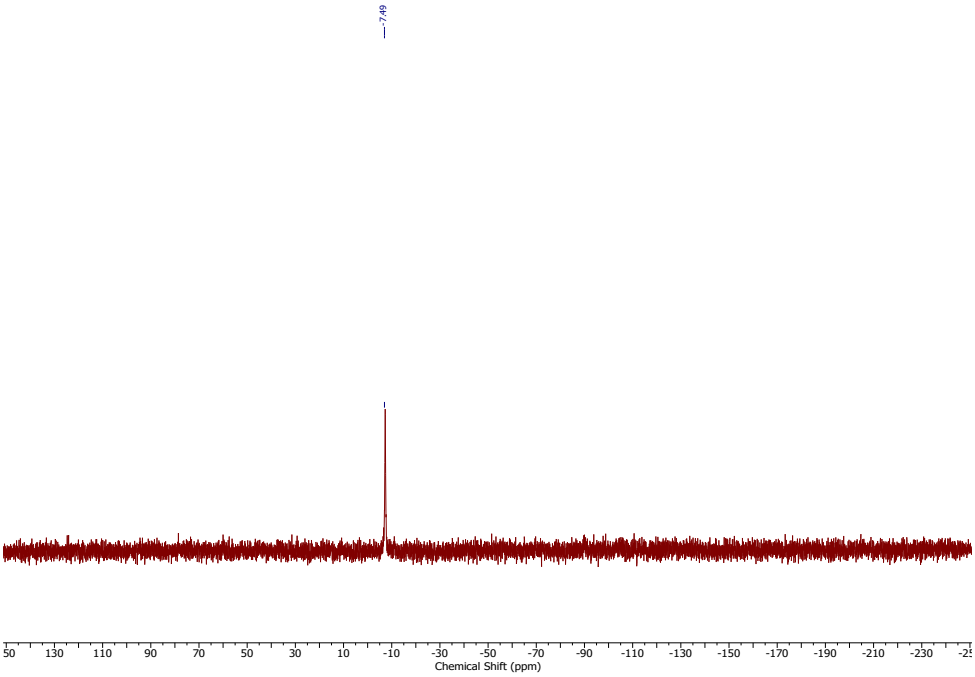

Figure D.15 ^{31}P NMR (202 MHz, DMSO) spectrum of **PL-ALPTCM**.

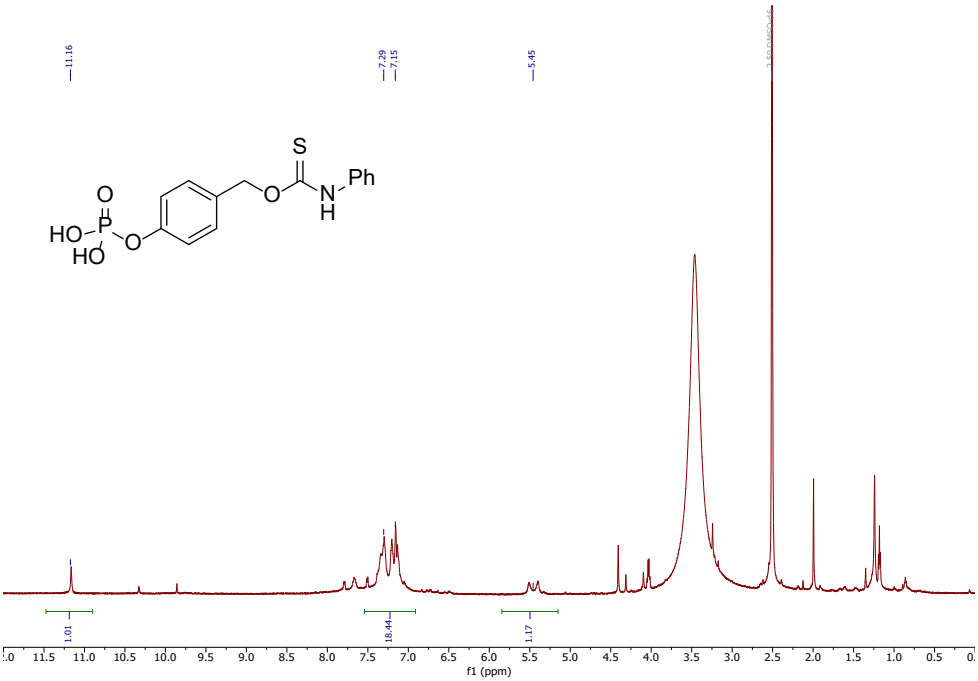

Figure D.16 ^{1}H NMR (500 MHz, DMSO) spectrum of **ALPTCM**.

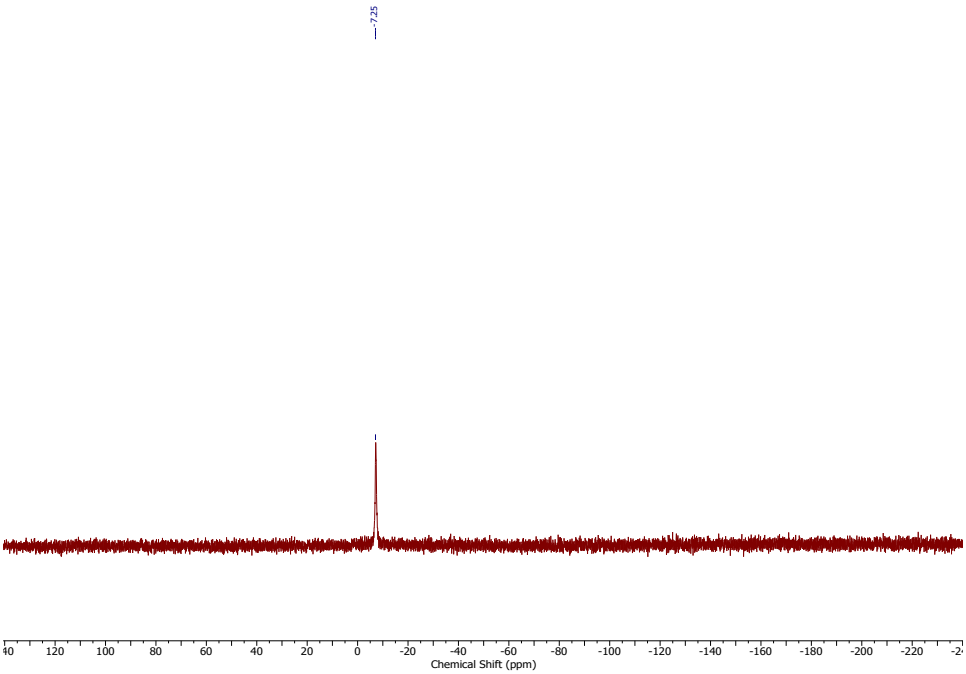

Figure D.17 ^{31}P NMR (243 MHz, DMSO) spectrum of **ALPTCM**.

REFERENCES CITED

1. Wang, R., Physiological implications of hydrogen sulfide: a whiff exploration that blossomed. *Physiol. Rev.* **2012,** *92* (2), 791-896.

2. Liu, Y.; Yang, R.; Liu, X.; Zhou, Y.; Qu, C.; Kikuiri, T.; Wang, S.; Zandi, E.; Du, J.; Ambudkar, I. S., Hydrogen sulfide maintains mesenchymal stem cell function and bone homeostasis via regulation of Ca^{2+} channel sulfhydration. *Cell stem cell* **2014,** *15* (1), 66-78.

3. Wei, H.-J.; Li, X.; Tang, X.-Q., Therapeutic benefits of H_2S in Alzheimer's disease. *J. Clin. Neurosci.* **2014,** *21* (10), 1665-1669.

4. Szabo, C., Roles of hydrogen sulfide in the pathogenesis of diabetes mellitus and its complications. *Antioxid. Redox Signal.* **2012,** *17* (1), 68-80.

5. Steiger, A. K.; Zhao, Y.; Pluth, M. D., Emerging roles of carbonyl sulfide in chemical biology: sulfide transporter or gasotransmitter? *Antioxid. Redox Signal.* **2018,** *28* (16), 1516-1532.

6. Levinn, C. M.; Cerda, M. M.; Pluth, M. D., Activatable small-molecule hydrogen sulfide donors. *Antioxid. Redox Signal.* **2020,** *32* (2), 96-109.

7. Levinn, C. M.; Cerda, M. M.; Pluth, M. D., Development and application of carbonyl sulfide-based donors for H_2S delivery. *Acc. Chem. Res.* **2019,** *52* (9), 2723-2731.

8. Ferm, R. J., The Chemistry Of Carbonyl Sulfide. *Chem. Rev.* **1957,** *57* (4), 621-640.

9. Beck, M. T.; Kauffman, G. B., COS and C_3S_2: The discovery and chemistry of two important inorganic sulfur compounds. *Polyhedron* **1985,** *4* (5), 775-781.

10. Svoronos, P. D. N.; Bruno, T. J., Carbonyl Sulfide: A Review of Its Chemistry and Properties. *Ind. Eng. Chem. Res.* **2002,** *41* (22), 5321-5336.

11. Leman, L.; Orgel, L.; Ghadiri, M. R., Carbonyl sulfide-mediated prebiotic formation of peptides. *Science* **2004,** *306* (5694), 283-286.

12. Huber, C.; Wächtershäuser, G., Peptides by Activation of Amino Acids with CO on (Ni,Fe)S Surfaces: Implications for the Origin of Life. *Science* **1998,** *281* (5377), 670.

13. Balazy, M.; Abu-Yousef, I. A.; Harpp, D. N.; Park, J., Identification of carbonyl sulfide and sulfur dioxide in porcine coronary artery by gas chromatography/mass spectrometry, possible relevance to EDHF. *Biochem. Biophys. Res. Commun.* **2003,** *311* (3), 728-734.

14. Kamboures, M. A.; Blake, D. R.; Cooper, D. M.; Newcomb, R. L.; Barker, M.; Larson, J. K.; Meinardi, S.; Nussbaum, E.; Rowland, F. S., Breath sulfides and pulmonary function in cystic fibrosis. *Proc. Natl. Acad. Sci. U.S.A.* **2005,** *102* (44), 15762-15767.

15. Sehnert, S. S.; Jiang, L.; Burdick, J. F.; Risby, T. H., Breath biomarkers for detection of human liver diseases: preliminary study. *Biomarkers* **2002,** *7* (2), 174-187.

16. Smeulders, M. J.; Pol, A.; Venselaar, H.; Barends, T. R. M.; Hermans, J.; Jetten, M. S. M.; Op den Camp, H. J. M., Bacterial CS_2 hydrolases from Acidithiobacillus thiooxidans strains are homologous to the archaeal catenane CS_2 hydrolase. *J. Bacteriol.* **2013,** *195* (18), 4046-4056.

17. Haritos, V. S.; Dojchinov, G., Carbonic anhydrase metabolism is a key factor in the toxicity of CO_2 and COS but not CS_2 toward the flour beetle Tribolium castaneum [Coleoptera: Tenebrionidae]. *Comp. Biochem. Physiol. Part - C: Toxicol. Pharmacol.* **2005,** *140* (1), 139-147.

18. Lorimer, G.; Pierce, J., Carbonyl sulfide: an alternate substrate for but not an activator of ribulose-1,5-bisphosphate carboxylase. *J. Biol. Chem.* **1989,** *264* (5), 2764-2772.

19. Ensign, S. A., Reactivity of Carbon Monoxide Dehydrogenase from Rhodospirillum rubrum with Carbon Dioxide, Carbonyl Sulfide, and Carbon Disulfide. *Biochem.* **1995,** *34* (16), 5372-5381.

20. Seefeldt, L. C.; Rasche, M. E.; Ensign, S. A., Carbonyl sulfide and carbon dioxide as new substrates, and carbon disulfide as a new inhibitor, of nitrogenase. *Biochem.* **1995,** *34* (16), 5382-5389.

21. Kernohan, J. C., The activity of bovine carbonic anhydrase in imidazole buffers. *Biochim. Biophys. Acta* **1964,** *81* (2), 346-356.

22. Chengelis, C. P.; Neal, R. A., Studies of carbonyl sulfide toxicity: Metabolism by carbonic anhydrase. *Toxicol. Appl. Pharmacol.* **1980,** *55* (1), 198-202.

23. Steiger, A. K.; Pardue, S.; Kevil, C. G.; Pluth, M. D., Self-Immolative Thiocarbamates Provide Access to Triggered H_2S Donors and Analyte Replacement Fluorescent Probes. *J. Am. Chem. Soc.* **2016,** *138* (23), 7256-7259.

24. Powell, C. R.; Foster, J. C.; Swilley, S. N.; Kaur, K.; Scannelli, S. J.; Troya, D.; Matson, J. B., Self-amplified depolymerization of oligo (thiourethanes) for the release of COS/H_2S. *Polym. Chem.* **2019,** *10* (23), 2991-2995.

25. Zhao, Y.; Pluth, M. D., Hydrogen sulfide donors activated by reactive oxygen species. *Angew. Chem. Int. Ed.* **2016,** *128* (47), 14858-14862.

26. Zhao, Y.; Henthorn, H. A.; Pluth, M. D., Kinetic insights into hydrogen sulfide delivery from caged-carbonyl sulfide isomeric donor platforms. *J. Am. Chem. Soc.* **2017,** *139* (45), 16365-16376.

27. Chauhan, P.; Jos, S.; Chakrapani, H., Reactive Oxygen Species-Triggered Tunable Hydrogen Sulfide Release. *Org. Lett.* **2018,** *20* (13), 3766-3770.

28. Zhu, C.; Suarez, S. I.; Lukesh, J. C., Illuminating and alleviating cellular oxidative stress with an ROS-activated, H_2S-donating theranostic. *Tetrahedron Lett.* **2021**, 152944.

29. Zhang, N.; Hu, P.; Wang, Y.; Tang, Q.; Zheng, Q.; Wang, Z.; He, Y., A Reactive Oxygen Species (ROS) Activated Hydrogen Sulfide (H_2S) Donor with Self-Reporting Fluorescence. *ACS Sens.* **2020,** *5* (2), 319-326.

30. Hu, Y.; Li, X.; Fang, Y.; Shi, W.; Li, X.; Chen, W.; Xian, M.; Ma, H., Reactive oxygen species-triggered off-on fluorescence donor for imaging hydrogen sulfide delivery in living cells. *Chem. Sci.* **2019,** *10* (33), 7690-7694.

31. Steiger, A. K.; Yang, Y.; Royzen, M.; Pluth, M. D., Bio-orthogonal "click-and-release" donation of caged carbonyl sulfide (COS) and hydrogen sulfide (H_2S). *Chem. Commun.* **2017,** *53* (8), 1378-1380.

32. Zhao, Y.; Bolton, S. G.; Pluth, M. D., Light-Activated COS/H_2S Donation from Photocaged Thiocarbamates. *Org. Lett.* **2017,** *19* (9), 2278-2281.

33. Hua, W.; Zhao, J.; Gou, S., A naphthalimide derivative can release COS and form H_2S in a light-controlled manner and protect cells against ROS with real-time monitoring ability. *Analyst* **2020,** *145* (11), 3878-3884.

34. Sharma, A. K.; Nair, M.; Chauhan, P.; Gupta, K.; Saini, D. K.; Chakrapani, H., Visible-light-triggered uncaging of carbonyl sulfide for hydrogen sulfide (H_2S) release. *Org. Lett.* **2017,** *19* (18), 4822-4825.

35. Štacko, P.; Muchová, L.; Vitek, L.; Klán, P., Visible to NIR light photoactivation of hydrogen sulfide for biological targeting. *Org. Lett.* **2018,** *20* (16), 4907-4911.

36. Powell, C. R.; Foster, J. C.; Okyere, B.; Theus, M. H.; Matson, J. B., Therapeutic delivery of H_2S via COS: small molecule and polymeric donors with benign byproducts. *J. Am. Chem. Soc.* **2016,** *138* (41), 13477-13480.

37. Powell, C. R.; Kaur, K.; Dillon, K. M.; Zhou, M.; Alaboalirat, M.; Matson, J. B., Functional N-Substituted N-Thiocarboxyanhydrides as Modular Tools for Constructing H_2S Donor Conjugates. *ACS Chem. Biol.* **2019,** *14* (6), 1129-1134.

38. Zhao, Y.; Steiger, A. K.; Pluth, M. D., Cysteine-activated hydrogen sulfide (H_2S) delivery through caged carbonyl sulfide (COS) donor motifs. *Chem. Commun.* **2018,** *54* (39), 4951-4954.

39. Yang, X.; Guo, Y.; Strongin, R. M., Conjugate Addition/Cyclization Sequence Enables Selective and Simultaneous Fluorescence Detection of Cysteine and Homocysteine. *Angew. Chem. Int. Ed.* **2011,** *50* (45), 10690-10693.

40. Zhao, Y.; Steiger, A. K.; Pluth, M. D., Cyclic Sulfenyl Thiocarbamates Release Carbonyl Sulfide and Hydrogen Sulfide Independently in Thiol-Promoted Pathways. *J. Am. Chem. Soc.* **2019,** *141* (34), 13610-13618.

41. Wallace, J. L.; Caliendo, G.; Santagada, V.; Cirino, G., Markedly reduced toxicity of a hydrogen sulphide-releasing derivative of naproxen (ATB-346). *Br. J. Pharmacol.* **2010,** *159* (6), 1236-1246.

42. Cerda, M. M.; Mancuso, J. L.; Mullen, E. J.; Hendon, C. H.; Pluth, M. D., Use of Dithiasuccinoyl-Caged Amines Enables COS/H_2S Release Lacking Electrophilic Byproducts. *Eur. J. Chem.* **2020,** *26* (24), 5374-5380.

43. Barany, G.; Merrifield, R. B., A new amino protecting group removable by reduction. Chemistry of the dithiasuccinoyl (DTS) function. *J. Am. Chem. Soc.* **1977,** *99* (22), 7363-7365.

44. Zhou, S.; Mou, Y.; Liu, M.; Du, Q.; Ali, B.; Ramprasad, J.; Qiao, C.; Hu, L.-F.; Ji, X., Insights into the Mechanism of Thiol-Triggered COS/H_2S Release from N-Dithiasuccinoyl Amines. *J. Org. Chem.* **2020,** *85* (13), 8352-8359.

45. Severino, B.; Corvino, A.; Fiorino, F.; Luciano, P.; Frecentese, F.; Magli, E.; Saccone, I.; Di Vaio, P.; Citi, V.; Calderone, V., 1,2,4-Thiadiazolidin-3,5-diones as novel hydrogen sulfide donors. *Eur. J. Med. Chem.* **2018,** *143*, 1677-1686.

46. Khodade, V. S.; Pharoah, B. M.; Paolocci, N.; Toscano, J. P., Alkylamine-Substituted Perthiocarbamates: Dual Precursors to Hydropersulfide and Carbonyl Sulfide with Cardioprotective Actions. *J. Am. Chem. Soc.* **2020,** *142* (9), 4309-4316.

47. Shahriari, M.; Zahiri, M.; Abnous, K.; Taghdisi, S. M.; Ramezani, M.; Alibolandi, M., Enzyme responsive drug delivery systems in cancer treatment. *J. Controlled Release* **2019,** *308*, 172-189.

48. Zheng, Y.; Yu, B.; Ji, K.; Pan, Z.; Chittavong, V.; Wang, B., Esterase-Sensitive Prodrugs with Tunable Release Rates and Direct Generation of Hydrogen Sulfide. *Angew. Chem. Int. Ed.* **2016,** *55* (14), 4514-4518.

49. Chauhan, P.; Bora, P.; Ravikumar, G.; Jos, S.; Chakrapani, H., Esterase activated carbonyl sulfide/hydrogen sulfide (H_2S) donors. *Org. Lett.* **2017,** *19* (1), 62-65.

50. Steiger, A. K.; Marcatti, M.; Szabo, C.; Szczesny, B.; Pluth, M. D., Inhibition of mitochondrial bioenergetics by esterase-triggered COS/H_2S donors. *ACS Chem. Biol.* **2017,** *12* (8), 2117-2123.

51. Levinn, C. M.; Steiger, A. K.; Pluth, M. D., Esterase-Triggered Self-Immolative Thiocarbamates Provide Insights into COS Cytotoxicity. *ACS Chem. Biol.* **2019,** *14* (2), 170-175.

52. Chauhan, P.; Gupta, K.; Ravikumar, G.; Saini, D. K.; Chakrapani, H., Carbonyl Sulfide (COS) Donor Induced Protein Persulfidation Protects against Oxidative Stress. *Asian J. Chem.* **2019,** *14* (24), 4717-4724.

53. Kang, J.; Li, Z.; Organ, C. L.; Park, C.-M.; Yang, C.-t.; Pacheco, A.; Wang, D.; Lefer, D. J.; Xian, M., pH-Controlled Hydrogen Sulfide Release for Myocardial Ischemia-Reperfusion Injury. *J. Am. Chem. Soc.* **2016,** *138* (20), 6336-6339.

54. Gilbert, A. K.; Zhao, Y.; Otteson, C. E.; Pluth, M. D., Development of acid-mediated H_2S/COS donors that respond to a specific pH window. *J. Org. Chem.* **2019,** *84* (22), 14469-14475.

55. Zhao, Y.; Steiger, A. K.; Pluth, M. D., Colorimetric Carbonyl Sulfide (COS)/Hydrogen Sulfide (H_2S) Donation from γ-Ketothiocarbamate Donor Motifs. *Angew. Chem. Int. Ed.* **2018,** *57* (40), 13101-13105.

56. Zhao, Y.; Cerda, M. M.; Pluth, M. D., Fluorogenic hydrogen sulfide (H_2S) donors based on sulfenyl thiocarbonates enable H_2S tracking and quantification. *Chem. Sci.* **2019,** *10* (6), 1873-1878.

57. Cerda, M. M.; Fehr, J. M.; Sherbow, T. J.; Pluth, M. D., Progress toward colorimetric and fluorescent detection of carbonyl sulfide. *Chem. Commun.* **2020,** *56* (67), 9644-9647.

58. Benavides, G. A.; Squadrito, G. L.; Mills, R. W.; Patel, H. D.; Isbell, T. S.; Patel, R. P.; Darley-Usmar, V. M.; Doeller, J. E.; Kraus, D. W., Hydrogen sulfide mediates the vasoactivity of garlic. *Proc. Natl. Acad. Sci. U.S.A.* **2007,** *104* (46), 17977-17982.

59. Zhao, W.; Zhang, J.; Lu, Y.; Wang, R., The vasorelaxant effect of H_2S as a novel endogenous gaseous K_{ATP} channel opener. *The EMBO journal* **2001,** *20* (21), 6008-6016.

60. Calvert, J. W.; Jha, S.; Gundewar, S.; Elrod, J. W.; Ramachandran, A.; Pattillo, C. B.; Kevil, C. G.; Lefer, D. J., Hydrogen sulfide mediates cardioprotection through Nrf2 signaling. *Circ. Res.* **2009,** *105* (4), 365-374.

61. Whiteman, M.; Li, L.; Rose, P.; Tan, C.-H.; Parkinson, D. B.; Moore, P. K., The effect of hydrogen sulfide donors on lipopolysaccharide-induced formation of inflammatory mediators in macrophages. *Antioxid. Redox Signal.* **2010,** *12* (10), 1147-1154.

62. Zhao, Y.; Biggs, T. D.; Xian, M., Hydrogen sulfide (H_2S) releasing agents: chemistry and biological applications. *Chem. Commun.* **2014,** *50* (80), 11788-11805.

63. Hartle, M. D.; Pluth, M. D., A practical guide to working with H_2S at the interface of chemistry and biology. *Chem. Soc. Rev.* **2016,** *45* (22), 6108-6117.

64. Powell, C. R.; Dillon, K. M.; Matson, J. B., A review of hydrogen sulfide (H_2S) donors: Chemistry and potential therapeutic applications. *Biochem. Pharmacol.* **2018,** *149*, 110-123.

65. Li, L.; Whiteman, M.; Guan, Y. Y.; Neo, K. L.; Cheng, Y.; Lee, S. W.; Zhao, Y.; Baskar, R.; Tan, C.-H.; Moore, P. K., Characterization of a novel, water-soluble hydrogen sulfide–releasing molecule (GYY4137) new insights into the biology of hydrogen sulfide. *Circulation* **2008,** *117* (18), 2351-2360.

66. Devarie-Baez, N. O.; Bagdon, P. E.; Peng, B.; Zhao, Y.; Park, C.-M.; Xian, M., Light-induced hydrogen sulfide release from “caged” gem-dithiols. *Org. Lett.* **2013,** *15* (11), 2786-2789.

67. Shukla, P.; Khodade, V. S.; SharathChandra, M.; Chauhan, P.; Mishra, S.; Siddaramappa, S.; Pradeep, B. E.; Singh, A.; Chakrapani, H., "On demand" redox buffering by H_2S contributes to antibiotic resistance revealed by a bacteria-specific H_2S donor. *Chem. Sci.* **2017,** *8* (7), 4967-4972.

68. Wu, D.; Si, W.; Wang, M.; Lv, S.; Ji, A.; Li, Y., Hydrogen sulfide in cancer: friend or foe? *Nitric Oxide* **2015,** *50*, 38-45.

69. Müller, I. A.; Kratz, F.; Jung, M.; Warnecke, A., Schiff bases derived from p-aminobenzyl alcohol as trigger groups for pH-dependent prodrug activation. *Tetrahedron Lett.* **2010,** *51* (33), 4371-4374.

70. Lloyd-Jones, G. C.; Moseley, J. D.; Renny, J. S., Mechanism and application of the Newman-Kwart O→ S rearrangement of O-aryl thiocarbamates. *Synthesis* **2008,** *2008* (05), 661-689.

71. Zonta, C.; De Lucchi, O.; Volpicelli, R.; Cotarca, L., Thione–Thiol Rearrangement: Miyazaki–Newman–Kwart Rearrangement and Others. In *Sulfur-Mediated Rearrangements II*, Springer: 2006; pp 131-161.

72. Perkowski, A. J.; Cruz, C. L.; Nicewicz, D. A., Ambient-Temperature Newman-Kwart Rearrangement Mediated by Organic Photoredox Catalysis. *J. Am. Chem. Soc.* **2015,** *137* (50), 15684-15687.

73. Pedersen, S. K.; Ulfkjaer, A.; Newman, M. N.; Yogarasa, S.; Petersen, A. U.; Solling, T. I.; Pittelkow, M., Inverting the Selectivity of the Newman-Kwart Rearrangement via One Electron Oxidation at Room Temperature. *J. Org. Chem.* **2018,** *83* (19), 12000-12006.

74. Eriksen, K.; Ulfkjaer, A.; Solling, T. I.; Pittelkow, M., Benzylic Thio and Seleno Newman-Kwart Rearrangements. *J. Org. Chem.* **2018,** *83* (18), 10786-10797.

75. Lu, S. C., Regulation of hepatic glutathione synthesis: current concepts and controversies. *The FASEB Journal* **1999,** *13* (10), 1169-1183.

76. Hauser, D. N.; Hastings, T. G., Mitochondrial dysfunction and oxidative stress in Parkinson's disease and monogenic parkinsonism. *Neurobiol. Dis.* **2013,** *51*, 35-42.

77. Rochette, L.; Zeller, M.; Cottin, Y.; Vergely, C., Diabetes, oxidative stress and therapeutic strategies. *Biochim. Biophys. Acta* **2014,** *1840* (9), 2709-2729.

78. Siasos, G.; Tsigkou, V.; Kosmopoulos, M.; Theodosiadis, D.; Simantiris, S.; Tagkou, N. M.; Tsimpiktsioglou, A.; Stampouloglou, P. K.; Oikonomou, E.; Mourouzis, K., Mitochondria and cardiovascular diseases—from pathophysiology to treatment. *Ann. Transl. Med.* **2018,** *6* (12).

79. Roussel, B. D.; Kruppa, A. J.; Miranda, E.; Crowther, D. C.; Lomas, D. A.; Marciniak, S. J., Endoplasmic reticulum dysfunction in neurological disease. *Lancet Neurol.* **2013,** *12* (1), 105-118.

80. Machamer, C. E., The Golgi complex in stress and death. *Front. Neurosci.* **2015,** *9*, 421.

81. Paul, B. D.; Snyder, S. H.; Kashfi, K., Effects of hydrogen sulfide on mitochondrial function and cellular bioenergetics. *Redox Biol.* **2021,** *38*, 101772.

82. Wang, H.; Shi, X.; Qiu, M.; Lv, S.; Liu, H., Hydrogen sulfide plays an important protective role through influencing endoplasmic reticulum stress in diseases. *Int. J. Biol. Sci.* **2020,** *16* (2), 264.

83. Zhang, Y.; Wang, Y.; Read, E.; Fu, M.; Pei, Y.; Wu, L.; Wang, R.; Yang, G., Golgi stress response, hydrogen sulfide metabolism, and intracellular calcium homeostasis. *Antioxid. Redox Signal.* **2020,** *32* (9), 583-601.

84. Paul, B. D.; Snyder, S. H., H_2S: a novel gasotransmitter that signals by sulfhydration. *Trends Biochem. Sci.* **2015,** *40* (11), 687-700.

85. Teng, H.; Wu, B.; Zhao, K.; Yang, G.; Wu, L.; Wang, R., Oxygen-sensitive mitochondrial accumulation of cystathionine β-synthase mediated by Lon protease. *Proc. Natl. Acad. Sci. U.S.A.* **2013,** *110* (31), 12679-12684.

86. Agrawal, N.; Banerjee, R., Human polycomb 2 protein is a SUMO E3 ligase and alleviates substrate-induced inhibition of cystathionine β-synthase sumoylation. *PloS one* **2008,** *3* (12), e4032.

87. Montoya, L. A.; Pluth, M. D., Organelle-targeted H_2S probes enable visualization of the subcellular distribution of H_2S donors. *Anal. Chem.* **2016,** *88* (11), 5769-5774.

88. Chen, J.; Zhao, M.; Jiang, X.; Sizovs, A.; Wang, M. C.; Provost, C. R.; Huang, J.; Wang, J., Genetically anchored fluorescent probes for subcellular specific imaging of hydrogen sulfide. *Analyst* **2016,** *141* (4), 1209-1213.

89. Liu, T.; Xu, Z.; Spring, D. R.; Cui, J., A lysosome-targetable fluorescent probe for imaging hydrogen sulfide in living cells. *Org. Lett.* **2013,** *15* (9), 2310-2313.

90. Zhu, H.; Liu, C.; Liang, C.; Tian, B.; Zhang, H.; Zhang, X.; Sheng, W.; Yu, Y.; Huang, S.; Zhu, B., A new phenylsulfonamide-based Golgi-targeting fluorescent probe for H_2S and its bioimaging applications in living cells and zebrafish. *Chem. Commun.* **2020,** *56* (29), 4086-4089.

91. Tang, Y.; Xu, A.; Ma, Y.; Xu, G.; Gao, S.; Lin, W., A turn-on endoplasmic reticulum-targeted two-photon fluorescent probe for hydrogen sulfide and bio-imaging applications in living cells, tissues, and zebrafish. *Sci. Rep.* **2017,** *7* (1), 1-9.

92. Qiao, Q.; Zhao, M.; Lang, H.; Mao, D.; Cui, J.; Xu, Z., A turn-on fluorescent probe for imaging lysosomal hydrogen sulfide in living cells. *RSC Adv.* **2014,** *4* (49), 25790-25794.

93. Wu, Z.; Liang, D.; Tang, X., Visualizing hydrogen sulfide in mitochondria and lysosome of living cells and in tumors of living mice with positively charged fluorescent chemosensors. *Anal. Chem.* **2016,** *88* (18), 9213-9218.

94. Szczesny, B.; Módis, K.; Yanagi, K.; Coletta, C.; Le Trionnaire, S.; Perry, A.; Wood, M. E.; Whiteman, M.; Szabo, C., AP39, a novel mitochondria-targeted hydrogen sulfide donor, stimulates cellular bioenergetics, exerts cytoprotective effects and protects against the loss of mitochondrial DNA integrity in oxidatively stressed endothelial cells in vitro. *Nitric oxide* **2014,** *41*, 120-130.

95. Mahato, S. K.; Bhattacherjee, D.; Bhabak, K. P., The biothiol-triggered organotrisulfide-based self-immolative fluorogenic donors of hydrogen sulfide enable lysosomal trafficking. *Chem. Commun.* **2020,** *56* (56), 7769-7772.

96. Chen, Y.; Zhao, R.; Tang, C.; Zhang, C.; Xu, W.; Wu, L.; Wang, Y.; Ye, D.; Liang, Y., Design and Development of a Bioorthogonal, Visualizable and Mitochondria-Targeted Hydrogen Sulfide (H_2S) Delivery System. *Angew. Chem. Int. Ed.* **2022,** *61* (6), e202112734.

97. Karwi, Q. G.; Bornbaum, J.; Boengler, K.; Torregrossa, R.; Whiteman, M.; Wood, M. E.; Schulz, R.; Baxter, G. F., AP39, a mitochondria-targeting hydrogen sulfide (H_2S) donor, protects against myocardial reperfusion injury independently of salvage kinase signalling. *Br. J. Pharmacol.* **2017,** *174* (4), 287-301.

98. Pomierny, B.; Krzyżanowska, W.; Jurczyk, J.; Skórkowska, A.; Strach, B.; Szafarz, M.; Przejczowska-Pomierny, K.; Torregrossa, R.; Whiteman, M.; Marcinkowska, M., The Slow-Releasing and Mitochondria-Targeted Hydrogen Sulfide (H_2S) Delivery Molecule AP39 Induces Brain Tolerance to Ischemia. *Int. J. Mol. Sci.* **2021,** *22* (15), 7816.

99. Zhao, F.-l.; Fang, F.; Qiao, P.-f.; Yan, N.; Gao, D.; Yan, Y., AP39, a mitochondria-targeted hydrogen sulfide donor, supports cellular bioenergetics and protects against Alzheimer's disease by preserving mitochondrial function in APP/PS1 mice and neurons. *Oxid. Med. Cell. Longev.* **2016,** *2016*.

100. Wang, H.; He, Z.; Yang, Y.; Zhang, J.; Zhang, W.; Zhang, W.; Li, P.; Tang, B., Ratiometric fluorescence imaging of Golgi H_2O_2 reveals a correlation between Golgi oxidative stress and hypertension. *Chem. Sci.* **2019,** *10* (47), 10876-10880.

101. Chen, X.; Khairallah, G. N.; Richard, A.; Williams, S. J., Fixed-charge labels for simplified reaction analysis: 5-hydroxy-1,2,3-triazoles as byproducts of a copper (I)-catalyzed click reaction. *Tetrahedron Lett.* **2011,** *52* (21), 2750-2753.

102. Yang, W.; Chan, P. S.; Chan, M. S.; Li, K. F.; Lo, P. K.; Mak, N. K.; Cheah, K. W.; Wong, M. S., Two-photon fluorescence probes for imaging of mitochondria and lysosomes. *Chem. Commun.* **2013,** *49* (33), 3428-3430.

103. Peng, B.; Thorsell, A. G.; Karlberg, T.; Schüler, H.; Yao, S. Q., Small molecule microarray based discovery of PARP14 inhibitors. *Angew. Chem. Int. Ed.* **2017,** *56* (1), 248-253.

104. Fang, L.; Trigiante, G.; Crespo-Otero, R.; Philpott, M. P.; Jones, C. R.; Watkinson, M., An alternative modular 'click-SNAr-click' approach to develop subcellular localised fluorescent probes to image mobile Zn^{2+}. *Org. Biomol. Chem.* **2019,** *17* (47), 10013-10019.

105. Chambers, J. M.; Hill, P. A.; Aaron, J. A.; Han, Z.; Christianson, D. W.; Kuzma, N. N.; Dmochowski, I. J., Cryptophane xenon-129 nuclear magnetic resonance biosensors targeting human carbonic anhydrase. *J. Am. Chem. Soc.* **2009,** *131* (2), 563-569.

106. Schindelin, J.; Arganda-Carreras, I.; Frise, E.; Kaynig, V.; Longair, M.; Pietzsch, T.; Preibisch, S.; Rueden, C.; Saalfeld, S.; Schmid, B.; Tinevez, J.-Y.; White, D. J.; Hartenstein, V.; Eliceiri, K.; Tomancak, P.; Cardona, A., Fiji: an open-source platform for biological-image analysis. *Nat. Methods* **2012,** *9* (7), 676-682.

107. Xu, A.; Tang, Y.; Lin, W., Endoplasmic reticulum-targeted two-photon turn-on fluorescent probe for nitroreductase in tumor cells and tissues. *Spectrochim. Acta A Mol. Biomol. Spectrosc.* **2018,** *204*, 770-776.

108. Sies, H.; Jones, D. P., Reactive oxygen species (ROS) as pleiotropic physiological signalling agents. *Nat. Rev. Mol. Cell Biol.* **2020,** *21* (7), 363-383.

109. Brieger, K.; Schiavone, S.; Miller, F. J.; Krause, K.-H., Reactive oxygen species: from health to disease. *Swiss Med. Wkly* **2012,** *142*, w13659.

110. Wauquier, F.; Leotoing, L.; Coxam, V.; Guicheux, J.; Wittrant, Y., Oxidative stress in bone remodelling and disease. *Trends Mol. Med.* **2009,** *15* (10), 468-477.

111. Wang, R., The Gasotransmitter Role of Hydrogen Sulfide. *Antioxid. Redox Signal.* **2003,** *5* (4).

112. Zhao, Y.; Biggs, T. D.; Xian, M., Hydrogen sulfide (H2S) releasing agents: chemistry and biological applications. *Chem Commun (Camb)* **2014,** *50* (80), 11788-805.

113. Szabo, C., A timeline of hydrogen sulfide (H_2S) research: From environmental toxin to biological mediator. *Biochem. Pharmacol.* **2018,** *149*, 5-19.

114. Gambari, L.; Lisignoli, G.; Gabusi, E.; Manferdini, C.; Paolella, F.; Piacentini, A.; Grassi, F., Distinctive expression pattern of cystathionine-β-synthase and cystathionine-γ-lyase identifies mesenchymal stromal cells transition to mineralizing osteoblasts. *J. Cell. Physiol.* **2017,** *232* (12), 3574-3585.

115. Behera, J.; Tyagi, S. C.; Tyagi, N., Role of hydrogen sulfide in the musculoskeletal system. *Bone* **2019,** *124*, 33-39.

116. Gambari, L.; Grigolo, B.; Grassi, F., Hydrogen Sulfide in Bone Tissue Regeneration and Repair: State of the Art and New Perspectives. *Int. J. Mol. Sci.* **2019,** *20* (20), 5231.

117. Hao, Y.-M.; He, D.-W.; Gao, Y.; Fang, L.-N.; Zhang, P.-P.; Lu, K.; Lu, R.-Z.; Li, C., Association of Hydrogen Sulfide with Femoral Bone Mineral Density in Osteoporosis Patients: A Preliminary Study. *Med. Sci. Monit.* **2021,** *27*, e929389-1.

118. Song, S.; Guo, Y.; Yang, Y.; Fu, D., Advances in pathogenesis and therapeutic strategies for osteoporosis. *Pharmacol. Ther.* **2022**, 108168.

119. Kearns, A. E.; Khosla, S.; Kostenuik, P. J., Receptor activator of nuclear factor kappaB ligand and osteoprotegerin regulation of bone remodeling in health and disease. *Endocr Rev* **2008,** *29* (2), 155-92.

120. Ha, H.; Kwak, H. B.; Lee, S. W.; Jin, H. M.; Kim, H.-M.; Kim, H.-H.; Lee, Z. H., Reactive oxygen species mediate RANK signaling in osteoclasts. *Exp. Cell Res.* **2004,** *301* (2), 119-127.

121. Domazetovic, V.; Marcucci, G.; Iantomasi, T.; Brandi, M. L.; Vincenzini, M. T., Oxidative stress in bone remodeling: role of antioxidants. *Clin. Cases Miner. Bone Metab.* **2017,** *14* (2), 209.

122. Rapposelli, S.; Gambari, L.; Digiacomo, M.; Citi, V.; Lisignoli, G.; Manferdini, C.; Calderone, V.; Grassi, F., A Novel H_2S-releasing Amino-Bisphosphonate which combines bone anti-catabolic and anabolic functions. *Sci Rep* **2017,** *7* (1), 11940.

123. Gambari, L.; Lisignoli, G.; Cattini, L.; Manferdini, C.; Facchini, A.; Grassi, F., Sodium hydrosulfide inhibits the differentiation of osteoclast progenitor cells via NRF2-dependent mechanism. *Pharmacol Res* **2014,** *87*, 99-112.

124. Xu, Z. S.; Wang, X. Y.; Xiao, D. M.; Hu, L. F.; Lu, M.; Wu, Z. Y.; Bian, J. S., Hydrogen sulfide protects MC3T3-E1 osteoblastic cells against H_2O_2-induced oxidative damage-implications for the treatment of osteoporosis. *Free Radic Biol Med* **2011,** *50* (10), 1314-23.

125. Gennari, L.; Merlotti, D.; Falchetti, A.; Eller Vainicher, C.; Cosso, R.; Chiodini, I., Emerging therapeutic targets for osteoporosis. *Expert Opin Ther Targets* **2020,** *24* (2), 115-130.

126. Khosla, S.; Oursler, M. J.; Monroe, D. G., Estrogen and the skeleton. *Trends Endocrinol Metab* **2012,** *23* (11), 576-81.

127. Grassi, F.; Tyagi, A. M.; Calvert, J. W.; Gambari, L.; Walker, L. D.; Yu, M.; Robinson, J.; Li, J. Y.; Lisignoli, G.; Vaccaro, C.; Adams, J.; Pacifici, R., Hydrogen Sulfide Is a Novel Regulator of Bone Formation Implicated in the Bone Loss Induced by Estrogen Deficiency. *J. Bone Miner. Res.* **2016,** *31* (5), 949-63.

128. Kim, J.; Kim, H.; Roh, H.; Kwon, Y., Causes of hyperhomocysteinemia and its pathological significance. *Arch. Pharmacal Res.* **2018,** *41* (4), 372-383.

129. Morris, A. A.; Kozich, V.; Santra, S.; Andria, G.; Ben-Omran, T. I.; Chakrapani, A. B.; Crushell, E.; Henderson, M. J.; Hochuli, M.; Huemer, M.; Janssen, M. C.; Maillot, F.; Mayne, P. D.; McNulty, J.; Morrison, T. M.; Ogier, H.; O'Sullivan, S.; Pavlikova, M.; de Almeida, I. T.; Terry, A.; Yap, S.; Blom, H. J.; Chapman, K. A., Guidelines for the diagnosis and management of cystathionine beta-synthase deficiency. *J Inherit Metab Dis* **2017,** *40* (1), 49-74.

130. Behera, J.; Bala, J.; Nuru, M.; Tyagi, S. C.; Tyagi, N., Homocysteine as a pathological biomarker for bone disease. *J. Cell. Physiol.* **2017,** *232* (10), 2704-2709.

131. Behera, J.; George, A. K.; Voor, M. J.; Tyagi, S. C.; Tyagi, N., Hydrogen sulfide epigenetically mitigates bone loss through OPG/RANKL regulation during hyperhomocysteinemia in mice. *Bone* **2018,** *114*, 90-108.

132. Behera, J.; Kelly, K. E.; Voor, M. J.; Metreveli, N.; Tyagi, S. C.; Tyagi, N., Hydrogen Sulfide Promotes Bone Homeostasis by Balancing Inflammatory Cytokine Signaling in CBS-Deficient Mice through an Epigenetic Mechanism. *Sci Rep* **2018,** *8* (1), 15226.

133. Zhai, Y.; Behera, J.; Tyagi, S. C.; Tyagi, N., Hydrogen sulfide attenuates homocysteine-induced osteoblast dysfunction by inhibiting mitochondrial toxicity. *J Cell Physiol* **2019,** *234* (10), 18602-18614.

134. Cunningham, B. P.; Brazina, S.; Morshed, S.; Miclau III, T., Fracture healing: a review of clinical, imaging and laboratory diagnostic options. *Injury* **2017,** *48*, S69-S75.

135. Schindeler, A.; McDonald, M. M.; Bokko, P.; Little, D. G., Bone remodeling during fracture repair: The cellular picture. *Semin Cell Dev Biol* **2008,** *19* (5), 459-66.

136. Thomas, J. D.; Kehoe, J. L., Bone Nonunion. *StatPearls [Internet]* **2020**.

137. James, A. W.; LaChaud, G.; Shen, J.; Asatrian, G.; Nguyen, V.; Zhang, X.; Ting, K.; Soo, C., A Review of the Clinical Side Effects of Bone Morphogenetic Protein-2. *Tissue Eng Part B Rev* **2016,** *22* (4), 284-97.

138. Ashley R. Poynton, J. M. L., Safety Profile for the Clinical Use of Bone Morphogenetic Proteins in the Spine. *Spine* **2002,** *27*, S40-S48.

139. Hettiaratchi, M. H.; Krishnan, L.; Rouse, T.; Chou, C.; McDevitt, T. C.; Guldberg, R. E., Heparin-mediated delivery of bone morphogenetic protein-2 improves spatial localization of bone regeneration. *Sci. Adv.* **2020,** *6* (1), eaay1240.

140. Zheng, Y.; Liao, F.; Lin, X.; Zheng, F.; Fan, J.; Cui, Q.; Yang, J.; Geng, B.; Cai, J., Cystathionine γ-Lyase–Hydrogen Sulfide Induces Runt-Related Transcription Factor 2 Sulfhydration, Thereby Increasing Osteoblast Activity to Promote Bone Fracture Healing. *Antioxid. Redox Signal.* **2017,** *27* (11), 742-753.

141. Song, A.; Hua, Y., Cystathionine γ-lyase-H2S facilitates mandibular defect healing via inducing osteogenic differentiation of bone marrow mesenchymal stem cells. *Arch. Oral Biol.* **2020,** *117*, 104821.

142. Jiang, X.; Chen, Y.; Lu, K.; Zhang, H.; Fan, X., GYY4137 promotes bone formation in a rabbit distraction osteogenesis model: a preliminary report. *J Oral Maxillofac Surg* **2015,** *73* (4), 732 e1-6.

143. Yang, M.; Zhang, K.; Zhang, X.; Zhang, Z.; Yin, X.; He, G.; Li, L.; Yang, X.; He, B., Treatment with hydrogen sulfide donor attenuates bone loss induced by modeled microgravity. *Can. J. Physiol. Pharmacol.* **2019,** *97* (7), 655-660.

144. Raggio, R.; Bonani, W.; Callone, E.; Dirè, S.; Gambari, L.; Grassi, F.; Motta, A., Silk Fibroin Porous Scaffolds Loaded with a Slow-Releasing Hydrogen Sulfide Agent (GYY4137) for Applications of Tissue Engineering. *ACS Biomater. Sci. Eng.* **2018,** *4* (8), 2956-2966.

145. Gambari, L.; Amore, E.; Raggio, R.; Bonani, W.; Barone, M.; Lisignoli, G.; Grigolo, B.; Motta, A.; Grassi, F., Hydrogen sulfide-releasing silk fibroin scaffold for bone tissue engineering. *Mater Sci Eng C Mater Biol Appl* **2019,** *102*, 471-482.

146. Whiteman, M.; Perry, A.; Zhou, Z.; Bucci, M.; Papapetropoulos, A.; Cirino, G.; Wood, M. E., Phosphinodithioate and Phosphoramidodithioate Hydrogen Sulfide Donors. *Handb Exp Pharmacol* **2015,** *230*, 337-63.

147. Gambari, L.; Grigolo, B.; Filardo, G.; Grassi, F., Sulfurous thermal waters stimulate the osteogenic differentiation of human mesenchymal stromal cells - An in vitro study. *Biomed Pharmacother* **2020,** *129*, 110344.

148. Berkmann, J. C.; Herrera Martin, A. X.; Ellinghaus, A.; Schlundt, C.; Schell, H.; Lippens, E.; Duda, G. N.; Tsitsilonis, S.; Schmidt-Bleek, K., Early pH changes in musculoskeletal tissues upon injury—Aerobic catabolic pathway activity linked to inter-individual differences in local pH. *Int. J. Mol. Sci.* **2020,** *21* (7), 2513.

149. Zhuang, L.; Li, K.; Wang, G.; Shou, T.; Gao, C.; Mao, Y.; Bao, M.; Zhao, M., Preconditioning with hydrogen sulfide prevents bone cancer pain in rats through a proliferator-activated receptor gamma/p38/Jun N-terminal kinase pathway. *Exp Biol Med (Maywood)* **2018,** *243* (1), 57-65.

150. Meng Lv, Y. L., Ting-Hui Xiao, Wei Jiang, Bo-Wen Lin, Xiao-Ming Zhang, Yi-Miao Lin, Zhong-Shi Xu, GYY4137 stimulates osteoblastic cell proliferation and differentiation via an ERK1/2-dependent anti-oxidant mechanism. *Am. J. Transl. Res.* **2017,** *9* (3), 1183-1192.

151. Zheng, Y.; Liao, F.; Lin, X.; Zheng, F.; Fan, J.; Cui, Q.; Yang, J.; Geng, B.; Cai, J., Cystathionine gamma-Lyase-Hydrogen Sulfide Induces Runt-Related Transcription Factor 2 Sulfhydration, Thereby Increasing Osteoblast Activity to Promote Bone Fracture Healing. *Antioxid Redox Signal* **2017,** *27* (11), 742-753.

152. Lee, Z. W.; Zhou, J.; Chen, C. S.; Zhao, Y.; Tan, C. H.; Li, L.; Moore, P. K.; Deng, L. W., The slow-releasing hydrogen sulfide donor, GYY4137, exhibits novel anti-cancer effects in vitro and in vivo. *PLoS One* **2011,** *6* (6), e21077.

153. Mo, S.; Hua, Y., Cystathionine gamma lyase-H_2S contributes to osteoclastogenesis during bone remodeling induced by mechanical loading. *Biochem. Biophys. Res. Commun.* **2018,** *501* (2), 471-477.

154. Gambari, L.; Lisignoli, G.; Cattini, L.; Manferdini, C.; Facchini, A.; Grassi, F., Sodium hydrosulfide inhibits the differentiation of osteoclast progenitor cells via NRF2-dependent mechanism. *Pharmacological research* **2014,** *87*, 99-112.

155. Jiang, X.; Chen, Y.; Lu, K.; Zhang, H.; Fan, X., GYY4137 promotes bone formation in a rabbit distraction osteogenesis model: a preliminary report. *Journal of Oral and Maxillofacial Surgery* **2015,** *73* (4), 732. e1-732. e6.

156. Gambari, L.; Amore, E.; Raggio, R.; Bonani, W.; Barone, M.; Lisignoli, G.; Grigolo, B.; Motta, A.; Grassi, F., Hydrogen sulfide-releasing silk fibroin scaffold for bone tissue engineering. *Materials Science and Engineering: C* **2019,** *102*, 471-482.

157. Cerda, M. M.; Hammers, M. D.; Earp, M. S.; Zakharov, L. N.; Pluth, M. D., Applications of synthetic organic tetrasulfides as H_2S donors. *Org. Lett.* **2017,** *19* (9), 2314-2317.

158. Hernández-González, A. C.; Téllez-Jurado, L.; Rodríguez-Lorenzo, L. M., Alginate hydrogels for bone tissue engineering, from injectables to bioprinting: A review. *Carbohydr. Polym.* **2020,** *229*, 115514.

159. Kabil, O.; Banerjee, R., Enzymology of H2S biogenesis, decay and signaling. *Antioxid. Redox Signal.* **2014,** *20* (5), 770-782.

160. Agidigbi, T. S.; Kim, C., Reactive oxygen species in osteoclast differentiation and possible pharmaceutical targets of ROS-mediated osteoclast diseases. *Int. J. Mol. Sci.* **2019,** *20* (14), 3576.

161. Zhao, Y.; Wang, H.; Xian, M., Cysteine-activated hydrogen sulfide (H_2S) donors. *J. Am. Chem. Soc.* **2011,** *133* (1), 15-17.

162. Vimalraj, S., Alkaline phosphatase: Structure, expression and its function in bone mineralization. *Gene* **2020,** *754*, 144855.

163. Golub, E. E.; Boesze-Battaglia, K., The role of alkaline phosphatase in mineralization. *Curr. opin. orthop.* **2007,** *18* (5), 444-448.

164. Konukoğlu, D., Bone markers. *Int. J. Med. Biochem.* **2019,** *2* (2), 65-78.

165. Laurer, H. L.; Hagenbourger, O.; Quast, S.; Herrmann, W.; Marzi, I., Sequential changes and pattern of bone-specific alkaline phosphatase after trauma. *Eur. J. Trauma* **2000,** *26* (1), 33-38.

166. Li, J.; Luo, X.; Wang, Q.; Zheng, L.-m.; King, I.; Doyle, T. W.; Chen, S.-H., Synthesis and biological evaluation of a water soluble phosphate prodrug of 3-aminopyridine-2-carboxaldehyde thiosemicarbazone (3-AP). *Bioorg. Med. Chem. Lett.* **1998,** *8* (22), 3159-3164.

167. Li, J.; Zheng, L.-m.; King, I.; Doyle, T. W.; Chen, S.-H., Syntheses and Antitumor Activities of Potent Inhibitors of Ribonucleotide Reductase 3-Amino-4-Methylpyridine-2-Carboxaldehyde-Thiosemicarba-zone (3-Amp), 3-Amino-Pyridine-2-Carboxaldehyde-Thiosemicarbazone (3-Ap) and its Water-Soluble Prodrugs. *Curr. Med. Chem.* **2001,** *8* (2), 121-133.

168. Goggins, S.; Naz, C.; Marsh, B. J.; Frost, C. G., Ratiometric electrochemical detection of alkaline phosphatase. *Chem. Commun.* **2015,** *51* (3), 561-564.

169. Goggins, S.; Marsh, B. J.; Lubben, A. T.; Frost, C. G., Signal transduction and amplification through enzyme-triggered ligand release and accelerated catalysis. *Chem. Sci.* **2015,** *6* (8), 4978-4985.

170. Sanchini, S.; Perruccio, F.; Piizzi, G., Rational design, synthesis and biological evaluation of modular fluorogenic substrates with high affinity and selectivity for PTP1B. *ChemBioChem* **2014,** *15* (7), 961-976.